THE UNIVERSITY OF CHICAGO

ENGINEERING APPROACHES FOR THE TREATMENT OF NEUROINFLAMMATION

A DISSERTATION SUBMITTED TO
THE FACULTY OF THE PRITZKER SCHOOL OF MOLECULAR ENGINEERING
IN CANDIDACY FOR THE DEGREE OF
DOCTOR OF PHILOSOPHY

BY
ERICA BUDINA

CHICAGO, ILLINOIS
MARCH 2024

Dedicated to my parents, Gentiana and Artan Budina, who immigrated to the United States 30 years ago with many hopes and dreams. My journey is a testament to your untold sacrifices and unwavering love. Thank you for always believing in me and encouraging me to shoot for the stars. *Ju dua*, I love you.

"Instructions for living a life:

Pay attention.

Be astonished.

Tell about it."

— Mary Oliver, from "Sometimes" (2008)

TABLE OF CONTENTS

LIST OF FIGURES

LIST OF TABLES

ACKNOWLEDGMENTS

"How lucky am I to have something that makes saying goodbye so hard" (A.A. Milne). During these 4.5 years of doctoral studies at the University of Chicago, I have been privileged to learn alongside some of the most brilliant, dedicated, and compassionate individuals. Their guidance and kindness, along with the unwavering love and support from my family and friends has been instrumental to my growth as both a scientist and a human being.

First and foremost, I want to express immense thanks to my advisor, Dr. Jeffrey Hubbell, for granting me the opportunity to conduct my dissertation research in his laboratory. I could not have wished for a better thesis advisor, and I am very grateful for the privilege I had to learn from him. Jeff's passion for scientific discovery and dedication to pursuing clinically impactful research inspired me to consistently put forth my best effort, pursue challenging and meaningful work, and grow into an independent scientist. I am grateful for his unwavering support, guidance, trust, patience, kindness, and encouragement over the years. Jeff's commitment to science is matched only by his profound respect and consideration for his team members. Thank you for fostering such a friendly, collaborative, and supportive laboratory environment.

I would like to thank my dissertation committee members, Dr. Anthony Reder and Dr. Aaron Esser-Kahn, for generously contributing their time to meet with me, engaging in thought-provoking discussions about my research projects, and offering helpful feedback. Both Dr. Reder's extensive clinical knowledge about multiple sclerosis pathology and treatment, and Dr. Esser-Kahn's interdisciplinary expertise engineering immunomodulatory materials were invaluable as I conducted my research. I am also grateful to Dr. Melody Swartz, Dr. Juan Mendoza, Dr. Cathryn Nagler, and Dr. Anita Chong for providing constructive feedback during my PhD studies.

I would like to thank my undergraduate research advisor, Dr. David Mooney, and my mentor in his laboratory, Dr. Brian Kwee, for their guidance and support early in my career.

In the Mooney laboratory, I first gained exposure to the intersection of immunology and bioengineering, and became fascinated by the discipline. I would also like to express my appreciation to Dr. Lauren Black and my mentor in his laboratory, Dr. Corin Williams, for giving me the opportunity to participate in scientific research for the first time as a high school student. I am very grateful to have had the privilege to learn from such dedicated and talented scientists. All of these individuals inspired me to pursue graduate studies.

Throughout my PhD studies, I have been very fortunate to train with exceptional mentors, who provided invaluable guidance and helped me grow as a scientist. I am very grateful to Dr. Shijie Cao, my collaborator and mentor on the serine butyrate project in Chapter 2, who pioneered butyrate engineering projects in our laboratory, introduced me to the field of metabolite engineering, provided kind guidance with experimental design and excellent training on various techniques, worked alongside me during countless 12+ hour experiment endpoint days, and continued to offer valuable feedback and support even after departing the Hubbell laboratory to start his own research group. Thank you to outstanding chemists, Dr. Michal Raczy, who played an instrumental role in the initial synthesis of serine butyrate, as well as, Anna Slezak and Taryn Beckman, for their continued assistance with synthesis.

I would also like to thank Dr. Jun Ishihara, Dr. Eiji Yuba, Dr. Aslan Mansurov, and Dr. Ako Ishihara, who taught me valuable protein purification techniques during the early months of my PhD and laid the groundwork for the cytokine engineering research I conducted in Chapter 3. My first year of PhD studies coincided with the beginning of the COVID-19 pandemic. I am very appreciative of Dr. Elyse Watkins, a role model and mentor, who took me under her wing during this challenging period. Elyse provided important advice as I refined the direction of my first research project and dedicated time to train me in essential immunophenotyping techniques, despite limited laboratory time due to pandemic shift schedules. I am also very grateful to Dr. Joe Reda, for their support as we navigated the highs and lows of graduate school at the same time, troubleshooting unsuccessful experiments

and enthusiastically brainstorming new ideas.

An integral part of my PhD research involved learning and optimizing complex mouse models of autoimmune diseases. I am very grateful to Ani Solanki and Mindy Nguyen of UChicago Animal Resource Center for providing invaluable mentorship, expertise, and assistance with mouse experiments. I also want to thank outstanding Research Specialists Ha-Na Shim, Kevin Hultgren, Zahra Khosravi, and Arjun Dhar for their willingness to always lend a helping hand during long tissue processing and immune cell isolation days. Thank you to Phil Ang of the Swartz laboratory for excellent assistance with immunofluorescence staining of spinal cord tissue. Thank you to Suzana Gomes, our extraordinary laboratory manager, for taking such good care of everyone.

It has been a joy to work alongside colleagues who uplift one another in science and in life. Thank you to all members of the Hubbell laboratory, past and present, for your support and friendship: Dr. Aaron Alpar, Dr. Jennifer Antane, Dr. Claudia Batistella, Taryn Beckman, Dr. Levi Bennish, Brendan Berg, Dr. Priscilla Briquez, Dr. Shijie Cao, Kevin Chang, Angela Chun, Camryn Garza, Dr. Taylor Gray, Suzana Gomes, Isabella Hansen, Dr. Ande Hesser, Samir Hossainy, Dr. Ako Ishihara, Dr. Jun Ishihara, Dr. Seounghun Kang, Dr. Marcin Kwissa, Dr. Abigail Lauterbach, Dr. Jialu Liu, Dr. Aslan Mansurov, Dr. Tiffany Marchell, Dr. Chitavi Maulloo, Dr. J. Emiliano Medellin, Dr. Nikolaos Mitrousis, Ryne Montoya, Lorenzo Netti, Salvador Norton de Matos, Dr. Michal Raczy, Dr. Joseph Reda, Sofia Reda, Kirsten Refvik, Dr. Lucas Shores, Anna Slezak, Nikola Stanic, Dr. Sheridan Swan, Dr. Andrew Tremain, Dr. Lisa Volpatti, Ivan Vuong, Dr. Rachel Wallace, Dr. Ruyi Wang, Thomas Wang, Dr. Elyse Watkins, Dr. Michael White, Dr. John-Michael Williford, and Dr. Eiji Yuba. I have learned so much from everyone on this team.

One of the most fulfilling aspects of graduate school has been sharing what I have learned with others. I would like to thank my mentees in the Hubbell laboratory: Angela Chun, Salvador Norton de Matos, and Sofia Reda for allowing me grow as a mentor and scientist.

It has been a privilege to teach you, learn from you, and watch you become exceptional researchers. I would also like to thank UChicago for providing me the opportunity to serve as a Teaching Assistant for the Biological Materials and Tissue Engineering courses at the Pritzker School of Molecular Engineering.

Outside the laboratory, I would also like to thank my UChicago classmates and friends: Bianca Edozie, Christopher Eom, Priya Mirmira, Thao Cao, Andrew Xu. I am so fortunate that our paths crossed at UChicago and we could navigate graduate school together. Thank you for encouraging me to occasionally step out of the laboratory and explore the vibrant city of Chicago.

Most importantly, I would like to thank my family for their unwavering love and support. Thank you to my brother, Alex, for always lifting my spirits and encouraging me to prioritize happiness. Above all, I am grateful for my parents, Gentiana and Artan Budina. This journey would not have been possible without you. Thank you for making countless, untold sacrifices to ensure that Alex and I had a wonderful childhood. Thank you for teaching me the value of hard work and education. Thank you for fostering in me a curiosity about the world. Thank you for supporting me during the best and worst of times, and for always encouraging me to keep trying. Thank you for instilling in me the importance of love and compassion. You have always been my ultimate role models, and my whole world.

ABSTRACT

The overall goal of this thesis is to develop engineering approaches for the treatment of multiple sclerosis (MS), an autoimmune disease of the central nervous system. For this purpose, we employ both chemical conjugation and protein engineering strategies to prolong the bioavailability and *in vivo* half-life of two immunoregulatory molecules. We then evaluate the ability of these engineered molecules to treat experimental autoimmune encephalomyelitis (EAE), a murine model of neuroinflammation, and characterize their respective impact on the immune system.

In Chapter 1, we introduce the mechanisms of self-tolerance and immunological drivers of autoimmunity, particularly in the context of MS. We then describe the immunopathology MS, and introduce murine models of neuroinflammation that recapitulate several features of MS. Lastly, we discuss the current standards of care and identify areas of unmet need in MS drug development. In Chapter 2, we develop serine butyrate (SerBut), an amino-acid conjugated butyrate prodrug, by esterifying butyrate to serine. First, we characterize the bioactivity and biodistribution of SerBut. We then evaluate the prophylactic efficacy of SerBut in EAE. We subsequently quantify immunological changes induced by SerBut in the CNS draining lymph nodes, spleen, and spinal cord. We also study the impact of SerBut administration on global immune responses to vaccination. In Chapter 3, we develop serum albumin interleukin-33 (SA IL-33), a recombinant fusion protein of the half-life prolonging blood protein, serum albumin, and the immunoregulatory cytokine, interleukin-33. First, we characterize SA IL-33 bioactivity, biodistribution, and toxicity. We then evaluate the prophylactic and therapeutic efficacy of SA IL-33 in chronic and relapsing-remitting EAE. We subsequently quantify immunological changes induced by SA IL-33 in the CNS draining lymph nodes, spleen, and spinal cord. In Chapter 4, we summarize the key findings of this thesis and describe opportunities for future investigation in the areas of protein and metabolite engineering for neuroimmunomodulation.

CHAPTER 1

INTRODUCTION

1.1 Overview of Autoimmune Diseases

Autoimmune diseases are group of more than 80 disorders including multiple sclerosis, rheumatoid arthritis, and systemic lupus erythematosus that affect more than 5% of the world's population, and their prevalence is on the rise [1]. Currently, more than 23.5 million Americans are living with an autoimmune disease [2]. Autoimmune diseases consist of aberrant immune responses against the body's own tissues and result in potentially debilitating clinical manifestations [3]. Autoimmune diseases impact women at a higher frequency than men, as women constitute approximately 78% of diagnosed patients [3], and are among the top ten causes of mortality in women under age 65 [4]. Due to the chronic nature of many autoimmune diseases, disease management presents significant healthcare and economic challenges. Epidemiological studies estimate that the cost of healthcare management for autoimmune disease patients exceeds $100 billion annually [2].

The immune system is designed to recognize and respond to "non-self" antigens from pathogens including bacteria, viruses, fungi and parasites in order to present infection and invasion [5]. However, it must remain unresponsive to "self" antigens from the host's tissues [5] and exist in a state of "self-tolerance" where an individual's immune system does not attack host tissues [6]. An autoimmune disease arises following the breakdown or failure of self-tolerance, causing the body's immune system to mistakenly attack and damage its own organs, tissues, and cells via the generation of autoreactive T cells, B cells, and antibodies against self-antigens [6]. Multiple sclerosis (MS) is a degenerative autoimmune disease of the central nervous system that occurs when the immune system mistakenly attacks and destroys myelin sheath that protects nerve fibers [7].

Here, we will introduce mechanisms of self-tolerance, immunological drivers of autoim-

munity, and various risk factors that trigger the onset of autoimmunity, particularly in the context of MS. We will then provide an overview of the immunopathology and disease progression of MS, and discuss the advantages and limitations of murine models employed in the study of neuroinflammation. Finally, we will describe the current standard of care and unmet needs in the treatment of MS.

1.2 Mechanisms of Immunological Tolerance

In healthy hosts, the immune system contains a series of checkpoints – collectively referred to as central and peripheral tolerance – that synergize to protect against the onset of autoimmunity without dampening the ability of the immune system to recognize and respond to pathogens [6]. Central tolerance mechanisms remove newly formed, strongly autoreactive lymphocytes as they develop in the bone marrow and thymus, whereas peripheral tolerance mechanisms remove weakly autoreactive lymphocytes in the secondary lymphoid organs and peripheral tissues that previously evaded elimination by central tolerance mechanisms [1].

1.2.1 Central Tolerance

Central tolerance occurs in the primary lymphoid organs the thymus and bone marrow, in which immature T and B lymphocytes, respectively, first encounter self-antigen [6]. A highly sophisticated and carefully controlled system has evolved in which newly developed T cells are "tested" to ensure that their newly recombined T cell receptor (TCR) does not strongly bind to self-derived peptide epitopes [6]. In the thymus, T cell precursor cells are exposed to self-peptide-major histocompatibility (MHC) complexes presented by antigen-presenting dendritic cells and thymic medullary epithelial cells [8]. Due to their expression of the autoimmune regulator gene (AIRE), medullary epithelial cells are able to present peripheral tissue-restricted self-antigens to T cell precursor cells in the thymus, allowing naive T cells to experience a wide variety of protein antigens otherwise unexpressed by standard

thymic-resident cells [9]. Lymphocyte precursors whose TCRs display high affinity for self-peptide-MHC complexes are subsequently eliminated from the repertoire of lymphocytes via clonal deletion, whereby they undergo apoptotic cell death, which is referred to as negative selection [6]. Lymphocyte precursors whose T cell receptors do not bind self-peptide-MHC complexes die due to neglect [10]. Lymphocyte precursors whose TCRs display weak affinity for self-peptide MHC complexes evade central tolerance and undergo positive selection, differentiating into CD4 or CD8 single positive thymocytes [10].

1.2.2 Regulatory T Cells

Thymic or "natural" regulatory T cells (tTregs) are a subset of $CD4^+$ T helper cells that derive from $CD4^+$ single-positive thymocytes and adopt a specific anti-inflammatory phenotype. The naive T cells which differentate into tTregs typically display TCRs with intermediate affinities or avidities for self-peptide MHC ligands, stronger than the affinities of TCRs that enable positive selection of conventional $CD4^+$ T cells and weaker than the affinities of TCRs that result in elimination by negative selection [11]. An estimated 80% of the Treg repertoire originates in the thymus [12]. Tregs constitutively express the cytokine IL-2Rα chain (CD25), the transcription factor FoxP3, and the inhibitory receptor CTLA-4 [13]. Sustained FoxP3 expression is essential for the development, function, and stability of Tregs [13]. Humans with loss-of function mutations in the *foxp3* gene develop IPEX (immune dysregulation, polyendocrinopathy, enteropathy, X-linked) syndrome, an early onset, fatal, T-cell mediated disease that causes a variety of inflammatory and autoimmune diseases including diabetes, thyroiditis, hemolytic anemia, hyper-IgE syndrome, exfoliative dermatitis, splenomegaly, lymphadenopathy, and cytokine storm in affected individuals [14].

Tregs play an essential role in maintaining self-tolerance by suppressing the proliferation and activation of various immune cell subsets, including the autoreactive lymphocytes that evade central tolerance [15]. Tregs secrete immunosuppressive cytokines including IL-10 [16],

TGF-β [17], and IL-35 [18]. Tregs also induce metabolic disruption of effector cells and antigen presenting cells (APCs) [19]. Through the expression of CD25, the high affinity receptor for IL-2, Tregs sequester IL-2, a critical stimuli of T cell proliferation and differentiation, from conventional T cells, resulting in cytokine deprivation-induced apoptosis of naive T cells lacking CD25 expression [6][20]. Tregs also express the ectoenzymes CD39 (ecto-nucleoside triphosphate diphosphohydrolase-1) [21] and CD73 (ecto-5'-ectonucleotidase) [22]. By converting extracellular ADP/ATP to AMP and dephosphorylating AMP to adenosine, respectively, these enzymes enable Tregs to suppress ATP-mediated inflammation such as IL-1β, IL-18, IL-6, and TNF-α cytokine production by APCs [23][24] and increase extracellular levels of the immunoregulatory metabolite, adenosine, which reportedly suppresses effector T cell function by activating the adenosine receptor 2A [25]. Tregs also promote immunosuppression via interactions with APCs. Tregs constitutively express high levels of CTLA-4. CTLA-4 binds to the co-stimulatory molecules CD80 and CD86 on APCs with higher affinity and avidity than CD28, which is expressed by conventional T cells [26]. Subsequently, Tregs prevent APCs from providing activating co-stimulation to conventional T cells by reducing CD80/CD86 interaction with CD28 [6][26]. It has also been shown that Tregs induce indoleamine 2,3-dioxygenase (IDO) expression on dendritic cells using a CTLA-4-dependent mechanism [27]. IDO catalyzes the degradation of tryptophan, resulting in the production of inhibitory molecules called kynurenines [19]. Tregs also express the surface molecule Lag-3 [28], which binds to MHC class II on immature dendritic cells, subsequently inhibiting their maturation, activation, and immunostimulatory capacity [11][29]. Additionally, Tregs express the surface protein TIGIT that engages the poliovirus receptor on mature dendritic cells, leading to elevated production of IL-10 and reduced IL-12p40 [30]. It has also been reported that activated Tregs that express granzyme molecules that induce the direct killing of effector T cells or APCs via perforin-dependent mechanisms [31][32].

1.2.3 Peripheral Tolerance

Following maturation, lymphocytes exit the thymus and bone marrow, and migrate to secondary lymphoid tissues such as the spleen and lymph nodes through the peripheral circulation. Several peripheral tolerance checkpoints exist that enable the elimination or inactivation of mature autoreactive lymphocytes in the secondary lymphoid tissues if these cells encounter their cognate self-antigen, become activated, and pose danger [6]. These mechanisms include deletion, anergy, exhaustion, and as well as expansion of peripherally-induced Tregs [33].

To become activated, a naive T cell must recognize two signals: a TCR-specific peptide bound to an MHC molecule and a co-stimulatory signal such as CD80 or CD86 on an APC. These molecules bind to the naive T cell's TCR and the receptor CD28, respectively [32]. Both the peptide-MHC complex and the costimulatory signal must be delivered to the T cell by the same APC (a dendritic cell, macrophage, or B cell) [34]. Upon encountering an antigen and co-stimulatory signal, naive T cells produce IL-2 and upregulate the alpha chain of the IL-2 receptor, which associates with the constitutively expressed IL-2β and γ chains to form a heterotrimeric IL-2 receptor that enables T cells to bind IL-2 with higher affinity [34]. Co-stimulation of CD28 plays a critical role in T cell activation, proliferation, and survival [32]. CD28 signaling stabilizes IL-2 mRNA and activates the transcription factors AP-1 and NFκB, which induce the transcription of the *il2* gene [34][35]. CD28 signaling also induces cell cycle progression by IL-2 independent mechanisms [36][37]. Furthermore, CD28 co-stimulation promotes T cell survival by increasing the expression of Bcl-XL on T cells, which has been shown to prevent apoptotic cell death caused by TCR cross-linking, Fas cross-linking, or IL-2 withdrawal [32][38].

In turn, when mature autoreactive T cells encounter their cognate antigen without co-stimulation, they are either eliminated by clonal deletion or enter a state of long term hypo-responsiveness called anergy [39][40]. Deletion occurs via extrinsic or intrinsic apop-

totic pathways [41]. The extrinsic apoptotic pathway is triggered when pro-apoptotic ligands such as FasL and TNF bind to "death receptors" such as Fas or TNF-R1, respectively, forming the death-inducing signaling complex, which activates the protease caspase-8 and downstream signaling molecules that commit the cell to apoptosis [42][43]. The intrinsic apoptotic pathway is triggered when Bcl-2 proteins such as Bim induce the permeabilization of the mitochondrial outer membrane, resulting the release of cytochrome c, which causes Apaf-1 mediated activation of the protease caspase-9 [43][44]. It has been shown that $Bcl2l11^{-/-}Fas^{lpr/lpr}$ mice that lack Bim and Fas function have defective peripheral tolerance, resulting in accelerated, fatal lymphadenopathy and more severe autoimmunity compared to mice that lack only one of the apoptosis inducers, suggesting that both pathways are important for the prevention of autoimmunity [43].

Alternatively, upon antigen recognition in the absence of co-stimulation, autoreactive T cells could be rendered anergic [45]. Anergy is defined as a state of long-term hyporesponsiveness to antigen stimulation [10]. TCR signaling in the absence of CD28 signaling poorly activates the MAPK, PI3K/Art and IKK pathways, resulting in reduced AP-1 and NFkB activity and subsequently anergy [46]. Anergic T cells display reduced production of the cytokines IL-2, IFN-γ, and TNF-α upon TCR stimulation and fail to proliferate [46]. Tregs and APCs have been shown to regulate anergy in autoreactive T cells [10]. Tregs express of CD39 and CD73, which convert ATP adenosine, resulting in elevated levels of extracellular adenosine [25]. The binding to adenosine receptor 2A on autoreactive T cells leads to cAMP-mediated signaling which antagonizes CD28-mediated signaling [46]. APCs can provide inhibitory second signals that induce anergy. For example, APCs express PD-L1 and PD-L2, which bind to PD-1 on T cells. PD-1 signaling has been shown to interfere with CD28-mediated activation of PI3K, leading to reduced IL-2 production and, subsequently, anergy [32][47]. Tolerogenic dendritic cells are a subset of dendritic cells, induced and maintained by IL-10 and TGF-β, that display an immature or semi-mature phenotype

characterized by low constitutive expression of positive costimulatory molecules [48][49]. Due to their ability to present low levels of antigen in the absence of co-stimulation, tolerogenic dendritic cells also induce anergy [48]. Although the mechanisms that mediate whether an autoreactive T cell exposed to self-antigen in the absence of co-stimulation undergoes deletion or anergy have not been fully elucidated, the decision may be impacted by the strength of the interaction between the TCR and the self-peptide-MHC [8][39][50]. In $CD8^+$ T cells, it has been demonstrated that continuous exposure to high doses of self-antigen leads to the induction of anergy while continuous exposure to low doses of self-antigen leads to clonal deletion [8][39][50].

Antigen exposure in the periphery can induce the expression of FoxP3, resulting the generation of Tregs extrathymically [51]. Peripherally induced Tregs (pTregs) are differentiated from mature, naive $FoxP3^-CD4^+$ T cells upon exposure to tissue-specific antigens or non-self-antigens from allergens, food, and commensal bacteria in the peripheral tissues [52][53][54]. Adoptive transfer studies have demonstrate that priming antigen-specific T cells with sub-immunogenic doses of their cognate antigen results in optimal induction of FoxP3 expression [55][53]. Like tTregs, pTregs also express CD25, FoxP3, and CTLA-4 [51][56]. These cells are involved in maintaining peripheral tolerance at sites of inflammation [53][56]. For example, in the intestinal mucosa-associated lymphoid tissues, pTregs differentiate in response to retinoic acid and TGF-β, and suppress the expansion of disease-causing $ROR\gamma t^+$ Th17 cells [6]. It has also been demonstrated that exposure to TGF-β *in vitro* induces *foxp3* gene expression in TCR-challenged $CD4^+$ conventional T cells, resulting in the generation of "induced" Tregs [57]. However, these *in vitro* generated iTregs may not fully recapitulate the functional or phenotypic characteristics of *in vivo* generated pTregs [53].

Following chronic, continuous exposure to antigen, some activated T cells enter a tolerogenic state called exhaustion [58][59]. Unlike anergy, which occurs in naive T cells due to the absence of co-stimulation, exhaustion occurs in activated T cells due to continuous TCR

stimulation from persistent antigen exposure in the presence of co-stimulation [60]. Exhausted T cells progressively lose their effector functions and upregulate multiple inhibitory receptors including CTLA-4, PD-1, LAG-3, TIM-3, and TIGIT as well as the transcription factor TOX [60][61]. Over time, these cells become unable to proliferate or secrete cytokines such as IL-2, TNF-α, and IFN-γ [60][61]. Due to this altered metabolic and gene-expression profile, exhausted T cells do not become functional memory T cells [59].

1.3 Risk Factors for Autoimmune Diseases

When central and peripheral self-tolerance mechanisms break down, autoreactive T cells, B cells, and antibodies against self-antigens mistakenly attack and damage the body's own organs, tissues, and cells, resulting in pathological autoimmunity [1][6]. Various genetic and environmental risk factors may predispose an individual to develop an autoimmune disease.

1.3.1 Genetic Factors

Although rare, mutations in single genes can contribute to autoimmunity [1]. For example, autoimmune polyendocrinopathy syndrome type 1 (APS1) is an autosomal-recessively inherited autoimmune disease characterized by hypoparathyroidism, Addison's disease, and chronic mucocutaneous candidiasis infection [62]. APS1 develops due to mutations in the autoimmune regulatory gene located on chromosome 21 [63], which encodes for the AIRE transcription factor that promotes ectopic expression of peripheral tissue-restricted self-antigens on thymic medullary epithelial cells [64]. When the AIRE protein is defective, autoreactive T cell precursors that should have been deleted in the thymus during negative selection evade central tolerance and escape to the periphery, resulting in multi-organ autoimmunity [62].

However, in many autoimmune diseases, multiple polymorphic genes with risk alleles contribute to one's risk for developing the disease [65]. Several genetic variants on chromosome 6p21.3 that encode for major histocompatibility complex molecules (also referred to

as human leukocyte antigens), proteins involved in antigen presentation and subsequently self-versus non-self-antigen recognition, confer susceptibility to developing autoimmune diseases [1][66][67]. For example, in the case of MS, risk of onset is elevated in individuals who have the MHC class II risk alleles *HLA-DRB1*15:01*, *HLA-DRB1*13:03*, *HLA-DRB1*03:01*, *HLA-DRB1*08:01* or *HLA-DQB1*03:02*, whereas having the MHC class I alleles *HLA-B*44:02*, *HLA-B*38:01*, *HLA-A*02:01*, and *HLA-B*55:01* may reduce susceptibility to MS [1][65][68][69][70]. It has been shown via MRI that MS patients with the *HLA-DRB1*15:01* allele display increased volume of inflammatory white matter lesions and reduced brain parenchymal volume during active disease [71], whereas patients with the *HLA-B*44:02* allele have reduced lesion burden and larger brain volume [72]. Over 200 non-MHC gene loci have also been implicated in MS susceptibility, including *il7r*, *il12ra*, *clec16*, and *cd226* [1][70][73].

1.3.2 Epigenetic Modifications

Autoimmune disease onset may also be impacted by epigenic aberrations in DNA methylation, histone modifications, or miRNA expression [1]. For example, in both the brain white matter and peripheral blood mononuclear cells of MS patients, there is hypomethylation (reduced methylation) of cytosines in the promoter of the *pad2* gene, which encodes for peptidylarginine deiminase 2 [74][75]. The PAD-2 enzyme catalyzes the conversion of arginine residues in myelin basic protein to citrullines, which contributes to myelin destabilization [76]. Hence, the decrease in *pad2* promoter methylation may contribute to the elevated levels of PAD-2 protein detected in MS patients [74][75]. Additionally, in the leukocytes of MS patients, it has also been shown that there is hypermethylation (increased methylation) of the promoter of the *shp1* gene, which encodes for the protein tyrosine phosphatase SHP-1 [77]. The SHP-1 protein acts as a negative regulator of cytokine signaling, pro-inflammatory gene expression, and CNS demyelination [77][78]. SHP-1 expression is reduced in lymphocytes

and myeloid cells of MS patients [78]. Hence, the increase in *shp1* promoter methylation may account for the reduced levels of SHP-1 protein in MS patients [77].

1.3.3 Infectious Agents

Infection by certain bacterial, viral, and fungal pathogens has been linked to elevated autoimmune disease risk, in part due to mechanisms such as molecular mimicry and epitope spreading [1]. Molecular mimicry occurs when pathogen-derived antigens whose peptide sequences resemble those of self-antigens cross-activate autoreactive T cells or B cells, leading to autoimmunity and tissue damage in genetically susceptible individuals [1][79]. An epitope is the component of an antigen that is recognized by T cells, B cells, or antibodies [80]. Epitope spreading occurs when autoreactivity towards the epitope type that causes the initial mimicry expands from the dominant epitope to the subdominant or "cryptic" epitopes, resulting in an immune response against several epitopes [1][81].

For example, Epstein-Barr virus infection may increase one's risk of developing MS [69][82]. Epstein-Barr virus (EBV) is human herpesvirus that infects 90% of adults worldwide and is the main cause of infectious mononucleosis [82][83]. Following infection, latent EBV remains in the body life-long [84]. An epidemiological study that followed more than 10 million US army personnel biennially between 1993 and 2013, 955 of whom were diagnosed with MS, showed that participants who converted to EBV seropositivity had a 32-fold increased risk of developing MS compared to participants that remained seronegative for EBV [69][82]. At the cellular level, EBV-infected B cell and plasma cell infiltrates have been detected in the white matter lesions of MS patients [85][86]. MS patients also display elevated EBV nuclear antigen 1 (EBNA-1)-specific $CD4^+$ T cells that cross-react with myelin basic protein peptide [79][87][88]. Antibodies that bind to EBNA-1 epitopes and cross react with CNS proteins such as GlialCAM have also been identified [89]. At the molecular level, it has been shown that there is structural homology between EBV nuclear antigen 1 epitopes

and several CNS proteins including myelin basic protein epitopes [69][90]. This molecular mimicry may lead to the activation of autoreactive T cells following EBV infection [79].

1.3.4 Commensal Microbiome

Autoimmune disease risk may also be impacted by the composition of the host's microbiome [1]. The commensal microbiome consists of living microorganisms, their genes, and metabolites that colonize body sites such as the gut, stomach, oral cavity, skin, urogenital tract, and respiratory tract [91][92]. Recently, the gut microbiota has been shown to play an important role in human health [91]. Healthy gut microbiota is characterized by diversity, a large number of different microbial species [93][94]; stability, the ability to maintain diversity under external perturbations [94][95]; and resilience, the ability to return to its pre-perturbation state [94][96]. The gut microbiota in the small and large intestine consist of more than 100 trillion microorganisms [97][98], including bacteria such as *Firmicutes*, *Bacteroidetes*, *Actinobacteria*, *Proteobacteria*, *Fusobacteria*, and *Verrucomicrobia*; fungi; viruses; archaea; and protozoans [91]. These microorganisms act in symbiosis with the host and play important roles in the extraction of energy and nutrients from food; the production of bioactive molecules such as vitamins, amino acids and lipids; the modulation of the host immune response; the protection against opportunistic pathogens; and in the prevention or repair of tissue damage to mucosal barriers [91][94][99].

Cross-talk between the microbiota and both the innate and adaptive immune system is important for maintaining homeostasis. This cross-talk is mediated by a variety of bacterial proteins and metabolites. Short chain fatty acids (SCFAs), including acetate, n-propionate, and n-butyrate, are metabolites secreted by the commensal bacteria *Bacteroidetes* and *Firmicutes* in the large intestine as the end product of anerobic fermentation of dietary fiber [100]. SCFAs are some of the best characterized microbial metabolites and have numerous immunomodulatory functions. Butyrate has been shown to epigenetically regulate gene ex-

pression by inhibiting classes I and IIa histone deacetylases (HDAC) [101][102]. Treatment of macrophages, the most abundant immune cell in the lamina propria, with n-butyrate reduces their secretion of LPS-induced pro-inflammatory mediators via HDAC inhibition [100]. Commensal microbe-derived butyrate also mediates the differentiation of colonic regulatory T cells via HDAC inhibition and upregulation of *foxp3* gene expression [102]. Notably, butyrate treatment also promotes the induction of FoxP3$^+$ Tregs even under Th1 and Th17 polarizing conditions [102]. Furthermore, administration of butyrate reduces the severity of CD4$^+$CD45RB^{hi} T cell transfer-induced colitis in *Rag1*$^{-/-}$ mice [102][103]. Alternatively, certain commensal microbes have been shown to promote Th17 responses [96][99][104]. For example, segmented filamentous bacteria colonize the small intestine by adhering to intestinal epithelial cells [99][104]. SFB colonization induces the production of serum amyloid A, which promotes lamina propria dendritic cell-mediated differentiation of SFB-specific RORγ t$^+$ Th17 T cells [99]. These cells produce IL-17A and IL-22 in the lamina propria [99][105] and protect the intestine from *Citrobacter rodentium* infection [99]. SFB also induce T cell-dependent secretory immunoglobulin A (IgA) production by plasma cells in the gut [106].

Changes in the composition of the microbiome can impact autoimmune disease incidence and progression [94][107]. Dysbiosis occurs due to the excessive growth of potentially harmful pathobionts normally present at low relative abundances, the reduction or complete loss of commensal microbes due to microbial killing or diminished proliferation, and/or reduction in microbiota diversity [96][108]. Dysbiosis has also been shown to impact the immune response to the microbiota, the integrity of the epithelia present in both intestines and blood-brain barrier [92]. Intestinal barrier dysfunction can cause low-grade movement of microbes to other body sites, resulting in inflammatory immune responses to these systemic microbes. [109].

The impact of the commensal microbiome has been studied in the context of relapsing-remitting multiple sclerosis (RRMS). Comparison of the fecal microbiota composition of

RRMS patients to those of healthy age- and sex-matched controls has shown that RRMS patients have distinct fecal microbiome profiles with an increased abundance of *Psuedomonas*, *Mycoplana*, *Haemophilus*, *Blautia*, and *Dorea genera* and decreased abundance of *Parabacteroides*, *Prevotella*, *Adlercreutzia*, *Collinsella*, and *Erysipelotrichaceae* compared to healthy controls [110]. Additionally, RRMS patients with active disease also displayed reduced species richness in comparison to RRMS patients in remission and healthy controls [110]. Another study comparing the gut microbiota of RRMS patients to that of healthy subjects also identified a significant decrease in the number of *Clostridium* and *Bacteroidetes* species in RRMS patients compared to healthy controls [111]. However, it important to note that fecal microbiota composition is also impacted by additional variables such as diet, age, sex, ethnicity, geographic location, and environmental factors such as smoking [109].

It has also been shown in a murine model of RRMS, the relapsing-remitting mouse model of spontaneously developing experimental autoimmune encephalomyelitis (EAE), that the commensal microbiota, is required trigger the onset of autoimmunity [96][112]. Germ-free mice displayed impaired Th17 $CD4^+$ T cell differentiation in the lamina propria and Peyer's patches, impaired B cell recruitment in the cervical lymph nodes, and reduced susceptibility to disease onset compared to conventionally housed mice, while microbial re-colonization induced the activation of autoreactive $CD4^+$ T cells and disease onset in more than 75% of mice [96][112]. Furthermore, transfer of the fecal microbiota of MS patients into germ-free mice reduced the proportion of IL-10^+FoxP3^+ Tregs in the mesenteric lymph nodes and exacerbated the severity of EAE compared to mice administered microbiota from healthy controls [113].

1.3.5 Sex Differences

Many autoimmune diseases are more prevalent in women than men [114]. For example, greater than 80% of patients diagnosed with Sjorgen's syndrome, lupus, autoimmune thy-

roid disease, and scleroderma of patients are women [114]. Multiple sclerosis occurs at a female to male ratio of 3:1, and its prevalence in women is rising [115]. Women are more likely to develop relapsing-remitting MS, experience first symptoms at a younger age, relapse more frequently, and develop a greater number of inflammatory lesions, while men have a higher risk of developing primary progressive MS and subsequently neurological damage [115]. Sex chromosomes and hormones may contribute these differences in disease susceptibility and progression [116][117]. Females have two X chromosomes, while males have one X chromosome and one Y chromosome. The X chromosome encodes for approximately 2000 genes, while the Y chromosome encodes for only 48 genes [117]. Several genes on the X chromosome, such as *foxp3*, *cd40l*, and *tlr7*, encode for proteins such as pattern recognition receptors, cytokine receptors, and transcription factors that are involved in immune cell function [116][117]. Although in human females, X inactivation, the silencing of one of the two X chromosomes, enables the expression of one set of X chromosome genes, about 15% of X chromosome genes escape X inactivation, which leads to higher X chromosome gene expression [116]. Sex hormones such as estrogens, progesterone, androgen, and prolactin may also influence disease onset and outcomes [115]. For example, elevated estrogen and progesterone levels reportedly contribute to the decrease in relapse rate observed during the third trimester of pregnancy in MS patients [115][118].

1.3.6 Additional Environmental Factors

Various environmental factors including nutrition and exposure to xenobiotics such as cigarette smoke, heavy metals, and certain pharmaceuticals also influence one's susceptibility to autoimmune disease [1]. For example, vitamin D is a fat-soluble hormone involved in calcium and phosphate metabolism [119]. In addition to its well established roles in regulating metabolism and bone health, vitamin D also impacts brain development and function, cell proliferation and apoptosis, blood pressure and insulin secretion, and immunomodulation

[120]. Additionally, vitamin D reportedly inhibits B cell proliferation and differentiation, promotes Th1 and Th17 $CD4^+$ T cell skewing towards the Th2 phenotype, and expands Tregs [121]. Humans obtain vitamin D from skin exposure to ultraviolet B radiation, and a diet rich in fatty fish (salmon and tuna) and vitamin D fortified foods (orange juice, dairy products, cereals) [120]. Vitamin D deficiency is a risk factor for several autoimmune diseases including MS [1]. The frequency of MS cases increases the farther one is from the equator, which is inversely correlated with duration and intensity of UVB sunlight exposure and, in turn, the amount of sunlight-derived vitamin D [120]. Furthermore, a 20-year study following 92,253 women revealed that taking dietary vitamin D supplements decreased one's risk of developing MS. Women who took 400 IU vitamin D or more per day had 41% reduced MS incidence than women who did not take vitamin D supplements [122].

1.4 Overview of Multiple Sclerosis Pathology, Treatment Options, and Preclinical Models

Multiple sclerosis (MS) is a chronic, inflammatory demyelinating disease of the central nervous system (CNS) that impacts more than 2.5 million people worldwide [123]. With the average age of onset being approximately 29 years of age [124], MS is the most common cause of non-traumatic neurological disability in young adults [125]. MS impacts women at disproportionally higher rates, as the female to male ratio of diagnosed patients is 3:1 [115]. MS is also one of the most expensive chronic diseases to manage, with annual costs exceeding $50,000 US dollars per patient [124]. MS is triggered by the environmental factors described above in genetically susceptible individuals. As the disease progresses, patients develop potentially disabling clinical manifestations including fatigue, pain, muscle weakness, sensory and vision loss, bladder and bowel dysfunction, and motor impairments [124].

1.4.1 Multiple Sclerosis Disease Courses

Although the symptoms are heterogeneous, multiple sclerosis can be categorized into four disease courses: clinically isolated syndrome, relapsing-remitting MS, secondary progressive MS, and primary progressive MS [126]. Clinically isolated syndrome is defined as the first episode of neurologic symptoms, in the form of vision problems, vertigo, loss of sensation in the face, or arm or leg weakness that could later develop into MS if subsequent episodes occur [126]. Approximately 85%, of patients are initially diagnosed with relapsing-remitting MS (RRMS) [7]. RRMS is characterized by an initial episode of neurological dysfunction, followed by remission, defined as a period of partial or complete clinical recovery during which disease does not worsen [126][7]. Subsequently, the patient experiences more relapses, defined as a discrete period of disease exacerbation during which new or increasing neurologic symptoms occur [126]. During relapses, inflammatory lesions develop in the CNS and are detected via MRI [7]. Patients with RRMS undergo recurring periods of relapse and remission, and disability accumulates, causing approximately 50% of untreated patients to eventually develop secondary progressive MS (SPMS) about 10 to 15 years after their RRMS diagnosis [7]. During SPMS, neurologic dysfunction steadily becomes more severe, resulting in decreased brain volume, increased axon loss, and uninterrupted progression of disability [126]. Approximately 15% of patients are initially diagnosed with primary progressive MS (PPMS) [126]. Unlike RRMS, PPMS patients do not experience relapse followed by remission. Rather, neurologic function progressively deteriorates over time from the initial onset of symptoms [126].

1.4.2 Immunopathology of Multiple Sclerosis

The immunopathology of MS is multifaceted. Although it is well-studied, many questions about disease initiation and progression remain unanswered. For example, whether multiple sclerosis is triggered in the periphery or in the central nervous system remains an open

question [7]. The "outside-in" hypothesis states that MS is initiated by the disruption of self-tolerance to CNS autoantigens due to the activation and differentiation of autoreactive T cells in the secondary lymphoid organs [123]. Although the dominant autoantigen has not been identified in multiple sclerosis, T cells autoreactive to CNS antigens of myelin basic protein (MBP) [127][128], myelin oligodendrocyte glycoprotein (MOG) [129], and proteolipid protein (PLP) [130] have been detected in both MS patients and healthy individuals [7]. These autoreactive cells, in turn, migrate from the peripheral tissues to the CNS, either by crossing the disrupted blood-brain barrier or the blood-cerebrospinal fluid barrier at the choroid plexus [7]. In the CNS, these cells become reactivated upon encountering their cognate antigen presented by APCs such as dendritic cells, macrophages, and microglia [7]. The influx of pathogenic, activated effector Th1 and Th17 $CD4^+$ T cells and $CD8^+$ T cells that cross the blood-brain barrier and enter the CNS also increases the production of pro-inflammatory cytokines and chemokines, which recruit and activate peripheral B cells as well as innate immune cells such as monocytes and macrophages into the inflammatory lesions [7]. Reactivated Th1 $CD4^+$ T cells produce the cytokines IFN-γ and TNF-α; Th17 $CD4^+$ T cells produce IL-17A, IL-21, IL-22 and IFN-γ; and $CD8^+$ effector T cells produce IL-17A, IFN-γ, and cytolytic granules [123]. The cytokine IFN-γ upregulates the expression of the HLA class I and class II molecules and subsequently enhances the ability of APCs to present antigen [123][131], while IL-17A diminishes the integrity of the blood brain barrier by inducing endothelial cell production of reactive oxygen species [70][123][132]. This inflammation cascade leads to the demyelination of the myelin sheath and oligodendrocyte cell body, the proliferation and activation of CNS-resident glial cells such as microglia and astrocytes, and tissue damage in the form of neuroaxonal degeneration [133]. The alternative "inside-out" hypothesis states that an event within the CNS, for example a viral infection of the brain, initially triggers the onset of MS, which subsequently results in the infiltration of autoreactive immune cells from the periphery [7][134].

Multiple sclerosis pathology is characterized by the formation of lesions or plaques in the brain and spinal cord consisting of infiltrating T cells, B cells, and monocytes [7][70]. These are sites of active demyelination in the white and grey matter [7]. Although inflammation occurs during all stages of MS, peripheral immune cell-mediated inflammation is more prevalent in the acute stages [7], while neurodegeneration is more prevalent in progressive stages [125]. T cell and B cell infiltrates are more pronounced in the white matter lesions of RRMS patients, while higher levels of plasma cells have been identified in the CNS of SPMS and PPMS patients even after T cell and B cell levels decline [135]. Additionally, progressive MS patients display an increase in grey matter lesions [70].

One key difference between human MS and experimental autoimmune encephalomyelitis (EAE), a murine model of neuroinflammation that recapitulates certain features of MS, is that $CD8^+$ T cells make up the majority of T cells present in CNS lesions of MS patients with established disease, outnumbering $CD4^+$ T cells by approximately 10 to 1 [123][136]. Upon encountering their cognate antigen presented by CNS APCs on MHC class I molecules, autoreactive $CD8^+$ T cells can induce cell killing by releasing the cytotoxic enzymes granzyme A and B [123]. Elevated levels of IFN-γ-producing $CD8^+$ cytotoxic T cells autoreactive towards MBP-derived peptides have been detected in MS patients, suggesting that these cells may contribute to oligodendrocyte injury [137]. In RRMS patients undergoing relapse, the levels of granzyme A and B in the cerebrospinal fluid are also elevated compared to the levels in remission patients and healthy controls, suggesting that $CD8^+$ T cells may be involved in RRMS pathogy during active disease [138]. Furthermore, immunohistochemistry analysis of CNS tissues of MS patients shows that cytotoxic $CD8^+$ T cell granules are located in close proximity to axons, suggesting that these cells may also contribute to axonal damage [123][139].

B cells also contribute to MS disease pathology. IgG oligoclonal bands – produced by clonally expanded, terminally differentiated B cells – are one of the hallmarks of disease,

detected in the cerebrospinal fluid of more than 95% of MS patients [123][140]. Furthermore, memory B-cells isolated from MS patients reportedly produce more GM-CSF and less IL-10 than those obtained from healthy individuals [123][141] and display elevated expression of the costimulatory molecules CD80 and CD86 [123][142]. During the early stages of disease, B cells migrate to the CNS and present autoantigens to T cells via the MHC class II molecule, resulting in their activation [123]. Transgenic mice engineered to express a MOG-specific B cell receptor while having B cells selectively deficient in MHC class II failed to develop MOG-induced EAE and exhibited reduced Th1 and Th17 responses, demonstrating that B cells may act as antigen presenting cells in murine models of neuroinflammation [143]. B cells also secrete pro-inflammatory cytokines and chemokines such as TNF-α, IL-6, and GM-CSF which activate resident CNS cells such as microglia and astrocytes [123].

SPMS patients with advanced disease reportedly contain tertiary lymphoid structures in the meningeal lymphatics [144][145]. These structures, which consist of aggregated plasma cells, B cells, T cells, and follicular dendritic cells, act as ectopic germinal centers and may contribute to late-stage, chronic CNS inflammation by promoting local B cell and T cell activation and maturation, which subsequently mediate glia cell damage and astrocyte dysfunction [144][145]. It has also been reported that β-synuclein-reactive $CD4^+$ T cells are enriched in the blood of SPMS patients and contribute to gliosis and neuronal destruction in the grey matter [70][146]. During chronic inflammation, CNS-resident immune cells such as microglia and astrocytes, in combination with B cells from ectopic germinal centers, also become activated and secrete soluble signals such as cytokines (e.g. GM-CSF), chemokines (e.g. CCL2), reactive oxygen species (ROS), and reactive nitrogen species (RNS) that prevent remyelination by inhibiting the generation of mature oligodendrocytes and further exacerbate neurodegeneration [7]. Furthermore, the release of ROS and RNS causes mitochondrial DNA mutations and injury in neurons [70][123]. During active demyelination, Fe^{3+} is also released from degenerating oligodendrocytes, causing oxidative stress. Under inflammatory

conditions, the x_c^- cysteine/glutamate antiporter is also upregulated in activated B cells, microglia, and astrocytes, resulting in the release of glutamate [147]. Excess glutamate production causes an influx of Ca^{2+} into neurons, leading to ionic imbalance, and subsequently cell death [123][147]. As the disease advances, sustained axonal and neuronal damage accumulate in both the white and grey matter, resulting in brain atrophy and worsening disability [148].

1.5 Experimental Autoimmune Encephalomyelitis Models

As MS is a complex disease, triggered by a combination of genetic and environmental factors, and progressing over decades with heterogeneous clinical, pathological, and immunological manifestations, no single experimental model recapitulates all of the features of disease [148][149]. In this dissertation, the experimental autoimmune encephalomyelitis (EAE) model has been used to investigate the ability of engineered molecules, described in subsequent chapters, to prevent the onset of neuroinflammation and suppress already-established disease in mice. These insights could be applied towards the development of therapeutics for the treatment of MS.

1.5.1 Active MOG_{35-55} Induced EAE

Active EAE can be induced in female C57BL/6 mice by peripherally immunizing the mice with MOG_{35-55} peptide emulsified in heat-inactivated *Mycobacterium tuberculosis*, also known as Complete Freud's Adjuvant (CFA), followed by pertussis toxin [148][150][151]. Myelin oligodendrocyte glycoprotein (MOG) is an immunoglobulin family protein expressed by CNS cells, particularly on the surface of myelin sheath, that protects axons and neurons [70][150][151]. MOG_{35-55} peptide is an encephalitogenic region of the MOG protein [150][151]. When presented by APCs on MHC class II, the antigen induces the activation, proliferation, and differentiation of autoreactive MOG-specific Th1 and Th17 $CD4^+$ T cells

in the secondary lymphoid organs, which subsequently migrate to the CNS and trigger the onset of inflammatory encephalopathy [7]. Immunization with antigens derived from alternative regions of the MOG protein, for example, MOG_{1-125}, induce B-cell mediated disease [152]. Administration of pertussis toxin after immunization with antigen disrupts the blood-brain barrier, enabling the entry of peripheral immune cells into the CNS [151]. If left untreated, EAE-bearing mice will develop clinical symptoms of disease approximately 10 to 18 days following the initial immunization [150][151]. Disease severity is assessed via a semi-quantitative, 5-point scale that progresses from no paralysis to tail paralysis to both hind limb and forelimb paralysis [150][151]. Peak disease score is defined as maximum disease score the EAE-bearing mouse attains during the entire experiment [150]. Recovery occurs when the peak disease score drops by at least 1 grade for at least 2 consecutive days [150]. In the majority of MOG_{35-55}-EAE bearing mice, inflammation persists due to the sustained priming of antigen-specific $CD4^+$ T cells, resulting in chronic disease until endpoint [150][151]. Prophylactic treatment is defined a treatment started before to the first clinical signs of disease appear [150]. The purpose of this treatment regimen is to assess whether the therapy can prevent or delay the onset of disease. Therapeutic treatment is defined as a treatment begun upon or after the onset of EAE symptoms [150]. The purpose of this treatment regimen is to assess whether a therapy can reverse already-established disease.

1.5.2 Active $PLP_{139-151}$ Induced EAE

Relapsing-remitting EAE can be induced in female SJL mice by immunizing the mice with $PLP_{139-151}$ peptide emulsified in CFA followed by pertussis toxin [151][153]. Proteolipid protein (PLP) is another component of CNS myelin [151][153]. $PLP_{139-151}$ peptide is an encephalitogenic region of the PLP protein [151][153]. When presented by APCs on MHC class II, this antigen also activates autoreactive PLP-specific $CD4^+$ T cells in the secondary lymphoid organs, which subsequently migrate to the CNS and trigger the onset of EAE [153].

Unlike MOG-EAE, immunization of SJL mice with $PLP_{139-151}$ results in a relapsing-remitting form of the demyelinating disease [151][153]. The first wave of disease occurs synchronously in nearly all mice approximately days 9 to 14 days following immunization [150]. Nearly all mice recover from the first wave of disease and subsequently enter remission, defined as a temporary reduction in CNS inflammation and disease symptoms [150][153]. A remission occurs when the disease score decreases by at least 1 grade, compared to the peak disease score, for at least 2 consecutive days [150][153]. Following remission, approximately 50 to 80% of the mice relapse non-synchronously within the first 5 to 7 weeks after disease induction [150][153]. A relapse occurs when the disease score increases by at least 1 grade, from the minimum score during remission, for at least 2 consecutive days [150]. Relapses are reportedly caused by epitope spreading, a process by which autoreactive T cells recognize secondary epitopes, peptides that are distinct from and non-cross reactive with the disease-inducing epitope [154][155]. These secondary epitopes can emerge due to the myelin destruction that occurs during the first wave of disease [7][155]. In SJL mice immunized with the dominant, non-cross reactive epitope, $PLP_{139-151}$, $CD4^+$ T cells autoreactive to the secondary encephalitogenic PLP epitope, $PLP_{178-191}$, have been identified during the first wave of disease [155]. When these $PLP_{178-191}$-specific $CD4^+$ T cells were adoptively transferred into naive mice, they induced the onset EAE in these mice [151][155]. Epitope spreading to $PLP_{139-151}$ has also been demonstrated in relapsing-remitting EAE mice originally immunized with $PLP_{178-191}$ [154].

1.5.3 Limitations of EAE Models

Although the EAE model has led to valuable insights about inflammation-mediated neurodegeneration and remains an essential preclinical research tool, the differences between EAE and human MS must be considered when using results from EAE models to make hypotheses about human disease [7]. MS arises spontaneously due to a combination of genetic and envi-

ronmental factors, while MOG and PLP-EAE are induced by active immunization with CNS antigens [148]. Two adjuvants are required for these models, CFA to sensitize mice to myelin antigens and stimulate the immune system, and pertussis toxin to permeabilize the blood-brain barrier [156][148][149]. The administration of adjuvants does not mimic physiological conditions. Although the use of adjuvants is not uncommon in murine models of immune disease [156], it should be noted as a limitation and difference from clinical pathology. EAE is also induced in inbred, genetically homogeneous mouse populations, which does not take into account the genetic heterogeneity of MS patients [148]. Furthermore, there are many genetic and phenotypic differences between the murine and human immune systems [7][157]. The type of immune cell infiltrates and the location of CNS inflammation also differ in these conditions. In MS, the dominant autoantigen has not been identified, while in EAE, mice are immunized with a single autoantigen, such as MOG_{35-55} or $PLP_{139-151}$, which leads to the activation of antigen-specific, autoreactive MHC class II-restricted $CD4^+$ T cells [7][149]. In contrast, $CD8^+$ T cells make up the majority of T cells present in CNS lesions of human MS patients [123][136]. The contribution of $CD8^+$ T cells and B cells to disease progression in already-established MS is not fully recapitulated in the MOG_{35-55} or $PLP_{139-151}$ EAE models [149]. In addition, human MS is characterized by inflammation and tissue damage in both the brain (particularly the forebrain, brain stem, and cerebellum) and spinal cord, while in EAE, the majority of inflammation and tissue damage is localized in the thoracic and lumbar spinal cord [7][149][150]. Furthermore, although some forms of EAE, for example MOG_{35-55}-CFA immunization in C57BL/6 mice, induce chronic disease can last for months, disease symptoms do not progressively worsen as during primary progressive or secondary progressive MS [149]. Despite its limitations, a number of FDA-approved MS drugs, including IFN-β, have undergone preclinical testing in EAE models [156].

1.6 Current Standard of Care in Multiple Sclerosis

Although there is currently no cure for MS, over the past 30 years, there have been many advances in the treatment of MS, particularly the relapsing-remitting form of the disease [158]. Available MS treatments include corticosteroids, disease modifying therapies, and monoclonal antibodies [158]. These therapies are effective in managing acute MS attacks and also reduce the frequency and severity of relapses [124].

1.6.1 Corticosteroids

Corticosteroids such as dexamethasone, betamethasone, methylprednisolone, and prednisone are synthetic compounds that mimic the functions of the immunosuppressive human hormone, cortisol [159][160]. Corticosteroids can be administered in short-term during an acute MS attack [161]. Corticosteroids dampen CNS inflammation via broad immunosuppression. Administration of corticosteroids has been shown to reduce blood-brain barrier disruption, suppress autoreactive T cell migration into the CNS, downregulate the expression of adhesion molecules on endothelial cells and monocytes, reduce proinflammatory (IFN-γ and TNF-α) cytokine and matrix metalloproteinase secretion, increase production of the immunoregulatory cytokines IL-10 and TGF-β, reduce the secretion of immunoglobulins, and inhibit MHC class II expression on macrophages and microglia [162].

Although corticosteroids are useful in reducing the severity of symptoms during relapse, short-term administration of corticosteroids alone does not impact long-term disease progression [158][162]. Side effects of short-term corticosteroid treatment can include stomach pain, insomnia, mood swings, appetite changes, headache, chest pain, heart palpitations, rash, and swelling of feet or hands [159]. However, long-term administration of high-dose corticosteroids is no longer recommended because it can lead to severe side effects including osteoporosis, increased incidence of bone fractures, avascular necrosis and infection, diabetes, skin atrophy, obesity, glaucoma, cataracts, fatty liver, and hypertension [159][161].

1.6.2 Disease Modifying Therapies

Disease modifying therapies are defined as treatments that alter the course of MS disease progression by suppressing or regulating immune cell function [125]. Disease modifying therapies are effective in treating relapsing-remitting MS and reduce the severity and frequency of MS relapses [125]. Interferon beta (IFN-β) was the first FDA-approved disease modifying agent for the treatment of RRMS [158]. IFN-β is an immunoregulatory, interferon type 1 cytokine [158][163]. Although its mechanism of action has not been fully elucidated, IFN-β treatment reportedly increases the production of immunoregulatory cytokines IL-4, IL-5, IL-10, IL-13, and TGF-β while reducing production of the disease-causing cytokines IL-17A, IFN-γ, and TNF-α [125][163]. IFN-β also suppresses T cell activation and migration to the CNS, as well as B cell antigen presentation [125][163]. Transcriptome analysis of MS patient mononuclear cells has revealed that long-term IFN-β treatment reverses the overexpression of proinflammatory and matrix metalloproteinase genes while upregulating the expression of genes involved in immunoregulation and neuroprotection [164]. Clinical trials in RRMS patients have shown that both IFN-β-1a [165][166] and IFN-β-1b [167] reduce the relapse rate, relapse severity, and inflammatory lesion burden detected via MRI compared to the placebo group [158][163]. Common adverse events associated with IFN-β treatment include influenza-like symptoms (fever, chills), headache, injection site reactions, and fatigue [163][168]. Less common adverse events occurring in patients administered IFN-β include mood changes, liver abnormalities, and kidney abnormalities [163][168]. Despite its efficacy in many patients, approximately one third of RRMS patients are unresponsive to IFN-β therapy [169], potentially due to the development of anti-drug antibodies [163].

Fingolimod is an orally administered sphingosine-1-receptor modulator that acts on lymphocytes [170][171][172]. Fingolimod administration prevents lymphocyte egress from the lymph nodes, spleen and thymus, which subsequently reduces disease-causing, autoreactive T cell infiltration into the CNS [170][171][172][173]. Fingolimod treatment increases the

percentage of $CD8^+CD28^-$ Treg cells in MS patients, thus reversing the low $CD8^+$ Treg to $CD8^+$ killer T cell ratio that may contribute to immune dysfunction in untreated MS patients [174]. In clinical trials, fingolimod treatment significantly reduces the relapse rate, number of inflammatory lesions measured by MRI, brain-volume loss, and risk of disability progression compared to the placebo control over a 24-month period in patients with RRMS [170][171][172]. Occasional adverse events associated with fingolimod treatment include headache, back pain, diarrhea, cough, elevated liver-enzyme levels, increased susceptibility to infections (herpes virus, fungal infections, flu), bradycardia, fatigue, reduced white blood cell levels, rash, hypertension, basal-cell carcinoma [125][170][171][172]. Less common adverse events occurring in patients administered fingolimod include pneumonia, macular edema, and reduction in blood neutrophil levels [125][170][171][172].

Additional disease modifying therapies used in the management of RRMS include dimethyl fumarate, teriflunomide, glatiramer acetate, and cladribine [125]. Dimethyl fumarate is a methyl ester of fumaric acid that exerts anti-inflammatory and cytoprotective effects via activation of nuclear factor erythroid 2-related factor 2 [158][175][176]. Teriflunomide inhibits dihydroorotate-dehydrogenase, a mitochondrial enzyme that catalyzes pyrimidine synthesis in proliferating cells [177]. Hence, teriflunomide administration dampens inflammation by reducing the proliferation of T and B cells [177]. Glatiramer acetate is a synthetic polypeptide mimic of myelin basic protein (MBP) that competes with MBP peptides for binding to major histocompatibility complex molecules and subsequently reduces autoreactive T cell activation in MS [158][178]. Cladribine is a purine analogue chemotherapy drug that preferentially depletes peripheral T and B cells by preventing their replication [179][180].

1.6.3 Monoclonal Antibodies

Natalizumab is a humanized monoclonal antibody that binds to and inhibits the $\alpha 4$ subunit of $\alpha_4\beta_1$ and $\alpha_4\beta_7$ integrins [181][182]. $\alpha_4\beta_1$ integrin is a transmembrane adhesion molecule

expressed by lymphocytes [158]. The binding of $\alpha_4\beta_1$ integrin to vascular endothelial adhesion molecule-1 (VCAM-1), expressed by endothelial cells in the blood vessels of the brain and spinal cord, enables autoreactive lymphocytes to cross the blood-brain barrier and enter the CNS [158][182]. Antagonism of this interaction by natalizumab reduces the transendothelial migration of lymphocytes across the CNS [158][182]. In clinical trials, natalizumab treatment significantly reduces the relapse rate, the number of new or enlarged inflammatory lesions detected by MRI, and risk of disability progression compared to the placebo control over a 24-month period in patients with RRMS [182] [183]. Occasional adverse events associated with natalizumab treatment include fever, chills, joint pain, nausea and vomiting, urinary tract infections, nasal inflammation, headache, dizziness, and joint pain [182][183]. Less common adverse events occurring in patients administered natalizumab include severe infusion allergic reactions, liver toxicity, increased susceptibility to infections, and increased risk of progressive multifocal leukoencephalopathy, a brain infection caused by the John Cunningham virus [125][158][182] [183]. In addition, discontinuation or noncompliance of the drug can lead to rebound disease activity [173].

Ocrelizumab is a humanized monoclonal antibody that binds to the CD20 [184]. CD20 is expressed on pre-B cells, naive B cells, and memory B cells; however, it is not expressed on stem cells, pro-B cells, or differentiated plasma cells that are involved in B cell reconstitution and the production protective IgG and IgM antibodies, respectively [173][184]. Ocrelizumab administration depletes pathogenic, CD20-expressing B cells by via completement-dependent cytotoxicity, antibody-dependent cytotoxicity, and apoptosis induction [184]. In MS, B cell depletion reportedly reduces the trafficking of peripheral B cells into the CNS, B-cell antigen presentation to T cells, and B-cell secretion of pathogenic cytokines [185]. Ocrelizumab is currently the only disease modifying therapy approved by the FDA for the treatment of primary progressive MS [173]. In clinical trials, ocrelizumab treatment significantly reduced disability progression and brain lesion volume compared to the placebo in PPMS patients

[186]. Mild side effects associated with ocrelizumab treatment include infusion site reactions (redness, swelling), body pain, diarrhea, and swelling of arms or legs [186]. Serious side effects include increased risk of colitis, herpes infections, respiratory infections, and skin infections [186].

1.6.4 Limitations of Existing Multiple Sclerosis Treatments

Multiple sclerosis disease modifying therapies manage acute attacks and reduce the frequency and severity of relapses by broadly suppressing the immune system [124]. However, in doing so, they can render patients more susceptible to both newly acquired and dormant infections, and are associated with a wide range of adverse events [124]. Furthermore, most available treatments are unable to significantly repair or regenerate damaged neurons, oligodendrocytes, or supporting glia, rendering them less effective in reversing progressive forms of MS characterized by neurodegeneration and axon dysfunction [125]. Hence, there remains an unmet need for new treatments to address these challenges.

CHAPTER 2

SUPPRESSION OF AUTOIMMUNE ARTHRITIS AND NEUROINFLAMMATION VIA AN AMINO ACID-CONJUGATED BUTYRATE PRODRUG WITH ENHANCED ORAL BIOAVAILABILITY

2.1 Abstract

Butyrate, a metabolite produced by commensal bacteria, has been extensively studied for its immunomodulatory effects on various immune cells, including regulatory T cells, macrophages, and dendritic cells. However, butyrate's development as a drug has been limited by its poor oral bioavailability due to its rapid metabolism in the gut, its low potency and thus high dosing, and its foul smell and taste. By esterifying butyrate to serine (SerBut), a design based on the concept of utilizing amino acid transporters to escape the gut and enhance systemic uptake thus increasing bioavailability, we developed an odorless and tasteless compound for oral administration. In the collagen antibody-induced arthritis (CAIA) and experimental autoimmune encephalomyelitis (EAE), murine models of rheumatoid arthritis and multiple sclerosis, we demonstrated that SerBut significantly ameliorated disease severity, modulated key immune cell populations both systemically and in disease-associated tissues, and reduced inflammatory responses without compromising the global immune response to vaccination. Our findings highlight SerBut as a promising next-generation therapeutic agent for autoimmune and inflammatory diseases.

2.2 Introduction

The gut microbiome has been associated with numerous diseases, with one of the key mechanisms involving immune regulation through the production of microbial metabolites [187][188][189][190]. Among these metabolites, short-chain fatty acids (SCFAs), such as butyrate, have gained significant attention due to their anti-inflammatory and immunomodulatory properties [191][192][193]. Derived from the microbial fermentation of dietary fiber in the colon, butyrate serves as a primary energy source for colonocytes and maintains intestinal homeostasis [191][194]. It is essential for protecting intestinal barrier function by facilitating tight junction assembly [195][196]. As an epigenetic modulator, butyrate is a histone deacetylase (HDAC) inhibitor and can thus alter chromatin structures and regulate gene expression [197][198][199]. Through HDAC inhibition, butyrate has been shown to upregulate forkhead box P3 (FoxP3) — a transcription factor involved in the development and function of regulatory T cells (Tregs) — as well as suppress nuclear factor κB (NFκB) activation, inhibit the production of interferon-γ (IFN-γ), and upregulate peroxisome proliferator-activated receptor γ (PPARγ) [102][103][200][201]. In addition to its broad anti-inflammatory activity, butyrate impacts immune cell migration, adhesion, cytokine expression, proliferation, activation, and apoptosis [202]. Apart from HDAC inhibition, butyrate can also exert anti-inflammatory effects on immune cells, such as dendritic cells and Tregs, via signaling through specific G-protein coupled receptors (GCPRs): GPR41, GPR43, and GPR109A [203][204][205][206]. Collectively, these properties of butyrate hold significant potential for the development of therapeutic strategies, particularly in the treatment of immunological disorders, including autoimmune diseases.

Autoimmune diseases, affect nearly 5% of the global population, and have increased in prevalence over the last few decades [207]. These disorders arise when the immune system mistakenly attacks the body's own cells and tissues, resulting in chronic inflammation and tissue damage [6]. The onset of autoimmune diseases may be influenced by a combination

of genetic and environmental factors [1]. Recent studies have underscored the pivotal role of the gut microbiome in modulating immune responses and influencing the development and progression of autoimmune diseases [189]. For instance, dysregulation of the gut microbiome, or dysbiosis, has been implicated in the pathogenesis of rheumatoid arthritis and multiple sclerosis [208][209][210][211]. Current therapeutics for autoimmune diseases, such as immunosuppressive agents, can provide symptom relief but often do not address underlying causes of these complex disorders. There is accumulating evidence that microbial metabolites, such as SCFAs, can impact the immune system and contribute to the development or regulation of autoimmune diseases [212]. Consequently, these findings highlight the potential of using microbial metabolites as therapeutic agents to treat autoimmune diseases by targeting the underlying mechanisms of these diseases and modulating the immune response.

In spite of this promise, oral administration of sodium butyrate has faced challenges due to its foul and persistent odor and taste, even when administered with enteric coatings or encapsulation [213]. Moreover, butyrate is not absorbed in the gut regions where it could exert therapeutic effects and is rapidly metabolized in the gut as an energy source, limiting its pharmacological impact [213]. Alternative routes of butyrate administration, such as intrarectal delivery or continuous intravenous infusion, are often deemed unfeasible for patients with chronic disorders [214][215][216][217]. Therefore, there is a need for innovative delivery methods for butyrate, including prodrugs that can enhance its systemic bioavailability.

To overcome these limitations, we sought to develop a prodrug strategy that enables butyrate to bypass metabolism in the gut, enter the bloodstream, and exert its therapeutic effects systemically after liberation. In this study, we designed an L-serine conjugate of butyrate (*O*-butyryl-*L*-serine, or here SerBut) that exploits the gut transport mechanisms of amino acids. Additionally, the conjugation effectively masked the odor and taste of free butyrate, important for facilitating patient compliance for potential clinical applications. We found that SerBut not only enhanced systemic bioavailability, but also facilitated its

crossing of the blood-brain barrier (BBB), thereby enabling access to the central nervous system (CNS). In a mouse model of collagen antibody-induced arthritis (CAIA), SerBut treatment showed a significant reduction in disease progression that was associated with a systemic increase in Tregs and an increase in the ratio of immunoregulatory M2 macrophages to proinflammatory M1 macrophages. In an experimental autoimmune encephalomyelitis (EAE) model of multiple sclerosis, SerBut significantly suppressed disease onset and severity, decreased immune cell infiltration in the spinal cord, and upregulated inhibitory markers such as PD-1 and CTLA-4 on $CD4^+$ T cells, increased Tregs, and downregulated activation markers on a variety of myeloid cells in the spinal cord-draining lymph nodes. SerBut treatment did not reduce vaccinal immune responses at either the humoral or cellular levels. Thus, in two disease models, SerBut administration modulated immune responses at both the myeloid and lymphoid compartments without unduly blunting protective immune responses.

2.3 Materials and Methods

2.3.1 Study Design

The objective of this study was to chemically conjugate L-serine to butyrate to improve butyrate's oral bioavailability and investigate the therapeutic potential of the conjugate, SerBut, in the context of CAIA and EAE, murine models of RA and MS, respectively.

In the biodistribution study, we quantified the butyrate content in various major organs following oral gavage of SerBut. In the RA model, mice were treated daily with either PBS or SerBut via oral gavage. Paw inflammation was assessed over time, and the pathology of inflamed paws and joints was evaluated using histology. Immune responses were analyzed by flow cytometry after sacrificing the mice at the end of the experiment when consistent RA scores were established. In the EAE model, we compared the efficacy of SerBut, PBS, free butyrate, and free L-serine in suppressing disease progression. Immune responses were

evaluated after sacrificing the mice when they reached a plateau in disease scores. In the vaccination study, we evaluated the global immunosuppressive effects of SerBut in comparison to the effects of FTY 720, an FDA-approved MS therapy. The study endpoint was determined based on previous reports that day 13 after OVA immunization was sufficient to induce anti-OVA IgG antibodies [218].

Sample size was determined using results obtained from previous and preliminary studies [218][219]. At least 5, and in most cases 7-9 independent biological replicates were examined for each group analyzed. See figure legends for details on sample size for each display figure. All experiments were replicated at least twice. Mice were randomly assigned to treatment groups. The individual who assessed clinical scores for RA and EAE experiments was distinct from the individual who administered the treatment and was blinded to the treatment group. The individual who performed fluorescent imaging and histology analysis was also blinded to treatment groups. Statistical methods are described in the "Statistical analysis" section.

2.3.2 Synthesis of SerBut

L-Serine (20 g, 0.19 mol) was added to trifluoroacetic acid (200 mL) and the suspension was stirred for 30 min until fully dissolved. Butyryl chloride (25.7 mL, 0.23 mol) was then added to the solution and the mixture was stirred for 2 hr at room temperature. The reaction was then transferred to an ice bath and diethyl ether (500 mL) was added, which resulted in a precipitation of a white solid. The resultant fine white precipitate was collected by filtration, washed with cold diethyl ether, and dried under vacuum to afford 26.3 g of *O*-butyryl-*L*-serine (0.15 mol, 79%). The final product was confirmed by 1H NMR (500MHz, DMSO-d_6) [ppm]: 0.88 (3H, t), 1.55 (2H, m), 2.32 (2H, t), 4.30 (1H, t), 4.43 (2H, d), 8.66 (2H, s), 14.06 (1H, s).

2.3.3 Mice

C57BL/6 mice, aged 8-12 wk, were purchased from Charles River (strain code: 027, Charles River). BALB/c mice, aged 6-10 wk were purchased from the Jackson Laboratory (strain code: 000651, JAX). C57BL/6 and BALB/c mice were maintained in a specific pathogen-free (SPF) facility at the University of Chicago. Mice were maintained on a 12 hr light/dark cycle at a room temperature of 20-24°C. All protocols used in this study were approved by the Institutional Animal Care and Use Committee of the University of Chicago.

2.3.4 Flow Cytometry and Antibodies

Flow cytometry was performed using a BD LSRFortessa, and data were analyzed using FlowJo 10.8.0. Antibodies against the following surface and intracellular markers were used in the CAIA and EAE mouse models: Arginase 1 (Invitrogen), CD3 (BioLegend), CD3 (BD Biosciences), CD4 (BioLegend), CD5 (BioLegend), CD8 (BioLegend), CD11b (BioLegend), CD11c (BD Biosciences), CD19 (BD Biosciences), CD25 (BioLegend), CD40 (BioLegend), CD45 (BD Biosciences), CD86 (BioLegend), CD206 (BioLegend), CTLA-4 (Invitrogen), F4/80 (BioLegend), FoxP3 (Invitrogen), Ly6C (BioLegend), Ly6G (BioLegend), I-A/I-E (BioLegend), IL-10 (BioLegend), iNOS (Invitrogen), PD-1 (BioLegend), and RORγt (BD Biosciences). The I-A(b) mouse MOG 38-49 GWYRSPFSRVVH (MOG tetramer, PE) was obtained from NIH Tetramer Core Facility. The antibodies used to stain myeloid cells and lymphoid cells are summarized in Table 2.1 and Table 2.2, respectively.

Table 2.1: Antibodies for Staining Myeloid Cells in SerBut *In Vivo* Experiments

Specificity	Fluorochrome	Clone Name	Dilution	Vendor
Arginase 1	PE-Cy7	A1exF5	1:200	Invitrogen
CD11b	BV 711	M1/70	1:200	Biolegend
CD11c	BV 421	HL3	1:200	BD Biosciences
CD40	PerCP-Cy5.5	3/23	1:200	Biolegend
CD86	AF 700	GL-1	1:200	Biolegend
CD206	PE	CO68C2	1:200	Biolegend
F4/80	APC	BM8	1:200	Biolegend
I-A/I-E	APC-Cy7	M5/114.15.2	1:200	Biolegend
iNOS	BUV 737	CXNFT	1:200	Invitrogen
Live/Dead	BV 510	N/A	1:500	Invitrogen
Ly6C	BV 605	HK1.4	1:200	Biolegend
Ly6G	AF 488	1A8	1:200	Biolegend

Table 2.2: Antibodies for Staining Lymphoid Cells in SerBut *In Vivo* Experiments

Specificity	Fluorochrome	Clone Name	Dilution	Vendor
CD3	BV 605	145-2C11	1:200	Biolegend
CD3	BUV 737	17A2	1:200	BD Biosciences
CD4	BV 605	RM4-5	1:200	Biolegend
CD4	BV 711	RM4-5	1:200	Biolegend
CD5	PE	53-7.3	1:200	Biolegend
CD8	AF 700	53-6.7	1:200	Biolegend
CD19	BUV 396	1D3	1:200	BD Biosciences
CD25	APC	QA19A49	1:200	Biolegend
CD45	BUV 395	30-F11	1:200	eBioscience
CD45	V450	30-F11	1:200	BD Biosciences
CLTA-4	PE-Cy7	UC10-4B9	1:200	Invitrogen
FoxP3	AF 488	FJK-16s	1:200	Invitrogen
IL-10	APC-Cy7	JES5-16E3	1:200	Biolegend
Live/Dead	BV 510	N/A	1:500	Invitrogen
MOG	PE	N/A	1:100	NIH Tetramer
PD-1	BV 711	29.1A12	1:200	Biolegend
RORγt	PerCP-Cy5.5	Q31-378	1:200	BD Biosciences

2.3.5 Mouse BMDC Isolation and Activation Study

Murine bone marrow-derived dendritic cells (BMDCs) were collected from 6-wk-old female C57BL/6 mice as described by Lutz et al [220]. BMDCs were seeded at 3 x 10^6 total cells/plate in petri dishes. Cells were cultured at 37°C and 5% CO_2 in the media: RPMI 1640 (Life Technologies), 10% HIFBS (Gibco), GM-CSF (20 ng/mL; recombinant mouse GM-CSF (carrier-free) from BioLegend) , 2 mM l-glutamine (Life Technologies), 1% antibiotic-antimycotic (Life Technologies). Media was replenished on days 3 and 6. Cells were used for experiments on day 9. Isolated BMDCs were plated in round-bottom 96 well plates at 100,000 cells per well in RPMI media and co-cultured with various concentrations of either NaBut or SerBut (from 0.02 to 1.8 mM) for 24 hr. Subsequently, LPS (1 µg/mL) was added for an additional 18 hr. The supernatant of cell culture was collected and analyzed by LEGENDplex assay (Biolegend) to determine the concentrations of cytokines. BMDCs were collected and stained with live/dead stain (Cat No. L34957, Invitrogen) and fluorescent antibodies against CD11c (BD Biosciences), CD80 (BioLegend), CD86 (Invitrogen), and I-A/I-E (BioLegend) were analyzed using flow cytometry (BD LSRFortessa). The antibodies used to stain SerBut-treated BMDCs are summarized in Table 2.3.

Table 2.3: Antibodies for Staining of BMDCs in SerBut *In Vitro* Experiments

Specificity	Fluorochrome	Clone Name	Dilution	Vendor
CD11c	PE-Cy7	HL3	1:200	BD Biosciences
CD80	PE	16-10A1	1:200	Biolegend
CD86	FITC	GL-1	1:200	Invitrogen
I-A/I-E	APC-Cy7	M5/114.15.2	1:200	Biolegend
Live/Dead	BV 510	N/A	1:500	Invitrogen

2.3.6 Biodistribution of SerBut

C57BL/6 mice were orally administered with 50.4 mg NaBut or 80 mg SerBut (both containing equivalent 40 mg butyrate). At 3 hr post-administration, mice were anesthetized under

isoflurane, blood was collected via cheek bleeding, and mice were then transcardially perfused with a minimum of 30 mL PBS containing 1 mM EDTA. Organs, including liver, mesenteric lymph nodes (mLNs), spleen, lung, spinal cord, and brain were collected, immediately frozen on dry ice, and then transferred to -80°C until further processing.

To extract butyrate from plasma or organs, a 1:1 v/v acetonitrile (ACN) to water solution was used. Plasma was mixed 1:1 with the ACN/water solution and centrifuged to remove denatured proteins. Organs were weighed, transferred to Lysing Matrix D tubes (MP Biomedical), and combined with the 1:1 v/v ACN/water solution. Samples were then lysed using a FastPrep-24 5G homogenizer (MP Biomedicals) and centrifuged. The supernatants were collected for butyrate measurement.

Samples were prepared and derivatized as described in the literature [193][221]. A 3-nitrophenylhydrazine (NPH) stock solution was prepared at 0.02 M in water:ACN 1:1 v/v. A 1-ethyl-3-(3-dimethylaminopropyl)carbodiimide (EDC) stock solution (with 1% pyridine added) was prepared at 0.25 M in water:ACN 1:1 v/v. The internal standard, 4-methylvaleric acid, was added. Samples were mixed with NPH and EDC stocks at a 1:1:1 volume ratio. The mixture was heated in a heating block at 60°C for 30 min. Samples were then filtered through 0.22 µm filters and transferred into HPLC vials, which were stored at 4°C before analysis.

An Agilent 6460 Triple Quad MS-MS was used to detect the derivatized butyrate. Both derivatized butyrate-NPH and 4-methylvaleric-NPH were detected in negative mode. Column: Thermo Scientific C18 4.6 × 50 mm, 1.8 µm particle size, at room temperature. Mobile phase A: water with 0.1% v/v formic acid. Mobile phase B: acetonitrile with 0.1% v/v formic acid. Injection volume: 5.0 µL. Flow rate: 0.5 mL/min. Gradient of solvent: 15% mobile phase B at 0.0 min; 100% mobile phase B at 3.5 min; 100% mobile phase B at 6.0 min; 15% mobile phase B at 6.5 min. The MS conditions were optimized using pure butyrate-NPH or 4-methylvaleric-NPH at 1 mM. The fragment voltage was set to 135 V,

and the collision energy was 18 V. Multiple reaction monitoring (MRM) of 222 → 137 was assigned to butyrate, and MRM of 250 → 137 was assigned to 4-methylvaleric acid as the internal standard. The ratio between MRM of butyrate and 4-methylvaleric acid was used to quantify butyrate concentration. The final butyrate content in each organ was normalized by organ weight.

2.3.7 Collagen-Antibody Induced Arthritis (CAIA) Model

BALB/c mice, aged 6 wk, were purchased from the Jackson Laboratory and housed in the animal facility at the University of Chicago for 2 weeks before immunization.

Mice were orally gavaged with PBS or SerBut (25 mg) once daily starting on day -14 at the age of 8 wk. CAIA was induced by passive immunization with an anti-collagen antibody cocktail (1 mg per mice, Arthrogen-CIA 5-Clone Cocktail Kit, Chondrex, Inc.) (on day 0, followed by an intraperitoneal injection of LPS (25 µg) on day 3. Mice were provided with soft (pine) bedding throughout the experiment. Arthritis severity was monitored daily after day 3 using the criteria for clinical scores according to instructions from Chondrex, Inc., as described previously [218].

On day 12, the thickness of mouse fore- and hindpaws was measured to assess the swelling resulting from arthritis. On day 13, mice were sacrificed, and the spleen and hock-draining LNs, including popliteal, axillary, and brachial LNs, were harvested for immunostaining followed by flow cytometry analysis. The paws were collected for histological analysis, as described previously [218]. In brief, paws were fixed in 2% paraformaldehyde (Thermo Scientific), decalcified in Decalcifer II (Leica), and stored in 70% ethanol until paraffin embedding. Paraffin-embedded paws were sliced into 5 µm-thick sections and stained with hematoxylin and eosin, or Masson's trichrome. The images were scanned with a CRi Panoramic SCAN 40x or MIDI 20x Whole Slide Scanner, or Olympus VS200 Slideview Research Slide Scanner, and analyzed using ImageJ and QuPath software.

2.3.8 Experimental Autoimmune Encephalomyelitis (EAE) Model

C57BL/6 female mice (7-8 wk old) were purchased from Charles River Laboratories and housed in the animal facility at the University of Chicago for 2 wk before immunization. Female C57BL/6 mice, aged 10 wk, were subcutaneously immunized in the dorsal flanks with an emulsion of MOG_{35-55} in Complete Freund's Adjuvant (MOG_{35-55}/CFA Emulsion, Hooke Laboratories) on day 0, followed by i.p. administration of pertussis toxin in PBS on both day 0 and day 1. The development of EAE was monitored, and clinical scores were measured daily from day 7 to day 20. The criteria for clinical scores was determined according to the instructions from Hooke Laboratories as described previously [219].

In the experiment to be described in Figure 2.9, mice were administered drinking water containing 100 mM NaBut, L-Serine (L-Ser), or SerBut from day -14 until the end of the study. On day 2 after EAE induction, PBS, NaBut (15 mg, molar equivalent to SerBut), L-Ser (12 mg, molar equivalent to SerBut), or SerBut (24 mg) were administered once daily. In the experiment to be described in Figure 2.15, mice were administered of PBS or SerBut (24 mg) twice daily by oral gavage from day 2 after EAE induction.

On day 21 or 22, mice were sacrificed. The spinal cords were collected and separated into three sections for immunofluorescence imaging, cytokine measurement through homogenization, or immunostaining for flow cytometry analysis. Blood was collected via cardiac puncture, and spleen, mesenteric LNs, spinal cord-draining LNs (sc-dLNs, including cervical LNs and iliac LNs), and spleen were harvested. Isolated single-cell suspension were collected for the immunostaining followed by the flow cytometry analysis. Cytokine from the plasma and spinal cord after homogenization were analyzed via LEGENDplex assay (BioLegend).

2.3.9 Immunofluorescance Imaging of Spinal Cord

Thoracic and lumbar spines of EAE mice were collected. The tissues were fixed in 2% paraformaldehyde (Thermo Scientific) and then stored in 70% ethanol until paraffin embed-

ding. Paraffin-embedded spinal cords were sliced into 5 µm-thick sections as previously described [219]. The sections were deparaffinized through a series of washes in xylene, ethanol, and double-distilled water, immersing them in each solution for 2 min. Antigen retrieval was performed using 1x pH 6.0 citrate buffer at 50-55°C for 45 min. Sections were blocked for 1 hr at room temperature with PBS containing 0.3% Triton-X and 5% normal goat serum. Primary antibodies against CD45 (clone 30-F11, BioLegend) and MBP (clone ab40390, Abcam) were applied at 1:100 dilution in blocking buffer and incubated for 16 hr at 4°C. Sections were washed and then incubated with donkey anti-rat IgG (H+L) AF647 (A48272, Invitrogen) and donkey anti-rabbit IgG (H+L) AF488 (2340683, Jackson ImmunoResearch) secondary antibodies for 16 hr at 4°C. After further washing, sections were mounted using Fluoromount-G Mounting Medium and imaged with an Olympus IX83 spinning-disc confocal fluorescence microscope. Image processing was performed using ImageJ and QuPath software.

2.3.10 Evaluation of Immune Responses to Vaccination and Safety Profile of SerBut

Mice were orally gavaged with PBS, SerBut (twice daily, 24 mg/dose), or FTY 720 (once daily, 0.02 mg/dose) starting on day -3 until the end of the experiment. On day 0, mice were immunized subcutaneously in the front hocks with 10 µg endotoxin-free ovalbumin (OVA), 50 µg alum, and 5 µg MPLA [218]. Mice were bled on day 9 and day 13, and plasma was analyzed for anti-OVA total IgG antibodies using a mouse anti-OVA IgG antibody assay kit (Chondrex). On day 13, mice were sacrificed, the hock-draining LNs and spleen were harvested and cells were isolated for the immunostaining followed by the flow cytometry analysis. One million cells from each spleen were seeded in a 96-well plate and incubated with OVA at 100 µg/mL for a 3-day restimulation. The supernatant of cell culture was collected, and cytokines were measured via LEGENDplex mouse Th cytokine assay (BioLegend). In addi-

tion, plasma samples collected on day 13 were analyzed using a biochemistry analyzer (Alfa Wassermann Diagnostic Technologies) according to the manufacturer's instructions. The panel included albumin, alanine amino-transferase, amylase, aspartate amino-transferase, blood urea nitrogen, calcium, creatine kinase, creatine, total bilirubin, and total protein.

2.3.11 Statistical Analysis

Statistical analysis and plotting of data were performed using Prism 9.0 (Graphpad), as indicated in the figure legends. One-way ANOVA with Dunnett's or Kruskal-Wallis test (if not normally distributed) for multiple comparisons was used in Figures 2.1c-h, Figures 2.9b, d-n, and Figures 2.20b-g. Student's T-test was used in Figures 2.5b-d, h-m and Figures 2.15b, d, f-o. Two-way ANOVA with Tukey's or Bonferroni's post-test was used in Figures 2.20h-m. In Figure 2.5b, Figure 2.9b, and Figure 2.15b, the area under curve (AUC) values of clinical scores were compared using one-way ANOVA with Dunnett's post-test, or Student's T-test. In Figure 2.9c and Figure 2.15c, the probability curve of EAE clinical scores remaining below 1.0 were compared between each two groups using the Log-rank (Mantel-Cox) test. Data represent mean ± s.e.m.; n is stated in the figure legend.

2.4 Results

2.4.1 Conjugation of L-Serine to Butyrate Maintained its Biological Activity While Enhancing Oral Bioavailability.

We conjugated L-serine to butyryl chloride using trifluoroacetic acid at room temperature, resulting in a 79% yield of the final product, *O*-butyryl-*L*-serine (SerBut) (Figure 2.1a, Figure 2.2). The conjugation effectively masked the unpleasant odor associated with free sodium butyrate or butyrate acid.

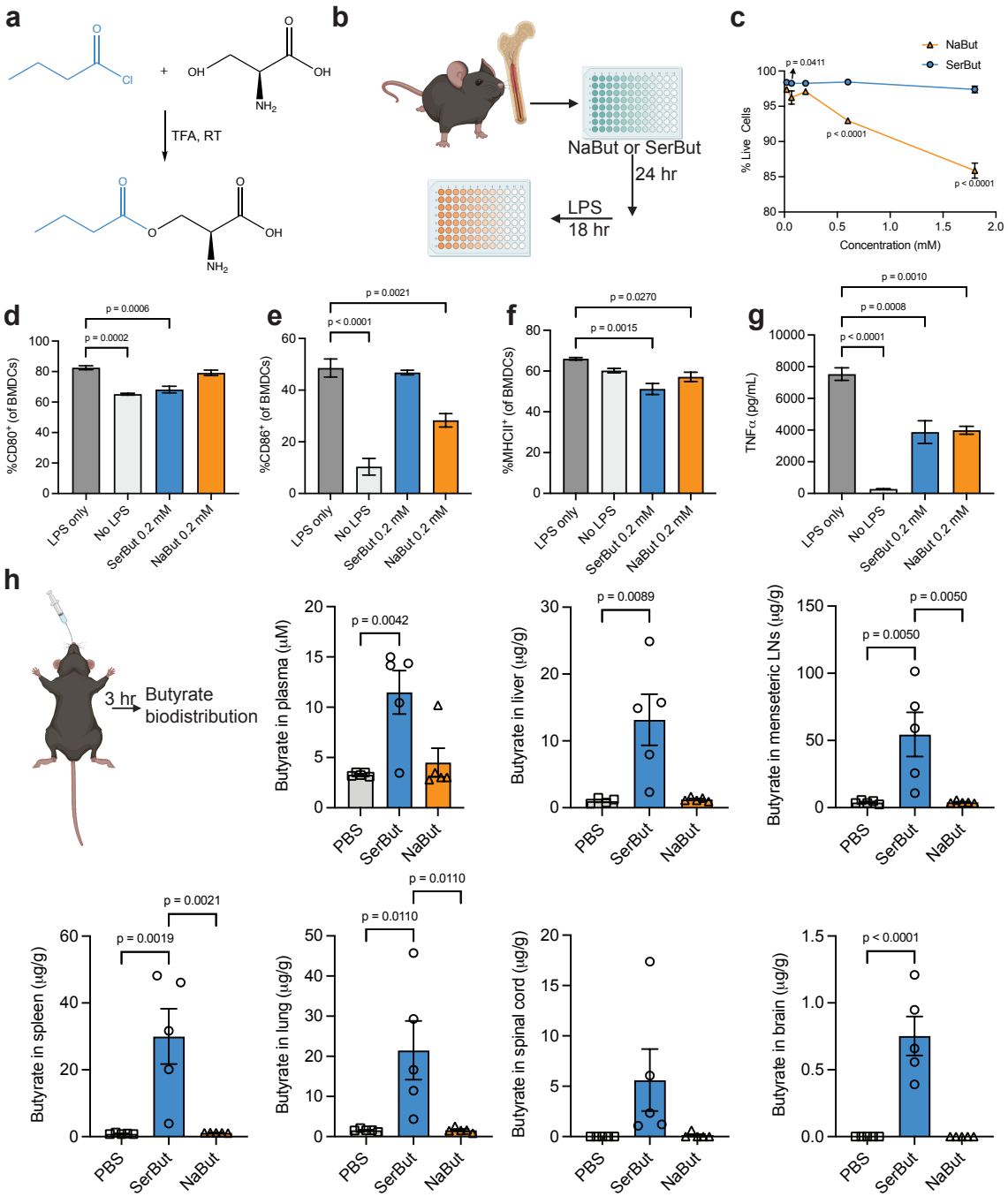

Figure 2.1: **Characterization of SerBut bioactivity and biodistribution.** (a) Chemical synthesis of serine conjugate with butyrate (SerBut). (b) Experimental schema of BMDCs incubated with sodium butyrate (NaBut) or SerBut at a series of concentrations for 24 hr, followed by LPS stimulation for 18 hr. (c) Percentage of live BMDCs after treatment. (d-f) Percentage of d) $CD80^+$, e) $CD86^+$, or f) MHC class II^+ cells analyzed by flow cytometry. (g) TNF-α concentration in the cell culture supernatant of BMDCs. n = 3 and the experiments were repeated twice. (Continued on next page.)

Figure 2.1: Continued: (h) Butyrate biodistribution after SerBut or NaBut oral administration in C57BL/6 mice. The amount of butyrate was detected and quantified in the plasma, liver, mesenteric lymph nodes (mLNs), spleen, lung, spinal cord, and brain. Blood was collected by cheek bleeding at 3 hr post-oral gavage. Mice were sacrificed and perfused at 3 hr post-oral gavage, and organs were collected for butyrate quantification. Butyrate was derivatized with 3-nitrophenylhydrazine and quantified by LC-MS/MS. n = 5 mice per group. Data represent mean ± s.e.m. Statistical analyses were performed using a one-way ANOVA with Dunnett's test. Figure 2.1b, h were created using BioRender.com.

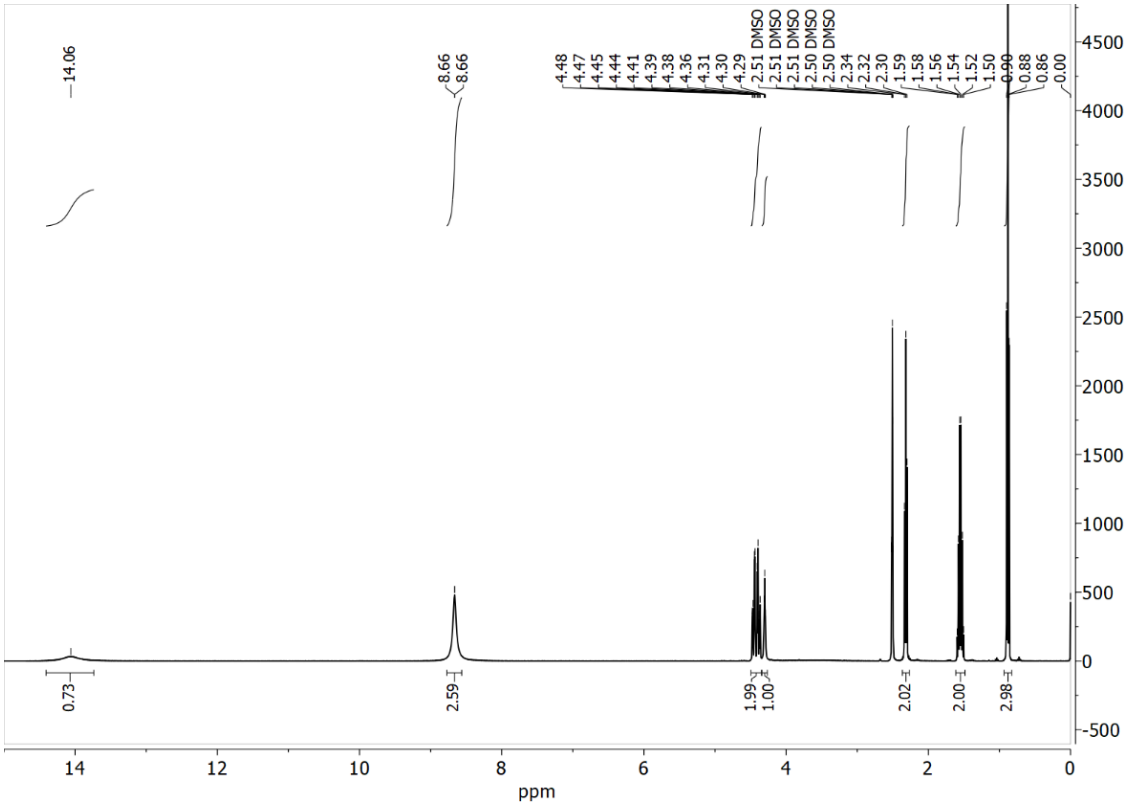

Figure 2.2: **^{1}H NMR spectrum of SerBut** (500MHz, DMSO-d_6) [ppm]: 0.88 (3H, t), 1.55 (2H, m), 2.32 (2H, t), 4.30 (1H, t), 4.43 (2H, d), 8.66 (2H, s), 14.06 (1H, s).

Butyrate is known to regulate myeloid cells, including the inhibition of dendritic cell (DC) maturation in response to proinflammatory stimuli [222]. We employed bone marrow-derived dendritic cells (BMDCs) to compare the biological effects of SerBut to free sodium butyrate (NaBut) (Figure 2.1b). BMDCs were first incubated with butyrate formulations for 24 hr, and then stimulated with lipopolysaccharide (LPS) for 18 hr. We found that NaBut

exhibited cytotoxicity to BMDCs at butyrate concentrations above 0.5 mM, while SerBut was well tolerated up to 1.8 mM (Figure 2.1c). Flow cytometry was used to compare the expression of MHC class II, CD80, and CD86 on BMDC surfaces. At the same concentration of 0.2 mM NaBut, SerBut showed similar suppression levels of MHC class II and CD80 (Figure 2.1d, e). Although SerBut did not suppress CD86 expression as effectively as NaBut at 0.2 mM (Figure 2.1f), we observed dose-dependent suppression of CD86 with SerBut at higher concentrations (Figure 2.3b). Similarly, SerBut suppressed the secretion of TNF-α from BMDCs (Figure 2.1g, Figure 2.3d). As demonstrated by suppression of LPS-stimulated BMDC activation, SerBut retains the biological activity of butyrate.

The primary site for amino acid absorption is the small intestine, where amino acid transporters are present in intestinal epithelial cells [223]. We conducted a biodistribution study to determine whether conjugating L-serine to butyrate enhances oral butyrate absorption and bioavailability. We measured free butyrate levels in plasma and several major organs after oral gavage of SerBut and compared them with NaBut (Figure 2.1h). We found that SerBut significantly increased plasma butyrate levels at 3 hr after oral administration compared to NaBut. In the liver, where orally administered drugs enter directly through the hepatic portal circulation, we observed elevated butyrate levels in mice treated with SerBut but not NaBut. In secondary lymphoid organs, we observed elevated butyrate in the mesenteric lymph nodes (mLNs) and spleen. Butyrate levels were also elevated in lungs at 3 hr post-administration of SerBut.

L-serine is an amino acid known to cross the BBB via the sodium-dependent system A and the sodium-independent alanine, serine, and cysteine transport system [224][225]. Montaser et al showed that utilizing the L-type amino acid transporter 1 enhances the efficient delivery of small prodrug across the BBB38 [226]. Therefore, we investigated whether L-serine conjugation could assist butyrate in entering the CNS, including the spinal cord and brain. Our findings revealed that SerBut significantly increased butyrate levels in both the

spinal cord (a remarkable level of approximately 43% that in the liver, as compared in micrograms of butyrate per gram of tissue) to even brain (to approximately 6%), whereas no exposure was observed after administration with NaBut (Figure 2.1h).

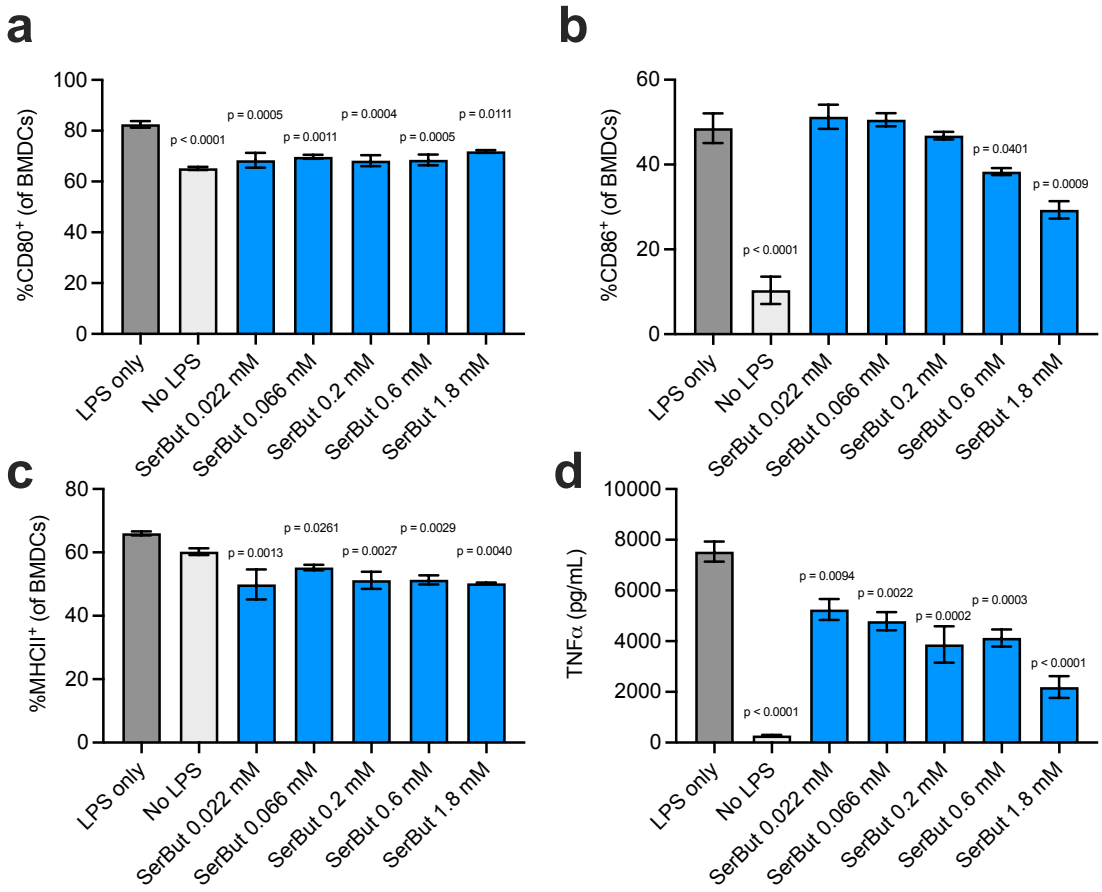

Figure 2.3: **SerBut suppresses BMDC activation.** BMDCs were incubated with SerBut at a series of concentrations for 24 hr, followed by LPS stimulation for 18 hr. (a-c) Percentage of a) $CD80^+$, b) $CD86^+$, or c) MHC class II^+ BMDCs analyzed by flow cytometry. (d) Concentration of TNF-α in the BMDC cell culture supernatant. Data represent mean $\pm$ s.e.m. Statistical analyses were compared between LPS only group with no LPS or SerBut-treated group, performed using a one-way ANOVA with Dunnett's test.

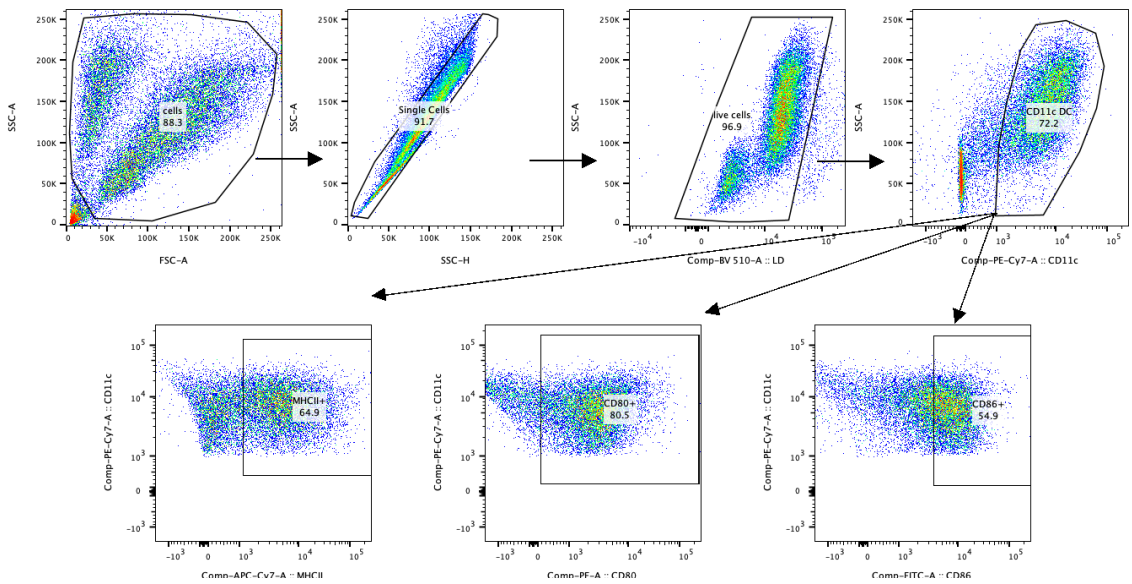

Figure 2.4: ***In Vitro* BMDC activation assay flow cytometry gating strategy.** Flow cytometry gating strategy for the identification of MHC class II$^+$, CD80$^+$, or CD86$^+$ BMDCs. This gating strategy was used in Figure 2.1c-f and Figure 2.3.

2.4.2 SerBut Suppresses Collagen Antibody-Induced Arthritis (CAIA) in Mice.

The composition of gut microbiota has been shown to affect the development of rheumatoid arthritis (RA) [208][209][227]. Previous research has shown that butyrate can improve RA symptoms by targeting key immune cells such as osteoclasts and T cells [228]. Furthermore, studies have demonstrated that butyrate supplementation effectively reduces arthritis severity in animal models by modulation of regulatory B cells [229]. Given SerBut's enhanced accumulation in crucial immune tissues following oral administration, we sought to evaluate its efficacy in the CAIA mouse model (Figure 2.5a). This model is induced by passive immunization with a cocktail of anti-collagen antibodies followed by LPS, which triggers a cascade of innate immune cell infiltration to the joints leading to inflammation and swelling within one week of immunization [218].

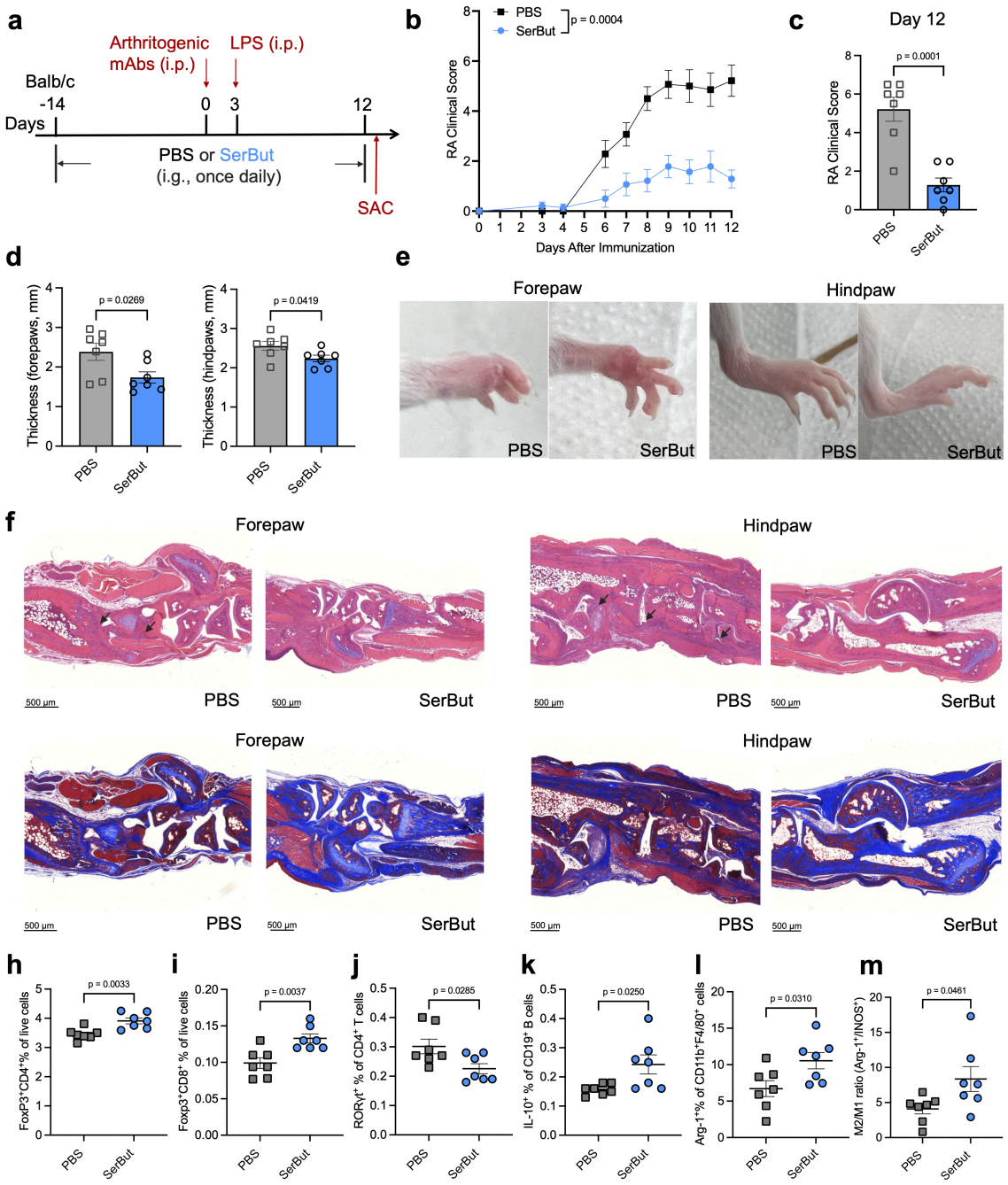

Figure 2.5: **SerBut suppresses collagen antibody-induced arthritis development.** (a) Experimental schema of the collagen antibody-induced arthritis (CAIA) model. Mice were orally gavaged with PBS or SerBut (25 mg) once daily beginning on day -14. CAIA was induced by passive immunization with anti-collagen antibody cocktail on day 0, followed by intraperitoneal injection of lipopolysaccharide (LPS). (b) Arthritis scores in mice measured daily after the immunization. (c) Arthritis scores from PBS or SerBut treated mice on day 12. (Continued on next page.)

Figure 2.5: Continued: (d) The thickness of forepaws or hindpaws measured on day 12 in mice treated with PBS or SerBut. (e) Representative images of paws after treatment. (f) Representative images of mouse joints from paws stained with hematoxylin and eosin on day 12 in each treatment group. Bar = 500 µm. Arrows indicate immune cell infiltration. (g) Representative images of mouse joints from paws stained with Masson's trichrome on day 12. Bar = 500 µm. Blue represents collagen staining. (h-i) Percentage of h) $FoxP3^+$ regulatory $CD4^+$ T cells or i) $FoxP3^+$ regulatory $CD8^+$ T cells of live cells in the spleen measured by flow cytometry. (j-m) Percentage of j) $ROR\gamma t^+$ of $CD4^+$ T cells and k) IL-10^+ of $CD19^+$ B cells, as well as l) Arg-1^+ of $CD11b^+F4/80^+$ macrophages, and m) M2/M1 macrophage ratio in the hock draining LNs. n = 7 mice per group. Data represent mean ± s.e.m. Statistical analyses were performed using Student's T-test.

Mice were pretreated with SerBut or PBS once daily by oral gavage, beginning two wk before the induction of arthritis. We observed that SerBut treatment significantly suppressed the development of arthritis in treated mice. In contrast, PBS-treated mice exhibited severe inflammation in the fore- and hindpaws, demonstrated by their increasing clinical scores over time and the measurements of paw thickness (Figure 2.5b-e). Histological analysis revealed that oral administration of SerBut effectively suppressed inflammatory responses in the paws and reduced joint pathology compared to PBS-treated mice (Figure 2.5f, g). In the CAIA model, anti-collagen antibodies binding to joint cartilage activates complement proteins, leading to the recruitment of immune cells such as macrophages and T cells to the affected joints [230][231]. This immune cell infiltration contributes to joint inflammation, tissue damage, and the clinical manifestations of arthritis. In our study, we observed that SerBut treatment effectively reduced immune cell infiltration into the joints (Figure 2.5f, Figure 2.6). Additionally, anti-collagen antibodies specifically target and degrade collagen in the joints, causing cartilage integrity and joint function loss, ultimately leading to arthritis symptoms [232]. We found that SerBut treatment also prevented collagen loss in the joints (Figure 2.5g, Figure 2.7, suggesting that SerBut may have therapeutic potential in mitigating joint damage and preserving collagen content in the autoimmune arthritis.

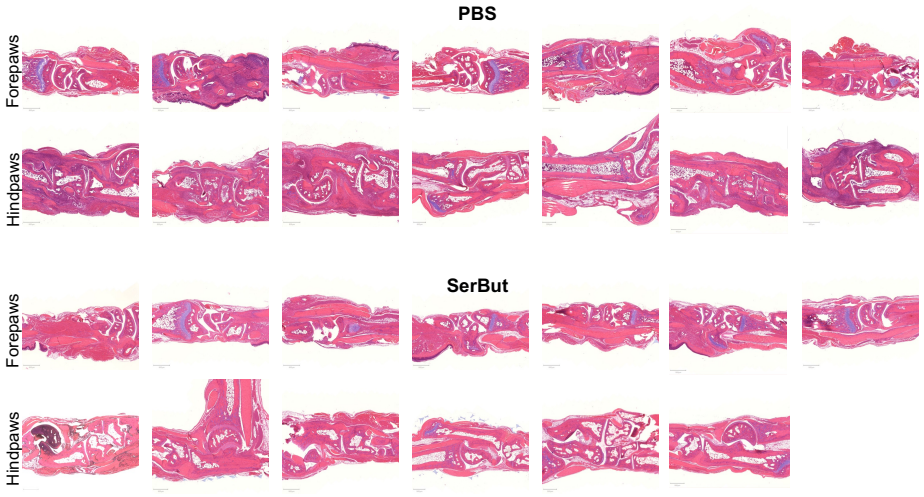

Figure 2.6: **Hematoxylin and eosin stained images of mouse joints.** Histology images of mouse joints from paws stained with hematoxylin and eosin, from the experiment in Figure 2.5. (One hindpaw sample from SerBut treatment group was excluded due to sample damage during processing.)

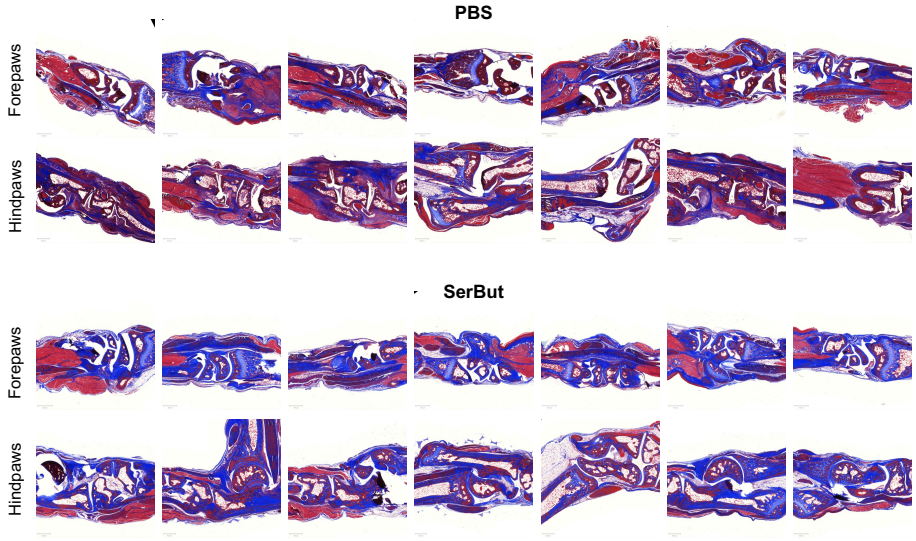

Figure 2.7: **Masson's trichrome stained images of mouse joints.** Histology images of mouse joints from paws stained with Masson's trichrome, from the experiment in Figure 2.5. Blue represents collagen staining.

To better understand the immunomodulatory effects of SerBut in CAIA, we analyzed immune cell populations in the spleen and hock-draining LNs using flow cytometry. Our

results showed that SerBut treatment increased FoxP3 expression in both $CD4^+$ and $CD8^+$ T cells in the spleen (Figure 2.5h, i), indicating that SerBut induced systemic Tregs in the RA disease setting. In the hock-draining LNs (Figure 2.5j), SerBut significantly reduced the proportion of Th17 cells, as evidenced by the decreased percentage of $ROR\gamma t^+$ $CD4^+$ T cells. Additionally, we observed a significant increase in IL-10-producing B cells within the hock-draining LNs (Figure 2.5k), which play a vital role in maintaining immune homeostasis [229][233]. Finally, the hock-draining LNs also demonstrated upregulation in Arg-1 expression on macrophages (Figure 2.5l), leading to an increased $M2(Arg1^+)/M1(iNOS^+)$ macrophage ratio in the hock-draining LNs (Figure 2.5m). The shift towards a higher proportion of immunoregulatory M2 macrophages suggests that SerBut promotes a more balanced immune response, which may be crucial for suppressing inflammation in the paws and reducing joint damage in the context of RA. Overall, these findings highlight the potential therapeutic utility of SerBut in treating RA by modulating the immune system at both the innate and adaptive levels, mitigating disease symptoms.

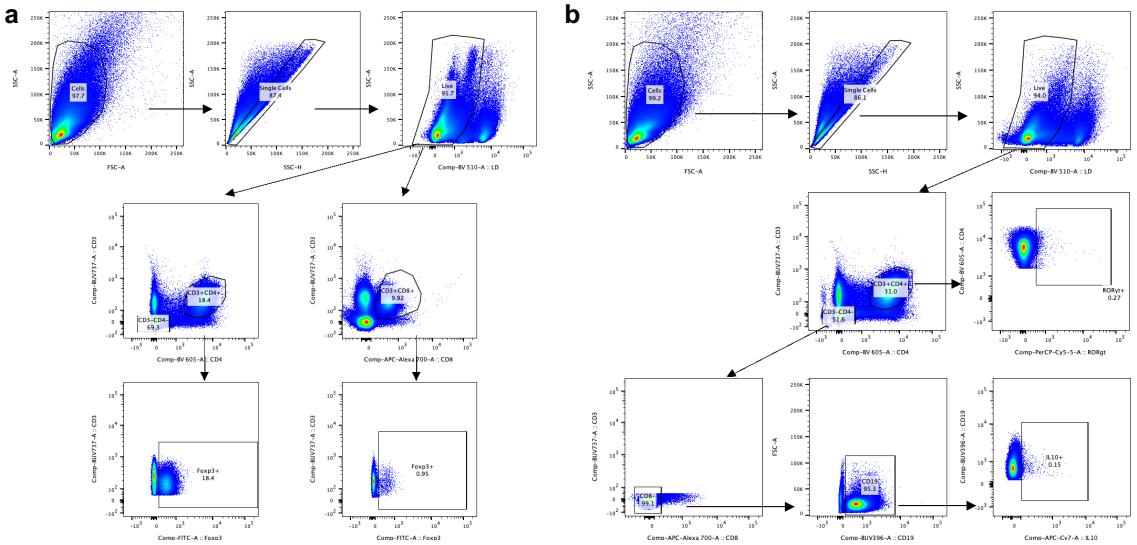

Figure 2.8: **Flow cytometry gating strategy for identification of T and B cells in the spleen and hock draining LNs of CAIA mice.** (a) Flow cytometry gating strategy for the identification of $FoxP3^+$ regulatory $CD4^+$ T cells or $FoxP3^+$ regulatory $CD8^+$ T cells in spleen. (b) Gating strategy for the identification of $ROR\gamma t^+$ of $CD4^+$ T cells, and IL-10^+ of $CD19^+$ B cells in the hock draining LNs, as shown in Figure 2.5h-m.

2.4.3 SerBut Suppresses EAE Development via Modulation of T Cells and Myeloid Cells in the Spinal Cord-Draining Lymph Nodes.

Multiple sclerosis (MS) is an autoimmune disease in which T cells become reactive to myelin autoantigens, resulting in a chronic demyelination of the CNS. Evidence suggests a connection between gut microbiota and MS [113][210][211][234][235][236][237], particularly dysbiosis in the gut microbiota of MS patients, which includes a reduction of SCFA-producing bacteria [111]. Oral administration of SCFAs, such as butyrate, has been shown to alleviate the severity of EAE, a mouse model of MS, by reducing Th1 cells and increasing Tregs [212][238]. Butyrate has also been shown to enhance remyelination in a mouse model of cuprizone-induced demyelination [239]. Our biodistribution study revealed that SerBut significantly increased butyrate levels in the brain and spinal cord, in addition to the lymphatic tissues, suggesting that it may have the potential to treat neuroinflammation.

We assessed the efficacy of SerBut in preventing EAE development. To minimize physiological stress from daily oral gavage, mice were administered drinking water containing 100 mM SerBut for the two wk preceding disease induction and were subsequently administered 24 mg SerBut via oral gavage once daily (Figure 2.9a). SerBut treatment significantly reduced the EAE clinical score in treated mice (Figure 2.9b). The treatment also delayed EAE onset, as is demonstrated by the lower percentage of SerBut-treated mice with a disease score greater than 1 (Figure 2.9c). Neither NaBut nor L-serine suppressed disease at molar equivalent doses.

A thorough analysis of immune cell populations in the spinal cord-draining LNs (SC-dLNs) revealed that SerBut treatment significantly increased PD-1 and CTLA-4 expression on $CD4^+$ T cells, expanded Tregs, and upregulated CTLA-4 expression on $CD4^+$ Tregs (Figure 2.9d-h).

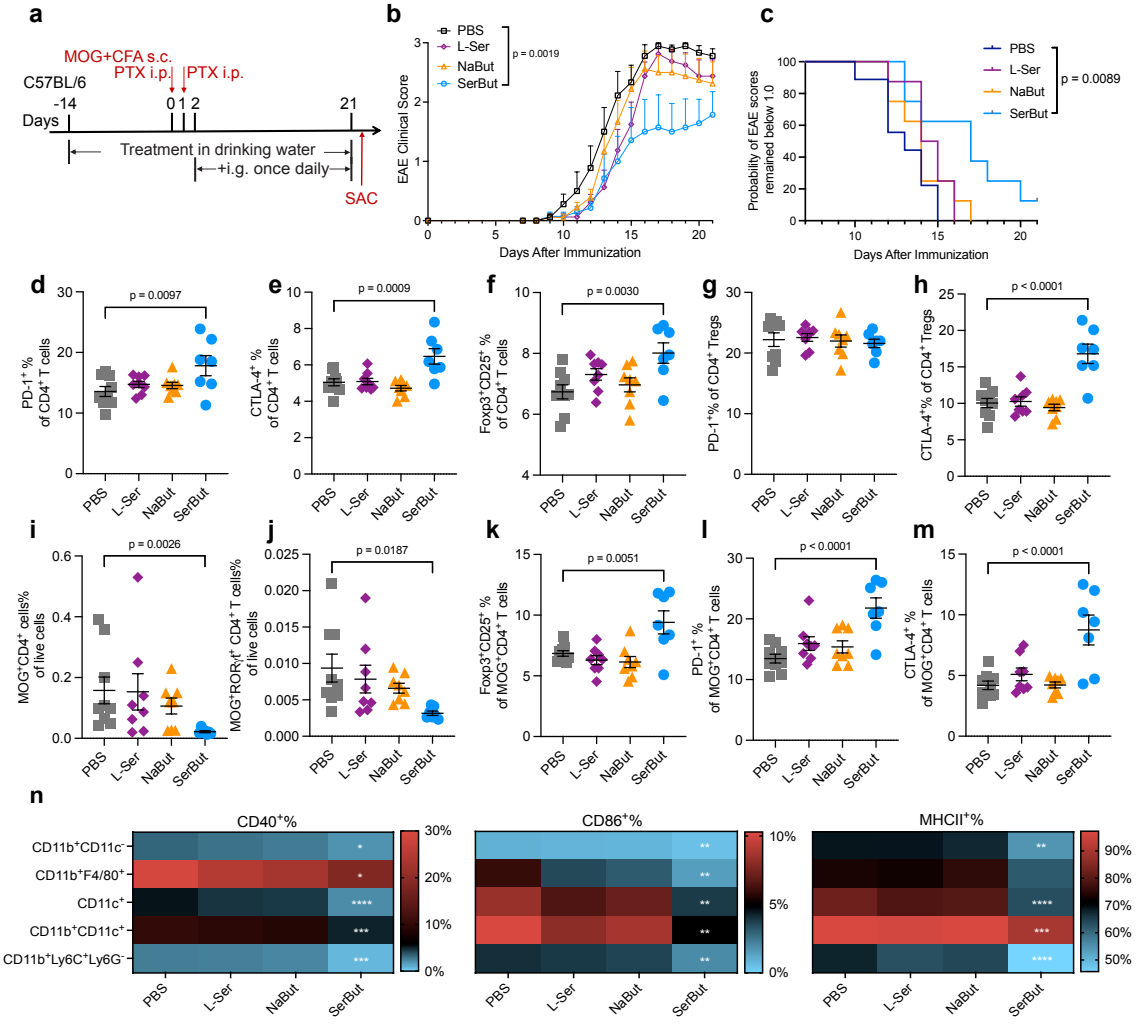

Figure 2.9: **SerBut ameliorates EAE development more effectively than free butyrate or serine.** (a) Experimental schema. EAE was induced in C57BL/6 mice using MOG_{35-55}/CFA with pertussis toxin. Mice were administered drinking water containing 100 mM NaBut, L-Serine (L-Ser), or SerBut from day -14 until the end of the study. On day 2 after EAE induction, PBS, NaBut (15 mg, molar equivalent to SerBut), L-Ser (12 mg, molar equivalent to SerBut), or SerBut (24 mg) were administered once daily. (b) Disease progression as indicated by the clinical score. The areas under the curve were compared, and statistical analyses were performed using a one-way ANOVA with Dunnett's test. (c) The probability that EAE clinical scores remained below 1.0 for the three treatment groups. Statistical analysis was performed using the Log-rank (Mantel-Cox) test comparing every two groups. (d-m) Phenotypes of $CD4^+$ T cells from the spinal cord-draining lymph nodes (SC-dLNs, i.e. the iliac and cervical LNs), including the percentage of d) PD-1^+, e) CTLA-4^+, or f) FoxP3^+ CD25^+ of total $CD4^+$ T cells; g) PD-1^+ or h) CTLA-4^+ of FoxP3^+CD25^+CD4^+ Tregs; the percentage of i) MOG Tetramer$^+$CD4^+ or j) RORγt$^+$CD4^+ T cells of total live cells; and k) Foxp3^+CD25^+, l) PD-1^+, m) CTLA-4^+ of MOG Tetramer$^+$CD4^+ T cells.

Figure 2.9: Continued: (n) Heatmap of the percentage of co-stimulatory molecules ($CD40^+$ or $CD86^+$) or MHC class II^+ cells of myeloid cells in the SC-dLNs, indicated by the color as shown in the corresponding scale bar. Data represent mean ± s.e.m. Statistical analyses were compared between PBS and each treatment group using one-way ANOVA with Dunnett's test or Kruskal-Wallis test (if not normally distributed). n = 8 mice per group.

These results suggest that SerBut may help suppress excessive immune responses during EAE by modulating key immune checkpoints and regulatory T cell populations. Additionally, in the SC-dLNs, SerBut treatment reduced the number of myelin oligodendrocyte glycoprotein (MOG)-specific T cells and $MOG^+ROR\gamma t^+CD4^+$ T cells (Th17 cells), antigen-specific pathogenic cells that contribute to EAE development (Figure 2.9i, j). SerBut treatment also increased FoxP3, PD-1, and CTLA-4 expression on these MOG^+CD4^+ T cells (Figure 2.9k-m), potentially preventing these cells from promoting inflammation and tissue damage in EAE. Consistent with disease score readouts, neither NaBut nor L-serine induced any changes to these cellular immune responses.

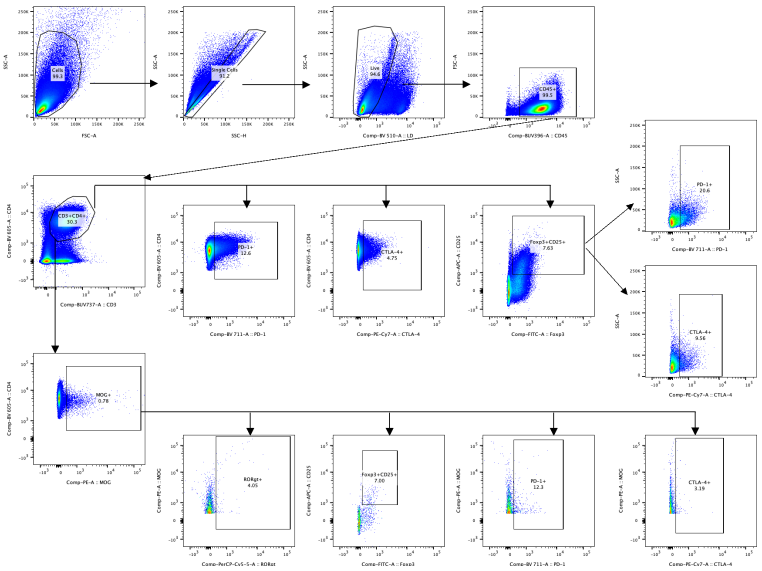

Figure 2.10: **Flow cytometry gating strategy for identification of $CD4^+$ T cell subsets in dLNs and spleen of EAE mice.** Flow cytometry gating strategy for the identification of PD-1^+, CTLA-4^+, or $FoxP3^+CD25^+$ of $CD4^+$ T cells, PD-1^+ or CTLA-4^+ of $FoxP3^+CD25^+CD4^+$ Tregs, MOG Tetramer$^+CD4^+$ or $CD4^+ROR\gamma t^+$ T cells, and $Foxp3^+CD25^+$, PD-1^+, CTLA-4^+ of MOG Tetramer$^+CD4^+$ T cells.

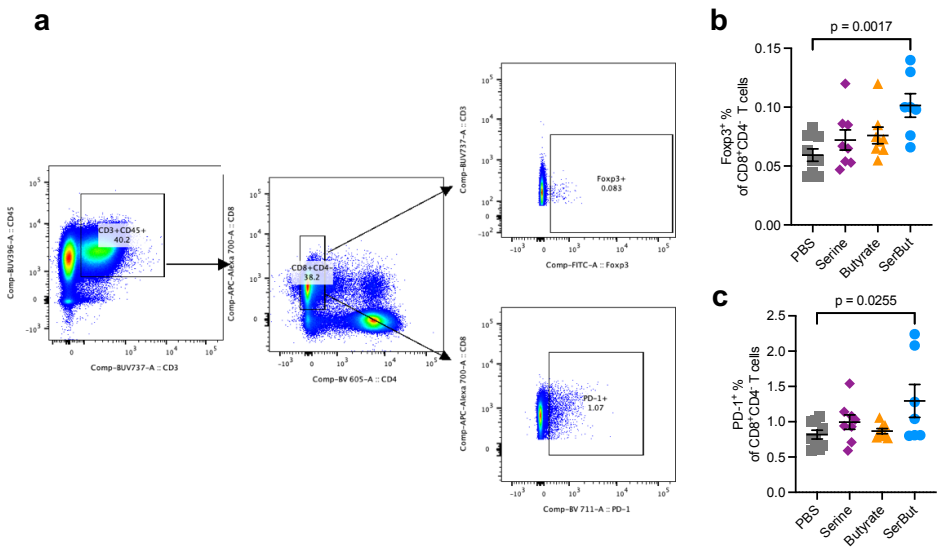

Figure 2.11: **Flow cytometry gating strategy for identification of CD8$^+$ T cell subsets in dLNs of EAE mice.** (a) The gating strategy and (b) the percentage of FoxP3$^+$ or (c) PD-1$^+$ of CD8$^+$CD4$^-$ T cells in the spinal cord-draining lymph nodes (SC-dLNs, iliac and cervical LNs) measured by flow cytometry, from the experiment in Figure 2.9. Data represent mean ± s.e.m. Statistical analyses were compared between PBS and each treatment group using one-way ANOVA with Dunnett's test. P values less than 0.05 were shown.

In the innate immune compartment, SerBut treatment reduced the expression of co-stimulatory markers, including CD40 and CD86, as well as the antigen-presenting molecule MHC class II, on various myeloid cells including CD11b$^+$CD11c$^-$ cells, CD11b$^+$F4/80$^+$ macrophages, CD11c$^+$ dendritic cells, CD11b$^+$CD11c$^+$ dendritic cells, and CD11b$^+$Ly6C$^+$ Ly6G$^-$ myeloid-derived suppressor cells (MDSCs) (Figure 2.9, Figure 2.12). As these myeloid cells play a crucial role in initiating and propagating immune responses, the reduction of co-stimulatory molecules and MHC class II expression on these cells suggests that SerBut treatment may inhibit their activation and function. This could lead to a dampening of the inflammatory response and contribute to EAE suppression. MDSCs are reported to have immunosuppressive functions, such as inhibiting T cell proliferation and promoting Treg expansion, in the context of EAE [240][241]. We observed not only a downregulation of activation markers on these cell types but also a significant increase in the percentage of

these cells in both SC-dLNs and mesenteric LNs (Figure 2.13). Overall, our results demonstrate that SerBut modulate the activity of various immune cell populations and reduces inflammatory responses in EAE-bearing mice. All these effects were observed exclusively with SerBut treatment and not with free L-serine nor NaBut, suggesting the importance of serine conjugation in enhancing butyrate's systemic and possibly CNS bioavailability.

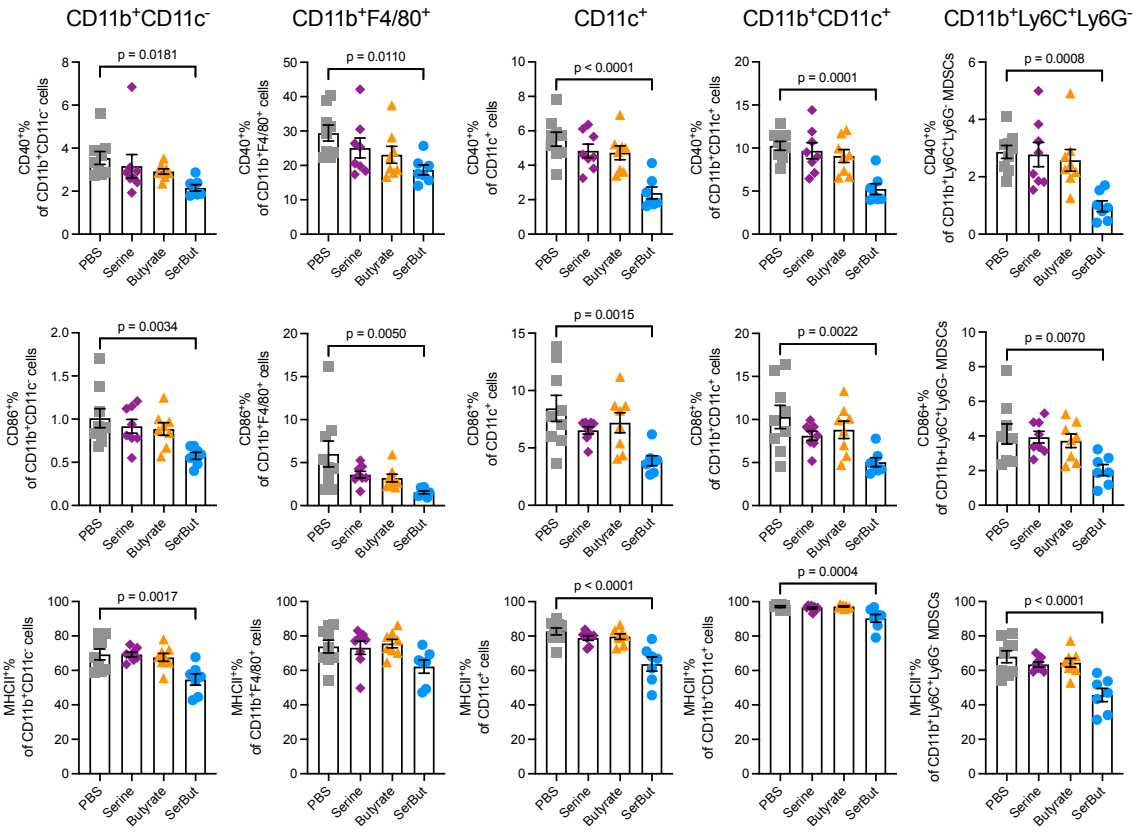

Figure 2.12: **Expression of co-stimulatory molecules and MHC class II on myeloid Cells from dLNs of EAE mice.** The percentage of co-stimulatory molecules ($CD40^+$ and $CD86^+$) and MHC class II^+ myeloid cells in the SC-dLNs from Figure 2.9n. Data represent mean ± s.e.m. Statistical analyses were compared between PBS and each treatment group using one-way ANOVA with Dunnett's test.

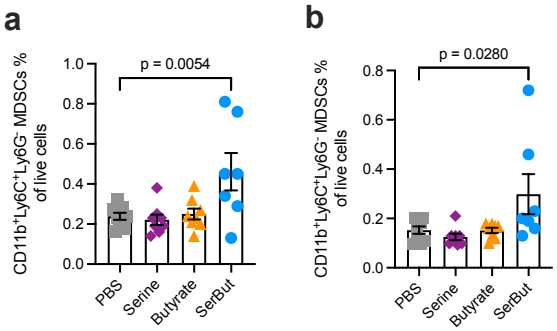

Figure 2.13: **CD11b$^+$Ly6C$^+$Ly6G$^-$ cells in LNs of EAE mice.** The percentage of CD11b$^+$Ly6C$^+$Ly6G$^-$ cells in the (a) spinal cord-draining LNs or (b) mesenteric LNs from the experiment in Figure 2.9. Data represent mean ± s.e.m. Statistical analyses were compared between PBS and each treatment group using one-way ANOVA with Dunnett's test.

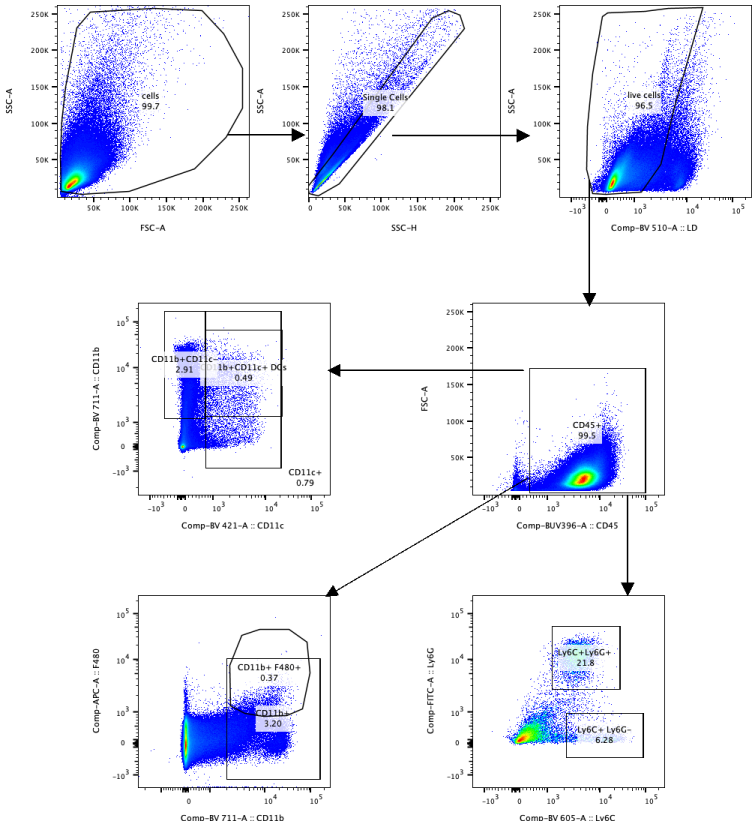

Figure 2.14: **Flow cytometry gating strategy for identifying myeloid cell subsets in dLNs and spleen of EAE mice.** Flow cytometry gating strategy for CD11b$^+$CD11c$^-$, CD11b$^+$F4/80$^+$, CD11c$^+$, and CD11b$^+$CD11c$^+$, CD11b$^+$Ly6C$^+$Ly6G$^-$ cells in Figure 2.9n, Figure 2.12, and Figure 2.13.

2.4.4 SerBut Administered Post-EAE Induction Suppresses Disease Progression and Inhibits Immune Responses in the Spinal Cord

We next sought to investigate whether administration of SerBut post-EAE induction could also suppress disease progression and induce immunological changes in the spinal cord. Mice were administered twice-daily gavage of SerBut after EAE induction (Figure 2.15a).

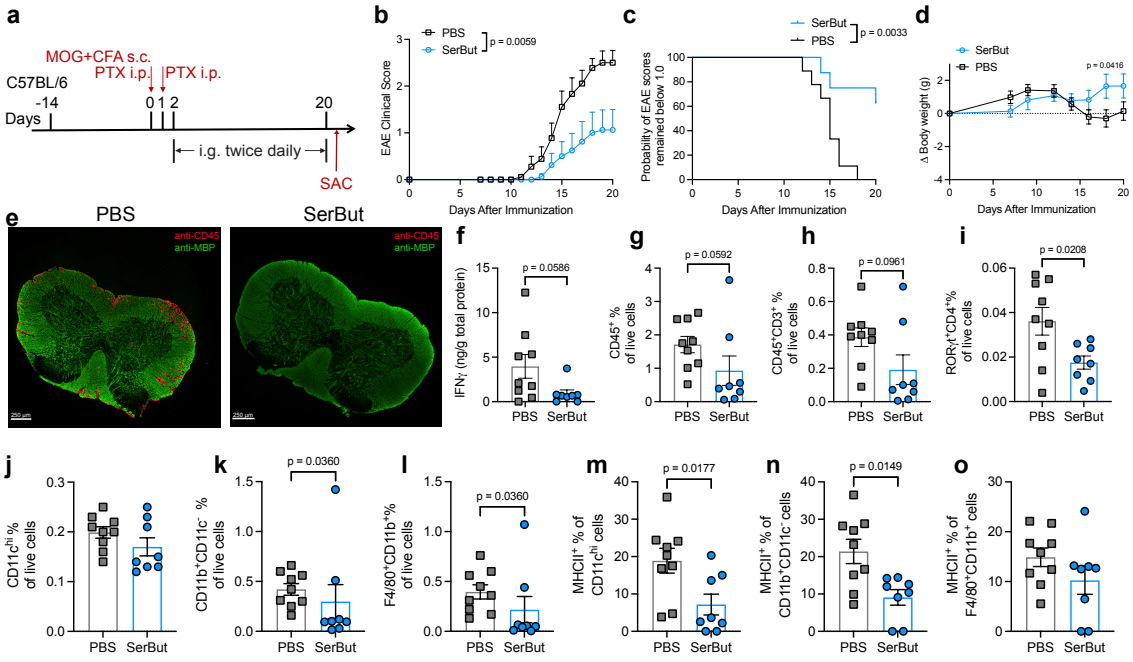

Figure 2.15: **Twice daily oral gavage of SerBut post-EAE induction suppresses disease progression.** (a) Experimental schema. EAE was induced in C57BL/6 mice using MOG_{35-55}/CFA followed by pertussis toxin. On day 2 after EAE induction, PBS (n = 9) or SerBut (n = 8) at 24 mg/dose was administered twice daily by oral gavage. (b) Disease progression as indicated by the clinical score. The areas under the curve were compared, and statistical analyses was performed using Student's T-test. (c) The probability of EAE clinical score remaining below 1.0 in the three treatment groups. Statistical analysis was performed using the Log-rank (Mantel-Cox) test. (d) Body weight change. (e) Representative immunofluorescence images of spinal cord sections from EAE mice treated with PBS or SerBut. Red: anti-CD45 staining; green: anti-myelin basic protein (MBP) staining. Bar = 250 µm. (f) The concentration of IFN-γ normalized by the total protein in the spinal cord homogenized supernatant. (g-l) The percentage of g) $CD45^+$, h) $CD3^+CD45^+$, i) $ROR\gamma t^+CD4^+$, j) $CD11b^+CD11c^-$, k) $F4/80^+CD11b^+$, and l) $CD11c^{hi}$ of live cells in the spinal cord. (m-o) The percentage of m) MHC class II^+ of $CD11b^+CD11c^-$, n) $F4/80^+CD11b^+$, or o) $CD11c^{hi}$ cells in the spinal cord. Data represent mean ± s.e.m. Statistical analyses were performed using Student's T-test.

We observed that the SerBut-treated mice had significantly lower EAE clinical scores compared to PBS-treated mice (Figure 2.15b). Only 2 out of 8 mice in the SerBut-treated group developed EAE with scores higher than 1 by the end of the study, and the rest remained healthy throughout the experiment (Figure 2.15c). Additionally, PBS-treated mice began to experience a significant drop in body weight starting on day 14, whereas the SerBut-treated mice continued to grow over time (Figure 2.15d).

When PBS-treated mice reached a plateau in disease score, we sacrificed both groups and examined the spinal cords to assess the impact of treatment. From immunofluorescence images with anti-CD45 and anti-myelin basic protein (MBP) staining, we observed substantial immune cell infiltration into the spinal cords of PBS-treated mice, but not in SerBut-treated mice (Figure 2.15e, Figure 2.16). The two mice from the SerBut-treated group that did not respond to treatment also showed corresponding immune cell infiltration into their spinal cords (Figure 2.16).

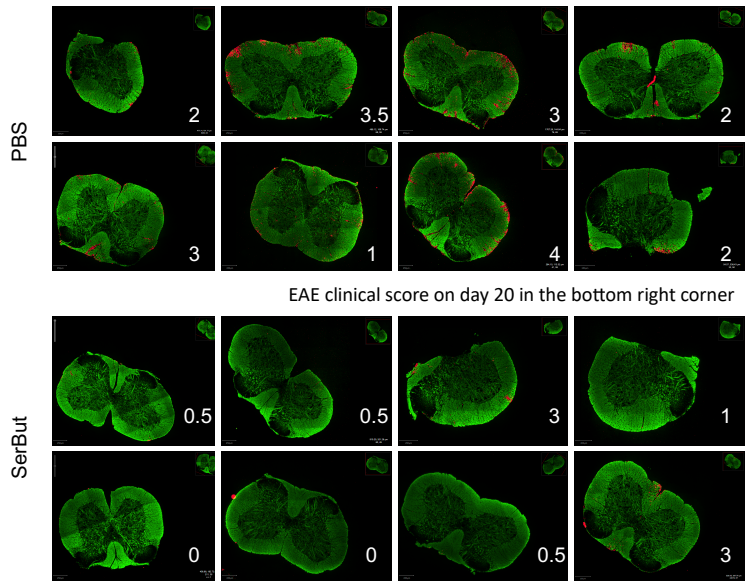

Figure 2.16: **Immunofluorescence images of spinal cord sections from PBS and SerBut-treated EAE mice.** Spinal cord sections were obtained from the experiment in Figure 2.15. The EAE clinical score on day 20 post-disease induction is displayed in the bottom right corner of each image. Red: anti-CD45 staining; green: anti-myelin basic protein (MBP) staining.

Additionally, we homogenized part of the spinal cord and measured IFN-γ levels. We observed a reduction in IFN-γ in the spinal cords of SerBut-treated mice (Figure 2.15). We also quantified the effect of SerBut treatment on the immune cell compartment in the spinal cord via flow cytometry. We observed a decrease in immune cell populations across most immune cell types in the spinal cord, including CD45$^+$ cells, CD3$^+$ T cells, and pathogenic Th17 cells (RORγt$^+$CD4$^+$ T cells) (Figure 2.15g-i), as well as macrophage-like CD11b$^+$CD11c$^-$ and CD11b$^+$F4/80$^+$ cells (Figure 2.15j-k). We did not observe a significant reduction in the CD11c$^+$ DC population (Figure 2.15l); however, there was a decrease in MHC class II on their surface, as well as on CD11b$^+$CD11c$^-$ cells, indicating diminished activation of these cells in the spinal cords of SerBut-treated mice (Figure 2.15m-o).

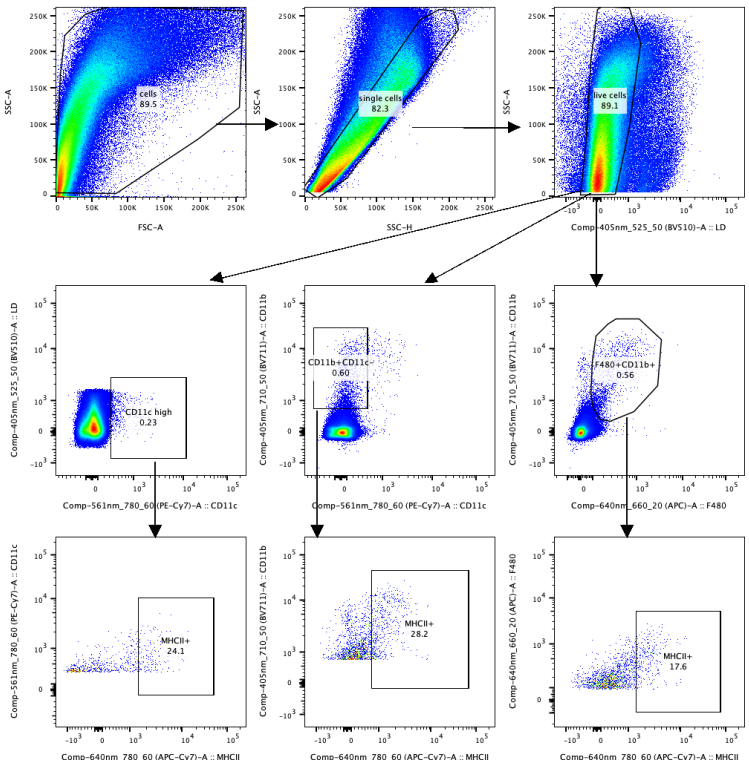

Figure 2.17: **Gating strategy for identification of myeloid cell subsets in the spinal cord of PBS and SerBut-treated EAE mice.** Flow cytometry gating strategy for CD11c^{hi}, CD11b$^+$CD11c$^-$, and CD11b$^+$F4/80$^+$ of live cells and MHC class II$^+$ of these myeloid cells in the spinal cord, from the experiment in Figure 2.15.

The reduced MHC class II on the myeloid cells was observed not only in the spinal cord, but also in the mesenteric LNs (Figure 2.18). In this experiment, we also noted that SerBut increased the frequency of Foxp3$^+$ Tregs both systemically in the spleen and locally in the SC-dLNs and mesenteric LNs (Figure 2.19), consistent with our findings in previous RA and EAE experiments. These findings suggested that SerBut exerts its immunomodulatory effects both systemically and in disease-related tissues.

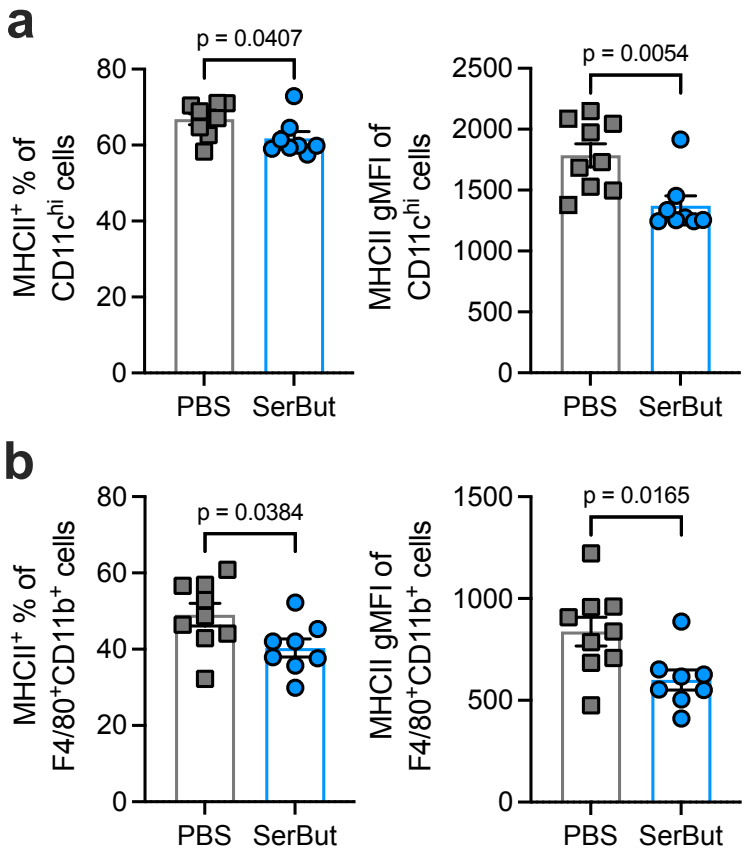

Figure 2.18: **SerBut treatment suppresses CD11c^{hi} dendritic cells and F4/80$^+$CD11b$^+$ macrophages in the mesenteric LNs.** The percentage of (a) MHC class II$^+$ and geometric mean fluorescent intensity (gMFI) of CD11c^{hi} dendritic cells and (b) F4/80$^+$CD11b$^+$ macrophages isolated from the mesenteric LNs, from the experiment in Figure 2.15. Data represent mean ± s.e.m. Statistical analyses were performed using Student's T-test.

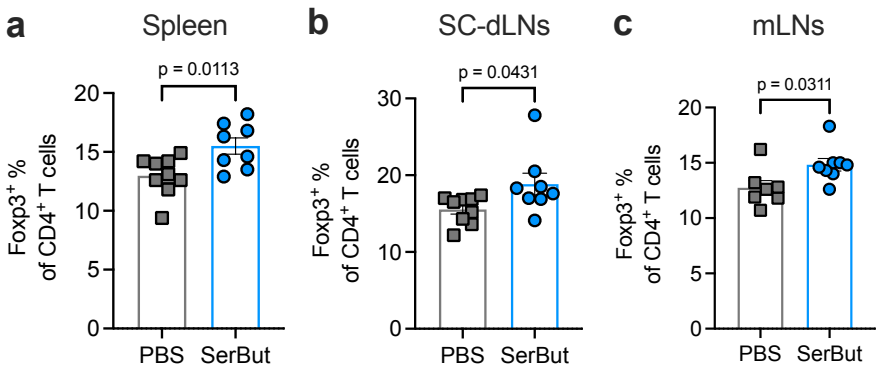

Figure 2.19: **SerBut treatment induces Treg expansion in several organs.** The percentage of FoxP3$^+$ of CD4$^+$ T cells in the (a) spleen, (b) spinal cord-draining LNs (SC-dLNs), and (c) mesenteric LNs (mLNs), from the experiment in Figure 2.15. Data represent mean ± s.e.m. Statistical analyses were performed using Student's T-test.

2.4.5 SerBut Does Not Impact Global Immune Responses to Vaccination or Alter Blood Chemistry Biomarkers

Several immune modulators employed in autoimmunity blunt systemic immune responses to vaccination or infection. As a benchmark, we employed fingolimod (FTY 720) is a widely used oral compound for treating MS [242]. FTY 720 targets the sphingosine-1-phosphate receptor and affects the immune system by sequestering lymphocytes in lymph nodes, reducing their migration to the CNS and ultimately supressing inflammation [243]. Studies have shown that oral prophylactic administration of FTY 720 in mice completely prevents the development of EAE, while therapeutic administration reduces the severity of EAE [243]. However, FTY 720 can inhibit global immune responses, as demonstrated in a previous study from our group, where FTY 720 administration to mice vaccinated with ovalbumin (OVA) and adjuvant prevented the generation of OVA-specific IgG [218]. To gain insight into whether SerBut might impact global immune responses to vaccination, we vaccinated mice with OVA, along with the adjuvants alum and monophosphoryl-lipid A (MPLA), which mimic the clinical vaccine adjuvant AS-04, through subcutaneous injections in the hock.

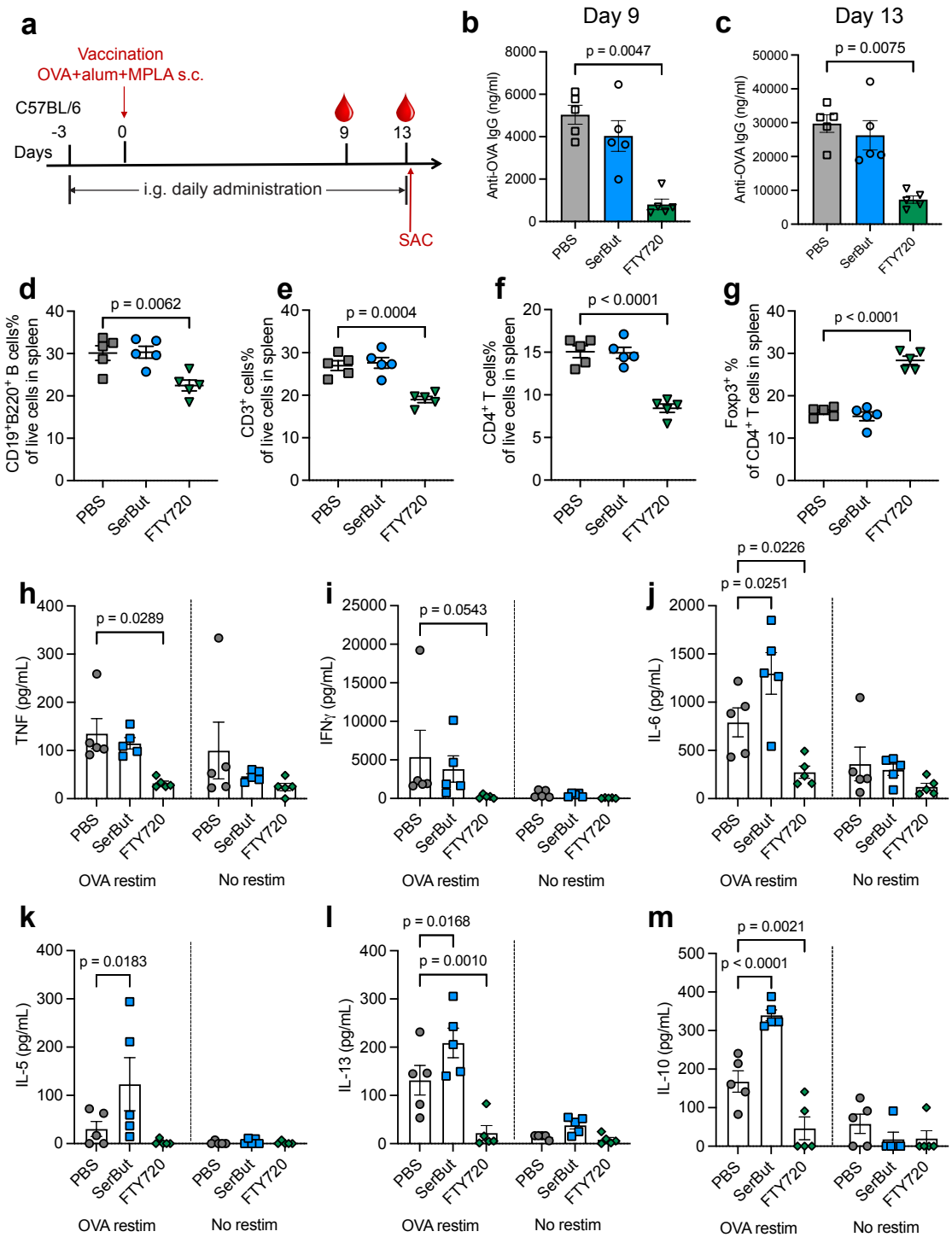

Figure 2.20: **SerBut does not impact immune responses to vaccination compared to FTY 720.** (a) Experimental schema. Mice were orally gavaged with PBS, SerBut (twice daily, 25 mg/dose), or FTY 720 (once daily, 0.02 mg/dose) beginning on day -3 until the end of the experiment. (Continued on next page.)

Figure 2.20: Continued: On day 0, mice were immunized subcutaneously in the front hocks with 10 µg endotoxin-free ovalbumin (OVA), 50 µg ALUM, and 5 µg MPLA. (b, c) Mice were bled on b) day 9 and c) day 13, and plasma was analyzed for anti-OVA IgG antibodies. (d-g) The percentage of d) $CD19^+B220^+$, e) $CD3^+$, f) $CD4^+$ of total live cells, and g) $FoxP3^+$ of $CD4^+$ T cells in the spleen. (h-m) Production of the cytokines h) TNF-α, i) IFN-γ, j) IL-6, k) IL-5, l) IL-13, and m) IL-10, measured in the supernatant of isolated splenocytes upon restimulation with OVA protein for 3 days. Data represent mean ± s.e.m. Statistical analyses were performed using one-way ANOVA (b-g) or two-way ANOVA (h-m) with Dunnett's post hoc test.

Mice were treated with either PBS, SerBut, or FTY 720 by oral gavage (Figure 2.20a). Blood collected on days 9 and 13 revealed OVA-specific IgG antibody generation in both PBS and SerBut-treated mice but much less so in FTY 720-treated mice, indicating that FTY 720, unlike SerBut, suppressed humoral responses to the OVA vaccination (Figure 2.20b, c).

To evaluate cellular responses, we sacrificed the mice and isolated immune cells from the spleen and hock-draining lymph nodes. FTY 720 reduced B cell ($CD19^+B220^+$), T cell ($CD3^+$), and $CD4^+$ T cell populations in both hock-draining LNs and the spleen (Figure 2.20d-f, Figure 2.22). Interestingly, FTY 720 substantially increased $FoxP3^+$ Tregs in both LNs and the spleen (Figure 2.20g, Figure 2.22). *In vitro* restimulation of splenocytes isolated from FTY 720-treated mice with OVA, revealed a significant reduction in cytokine production, including TNF-α, IFN-γ, IL-6, IL-5, IL-13, and IL-10 (Figure 2.20h-m), indicating that FTY 720 suppressed antigen-specific T cell responses to OVA. In contrast, SerBut treatment did not suppress these cellular responses, although interestingly, we did observe some increase in the production of cytokines IL-6, IL-5, IL-13, and IL-10 following SerBut treatment (Figure 2.20h-m).

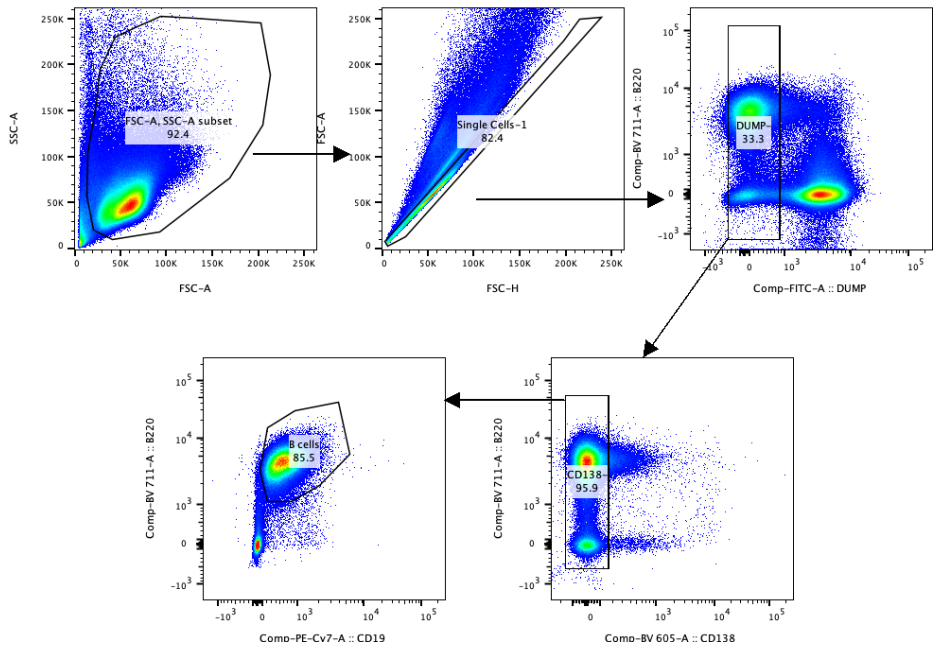

Figure 2.21: **Flow cytometry gating strategy for identifying B cell subsets in SerBut vaccination study.** Gating strategy for identifying $CD19^{+}B220^{+}$ cells in Figure 2.20c and Figure 2.20d. Dump gate used to exclude cells stained with FITC antibody against F4/80, CD11c, Gr-1, CD4, and CD8.

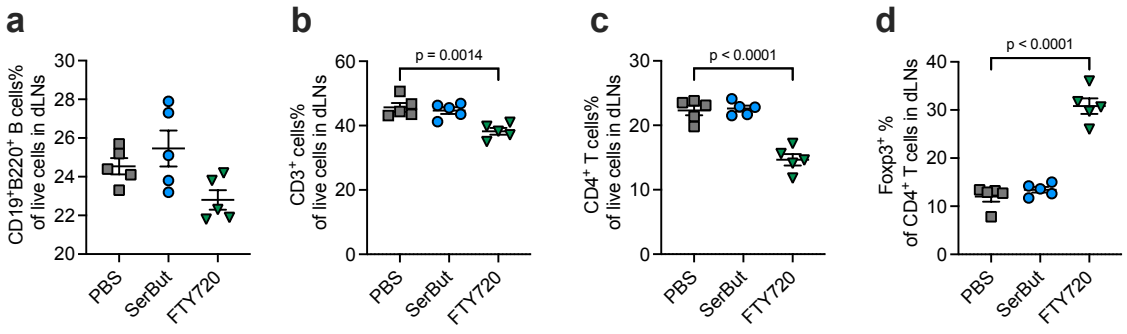

Figure 2.22: **Impact of SerBut and FTY 720 administration on B cell and T cells in dLNs following vaccination.** Percentages of (a) $CD19^{+}B220^{+}$, (b) $CD3^{+}$, (c) $CD4^{+}$ of total live cells and (d) $FoxP3^{+}$ of $CD4^{+}$ T cells in the hock-draining LNs, from the experiment in Figure 2.20. Data represent mean ± s.e.m. Statistical analyses were performed using one-way ANOVA with Dunnett's post hoc test.

We also conducted biochemistry analysis on the mouse serum from the vaccination study to determine if the SerBut or FTY 720 treatment induced organ toxicity in addition to effects

on immune responses (Figure 2.23). Compared to PBS, SerBut treatment did not induce significant changes in the key readouts from the biomarker panel, which included markers of liver, pancreas, and kidney toxicity. FTY 720 induced a modest reduction in blood urea nitrogen levels but no additional changes. Overall, these findings suggest that SerBut did not have a significant impact on global immune responses to vaccination and is safe for mice when administered at the indicated dose via twice-daily oral gavage.

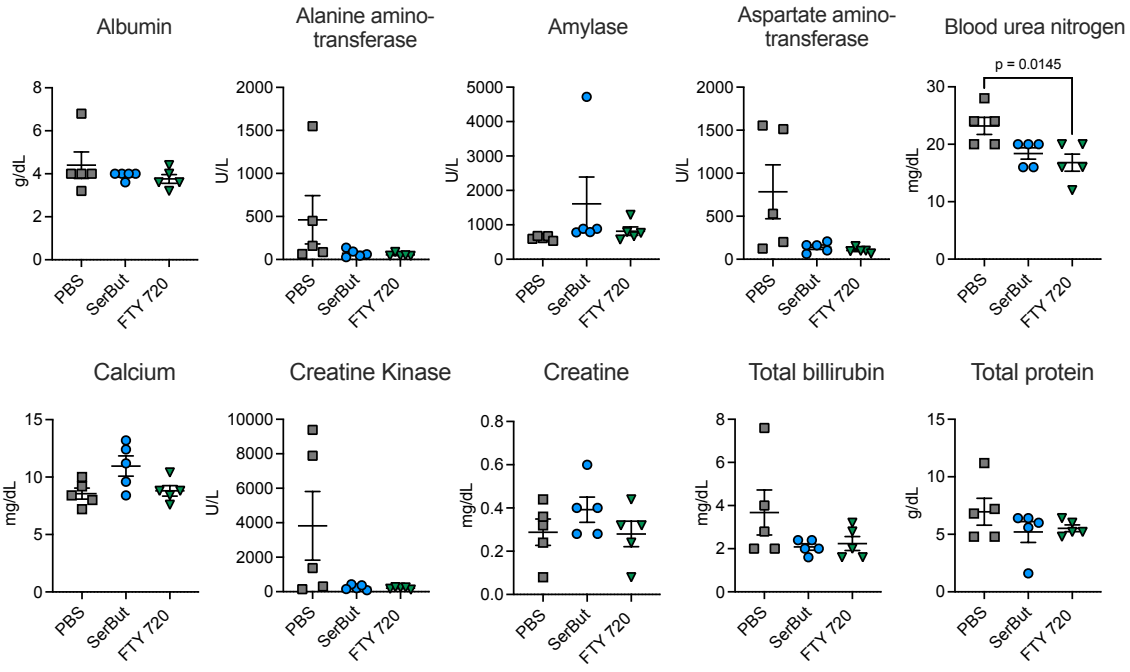

Figure 2.23: **Biochemistry analysis of mouse serum samples.** Biochemistry analysis of mouse serum samples from the experiment in Figure 2.20. Data represent mean ± s.e.m. Statistical analyses were compared between every two groups using one-way ANOVA with Tukey's test.

2.5 Discussion

In this study, we investigated the therapeutic potential of SerBut in treating CAIA and EAE, murine models of RA and MS, respectively. Orally administered free butyrate can be absorbed and quickly metabolized by host tissues and cells via butyryl-CoA/acetate CoA transferase and phosphotransbutyrylase-butyrate kinase pathways [244]. In the colon, bu-

tyrate is primarily consumed by the colonocytes as an energy source [213]. By employing a simple chemical strategy to conjugate serine to butyrate, we improved the oral bioavailability of butyrate including into the CNS, creating a prodrug candidate that offers several advantages, including a lack of unpleasant odor and taste, and higher efficacy compared to free butyrate. Our results demonstrated that SerBut significantly ameliorated the severity of both diseases, modulated key immune cell populations, and reduced inflammatory responses, all without compromising global immune responses to vaccination.

Butyrate, a key metabolite from commensal bacteria, has multiple modulating effects across different types of immune cells. It has been shown to facilitate peripheral generation of Tregs through both direct upregulation of FoxP3 by HDAC inhibition [102][201], and indirect effects from the induction of tolerogenic DCs [203][245]. In our study, we demonstrated that SerBut treatment increased peripheral Tregs in both CAIA and EAE settings, as well as in both local LNs and spleen (Figure 2.5h, Figure 2.5f, k, Figure 2.11b, Figure 2.19). Notably, we observed enhanced biodistribution of SerBut in these tissues after oral administration, which is not limited to gut tissues as previously reported [246][247]. Butyrate has also been shown to modulate the differentiation of macrophages and DCs [213]. Through HDAC inhibition, butyrate downregulates LPS-induced proinflammatory cytokines produced by macrophages [100], and activates macrophage metabolism towards oxidative phosphorylation through upregulation of Arg-1, promoting an anti-inflammatory M2 phenotype [248]. In our CAIA studies, enhancing the systemic bioavailability of butyrate through SerBut significantly increased the M2/M1 macrophage ratio in hock-draining LNs, which could exert direct anti-inflammatory effects on paw and joint inflammation. Moreover, butyrate has been shown to suppress DC activation and induce tolerogenic DCs through a combination of signaling via GPR109A and HDAC inhibition [203]. In our study, we observed a similar effect from SerBut compared to free NaBut in suppressing LPS-induced activation, including co-stimulatory markers CD80 and CD86, and MHC class II expression of BMDCs isolated from

mice. Consistently, in the EAE model, we observed downregulation of these costimulatory markers and MHC class II on various myeloid cells across different tissues, suggesting the important roles butyrate can play in suppressing disease progression through this pathway while delivered systemically.

Myeloid cells, such as DCs and macrophages, play a crucial role in antigen presentation and T cell activation. For instance, CD86 interacts with CD28 on T cells, promoting their activation and proliferation [249][250]. CTLA-4 is a surface receptor predominantly expressed on T cells, particularly on Tregs, and competes with CD28 for binding to CD86 on myeloid cells, delivering an inhibitory signal to T cells [251]. Intriguingly, in the EAE experiment, we observed that SerBut treatment significantly increased CTLA-4 expression on both total $CD4^+$ T cells, and Tregs in the spinal cord-draining LNs. This concurrent upregulation of CTLA-4 on T cells, and downregulation of CD86 on myeloid cells can synergistically contribute to a more profound suppression of immune activation, ultimately dampening autoimmune responses.

In the EAE experiment, we have shown that twice-daily administration of SerBut significantly reduces immune cell infiltration into the spinal cord. We do not know if this CNS effect is modulated directly as a result of the butyrate that crosses the BBB or whether its effect on peripheral immune cells indirectly impacts the CNS. Additionally, the effect of butyrate on BBB (or blood-spinal cord barrier) endothelial cell functions and integrity warrants further investigation.

We have shown that SerBut has several potential benefits over free NaBut for clinical translation: serine conjugation to butyrate masks its odor and taste, yields higher bioavailability, and demonstrates superior efficacy in suppression of autoimmune disease models than NaBut. The dose used in these studies can be converted to 6 grams per dose for human clinical trials, which could be formulated as powder that could be added drinking water for daily consumption. Importantly, SerBut did not negatively impact global immune responses

to vaccination, as demonstrated by the generation of equivalent OVA-specific IgG humoral and cellular immune responses in both PBS and SerBut-treated mice. Although we observed effective immune modulation in the context of autoimmune arthritis and EAE, the immune response elicited by a strong, Th1-biasing adjuvant (the TLR4 agonist MPLA in the alum depot) was sufficient to overcome the effects of SerBut [252].

The findings of our study provide evidence for the potential of SerBut as a next-generation therapeutic agent for RA and MS. Further studies, including preclinical and clinical studies, are needed to better understand the long-term safety and efficacy of SerBut in the context of rheumatoid arthritis, multiple sclerosis, and other autoimmune and inflammatory diseases. Given its broad immunomodulatory effects shown in our study, it would be valuable to explore the potential of SerBut in treating a broader range of immune-related conditions.

2.6 Author Contributions

This chapter and the accompanying figures are adapted from the manuscript "Suppression of autoimmune arthritis and neuroinflammation via an amino acid-conjugated butyrate prodrug with enhanced oral bioavailability" by Shijie Cao* (* = equal contribution), Erica Budina* (* = equal contribution), Michal M. Raczy, Ani Solanki, Mindy Nguyen, Taryn N. Beckman, Joseph W. Reda, Kevin Hultgren, Phillip Ang, Anna J. Slezak, Lauren A. Hesser, Aaron T. Alpar, Kristen C. Refvik, Lucas S. Shores, Ishita Pillai, Rachel P. Wallace, Arjun Dhar, Elyse A. Watkins, Jeffrey A. Hubbell. This manuscript is currently in press in *Nature Biomedical Engineering.* * Shijie Cao and Erica Budina contributed equally to this work. J.A.H. oversaw all research. S.C., E.B., and J.A.H. designed most of experiments. S.C., M.M.R., T.N.B., and A.J.S. synthesized materials. S.C., E.B., M.M.R., A.S., M.N., T.N.B., J.W.R., K.H., P.A., L.A.H., A.T.A., K.C.R., L.S.S., I.P., R.P.W., A.D., and E.A.W. performed experiments. S.C. and E.B. analyzed experiments. S.C., E.B., and J.A.H. wrote the manuscript. All authors contributed to the article and approved the submitted version.

2.7 Acknowledgements

This work was supported by the Chicago Immunoengineering Innovation Center of the University of Chicago and the Alper Family Fund. We thank Yue Wang from Prof. Melody Swartz's laboratory for providing mouse BMDCs. We thank Dr. Abbey Lauterbach for helping on interpreting histology images. We thank the Cytometry and Antibody Technology Core Facility (Cancer Center Support Grant P30CA014599), the Human Tissue Resource Center, the Integrated Light Microscopy Core, and the Mass Spectrometry Facility (National Science Foundation instrumentation grant CHE-1048528) at the University of Chicago.

2.8 Competing Interests

S.C., E.B., M.M.R., E.A.W. and J.A.H. are inventors on a patent filed by the University of Chicago on uses of SerBut.

CHAPTER 3

ACTIVITY-ATTENUATED SERUM ALBUMIN-FUSED INTERLEUKIN-33 SUPPRESSES EXPERIMENTAL AUTOIMMUNE ENCEPHALOMYELITIS

3.1 Abstract

Interleukin-33 (IL-33) is an immunoregulatory cytokine that reduces the severity of experimental autoimmune encephalomyelitis (EAE), a murine model of multiple sclerosis (MS), but displays poor pharmacokinetics and immunotoxicity that hinder its clinical translation. To address these limitations, we developed an activity-attenuated IL-33 by recombinant fusion to serum albumin (SA). SA IL-33 displayed fewer adverse events at immunity-modulating doses and enhanced bioavailability in the secondary lymphoid organs (SLOs), sites of T cell priming in autoimmunity, compared to unmodified IL-33 (WT IL-33). Prophylactic subcutaneous SA IL-33 administration prevented EAE development with superior efficacy to WT IL-33 and similar efficacy to fingolimod, an FDA-approved MS drug that systemically suppresses immunity. Therapeutic SA IL-33 administration also significantly reduced disease score in both chronic and relapsing-remitting EAE. SA IL-33 promoted immunoregulation by reducing the infiltration of $CD45^+$ cells including disease-causing Th17 T cells in the spinal cord, while expanding type 2 immune cells including ILC2s, $ST2^+$ Tregs, Th2 T cells, and M2-polarized macrophages in the SLOs of EAE-bearing mice. These findings suggest that SA IL-33 is a promising therapeutic for neuroinflammatory diseases.

3.2 Introduction

Multiple sclerosis (MS) is an inflammatory, degenerative disease of the central nervous system (CNS) that impacts more than 2.5 million people worldwide [123]. Disease is caused by the activation and migration of autoreactive lymphocytes and innate immune cells into the CNS [7]. This inflammation cascade leads to demyelination of the myelin sheath and oligodendrocyte cell body, activation and proliferation of glial cells, and neuroaxonal degeneration, resulting in disabling clinical manifestations including fatigue, pain, sensory and vision loss, and motor impairment [124]. Although current MS disease-modifying therapies manage acute attacks and reduce the frequency of relapses, these treatments act by broadly suppressing the immune system, increasing susceptibility to infections; require lifelong treatment; and are less effective in halting progressive forms of MS [125]. Hence, there remains an unmet need for MS treatments that can restore homeostasis without broadly suppressing the immune system.

Interleukin-33 (IL-33) is an 18 kD cytokine that induces type 2 immunity [253][254]. Originally described as an alarmin secreted by necrotic epithelial cells following helminth infection [254][255] and allergen exposure [256], recent studies show that IL-33 also promotes immunoregulation and tissue repair [257]. IL-33 expands a subset of $FoxP3^+CD4^+$ Tregs that co-express ST2 (IL-33R) [258][259][260][261][262]. $ST2^+$ Tregs have been shown to suppress $CD4^+$ T cell proliferation more effectively than $ST2^-$ Tregs *in vitro*, and secrete elevated levels of the immunoregulatory cytokines IL-10 and TGF-β [260]. IL-33 also synergizes with TGF-β to induce naive $CD4^+$ T cell differentiation into $ST2^+$ Tregs [258]. Upon IL-33 stimulation, $ST2^+$ Tregs produce amphiregulin, a ligand for epidermal growth factor receptor that promotes tissue repair following inflammation-mediated tissue damage [257][263][264]. IL-33 also expands other ST2-expressing immune cells including Th2 T cells [265], type 2 innate lymphoid cells (ILC2s) [266], M2-polarized macrophages [267], and dendritic cells (DCs) [268] that may modulate Treg phenotype [263][269]. Upon IL-33 stimulation, Th2 T

cells [254] and ILC2s [266] produce the type 2 cytokines, IL-5 and IL-13. IL-33 synergizes with IL-13 to induce M2 macrophage polarization through increased arginase-1 production [267]. M2-macrophages secrete IL-10 and TGF-β, which also promote Treg differentiation and maintenance [263]. Stimulation of CD11c$^+$ DCs with IL-33 increases IL-2 production, resulting in ST2$^+$ Treg expansion [268]. IL-33 also suppresses disease-causing Th17 T cells [270][271][272][273][274] by reducing the expression of the pro-inflammatory genes *tbx21*, *ifng*, and *csf2* [270]. Furthermore, IL-33-stimulated Th17 cells inhibit the proliferation of responder T cells *in vitro*, suggesting that IL-33 may skew their phenotype from pathogenic to immunoregulatory [270].

Cytokine therapies that suppress pathogenic immune responses and expand regulatory populations are promising for treatment of autoimmune diseases [275]. As Th17 and Th1 T cells may contribute to MS pathogenesis [7], there is great interest in developing an IL-33 therapy to skew the immune response towards a Treg or Th2 phenotype, particularly in the secondary lymphoid organs (SLOs), sites of autoreactive T cell priming [276][277][278]. However, the clinical utility of unmodified IL-33 is hindered by its short plasma half-life [279] and immunotoxicity through the induction of type 2 cytokine expression and associated cellular responses [280]. In a study evaluating the impact of recombinant IL-33 on experimental autoimmune encephalomyelitis (EAE), a murine model of neuroinflammation, daily cytokine administration was required to achieve moderate disease suppression [281]. Because unmodified IL-33 has a molecular weight of less than 40 kD, the threshold size of renal clearance [282], and lacks recycling mechanisms such as binding to neonatal Fc receptor, it is rapidly degraded by proteolytic enzymes in the bloodstream or cleared by the kidneys [279]. This results in poor trafficking and persistence in the SLOs [279]. Hence, it must be administered frequently to achieve therapeutic efficacy, which could lead to dose-limiting toxicity [283].

Serum albumin (SA) is the most abundant protein in blood plasma [284]. We have previously shown that recombinant fusion of interleukin-4 (IL-4) to SA extends the plasma

half-life of IL-4 and increases its persistence in the SLOs [219]. These effects are mediated, in part, by the protein's interaction with the neonatal Fc receptor [219]. Here, we focused on a cytokine that expands both Treg subsets and protective type 2 immune cells, with the objective of restoring homeostasis during an overactive Th17 response. For this purpose, we recombinantly fused IL-33 to SA, generating SA IL-33. We then evaluated the impact of SA IL-33 therapy on multiple models of EAE and performed extensive immunophenotyping to characterize its impact on the immune system. SA fusion not only extended the plasma half-life of IL-33 and increased its persistence in the SLOs, but also attenuated the cytokine's bioactivity, reducing drug-related adverse events in both healthy and disease-bearing mice at immunity-modulating doses. Prophylactic administration of SA IL-33 prevented the development of EAE. Furthermore, therapeutic treatment reduced the severity of both chronic and relapsing-remitting disease. At the cellular level, SA IL-33 suppressed the infiltration of $CD45^+$ cells, including disease-causing MOG $Tetramer^+$ Th17 T cells, as well as IFN-γ and TNF-α levels in the spinal cord homogenate of EAE-bearing mice. Strikingly, SA IL-33-treated mice also displayed elevated levels of spinal cord amphiregulin, a tissue-repair associated growth factor. In the SLOs, SA IL-33 treatment expanded ILC2s, M2 macrophages, $ST2^+$ Tregs, and Th2 T cells, altogether suggesting that this engineered molecule ameliorates neuroinflammation by promoting immunoregulation with minimal immunotoxicity.

3.3 Materials and Methods

3.3.1 Mice

Female, 8-wk-old C57BL/6 mice were purchased from Charles River. Female 6-wk-old SJL/JCrHsd mice were purchased from Envigo. The mice were acclimated at the University of Chicago Animal Facility for 2 wk prior to use. All experiments and procedures in this study were performed in accordance with the Institutional Animal Care and Use Committee

at the University of Chicago.

3.3.2 Expression and Purification of Recombinant SA IL-33

To produce SA IL-33, codon optimized DNA sequences encoding mouse serum albumin without its pro-peptide (amino acids 25-608 of the entire serum albumin sequence), mouse IL-33 and a $(GGGS)_2$ linker were synthesized and subcloned into the mammalian expression vector pcDNA3.1(+) by GenScript Biotech. To enable affinity purification, a sequence encoding for a hexahistidine (H_6) tag was added along the C-terminus. The amino acid sequence of SA IL-33 is displayed in Table 3.1. SA IL-33 was expressed in suspension-adapted HEK 293F cells (Gibco) cultured in FreeStyle 293 Expression Medium (Gibco). On the day of transfection, HEK cells were resuspended in fresh media at a density of 1 x 10^6 cells mL^{-1}. A mixture of 1 µg mL^{-1} SA IL-33 plasmid DNA and 2 µg mL^{-1} linear 25 kD polyethyleneimine (Polysciences) prepared in OptiPRO Serum Free Medium (Gibco) was added to suspension cells sequentially. The transfected cells were incubated at 37°C in 5% CO_2 with orbital shaking at 135 rpm. After 7 days of culture, the HEK cell supernatant was collected, centrifuged at 4,000g for 10 min, and filtered through a 0.22-µm filter (Corning). Protein purification was carried out using an ÄKTA Pure 25 Chromatography System (Cytiva) as described previously [219][218][285][286][287][288][289]. Briefly, affinity chromatography was performed by loading the supernatant into a 5 mL HisTrap HP column (Cytiva). The column was washed with binding buffer (20 mM NaH_2PO_4, 0.5 M NaCl, 20 mM imidazole at pH 7.4). The H_6-tagged protein was eluted from the column by flowing a gradient of elution buffer (500 mM imidazole, 20 mM NaH_2PO_4, 0.5 M NaCl at pH 7.4). The protein was then loaded into a HiLoad Superdex 200 Prep Grade column (Cytiva) for further purification by size exclusion chromatography and eluted in phosphate buffered saline. All purification steps were performed at 4°C.

Table 3.1: Amino Acid Sequence of SA IL-33

Protein Name	Amino Acid Sequence
SA-IL-33-H_6	EAHKSEIAHRYNDLGEQHFKGLVLIAFSQYLQKCSYDEHAK LVQEVTDFAKTCVADESAANCDKSLHTLFGDKLCAIPNLRE NYGELADCCTKQEPERNECFLQHKDDNPSLPPFERPEAEA MCTSFKENPTTFMGHYLHEVARRHPYFYAPELLYYAEQYN EILTQCCAEADKESCLTPKLDGVKEKALVSSVRQRMKCSSM QKFGERAFKAWAVARLSQTFPNADFAEITKLATDLTKVNKE CCHGDLLECADDRAELAKYMCENQATISSKLQTCCDKPLLK KAHCLSEVEHDTMPADLPAIAADFVEDQEVCKNYAEAKDVF LGTFLYEYSRRHPDYSVSLLLRLAKKYEATLEKCCAEANPPA CYGTVLAEFQPLVEEPKNLVKTNCDLYEKLGEYGFQNAILVR YTQKAPQVSTPTLVEAARNLGRVGTKCCTLPEDQRLPCVED YLSAILNRVCLLHEKTPVSEHVTKCCSGSLVERRPCFSALTVD ETYVPKEFKAETFTFHSDICTLPEKEKQIKKQTALAELVKHK PKATAEQLKTVMDDFAQFLDTCCKAADKDTCFSTEGPNLVT RCKDALAGGGGSGGGSSIQGTSLLTQSPASLSTYNDQSVSFVL ENGCYVINVDDSGKDQEQDQVLLRYYESPCPASQSGDGVDG KKLMVNMSPIKDTDIWLHANDKDYSVELQRGDVSPPEQAFF VLHKKSSDFVSFECKNLPGTYIGVKDNQLALVEEKDESCNNI MFKLSKIHHHHHH

3.3.3 Characterization of Recombinant SA IL-33 Protein Purity

SDS-PAGE was performed as described previously [218][219][285][286][287][288][289]. Briefly, the purified SA IL-33 protein was loaded onto a 4-20% Mini-PROTEAN TGX precast polyacrylamide gel (Bio-Rad) and gel electrophoresis was performed. To visualize the protein bands, the gel was then stained with SimplyBlue SafeStain (Invitrogen), according to the manufacturer's instructions. Gel images were acquired using a ChemiDoc XRS+ Gel Imaging System (Bio-Rad). SA IL-33 was verified to be $> 90\%$ pure. To validate that the protein band on the SDS-PAGE gel corresponded to the H_6-tagged SA IL-33, an anti-histidine Western blot was performed as described previously [219][285][286][287][288][289]. Briefly, purified SA IL-33 was separated on a 4-20% Mini-PROTEAN TGX gel (Bio-Rad) and transferred onto a PVCF membrane (Thermo Fisher Scientific). The H_6-tagged protein was stained with

an HRP anti-histidine tag antibody (clone J099B12, Biolegend) at 1:2500 dilution [289]. The membrane was developed via Clarity Max Western ECL substrate (Bio-Rad) and imaged using the ChemiDoc XRS+ Gel Imaging System (Bio-Rad). The purified protein was confirmed to contain < 0.01 endotoxin units mL^{-1} via a HEK-Blue human TLR-4 reporter cell line (InvivoGen) assay, performed according to the manufacturer's instructions. The concentration of the protein was determined using a NanoDrop spectrophotometer (Thermo Fisher Scientific) by measuring the absorbance at 280 nm.

3.3.4 WT IL-33 and SA IL-33 Binding to Mouse ST2 (IL-33 Receptor)

The binding of WT and SA IL-33 to mouse ST2/IL-33R was assessed using an enzyme-linked immunosorbent assay (ELISA). Flat bottom, 96-well plates were coated with 4 µg mL^{-1} recombinant mouse ST2/IL-33R Fc Chimera Protein (R&D Systems) in PBS overnight at 4°C. The following day, the wells were washed three times in PBS-T (PBS supplemented with 0.05% (v/v) Tween-20 (Bio-Rad)) and then blocked with PBS supplemented with 2% (w/v) bovine serum albumin (Sigma Aldrich) and 0.1% (v/v) Tween-20 for 1 hr at room temperature. After blocking, wells were washed once with PBS-T and incubated with the indicated concentrations of WT IL-33 or SA IL-33 for 2 hr at room temperature. Following three PBS-T washes, the wells were then incubated with a biotinylated antibody against mouse IL-33 (R&D Systems) for 2 hr at room temperature. The wells were then washed three times with PBS-T and incubated with a horseradish peroxide-conjugated antibody against mouse IL-33 (R&D Systems) for 1 hr at room temperature. After five washes with PBS-T, the ST2-receptor bound IL-33 was detected via tetramethylbenzidine (TMB) substrate (Thermo Fisher Scientific). Stop Solution (1N H_2SO_4) was added to the TMB wells after 20 min incubation at room temperature. The absorbance (optical density) was measured at 450 nm and 570 nm using an Epoch Microplate Spectrophotometer (BioTek). The background signal at 570 nm was subtracted from the optical density at 450 nm, as described previously

[290][291]. The affinity (dissociation constant, K_d) of WT IL-33 and SA IL-33 against ST2/IL-33R was calculated using a nonlinear, four parameter, dose-response curve fit model in Prism software (v.9, GraphPad).

3.3.5 Plasma Pharmacokinetics of WT IL-33 and SA IL-33

Female, 8-wk-old, naive C57BL/6 mice (Charles River) were administered 26 µg WT IL-33 or SA IL-33 (equivalent to 26 µg WT IL-33) by subcutaneous injection in the dorsal flank. Mice were bled 2, 4, 8, 12, 24, 36, 48, 72, and 96 hr after IL-33 administration. Blood was stored in EDTA-containing heparinized tubes (BD Biosciences). Plasma was separated by centrifugation at 1,000g for 10 min. The concentration of IL-33 in the plasma was measured using a Mouse IL-33 DuoSet ELISA (R&D Systems) according to the manufacturer's instructions. The *in vivo* half-life of WT IL-33 and SA IL-33 was estimated using a one-phase, exponential decay model in Prism software (v.9, GraphPad).

3.3.6 Tissue Biodistribution of WT IL-33 and SA IL-33

Female, 8-wk-old, naive C57BL/6 mice (Charles River) were administered 26 µg WT IL-33 or SA IL-33 (equivalent to 26 µg WT IL-33) by subcutaneous injection in the dorsal flank. Following cardiac perfusion with PBS, the iliac lymph nodes, cervical lymph nodes, brachial lymph nodes, spleen, liver, spinal cord, brain, kidney, lungs, and heart were collected 6 hr or 48 hr post-IL-33 administration. Organs were immersed in Lysing Matrix D tubes (MP Biomedicals) containing Tissue Protein Extraction Reagent (Thermo Fisher Scientific) supplemented with Complete Protease Inhibitor (Roche), and homogenized using a FastPrep-24 5G bead beating grinder and lysis system (MP Biomedicals) for 40 sec at 5,000 beats minute^{-1}, as described previously [219][286][287]. To separate tissue homogenate from debris, samples were centrifuged at 10,000g for 10 min, and the supernatant was collected. The concentration of IL-33 in the tissue homogenate was then measured using a Mouse IL-33

DuoSet ELISA (R&D Systems), according to the manufacturer's instructions. IL-33 levels were normalized by total protein content, which was measured using the BCA Protein Assay (Pierce), according to the manufacturer's instructions.

3.3.7 Isolation of Type 2 Innate Lymphoid cells (ILC2s) from Murine Lungs

Lung tissues from female, 8-wk-old, naive C57BL/6 mice (Charles River) were perfused in PBS and mechanically dissociated [290][292]. Tissues were then digested with Collagenase D (2mg mL^{-1}, Sigma Aldrich) and Collagenase IV (2mg mL^{-1}, Gibco) in Dulbecco's Modified Eagle Medium (DMEM) (Gibco) supplemented with 5% heat-inactivated FBS (Gibco) and 1.2 mM $CaCl_2$ (Sigma Aldrich) for 1 hr at 37°C [290][292]. Lung cell suspensions were strained through a sterile, 70 µm filter (Corning). Red blood cells were lysed using ACK Lysing Buffer (Gibco) for 5 min at 4°C. The lysing buffer was quenched with 25 mL DMEM containing 10% FBS. Single cell suspensions were then washed once with DMEM and resuspended in Roswell Park Memorial Institute (RMPI) Medium 1640 medium (Gibco) supplemented with 10% FBS, 1% Penicillin-Streptomycin (Pen-Strep) (Gibco) and 50 µM β-mercaptoethanol (Sigma Aldrich). ILC2s were isolated from mouse lung cell suspensions by immunomagnetic negative selection using an EasySep Mouse ILC2 Enrichment Kit (Stem Cell Technologies) according to the manufacturer's instructions. Briefly, cells were resuspended in PBS supplemented with 2% FBS and 1 mM EDTA (Invitrogen), diluted to 1 x 10^8 cells mL^{-1}, and incubated with mouse ILC2 enrichment cocktail and magnetic Streptavidin RapidSpheres that bound to non-ILC2s. Mouse ILC2s were subsequently separated from non-ILC2s via the EasySep magnet. Cells were then cultured in RMPI 1640 medium supplemented with 10% FBS, 1% Pen-strep and 50 µM β-mercaptoethanol, and rested for 6 hr at 37°C in 5% CO_2 prior to the *in vitro* bioactivity assay.

3.3.8 In Vitro Bioactivity of WT IL-33 and SA IL-33 in Murine Lung ILC2s

Murine ILC2s (50,000 cells/well) cultured in a 96-well plate (Corning) were stimulated with various concentrations of recombinant mouse IL-33 (WT IL-33) (Biolegend) or SA IL-33 for 18 hr at 37°C in 5% CO_2. The production of cytokines IL-5, IL-10, and IL-13 in the ILC2 supernatant following IL-33 treatment was measured via LEGENDplex Mouse Th Cytokine assay (Biolegend) according to the manufacturer's instructions. Cells were washed once with PBS and stained with LIVE/DEAD Fixable Aqua Dead Cell Stain Kit (Biolegend) at 1:500 dilution and anti-mouse CD16/32 antibody at 1:200 dilution in PBS at 4°C for 20 min. Cells were then washed once with FACS buffer (PBS supplemented with 2% FBS and 2 mM EDTA) and stained with the following cell surface antibodies diluted 1:200 in FACS buffer for 45 min at 4°C: anti-B220, CD3ϵ, CD4, CD5, CD8α, CD11b, CD11c, CD19, CD25, CD45, FcϵRIα, Gr-1, ICOS, NK1.1, ST2, TCR-β, TCR-$\gamma\delta$, TER-119, and Thy1.2. Cells were then fixed in 2% paraformaldehyde (Sigma Aldrich) for 1 hr at 4°C, washed three times, and resuspended in FACS buffer. Data was acquired on an LSR-Fortessa (BD Biosciences) and analyzed using FlowJo Software (v.10, BD Biosciences). The antibodies used in this experiment are summarized in Table 3.2. The EC_{50} of IL-33-induced CD25 upregulation in mouse ILC2 cells was calculated using a nonlinear, four parameter, dose response curve fit model in Prism software (v.9, GraphPad).

Table 3.2: Antibodies for Staining ILC2s in IL-33 Bioactivity Assay

Specificity	Fluorochrome	Clone Name	Dilution	Vendor
B220	FITC	RA3-6B2	1:200	Biolegend
CD3ϵ	FITC	500A2	1:200	Biolegend
CD4	FITC	GK1.5	1:200	Biolegend
CD5	FITC	53-7.3	1:200	Biolegend
CD8α	FITC	53-6.7	1:200	Biolegend
CD11b	FITC	M1/70	1:200	Biolegend
CD11c	FITC	N418	1:200	Biolegend
CD16/32	N/A	93	1:200	Biolegend
CD19	FITC	6D5	1:200	Biolegend
CD25	PerCP-eFluor 710	PC 61.5	1:200	eBioscience
CD45	BUV 395	30-F11	1:200	BD Biosciences
FcϵRIα	FITC	MAR-1	1:200	Biolegend
Gr-1	FITC	RB6-8C5	1:200	Biolegend
ICOS	APC	DX29	1:200	BD Biosciences
Live/Dead	BV 510	N/A	1:500	eBioscience
NK1.1	FITC	PK136	1:200	Biolegend
ST2	PE	U29-93	1:200	BD Biosciences
TCR-β	FITC	H57-597	1:200	Biolegend
TCR-$\gamma\delta$	FITC	GL3	1:200	Biolegend
TER-119	FITC	TER-119	1:200	Biolegend
Thy1.2	PE-Cy7	53-2.1	1:200	Biolegend

3.3.9 In Vitro Bioactivity of WT IL-33 and SA IL-33 in Human Embryonic Lidney (HEK)-Blue IL-33 Cells

The HEK-Blue IL-33 reporter cell line was developed by InvivoGen and consists of HEK293 cells transfected with the human IL1RL1 gene [293][294]. These cells also express an NF-κB/AP-1-inducible secreted embryonic alkaline phosphatase (SEAP) reporter [293][294]. The binding of IL-33 to IL-33R on HEK-Blue IL-33 cells triggers a signaling cascade that induces NF-κB activation and, in turn, SEAP production, measured using QUANTI-Blue reagent [293][294]. HEK-Blue IL-33 cells (InvivoGen) were cultured in DMEM supplemented with 4.5 g/L glucose (Gibco), 2 mM L-glutamine (Gibco), 10% heat-inactivated FBS, 1% Pen-Strep, and 100 µg/mL Normocin (InvivoGen), according to the manufacturer's instruc-

tions. HEK-Blue IL-33 cells (50,000 cells/well) seeded on a 96-well plate (Corning) in a total volume of 200 µL/well were stimulated with the indicated concentrations of WT IL-33 (Biolegend) or SA IL-33 overnight at 37°C in 5% CO_2. A total of 20 µL of HEK-Blue IL-33 supernatant was diluted in 180 µL QUANTI-Blue Solution (InvivoGen) in a flat-bottom 96-well plate and incubated at 37°C for 1 hr. Untreated supernatant was used as the negative control. SEAP levels were detected at 620 nm using an Epoch Microplate Spectrophotometer (BioTek). The EC_{50} of IL-33-induced SEAP levels was calculated using a nonlinear, four parameter, dose response curve fit model in Prism software (v.9, GraphPad).

3.3.10 In Vivo Assessment of IL-33 Toxicity in Healthy Mice

To assess the impact of IL-33 administration on naive mice, female 8-wk-old, C57BL/6 mice (Charles River) were subcutaneously injected with PBS, 26 µg of WT IL-33, or equimolar SA IL-33 in the dorsal flank. 24 hr after treatment, blood was collected and stored in EDTA-containing, heparinized tubes. The plasma was separated by centrifugation at 1,000g for 10 min. The concentration of the cytokines IL-5, IL-6, IL-9, IL-10, and IL-13 in the plasma was quantified using the LEGENDplex Mouse Th Cytokine Panel (Biolegend), according to the manufacturer's instructions. Any values below limit of detect were considered as the limit of detection.

3.3.11 MOG_{35-55} Experimental Autoimmune Encephalomyelitis Model

Female, 8-wk-old, C57BL/6 mice were purchased from Charles River and allowed to acclimate in the animal facility for 2 wk. Experimental autoimmune encephalomyelitis (EAE) was induced, as described previously [219], by subcutaneously immunizing 10-wk-old mice with MOG_{35-55} antigen emulsified in Complete Freund's Adjuvant (CFA) (Hooke Laboratories) in the dorsal flank. To promote permeability of the blood-brain barrier, 2 hr after MOG_{35-55} immunization, and again on the following day, pertussis toxin from *Bordetella pertussis*

(Hooke Laboratories) dissolved in PBS was administered intraperitoneally, according to the manufacturer's instructions. EAE disease score was determined daily from day 7 until study endpoint by a blinded investigator according to the clinical score criteria established by Hooke Laboratories, as described previously [219]. In prophylactic treatment experiments, mice were administered PBS, WT IL-33, or SA IL-33 subcutaneously in the dorsal flank every other day from day 8 post-immunization until study endpoint, unless otherwise specified. As a positive control, mice were administered fingolimod (FTY 720) orally (1 mg/kg body weight) from day 8 until study endpoint. In therapeutic treatment experiments, EAE-bearing mice with already-established disease were subcutaneously administered PBS or SA IL-33 in the dorsal flank every other day from day 20 post-immunization until study endpoint. FTY 720 was administered orally (1 mg/kg body weight) every day from day 20 until study endpoint. To prevent cage effects, treatments were assigned evenly across all cages. In therapeutic treatment experiments, the average clinical score at the start of treatment was the same across all treatment groups.

3.3.12 $PLP_{139-151}$ Relapsing-Remitting EAE Model

Female, 6-wk-old, SJL/JCrHsd mice were purchased from Envigo and allowed to acclimate in the animal facility for 2 wk. EAE was induced, as described previously [290], by subcutaneously immunizing 8-wk-old mice with $PLP_{139-151}$ antigen emulsified in CFA (Hooke Laboratories) in the dorsal flank. Approximately 2 hr after $PLP_{139-151}$ immunization, and again on day 2 post-immunization, pertussis toxin (Hooke Laboratories) dissolved in PBS was administered intraperitoneally, according to the manufacturer's instructions. EAE disease score was determined daily from day 7 to endpoint by a blinded investigator according to the scoring criteria established by Hooke Laboratories, as described previously [290]. After the first episode of paralysis, mice were subcutaneously administered PBS or SA IL-33 in the dorsal flank every other day from day 18 post-immunization until day 36. FTY 720 was

administered orally (1 mg/kg body weight) every day from day 18 to day 36. To prevent cage effects, treatments were assigned evenly across all cages. The average clinical score at the start of treatment was the same across all groups. The acute phase was defined as the first episode of disease [150][153][290][295]. Remission was defined as a period of clinical improvement following the first episode of disease or a relapse, during which the peak disease score decreased by ≥ 1 grade for ≥ 2 consecutive days [150][153][290][295]. Relapse was defined as an increase in the minimum remission disease score by ≥ 1 grade [150][153][290][295].

3.3.13 Preparation of Single-Cell Suspensions from EAE Tissues

At the endpoint of EAE experiments, the spinal cord, cervical and iliac lymph nodes (CNS-dLNs), and spleen were harvested from each mouse. Spinal cord and CNS-dLNs were incubated with Collagenase D (2mg mL^{-1}, Sigma Aldrich) in DMEM (Gibco) supplemented with 10% heat-inactivated FBS (Gibco) and 1.2 mM $CaCl_2$ (Sigma Aldrich) for 45 min at 37°C [290][291]. Lymph nodes, spinal cords, and spleens were mechanically dissociated and strained through a sterile, 70 µm filter (Corning). Red blood cells in the spleen suspensions were lysed using ACK Lysing Buffer (Gibco) for 5 min and quenched with 25 mL DMEM supplemented with 10% FBS [290][291]. Single cell suspensions were then washed once with DMEM supplemented with 10% FBS and resuspended in RMPI 1640 medium (Gibco) supplemented with 10% FBS and 1% Pen-Strep (Gibco).

3.3.14 Flow Cytometry of EAE Tissues

Single-cell suspensions of the spinal cord, CNS-dLNs, and spleen from EAE-bearing mice were added to 96-well U-bottom plates. Cells were washed once with PBS and stained with LIVE/DEAD Fixable Aqua or Violet Dead Cell Stain Kit at 1:500 dilution and anti-mouse CD16/32 antibody at 1:200 dilution in PBS at 4°C for 20 min. Cells were then washed once with FACS buffer (PBS supplemented with 2% FBS and 2 mM EDTA) and stained

with the following cell surface antibodies diluted 1:200 in FACS buffer for 45 min at 4°C: anti-B220, CD3ϵ, CD4, CD5, CD8α, CD11b, CD11c, CD19, CD25, CD45, CD69, CD86, FcϵRIα, F4/80, Gr-1, ICOS, KLRG1, MHC class II (I-A/I-E), NK1.1, PD-1, ST2, TCR-β, TCR-$\gamma\delta$, TER-119, and Thy1.2. To detect MOG-specific cells, the cells were washed once in PBS and stained with PE-conjugated MOG_{38-49} Tetramer (NIH Tetramer Core Facility) diluted 1:100 in PBS for 45 min at room temperature. For intracellular staining, cells were fixed and permeabilized for 1 hr at 4°C (Foxp3/Transcription Factor Fixation and Permeabilization Kit, eBioscience). Cells were then washed twice and stained overnight at 4°C with the following intracellular antibodies diluted 1:200 in Permeabilization buffer (eBioscience): anti-Arginase-1, CD206, CTLA-4, FoxP3, GATA3, and RORγt. After staining, cells were washed twice and resuspended in FACS buffer. Data was acquired on an LSR-Fortessa (BD Biosciences) and analyzed using FlowJo Software (v.10, BD Biosciences). The antibodies used to stain ILC2s in CNS-dLNs and spleen, T cells in the spinal cord, myeloid cells in the spinal cord, T cells in the CNS-dLNs and spleen, and myeloid cells in the CNS-dLNs and spleen are summarized in the Tables 3.3, 3.4, 3.5, 3.6, and 3.7, respectively.

Table 3.3: Antibodies for Staining ILC2s in EAE CNS-dLNs and Spleen

Specificity	Fluorochrome	Clone Name	Dilution	Vendor
B220	FITC	RA3-6B2	1:200	Biolegend
CD3ϵ	FITC	500A2	1:200	Biolegend
CD4	FITC	GK1.5	1:200	Biolegend
CD5	FITC	53-7.3	1:200	Biolegend
CD8α	FITC	53-6.7	1:200	Biolegend
CD11b	FITC	M1/70	1:200	Biolegend
CD11c	FITC	N418	1:200	Biolegend
CD16/32	N/A	93	1:200	Biolegend
CD19	FITC	6D5	1:200	Biolegend
CD25	PerCP-eFluor 710	PC 61.5	1:200	eBioscience
CD45	BUV 395	30-F11	1:200	BD Biosciences
CD69	BUV 737	H1.2F3	1:200	BD Biosciences
FcϵRIα	FITC	MAR-1	1:200	Biolegend
GATA3	BV 421	L50-923	1:200	BD Biosciences
Gr-1	FITC	RB6-8C5	1:200	Biolegend
ICOS	APC	DX29	1:200	BD Biosciences
KLRG1	BV 605	2F1/KLRG1	1:200	Biolegend
Live/Dead	BV 510	N/A	1:500	eBioscience
NK1.1	FITC	PK136	1:200	Biolegend
TCR-β	FITC	H57-597	1:200	Biolegend
TCR-$\gamma\delta$	FITC	GL3	1:200	Biolegend
TER-119	FITC	TER-119	1:200	Biolegend
Thy1.2	PE-Cy7	53-2.1	1:200	Biolegend
ST2	PE	U29-93	1:200	BD Biosciences

Table 3.4: Antibodies for Staining T Cells in EAE Spinal Cord

Specificity	Fluorochrome	Clone Name	Dilution	Vendor
CD3ϵ	BUV 395	145-2C11	1:200	BD Biosciences
CD4	BUV 496	GK1.5	1:200	BD Biosciences
CD8α	BV 605	53-6.7	1:200	Biolegend
CD16/32	N/A	93	1:200	Biolegend
CD45	APC-Cy7	30-F11	1:200	BD Biosciences
CD45	BV 786	30-F11	1:200	BD Biosciences
Live/Dead	BV 421	N/A	1:500	eBioscience
MOG	APC	N/A	1:100	NIH Tetramer
RORγt	APC	Q31-378	1:200	BD Biosciences
RORγt	BV 786	Q31-378	1:200	BD Biosciences

Table 3.5: Antibodies for Staining Myeloid Cells in EAE Spinal Cord

Specificity	Fluorochrome	Clone Name	Dilution	Vendor
CD11b	PerCP-Cy5.5	M1/70	1:200	BD Biosciences
CD11c	PE-Cy7	HL3	1:200	Biolegend
CD16/32	N/A	93	1:200	Biolegend
CD45	BV 786	30-F11	1:200	BD Biosciences
CD86	BUV 396	GL1	1:200	BD Biosciences
CD206	PE	Y17-505	1:200	BD Biosciences
F4/80	APC	T45-2342	1:200	BD Biosciences
I-A/I-E	APC-Cy7	M5/114.15.2	1:200	Biolegend
Live/Dead	BV 421	N/A	1:500	eBioscience

Table 3.6: Antibodies for Staining T Cells in EAE CNS-dLNs and Spleen

Specificity	Fluorochrome	Clone Name	Dilution	Vendor
CD3ϵ	BUV 395	145-2C11	1:200	BD Biosciences
CD4	BUV 496	GK1.5	1:200	BD Biosciences
CD8α	BUV 737	5H10-1	1:200	BD Biosciences
CD16/32	N/A	93	1:200	Biolegend
CD25	APC-Cy7	PC61	1:200	BD Biosciences
CD152	PerCP-Cy5.5	UC10-4B9	1:200	Biolegend
CD279	PE-Cy7	J43	1:200	BD Biosciences
FoxP3	AF 488	MF23	1:200	BD Biosciences
GATA3	BV 421	L50-923	1:200	BD Biosciences
Live/Dead	BV 510	N/A	1:500	eBioscience
MOG	APC	N/A	1:100	NIH Tetramer
RORγt	BV 786	Q31-378	1:200	BD Biosciences
ST2	PE	U29-93	1:200	BD Biosciences

Table 3.7: Antibodies for Staining Myeloid Cells in EAE CNS-dLNs and Spleen

Specificity	Fluorochrome	Clone Name	Dilution	Vendor
Arginase-1	AF 488	A1exF5	1:200	eBioscience
CD11b	PE-Cy7	M1/70	1:200	BD Biosciences
CD16/32	N/A	93	1:200	Biolegend
CD45	APC-Cy7	30-F11	1:200	BD Biosciences
CD86	BUV 396	GL1	1:200	BD Biosciences
CD206	BV 785	C068C2	1:200	Biolegend
F4/80	PE	T45-2342	1:200	BD Biosciences
Live/Dead	BV 510	N/A	1:500	eBioscience

3.3.15 Ex Vivo Myelin Oligodendrocyte Glycoprotein Restimulation Assay

For *ex vivo* restimulation assays, 5.0 x 10^5 cells isolated from CNS-dLNs or spleen of PBS, SA IL-33, or FTY 720-treated EAE-bearing mice were resuspended in RMPI 1640 medium supplemented with 10% FBS and 1% Pen-Strep, and seeded in 96-well U-bottom plates, as described previously [219][290]. The cells were restimulated with a final concentration of 50 µg mL^{-1} mouse Myelin Oligodendrocyte Glycoprotein (MOG) Protein (Anaspec) for 72 hr at 37°C with 5% CO_2 [219][290]. After 72 hr, cells were centrifuged at 1,000g for 5 min and the supernatant was collected for cytokine analysis using LEGENDplex Mouse Th Cytokine Panel (Biolegend).

3.3.16 Detection of Cytokines in the Spinal Cord Homogenate of EAE Mice

Spinal cords of PBS, SA IL-33, or FTY 720-treated EAE-bearing mice were immersed in Lysing Matrix D tubes (MP Biomedicals) containing Tissue Protein Extraction Reagent supplemented with Complete Protease Inhibitor, and homogenized using a FastPrep-24 5G bead beating grinder and lysis system for 40 sec at 5,000 beats per min. To separate the homogenate from tissue debris, samples were centrifuged at 10,000g for 10 min and the supernatant was collected. The concentration of cytokines in the tissue homogenate was then measured using a LEGENDplex Mouse Th Cytokine assay (Biolegend), LEGENDplex Mouse Free Active TGF-β1 assay (Biolegend), and Mouse Amphiregulin DuoSet ELISA kit (R&D Sytems), according to the manufacturer's instructions. Cytokine levels were normalized by total protein content. Total protein content was measured using the BCA Protein Assay (Pierce), according to the manufacturer's instructions.

3.3.17 Statistical Analysis

Prism software (v.9, GraphPad) was used to evaluate statistically significant differences between experimental groups. For multiple comparisons, one-way analysis of variance (ANOVA)

followed by the Tukey post hoc test was performed, unless otherwise specified. For comparison of two experimental groups, a two-tailed Student's T-test was used, unless otherwise specified. For comparison of two survival curves, the Log-rank (Mantel-Cox) test was performed. All statistical analyses are stated in the figure legends.

3.4 Results

3.4.1 Fusion of IL-33 to Serum Albumin Prolongs IL-33 Persistence in the Plasma and Secondary Lymphoid Organs

To generate SA IL-33, murine IL-33 was recombinantly fused to murine SA via a $(GGGS)_2$ flexible linker (Table 3.1, Figure 3.1a). SA IL-33 was expressed in HEK293F cells and purified via affinity-based nickel chromatography followed by size exclusion chromatography (Figure 3.2a). SDS-PAGE (Figure 3.2b) and anti-histidine western blot (Figure 3.2c) analysis of H_6-tagged SA IL-33 revealed a single protein band between the 75 and 100 kD size standards, consistent with the expected molecular weight of SA IL-33 (approximately 84 kD). IL-33 binds to the extracellular domain of ST2 (IL-33R) [254], which recruits interleukin-1 receptor accessory protein (IL-1RAcP), forming a receptor complex [296][297]. Protein folding predictions, performed using AlphaFold, identified a conformation in which SA IL-33 bound to the IL-33 co-receptors, ST2 and IL-1RAcP (Figure 3.1b). SA IL-33 binding to murine ST2 was confirmed via ELISA, with both WT and SA IL-33 binding to ST2 in a dose-dependent manner (Figure 3.1c). SA-fusion moderately increased the dissociation constant (K_d) of IL-33 by approximately 3.2-fold.

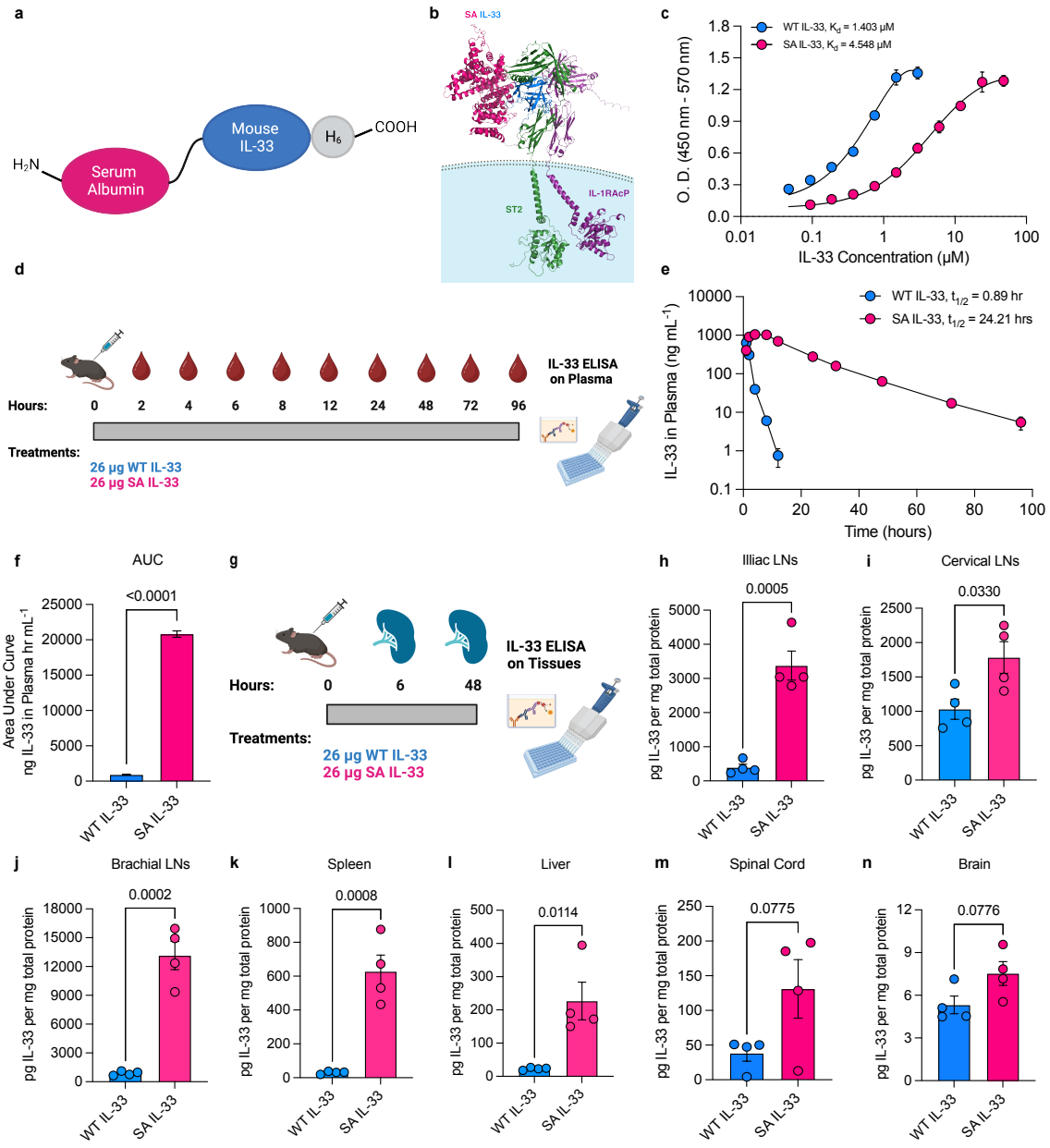

Figure 3.1: **SA fusion prolongs the persistence of IL-33 in the plasma and SLOs.** (a) Schematic of SA recombinantly fused to IL-33 via a $(GGGS)_2$ linker. (b) Protein folding prediction of SA IL-33 binding to primary IL-33 receptor, ST2, and co-receptor, IL-1RAcP. Image generated using AlphaFold. (c) Affinity (dissociation constant, K_d) of WT IL-33 and SA IL-33 against immobilized ST2 was measured using ELISA (n = 3). (d) Experimental design of pharmacokinetics study. Naive C57BL/6 mice were administered 26 μg WT IL-33 or molar e.q. SA IL-33 via s.c. injection. Blood was collected at the indicated time points and the concentration of IL-33 in the plasma was measured using ELISA (n = 3). (e, f) The e) half-life and f) area under the curve of WT and SA IL-33 in the plasma were estimated using a one-phase exponential decay model (GraphPad Prism). Continued on next page.

Figure 3.1: Continued: (g) Overview of tissue biodistribution study. Naive mice were administered 26 µg WT IL-33 or molar e.q. SA IL-33 via s.c. injection. The amount of IL-33 in the (h) iliac LNs, (i) cervical LNs, (j) brachial LNs, (k) spleen, (l) liver, (m) spinal cord, and (n) brain was determined 6 hr after s.c. injection. Organs were perfused in PBS and then homogenized for protein extraction. IL-33 levels were quantified using ELISA and normalized by total protein content (n = 4). Data represent means ± s.e.m. Statistical analysis in Figure 3.1f,h-n was performed using unpaired, two-tailed Student's T-test. P-values $<$ 0.05 are shown. Diagrams in Figure 3.1a,d,g were generated using BioRender.com.

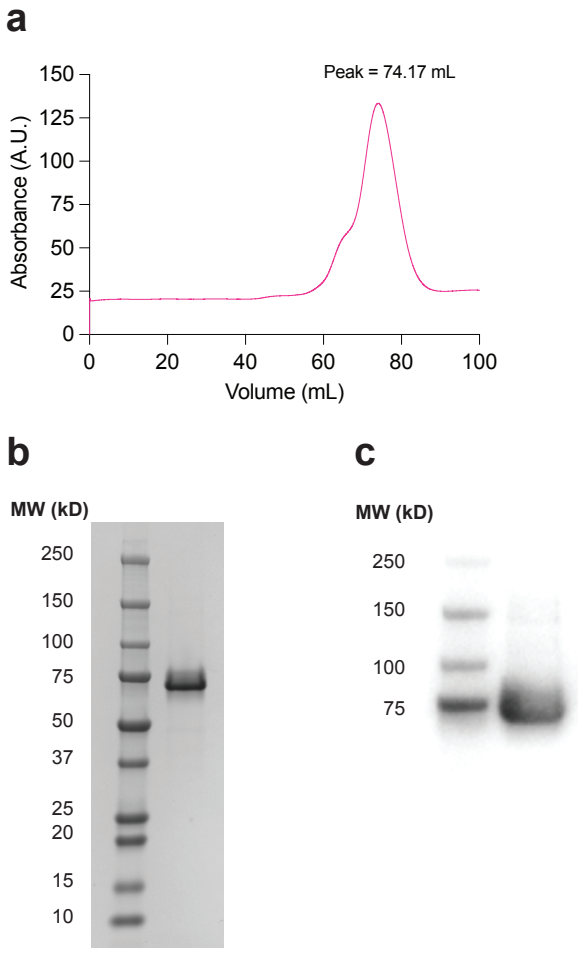

Figure 3.2: **Purification of SA IL-33.** SA IL-33 was recombinantly expressed in HEK-293F cells and purified via nickel-based chromatography. The eluted fractions were then loaded onto a size exclusion column and purified by size exclusion chromatography (a) Size-exclusion chromatogram of affinity-purified SA IL-33. (b) SDS-PAGE analysis of SA IL-33 under non-reducing conditions. (c) Anti-histidine western blot analysis of hexahistidine-tagged SA IL-33.

SA has a long plasma half-life, in part, due to its ability to undergo neonatal Fc receptor-mediated recycling [284]. To assess the impact of SA fusion on IL-33 pharmacokinetics, we subcutaneously administered naive mice with WT or equimolar SA IL-33 and quantified the amount of IL-33 in the plasma 2 hr to 96 hr post-injection (Figure 3.1d). IL-33 fusion to SA increased its plasma half-life ($t_{1/2}$) from approximately 0.9 hr to 24.2 hr (Figure 3.1e), resulting in a significantly larger area-under-the-curve (Figure 3.1f). We subsequently evaluated the impact of SA on IL-33 persistence (Figure 3.1g) in the lymph nodes, spleen, spinal cord, brain, and additional peripheral organs both 6 hr (Figure 3.1h-n, Figure 3.3a-c) and 48 hr (Figure 3.4a-j) post s.c. injection. We observed elevated IL-33 biodistribution in the iliac LNs, cervical LNs, brachial LNs, and spleen SLOs 6 hr and 48 hr, as well as in the spinal cord 48 hr post s.c. SA IL-33 injection. Likely due to its prolonged half-life, SA also increased IL-33 levels in peripheral organs including the liver, lungs, kidney, and heart at these time points (Figure 3.1l, Figure 3.3a-c, Figure 3.4e-h). Together, these data suggest that IL-33 fusion to SA prolongs the cytokine's *in vivo* plasma half-life and increases its persistence in various immunologically relevant organs for at least 48 hr post-administration.

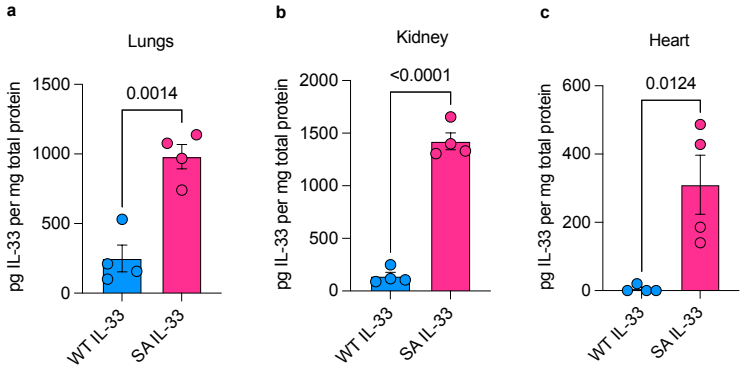

Figure 3.3: **Biodistribution of WT and SA IL-33 in the lungs, kidney, and heart 6 hr after s.c. administration.** Tissue biodistribution study was described in Figure 3.1g. The amount of IL-33 in the (a) lungs, (b) kidney, and (c) heart was determined 6 hr after s.c. WT or SA IL-33 injection. Tissues were perfused in PBS and then homogenized for protein extraction. IL-33 levels were quantified using ELISA and normalized by total protein content (n = 4). Data represent means ± s.e.m. Statistical analysis was performed using unpaired, two-tailed Student's T-test. P-values < 0.05 are shown.

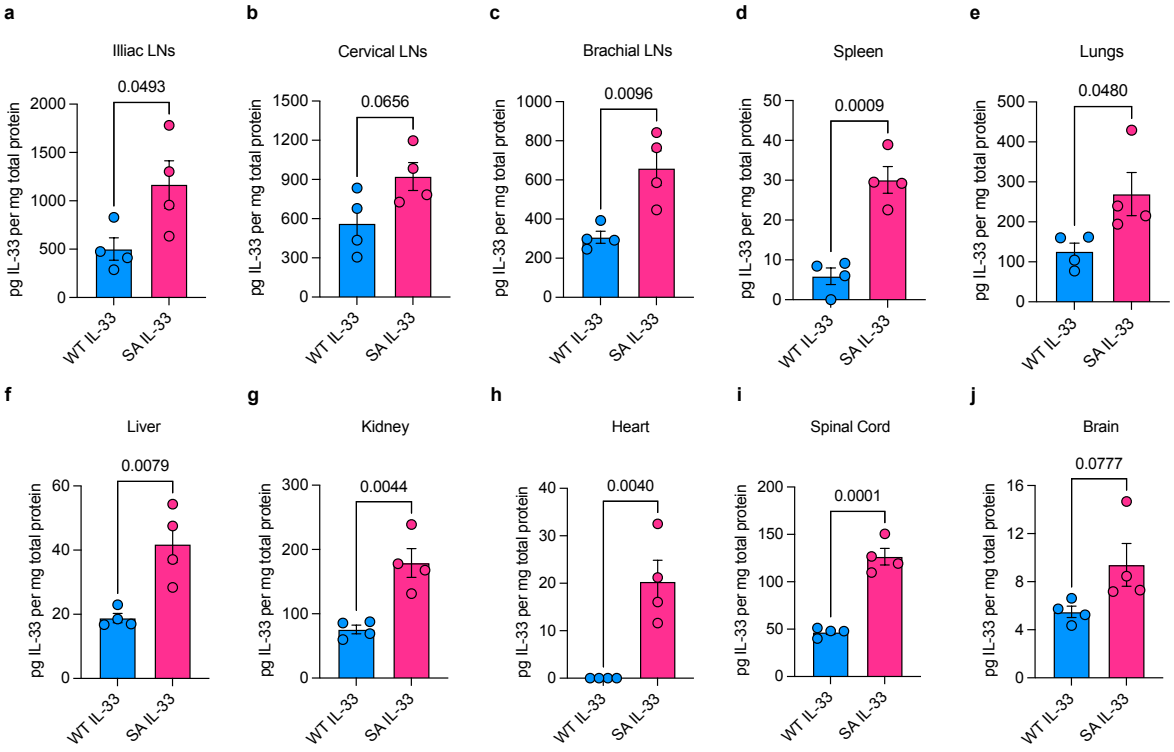

Figure 3.4: **Biodistribution of WT and SA IL-33 48 hr after s.c. administration.** Tissue biodistribution study was described in was described in Figure 3.1g. The amount of IL-33 in the (a) iliac LNs, (b) cervical LNs, (c) brachial LNs, (d) spleen, (e) lungs, (f) liver, (g) kidney, (h) heart, (i) spinal cord, and (j) brain was determined 48 hr after s.c. injection. Organs were perfused in PBS and then homogenized for protein extraction. IL-33 levels were quantified using ELISA and normalized by total protein content (n = 4). Data represent means ± s.e.m. Statistical analysis was performed using unpaired, two-tailed Student's T-test. P-values < 0.05 are shown.

3.4.2 Serum Albumin Attenuates IL-33 Bioactivity and Immunotoxicity.

IL-33 expands ST2-expressing ILC2s [269][298], immune cells present at various surveillance sites including in the lymph nodes, spleen, liver, and lungs [266][299]. In response to IL-33, ILC2s upregulate surface markers CD25 and ICOS [292], and secrete elevated levels of the type 2 cytokines IL-5 and IL-13 [266]. We hypothesized that fusion of SA, a bulky 66.5 kD protein [284], to IL-33, may attenuate IL-33 bioactivity due to steric hinderance. To assess its impact on IL-33 bioactivity, murine lung ILC2s were stimulated with various

concentrations of WT IL-33 or SA IL-33 *in vitro* for 18 hr (Figure 3.5a). Both WT IL-33 and SA IL-33 upregulated CD25 expression (Figure 3.5b, Figure 3.6) on ILC2s, and increased IL-5 (Figure 3.5c), IL-10 (Figure 3.5d), and IL-13 (Figure 3.5e) production in a dose-dependent manner. Remarkably, IL-33 fusion to SA reduced its bioactivity, increasing the EC_{50} of IL-33-induced CD25 upregulation by approximately 148-fold in murine ILC2s. Upon binding to ST2 and IL-1RAcP, IL-33 signals by recruiting the adaptor protein MyD88 followed by IRAK1, IRAK4, and TRAF6 [296][297], subsequently activating the MAPK and IκK pathways that recruit downstream signaling molecules p38, JNK, ERK1/2, and NF-κB [296][297]. Given the reported sequence homology of murine and human IL-33 [300], we also assayed the bioactivity of SA IL-33 in (human) HEK-Blue IL-33 reporter cells (Figure 3.7) which, upon IL-33 stimulation, signal through the MyD88, AP-1, and NFκB pathways, producing SEAP [294]. IL-33 fusion to SA also increased the EC_{50} of IL-33-induced SEAP production by approximately 233-fold in HEK-Blue IL-33 cells, suggesting that SA may attenuate IL-33 signaling via these pathways.

Although IL-33 plays a protective role in neuroinflammatory diseases [263], overabundant IL-33 signaling may also contribute to the production of excess type 2 cytokines, as well as mast cell, basophil, and eosinophil degranulation, maturation, and survival [280]. As these cells have been linked to conditions such as airway inflammation and allergy-associated anaphylactic shock [280], adverse effects associated with IL-33 treatment must be monitored. To characterize the immunotoxicity of SA IL-33 in naive mice, we measured plasma cytokine levels 24 hr after s.c. administration of PBS, WT IL-33, or equimolar SA IL-33 (Figure 3.5f). A single dose of SA IL-33 induced significantly lower IL-5 (Figure 3.5g), IL-6 (Figure 3.5h), IL-9 (Figure 3.5i), IL-10 (Figure 3.5j), and trended towards lower IL-13 (Figure 3.5k) production compared to WT IL-33 in the plasma.

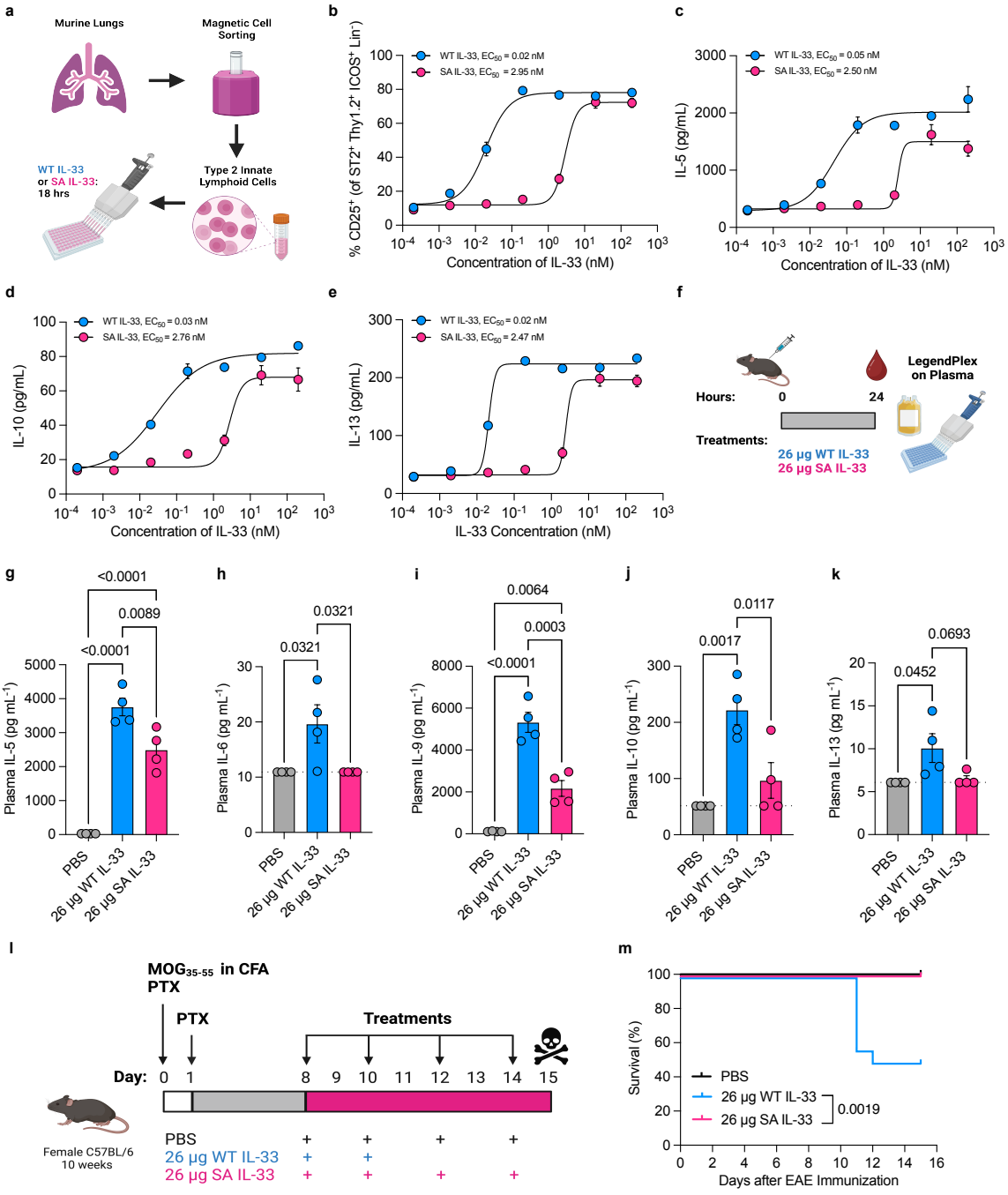

Figure 3.5: **SA fusion attenuates the bioactivity and potential type 2 immunotoxicity of IL-33.** (a) Overview of *in vitro* IL-33 bioactivity assay in murine ILC2s. (b-e). Dose-response relationship of b) CD25 upregulation and c) IL-5, d) IL-10, e) IL-13 production following 18 hr *in vitro* stimulation of ILC2s with the indicated concentrations of WT IL-33 or SA IL-33 was determined by flow cytometry and LEGENDplex (n = 3). EC_{50}, half maximum concentration, was calculated using a nonlinear, four parameter, dose-response curve fit model (GraphPad Prism). Continued on next page.

Figure 3.5: Continued: Lineage$^-$ cells were defined as cells that do not express CD3, CD4, CD8α, CD11b, CD11c, CD19, B220, TER-119, Ly6C, Ly6G, NK1.1, FcϵRIα, CD5, TCR-$\gamma\delta$, and TCR-β. (f) Overview of *in vivo* IL-33 toxicity study in naive C57BL/6 mice. Mice were administered PBS, 26 µg WT IL-33 or molar e.q. SA IL-33 via s.c. injection (n = 4 mice/group). Blood was collected after 24 hr. (g-k) The concentration of g) IL-5, h) IL-6, i) IL-9, j) IL-10, and k) IL-13 in the plasma was measured using LEGENDplex. Values below the limit of detect were considered as the limit of detection. (i) Overview of IL-33 toxicity study in EAE-bearing mice. EAE was induced in C57BL/6 mice by s.c. immunization with MOG_{35-55}/CFA followed by i.p. injections of PTX on days 0 and 1. Mice were administered s.c. PBS, s.c. 26 µg WT IL-33 or molar e.q. SA-IL-33 every other day from day 8 after MOG_{35-55} immunization (n = 14-16 mice/group, pooled from two independent experiments). WT IL-33 treatment was discontinued after day 10 because 7 out of 14 mice became moribund. Data represent means ± s.e.m. Statistical analysis was performed using ordinary one-way ANOVA with Tukey's multiple comparisons tests in (g-k) or Log-rank (Mantel-Cox) test comparing every two groups in (m). P-values < 0.05 are shown. Diagrams in (a, f, l) were created in BioRender.com.

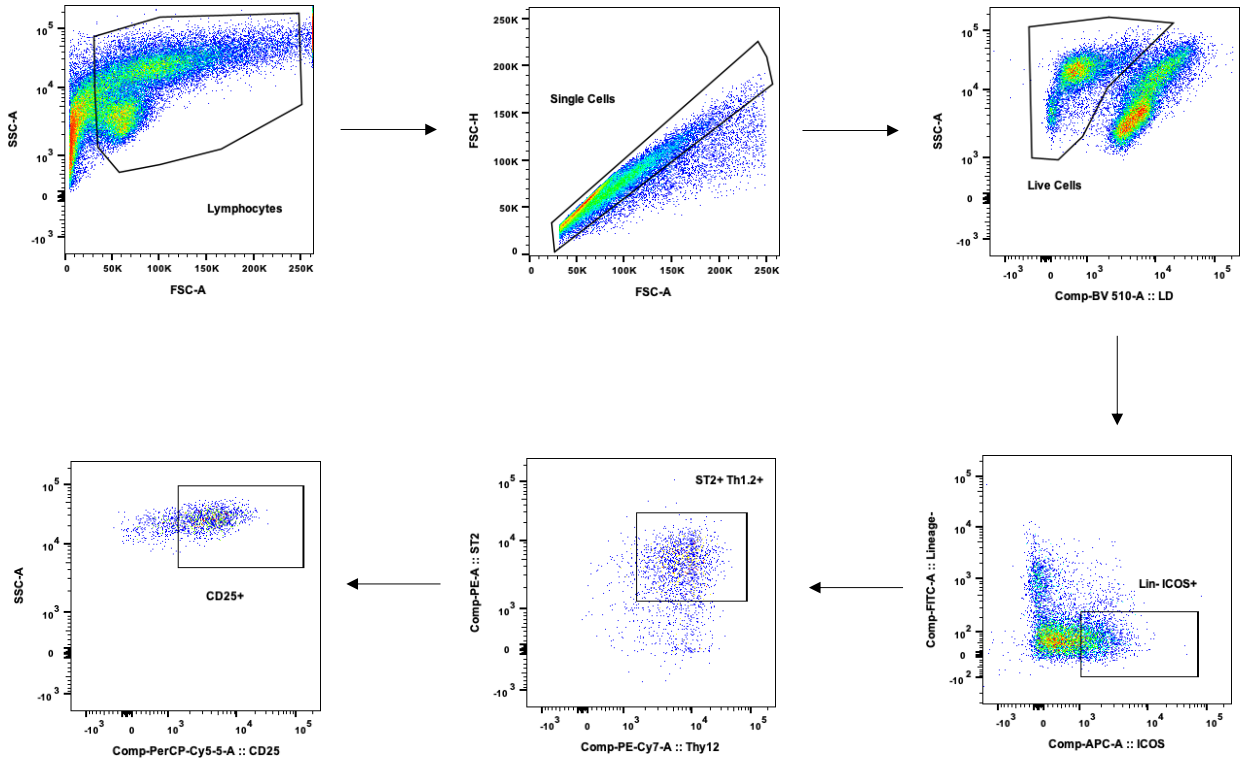

Figure 3.6: **Flow cytometry gating strategy for identification of lung CD25$^+$ ILC2s following *in vitro* IL-33 stimulation.** ILC2s were harvested from murine lungs and stimulated with the indicated concentrations of WT IL-33 or SA IL-33 for 18 hr as described in Figure 3.5a.

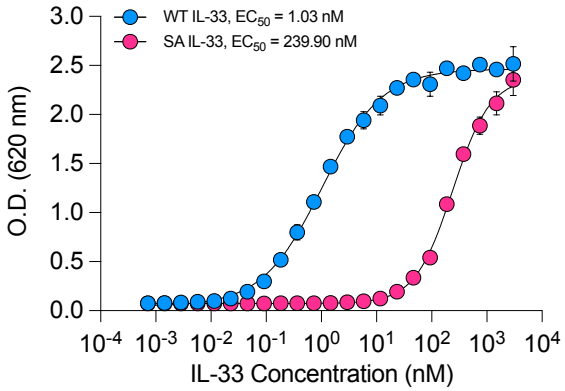

Figure 3.7: **Bioactivity of mouse WT IL-33 and SA IL-33 in IL-33R-expressing human cells.** Dose-response relationship of HEK-Blue IL-33 cell production of SEAP following overnight stimulation with the indicated concentrations of mouse WT and SA IL-33 (n = 3). The NF-κB/AP-1-mediated SEAP response was quantified using QUANTI-Blue solution, a SEAP detection regent. Optical density (OD) was read at 620 nm. EC_{50}, half maximum concentration, was calculated using a nonlinear, four parameter, dose-response curve fit model (GraphPad Prism).

Next, we assessed the toxicity of SA IL-33 in EAE-bearing mice by s.c. administering PBS, WT IL-33, or equimolar SA IL-33 every-other day beginning on day 8 post disease induction (Figure 3.5l). Unexpectedly, following two doses of WT IL-33, 50% of mice (7 out of 14 mice) became moribund and had to be euthanized, whereas no mortality occurred in mice that received equimolar SA IL-33 (Figure 3.5m). Overall, the reduction in type 2 cytokine production and lack of mortality in SA IL-33-treated mice in healthy and disease-bearing mice, respectively, suggests that in the contexts evaluated, activity-attenuated SA IL-33 may be less toxic than WT IL-33 and thus more amenable to clinical translation.

3.4.3 Prophylactic SA IL-33 Prevents the Development and Progression of MOG_{35-55}-Induced EAE

We next evaluated the impact of prophylactic SA IL-33 administration on EAE development. Active EAE was induced in C57BL/6 mice via immunization with MOG_{35-55} antigen emulsified in Complete Freud's Adjuvant followed by pertussis toxin [156]. To identify the dose

of SA IL-33 required for disease prevention, we first s.c. administered mice with PBS, 13 µg SA IL-33, 26 µg SA IL-33, or 39 µg SA IL-33 every other day beginning on day 8 (Figure 3.8a). Subcutaneous administration was selected due to its clinical convenience [301]. As a positive control, we also orally gavaged mice daily with FTY 720, an FDA-approved, clinically used MS drug [302], from day 8 until endpoint (Figure 3.8a). Mice that received PBS developed severe hindlimb paralysis by day 15 post-disease induction, as indicated by the elevated EAE clinical score and percentage of mice with disease score greater than 1 (Figure 3.8b-d, Figure 3.9a). In contrast, treatment with 26 µg SA IL-33 or 39 µg SA IL-33 prevented disease development in nearly all mice, demonstrating similar efficacy to FTY 720 (Figure 3.8b-d, Figure 3.9c-e). Treatment with 13 µg SA IL-33 also delayed disease onset, but ultimately did not prevent disease development (Figure 3.8b-d, Figure 3.9b). Therefore, we selected the 26 µg dose of SA IL-33 as the lowest dose required to prevent EAE onset for further studies.

After identifying the optimal SA IL-33 dose, we then compared the efficacy of SA IL-33 to WT IL-33 (activity-equivalent dose determined based on assay in Figure 3.5b) in prophylactic EAE (Figure 3.8e). We hypothesized that despite its activity-attenuation, SA IL-33's extended bioavailability, and prolonged residence in the SLOs and spinal cord would enable improved disease prevention. When administered at an activity-equivalent dose to WT IL-33, SA IL-33 was significantly more effective in preventing EAE onset (Figure 3.8f-h, Figure 3.10a-d). After monitoring the mice long-term (until day 21), we observed that none of the SA IL-33-treated mice exhibited clinical symptoms, whereas 5 out 8 of the WT IL-33-treated mice developed disease by endpoint (Figure 3.8f-h, Figure 3.10). Taken together, these findings suggest that IL-33 fusion to SA enhances the cytokine's ability to prevent the onset of EAE.

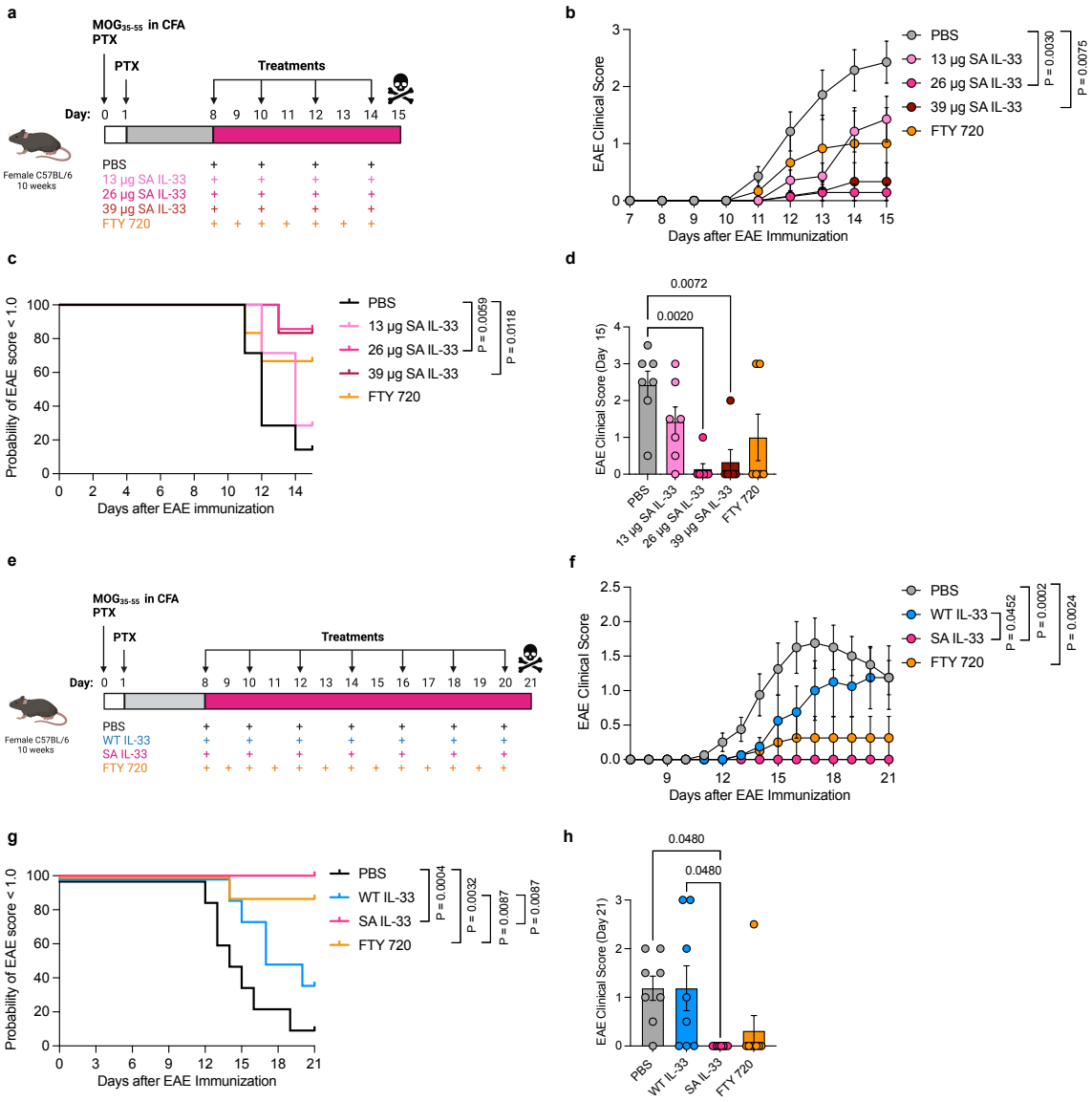

Figure 3.8: **Prophylactic SA IL-33 therapy prevents the development and progression of MOG_{35-55}-induced EAE.** (a) Overview of experimental design. EAE was induced in C56BL/6 mice by s.c. immunization with MOG_{35-55}/CFA followed by i.p. injections of PTX on days 0 and 1. Mice were prophylactically administered s.c. PBS or s.c. 13 µg SA IL-33, s.c. 26 µg SA IL-33, s.c. 39 µg SA IL-33 (all molar e.q. to WT IL-33) every other day, or oral gavage of FTY 720 (1 mg/kg body weight) daily from day 8 after MOG_{35-55} immunization (n = 6-7 mice/group). (b) Disease progression. Clinical score of paralysis severity was assessed daily by a blinded investigator. (c) Disease severity, indicated by the probability of EAE clinical scores remaining below a grade of 1.0. (d) Disease score at endpoint. Mice were sacrificed on day 15 to collect tissues for analysis. (e) Overview of experimental design. EAE was induced as described in (a). Continued on next page.

Figure 3.8: Continued: Mice were prophylactically administered s.c. PBS, s.c. 176 ng WT IL-33 (bioactivity equivalent to SA IL-33 as determined in Figure 3.5b), or s.c. 26 µg SA IL-33 every other day, or oral gavage of FTY 720 (1 mg/kg body weight) daily from day 8 after MOG_{35-55} immunization (n = 8 mice/group). (f) Disease progression. Clinical score of paralysis severity was assessed daily by a blinded investigator. (g) Disease severity, indicated by the probability of EAE clinical scores remaining below a grade of 1.0. (h) Disease score at endpoint. Mice were sacrificed on day 21 to collect tissues for analysis. Data represent means ± s.e.m. Statistical analysis on disease score area under the curve (AUC) (from d8 to d15 in (b) and d8 to d21 in (f)) and at endpoint (d, h) was performed using ordinary one-way ANOVA with Tukey's multiple comparisons tests, and on disease severity (c, g) using Log-rank (Mantel-Cox) test comparing every two groups. P-values < 0.05 are shown. Diagrams in (a, e) were created in BioRender.com.

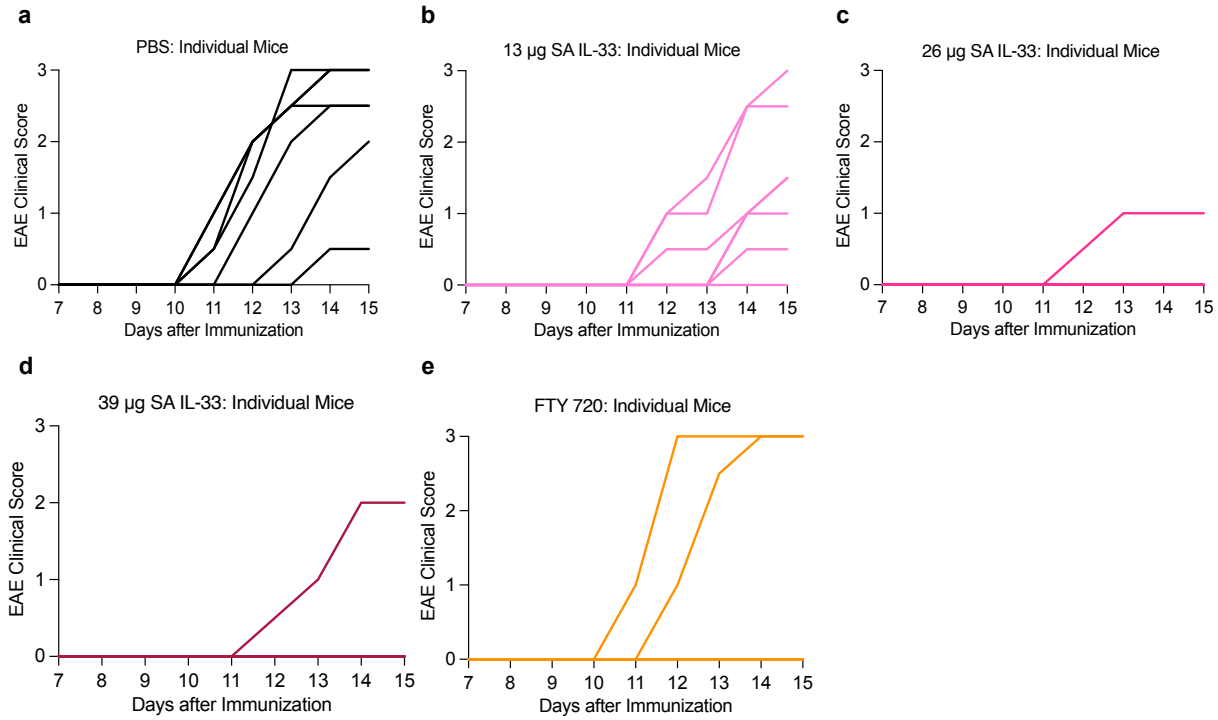

Figure 3.9: **Clinical scores of individual EAE-bearing mice in prophylactic SA IL-33 dosing study.** (a-e) Mice were treated with a) PBS, b) 13 µg SA IL-33, c) 26 µg SA IL-33, d) 39 µg SA IL-33, or FTY 720, as described in Figure 3.8a.

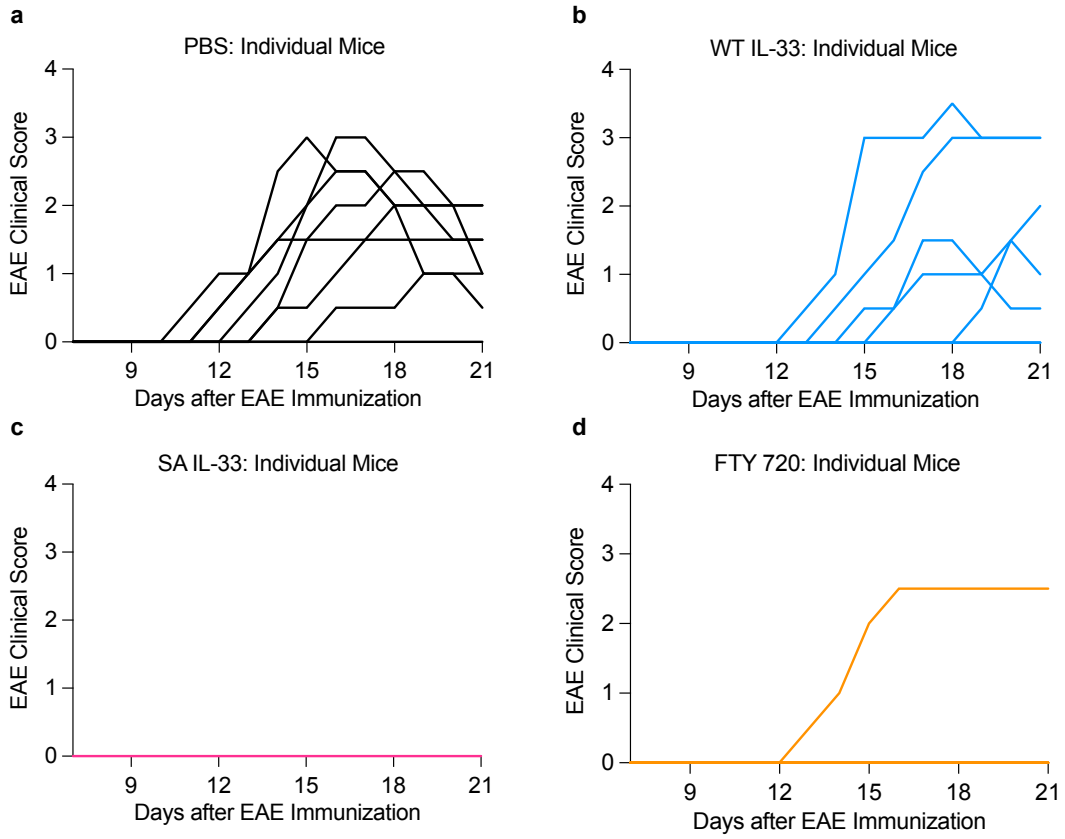

Figure 3.10: **Clinical scores of individual EAE-bearing mice in prophylactic WT IL-33 vs. SA IL-33 comparison study.** (a-d) Mice were treated with a) PBS, b) WT IL-33, c) SA IL-33, or d) FTY 720, as described in Figure 3.8e.

3.4.4 SA IL-33 Suppresses Leukocyte Infiltration and Proinflammatory Cytokine Production in the Spinal Cord of EAE-Bearing Mice

A hallmark of MS and EAE is the infiltration of pathogenic leukocytes into CNS [156]. EAE occurs when autoreactive, MOG-specific RORγt$^+$ Th17 T cells, primed in the SLOs, breach the disrupted blood-brain barrier and enter the spinal cord, where these cells become reactivated, triggering an inflammation cascade that leads to chronic hindlimb paralysis [156]. To assess the impact of prophylactic SA IL-33 therapy on leukocyte phenotype, we isolated cells from the spinal cord tissue at the study endpoint, stained them for T cell and myeloid cell markers, and performed immunophenotyping via flow cytometry (Figures 3.11, 3.12,

3.13, 3.14, and 3.15). In the spinal cord, SA IL-33 administration significantly reduced the percentage of $CD45^+$ lymphocytes (Figure 3.11a), $CD4^+$ T cells (Figure 3.11b), and disease-causing $ROR\gamma t^+$ Th17 cells (Figure 3.11c) compared to PBS. Additionally, in a repeated experiment (Figure 3.12a), we also stained for MOG $Tetramer^+$ cells and observed that SA IL-33 treatment significantly reduced the percentage of MOG $Tetramer^+$ $CD4^+$ T cells (Figure 3.12b) and MOG^+ $ROR\gamma t^+$ Th17 cells (Figure 3.12c). As expected, administration of the positive control, FTY 720, significantly reduced the levels of $CD4^+$ T cells (Figure 3.11b), $ROR\gamma t^+$ Th17 cells (Figure 3.11c), MOG $Tetramer^+$ $CD4^+$ T cells (Figure 3.12b), and MOG $Tetramer^+$ $ROR\gamma t^+$ Th17 cells (Figure 3.12c) in the spinal cord.

Infiltrating peripheral and CNS-resident myeloid cells also contribute to the CNS inflammation cascade [156]. M1-polarized macrophages secrete proinflammatory cytokines and chemokines that recruit additional immune cells [156]. These antigen presenting cells (APCs) present myelin antigens to autoreactive T cells, promoting their continued re-activation [156]. In the spinal cord, SA IL-33 administration significantly reduced the percentage of $CD11b^+F4/80^+$ macrophages (Figure 3.11d) and proinflammatory $CD86^+$ M1-polarized macrophages (Figure 3.11e), as well as trended towards increasing the percentage of immunoregulatory $CD206^+$ M2-polarized macrophages (Figure 3.11f), overall significantly lowering the M1 to M2 macrophage ratio compared to PBS (Figure 3.11g). Additionally, SA IL-33 administration significantly reduced the percentage of $CD11c^+MHCII^{high}F4/80^-$ (Figure 3.11h) and $CD11b^+CD11c^+MHCII^{high}F4/80^-$ (Figure 3.11i) DCs compared to PBS. Conversely, FTY 720 treatment did not impact myeloid cell levels (Figure 3.11d-i).

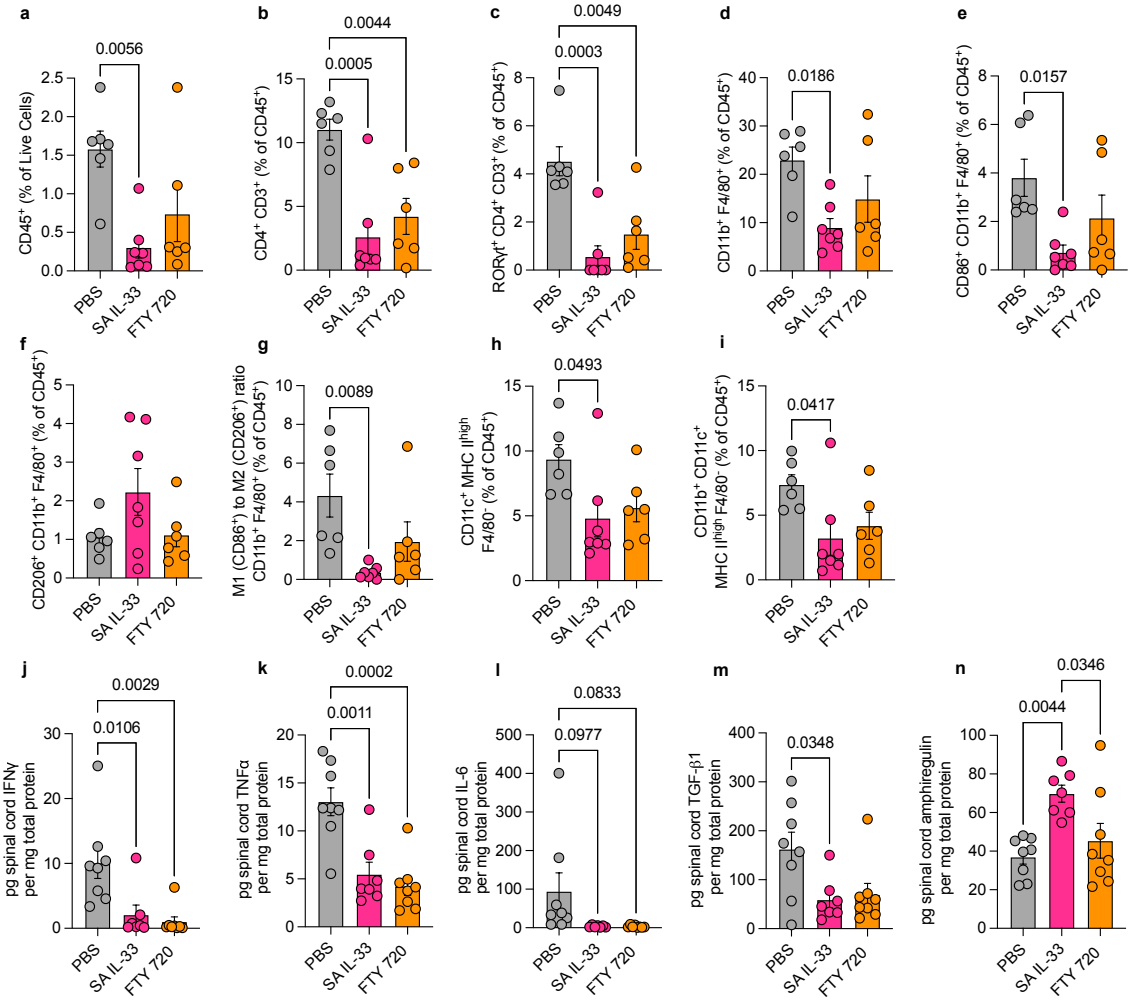

Figure 3.11: **SA IL-33 treatment suppresses leukocyte infiltration and proinflammatory cytokine production in the spinal cord of EAE-bearing mice.** MOG_{35-55} EAE-bearing mice were prophylactically administered s.c. PBS or s.c. 26 µg SA IL-33 (molar e.q. to WT IL-33) every other day, or oral gavage FTY 720 (1 mg/kg body weight) daily from day 8 after immunization as described in Figure 3.8a (n = 6-7 mice/group). On day 15, spinal cords were excised, and cells were processed for flow cytometric analysis. In a repeated experiment (disease scores shown in Figure 3.12a, n = 8 mice/group), spinal cords were homogenized for cytokine analysis. (a-i) Percentage of a) $CD45^+$ of live cells and b) $CD4^+CD3^+$, c) $ROR\gamma t^+CD4^+$, d) $CD11b^+F4/80^+$, e) $CD86^+CD11b^+F4/80^+$, f) $CD206^+CD11b^+F4/80^+$ of $CD45^+$ cells in the spinal cord. g) M1 to M2 macrophage ratio in the spinal cord. Percentage of h) $CD11c^+MHCII^{high}F4/80^-$ and i) $CD11b^+CD11c^+MHCII^{high}F4/80^-$ of $CD45^+$ cells in the spinal cord. (j-n) The concentration of j) IFN-γ, k) TNF-α, l) IL-6, m) free active TGF-β1, and n) amphiregulin in the spinal cord homogenate was measured using LEGENDplex or ELISA and normalized by total protein. Any values below the limit of detect were considered as the limit of detection. Data represent means ± s.e.m. Statistical analysis was performed using ordinary one-way ANOVA with Tukey's multiple comparisons tests. P-values < 0.05 are shown.

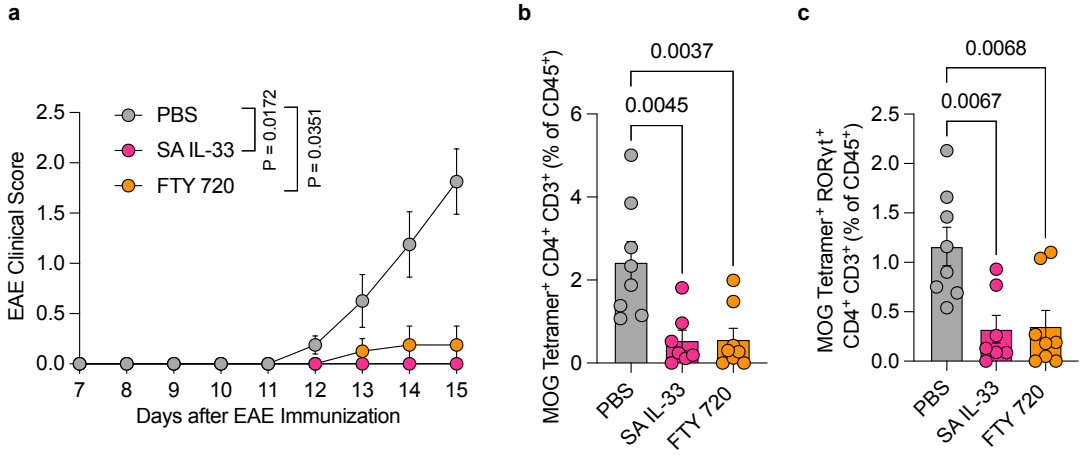

Figure 3.12: **Impact of prophylactic SA IL-33 therapy on MOG-Tetramer CD4$^+$ T cells in the spinal cord of EAE-bearing mice.** (a) Disease progression. Data is from a repeated experiment of the prophylactic SA IL-33 study described in Figure 3.8a. (b, c) Percentage of b) MOG Tetramer$^+$CD4$^+$CD3$^+$ and c) MOG Tetramer$^+$RORγt$^+$CD4$^+$CD3$^+$ of CD45$^+$ cells in the spinal cord. Data represent means ± s.e.m. Statistical analysis was performed using ordinary one-way ANOVA with Tukey's multiple comparisons tests. P-values < 0.05 are shown.

During EAE, the proinflammatory cytokines secreted by these immune cells contribute to blood-brain barrier disruption, recruit additional peripheral cells, and activate CNS-resident immune cells including microglia and astrocytes, resulting in CNS tissue damage [156]. We observed that SA IL-33 and FTY 720 treatment significantly reduced IFN-γ (Figure 3.11j) and TNF-α (Figure 3.11k), and trended towards reducing IL-6 (Figure 3.11l) levels in the spinal cord homogenate. SA IL-33 also reduced the concentration of TGF-β1 (Figure 3.11m), which in combination with IL-6 promotes Th17 T cell differentiation [303]. Strikingly, SA IL-33 treatment significantly increased the production of amphiregulin (Figure 3.11n), a growth factor associated with IL-33-induced tissue repair [263], in the spinal cord. Overall, these results support the flow cytometric findings, which indicate that SA IL-33 treatment suppressed disease-causing T cells and myeloid cells in the spinal cord.

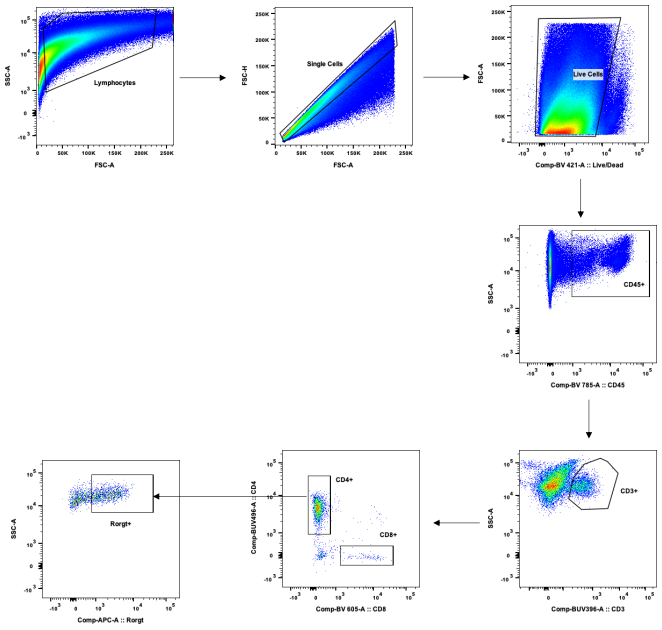

Figure 3.13: **Flow cytometry gating strategy for identification of T cells in the spinal cord of EAE-bearing mice.** This gating strategy was used in Figure 3.11a-c and Figure 3.24d-f.

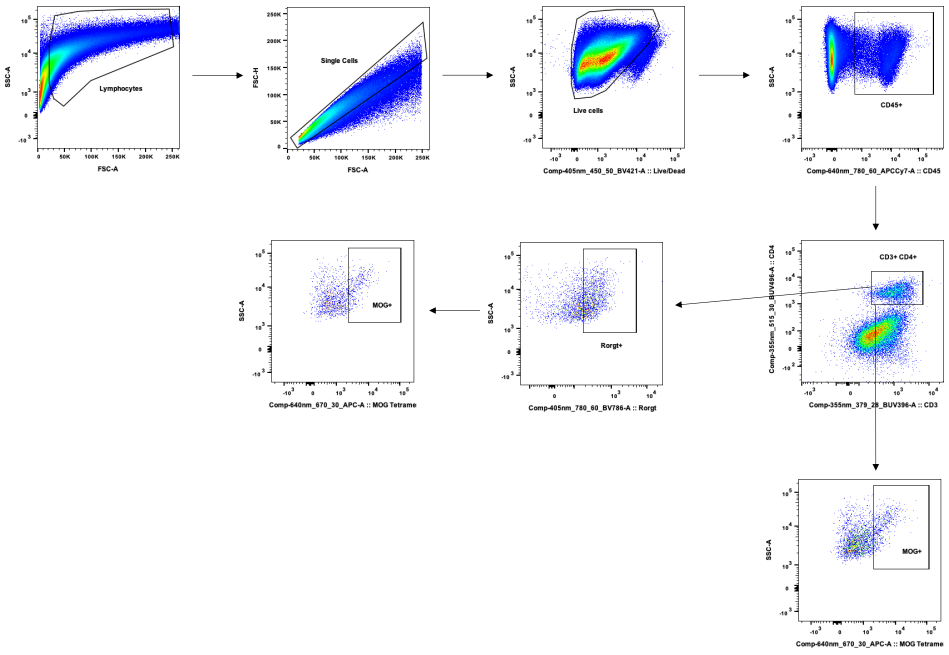

Figure 3.14: **Flow cytometry gating strategy for identification of MOG Tetramer$^+$ T cells in the spinal cord of EAE-bearing mice.** This gating strategy was used in Figure 3.12b,c and Figure 3.26.

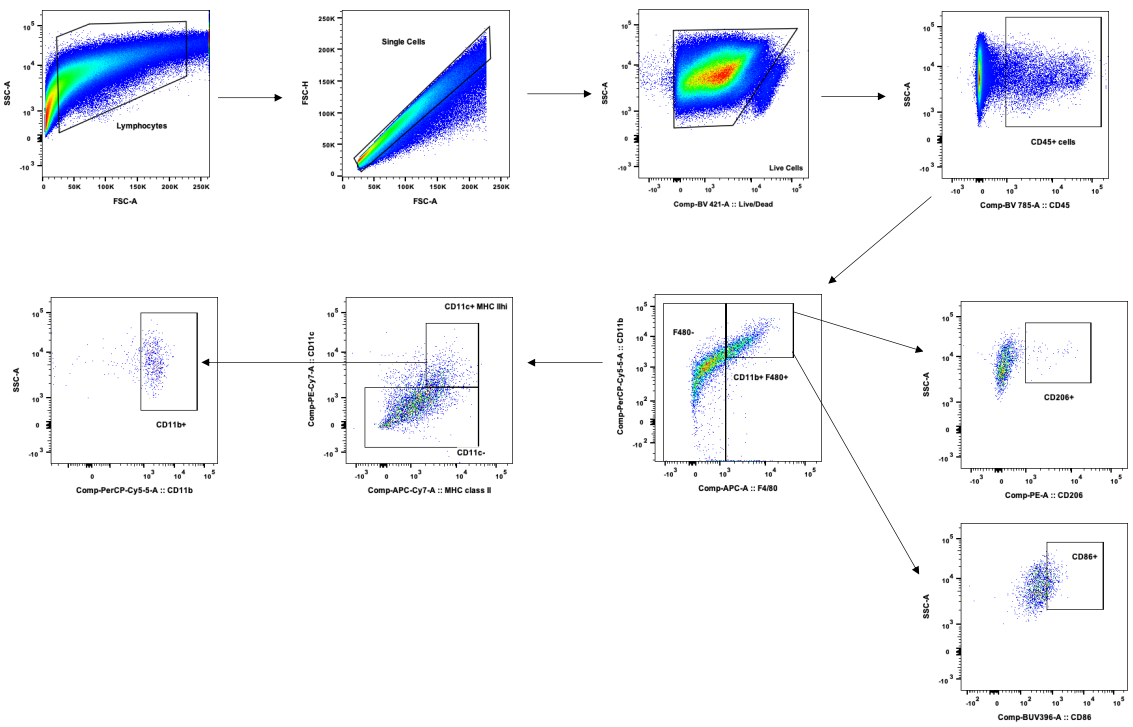

Figure 3.15: **Flow cytometry gating strategy for identification of myeloid cells in the spinal cord of EAE-bearing mice.** This gating strategy was used in Figure 3.11d-i.

3.4.5 SA IL-33 Expands the Protective Type 2 Response and Reduces Proinflammatory Cytokine Production in the Secondary Lymphoid Organs of EAE-Bearing Mice.

As IL-33 expands type 2 immune cells including ILC2s, GATA3$^+$ Th2 T cells, ST2$^+$FoxP3$^+$ Tregs, and M2 macrophages [263], we hypothesized that SA IL-33 would promote type 2 skewing in the SLOs of EAE-bearing mice. To assess the impact of prophylactic SA IL-33 therapy on immune cell phenotypes in the SLOs, we isolated cells from cervical and iliac lymph nodes (CNS-dLNs) and performed immunophenotyping (Figures 3.16, 3.17, 3.18, 3.19, 3.20, 3.21, 3.22, and 3.23).

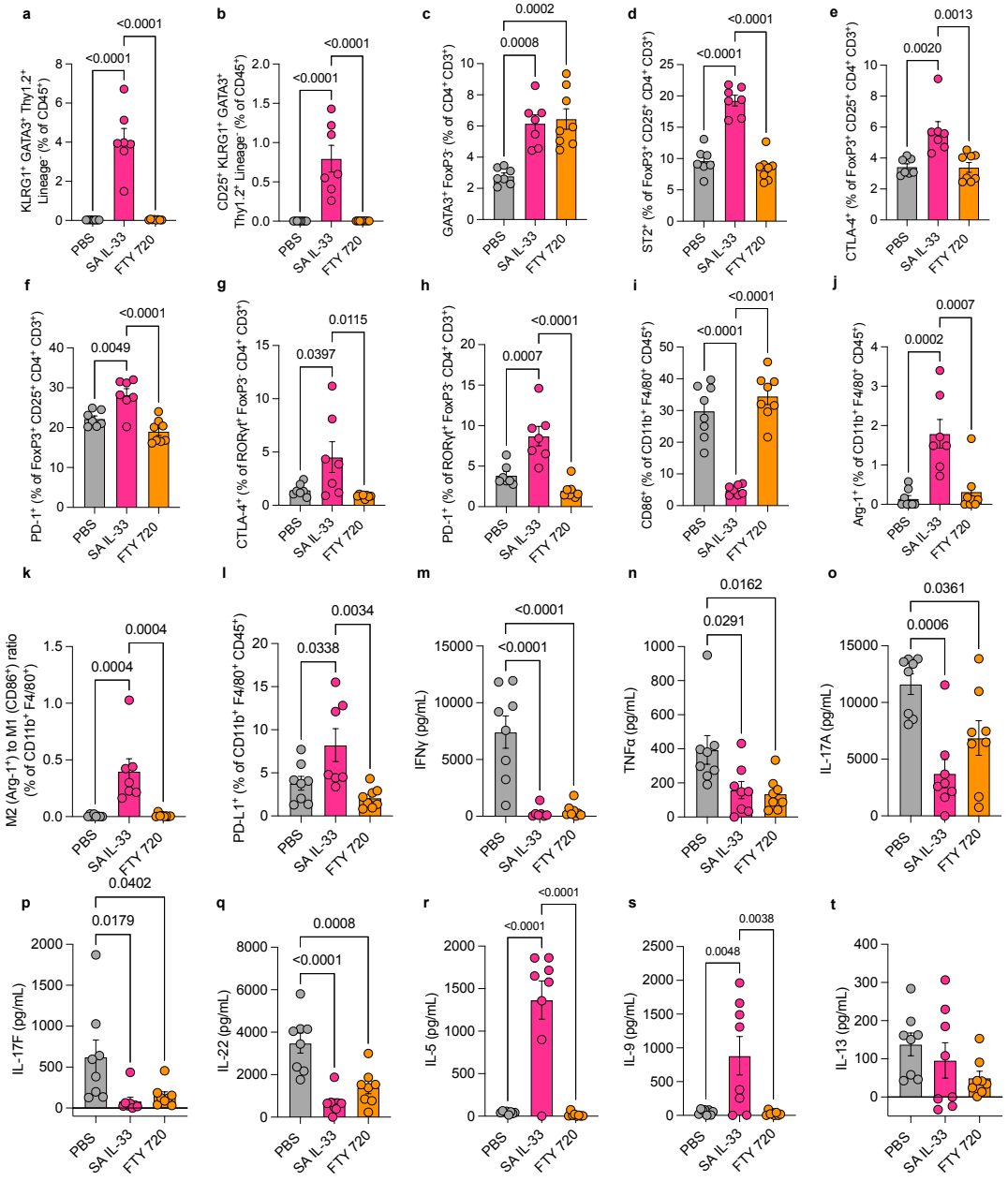

Figure 3.16: **SA IL-33 expands protective type 2 immune cells and reduces proinflammatory cytokine production in the CNS-dLNs of EAE-bearing mice.** MOG_{35-55} EAE-bearing mice were prophylactically administered s.c. PBS or s.c. 26 µg SA IL-33 (molar e.q. to WT IL-33) every other day, or oral gavage FTY 720 (1 mg/kg body weight) daily from day 8 after immunization as described in Figure 3.8e (n = 8 mice/group). On day 21, the iliac and cervical LNs (CNS draining lymph nodes, CNS-dLNs) were excised, and cells were processed for flow cytometric analysis. In a repeated experiment (disease scores shown in Figure 3.12a, n = 8 mice/group), lymphocytes were restimulated *ex vivo* for 72 hr with MOG protein, and cytokine production was measured. Continued on next page.

Figure 3.16: Continued: (a-i) Percentage of a) KLRG1$^+$GATA3$^+$Thy1.2$^+$Lin$^-$ and b) CD25$^+$KLRG1$^+$GATA3$^+$Thy1.2$^+$Lin$^-$ of CD45$^+$ cells; c) GATA3$^+$FoxP3$^-$ of CD4$^+$ cells; d) ST2$^+$, e) CTLA-4$^+$, and f) PD-1$^+$ of FoxP3$^+$CD25$^+$CD4$^+$ cells; g) CTLA-4$^+$ and h) PD-1$^+$ of RORγt$^+$FoxP3$^-$CD4$^+$ cells; and i) CD86$^+$ and j) Arg-1$^+$ of CD11b$^+$F4/80$^+$ cells in the CNS-dLNs. (k) M2 to M1 macrophage ratio in the CNS-dLNs. (l) Percentage of PD-L1$^+$ of CD11b$^+$F4/80$^+$ cells in the CNS-dLNs. (m-t) The production of m) IFN-γ, n) TNF-α, o) IL-17A, p) IL-17F, q) IL-22, r) IL-5, s) IL-9, and t) IL-13 was measured in the supernatant of CNS-dLN derived cells from EAE-bearing mice following *ex vivo* restimulation with MOG protein for 72 hr. Values represent the difference between cytokine production of MOG-restimulated and unstimulated cells. Data represent means ± s.e.m. Statistical analysis was performed using ordinary one-way ANOVA with Tukey's multiple comparisons tests. P-values < 0.05 are shown.

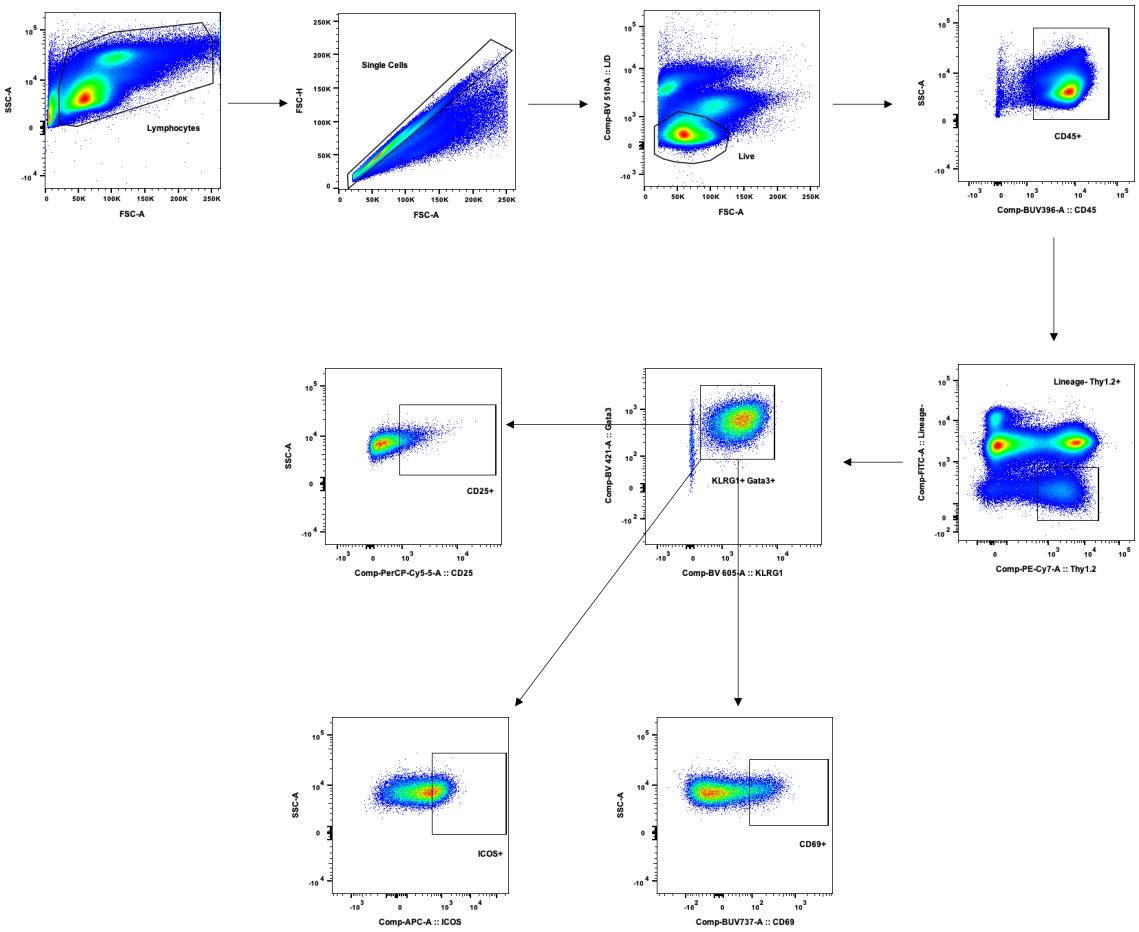

Figure 3.17: **Flow cytometry gating strategy for identification of ILC2s in the CNS-dLNs and spleen of EAE-bearing mice.** This gating strategy was used in Figure 3.16a,b; Figure 3.20a,b; Figure 3.21a-d; Figure 3.24h,i; Figure 3.27; and Figure 3.30d,e.

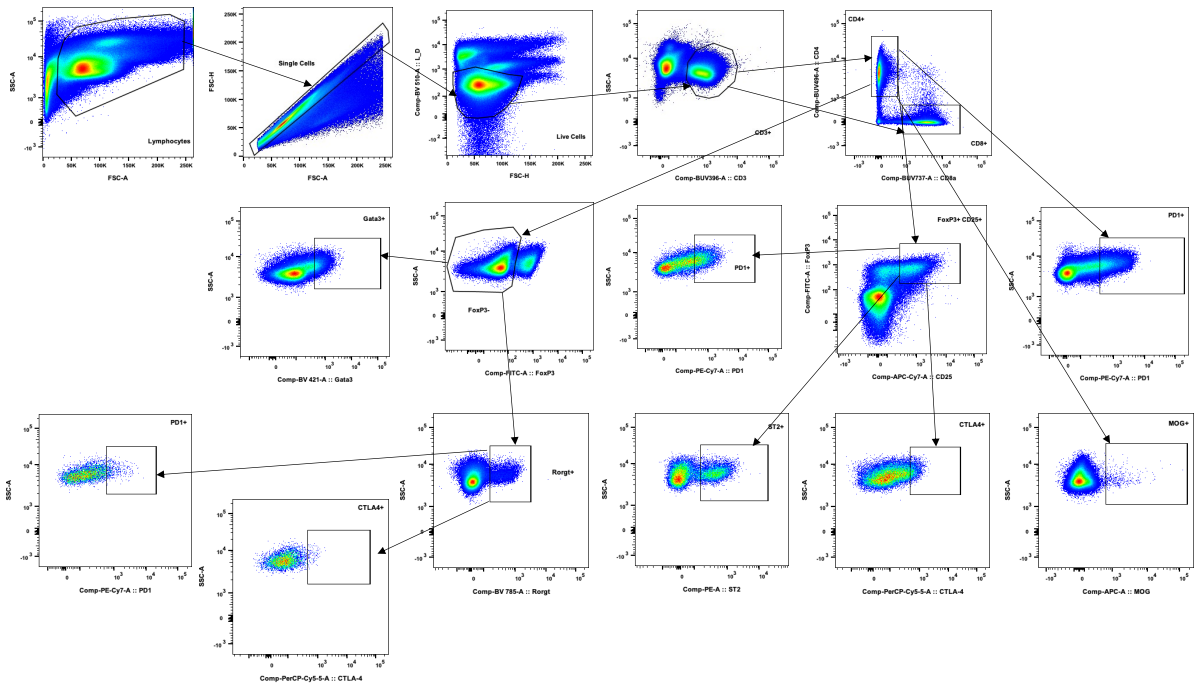

Figure 3.18: **Flow cytometry gating strategy for identification of CD4$^+$ T cell subsets in the CNS-dLNs and spleen of EAE-bearing mice.** This gating strategy was used in Figure 3.16c-h; Figure 3.20c-g; Figure 3.23a-d; Figure 3.24j-m; Figure 3.20c-g; Figure 3.23a-d; Figure 3.28a-d; Figure 3.29a-d; and Figure 3.30f-h.

On ILC2s, IL-33 upregulates the transcription factor GATA3, which is required for their differentiation and maintenance [298]. Activated ILC2s also express the surface markers CD25, ICOS, and CD69 [304]. Prophylactic SA IL-33 administration significantly increased the percentage of KLRG1$^+$GATA3$^+$Th1.2$^+$Lin$^-$ ILC2s in both the CNS-dLNs (Figure 3.16a) and spleen (Figure 3.20a) compared to PBS and FTY 720. Furthermore, SA IL-33 elevated the percentage of ILC2s expressing the activation markers CD25, CD69, and ICOS in both the CNS-dLNs (Figure 3.16b, Figure 3.21a,b) and spleen (Figure 3.20b, Figure 3.21c-d).

SA IL-33 treatment also modulated T cell phenotype in the SLOs. IL-33 acts as a chemoattractant for Th2 T cells [305] and upregulates their expression of the canonical transcription factor GATA3 via the NF-κB and STAT5 pathways [306]. Prophylactic SA IL-

33 administration significantly increased the percentage of GATA3$^+$ Th2 T cells in both the CNS-dLNs (Figure 3.16c) and spleen (Figure 3.20c) compared to PBS. FTY 720 elevated the percentage of Th2 T cells in the CNS-dLNs. IL-33 also promotes the expansion of ST2$^+$FoxP3$^+$ Tregs, a Th2-skewing Treg subset that contributes to the protective effects of IL-33 in allogenic cardiac transplantation [307], graft-versus-host-disease [268], and colitis [258][308]. Notably, prophylactic SA IL-33 significantly increased the expression of ST2 on FoxP3$^+$CD25$^+$ Tregs in both the CNS-dLNs (Figure 3.16d) and spleen (Figure 3.20d), without altering the levels of FoxP3$^+$CD25$^+$ Tregs in the CNS-dLNs (Figure 3.23b) or spleen (Figure 3.23d). Additionally, prophylactic SA IL-33 significantly elevated the expression of the immune checkpoint markers CTLA-4 and PD-1 on FoxP3$^+$CD25$^+$ Tregs in both the CNS-dLNs (Figure 3.16e,f) and spleen (Figure 3.20e,f). These results suggest that SA IL-33 may enhance the immunosuppressive capacity of Tregs.

Apart from its role in Th2 skewing, IL-33 reportedly suppresses the function of RORγt$^+$ Th17 T cells [270][271][272][273][274], a key driver of disease in EAE [156]. Prophylactic SA IL-33 treatment also significantly reduced the percentage of RORγt$^+$FoxP3$^-$ Th17 T cells in the spleen (Figure 3.23c), while increasing CTLA-4 and PD-1 expression on Th17 T cells in the CNS-dLNs (Figure 3.16g,h) and PD-1 expression on Th17 T cells in the spleen (Figure 3.20g). In contrast, FTY 720 increased the level of RORγt$^+$FoxP3$^-$ Th17 T cells in the SC-dLNs (Figure 3.23a), an outcome that is expected and likely occurs due to its role as an S1P receptor modulator that prevents cell egress from the lymph nodes [170][302]. As the SLOs are important sites of T cell priming in EAE [156], we also stained for MOG Tetramer$^+$ cells in the SLOs (Figure 3.22). We observed that prophylactic SA IL-33 treatment significantly reduced the percentage of MOG Tetramer$^+$ CD4$^+$ T cells in the spleen (Figure 3.22b) and trended towards reducing these cells in the CNS-dLNs (Figure 3.22a).

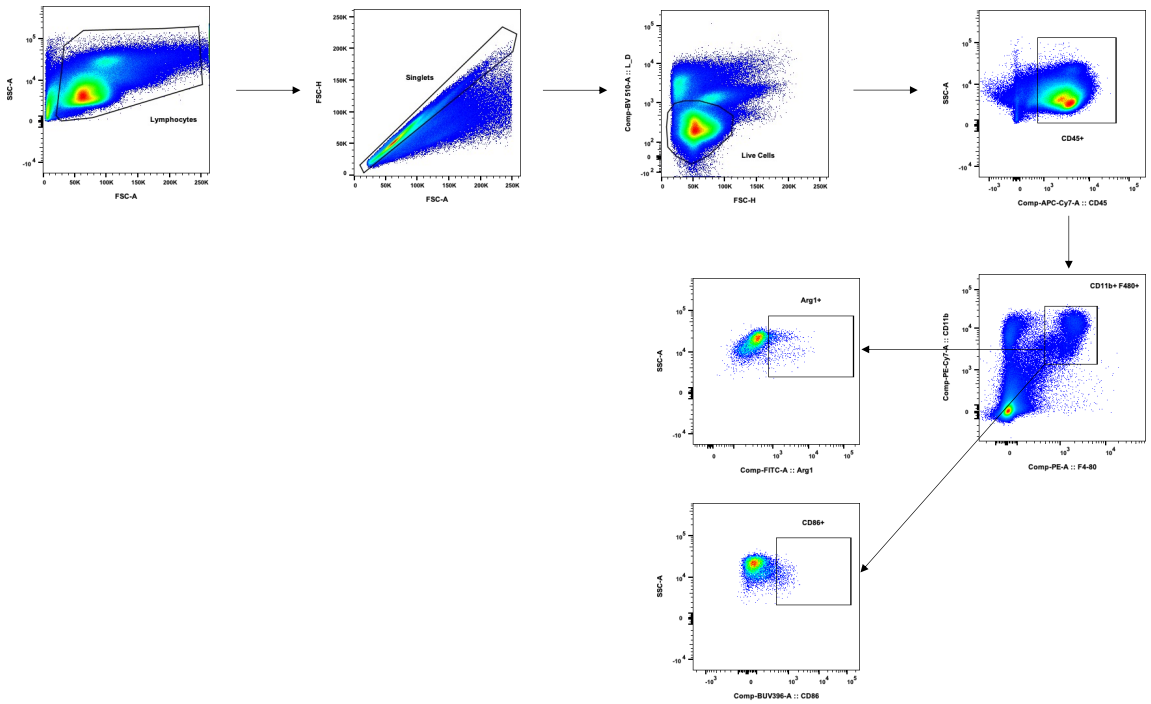

Figure 3.19: **Flow cytometry gating strategy for identification of myeloid cells in the CNS-dLNs and spleen of EAE-bearing mice.** This gating strategy was used in Figure 3.16i-l and Figure 3.30i-k.

In both the CNS-dLNs and spleen, prophylactic SA IL-33 treatment significantly reduced the percentage of proinflammatory CD86$^+$ M1-polarized macrophages (Figure 3.16i), while increasing the percentage of immunoregulatory Arg-1$^+$ M2-macrophages (Figure 3.16j), and the M2 to M1 macrophage ratio (Figure 3.16k) compared to PBS and FTY 720. These results align with a previous study demonstrating that IL-33 synergizes with IL-13 to promote M2 macrophage polarization by increasing Arg-1 expression [267]. Furthermore, SA IL-33-treated mice also displayed elevated PD-L1 levels on CD11b$^+$F4/80$^+$ macrophages in the CNS-dLNs (Figure 3.16l). The reduction in CD86 and increase in PD-L1 expression on myeloid cells coupled with the increase in CTLA-4 and PD-1 expression on T cells suggests that the CD86-CTLA-4 and PD-1-PD-L1 axes may contribute to SA IL-33-mediated immunoregulation in EAE.

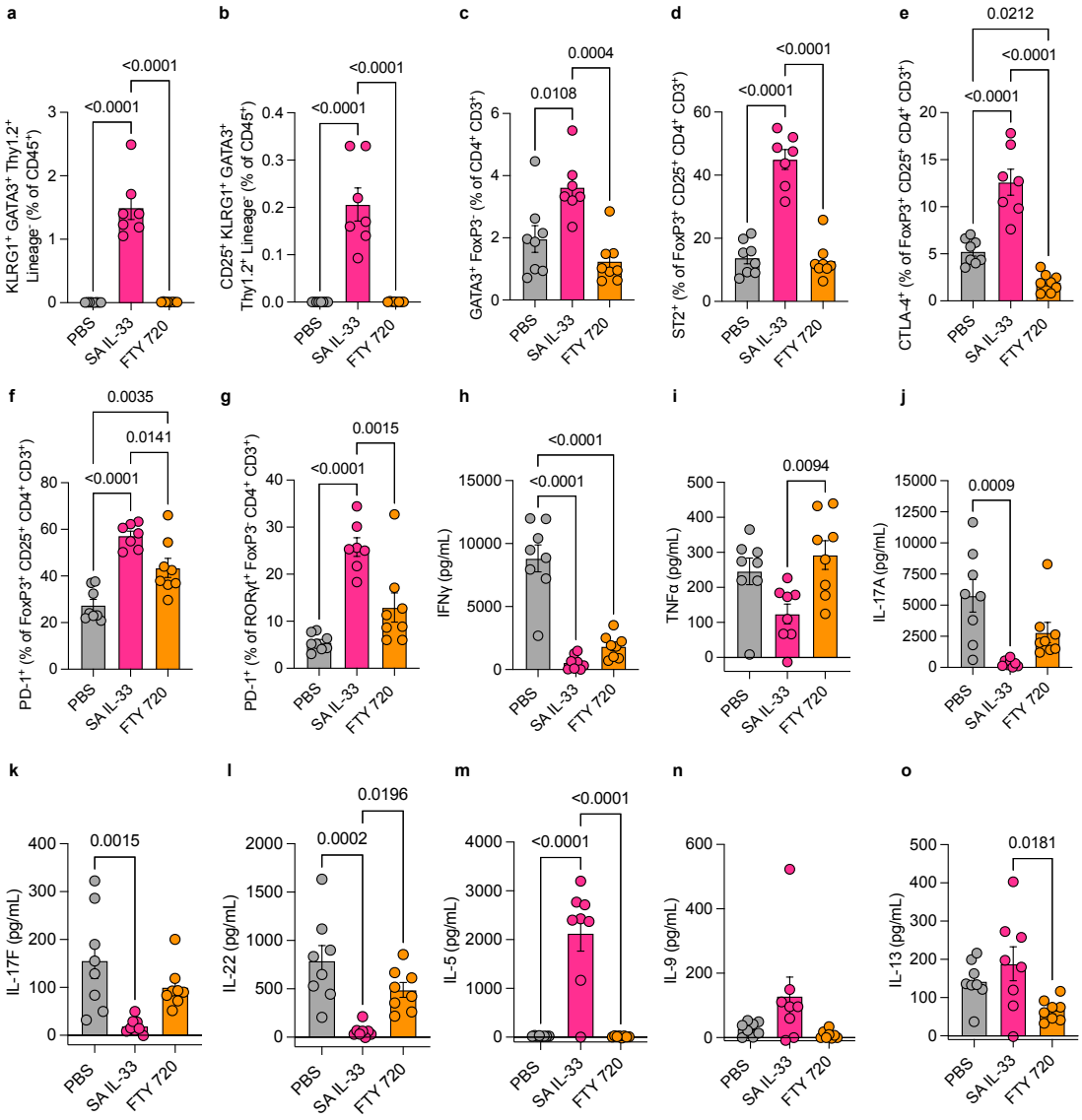

Figure 3.20: **Impact of prophylactic SA IL-33 therapy on protective type 2 immune cells and proinflammatory cytokine production in the spleen of EAE-bearing mice.** MOG_{35-55} EAE-bearing mice were prophylactically administered s.c. PBS or s.c. 26 µg SA IL-33 (molar e.q. to WT IL-33) every other day, or oral gavage FTY 720 (1 mg/kg body weight) daily from day 8 after immunization, as described in Figure 3.8e (n = 8 mice/group). On day 21, the spleen was excised and cells were processed for flow cytometric analysis. In a repeated experiment (disease scores shown in Figure 3.12a, n = 8 mice/group), spleen-derived cells were restimulated *ex vivo* for 72 hr with MOG protein and cytokine production was measured. (a-g) Percentage of a) $KLRG1^+GATA3^+Thy1.2^+Lin^-$ and b) $CD25^+KLRG1^+GATA3^+Thy1.2^+Lin^-$ of $CD45^+$ cells; c) $GATA3^+FoxP3^-$ of $CD4^+$ cells; d) $ST2^+$, e) CTLA-4^+, and f) PD-1^+ of $FoxP3^+CD25^+CD4^+$ cells; and g) PD-1^+ of $ROR\gamma t^+FoxP3^-CD4^+$ cells in the spleen. Continued on next page.

Figure 3.20: Continued: (h-o) The production of h) IFN-γ, i) TNF-α, j) IL-17A, k) IL-17F, l) IL-22, m) IL-5, n) IL-9, and o) IL-13 was measured in the supernatant of spleen-derivced cells from EAE-bearing mice following *ex vivo* restimulation with MOG protein for 72 hr. Values represent the difference between cytokine production of MOG-restimulated and unstimulated cells. Data represent means ± s.e.m. Statistical analysis was performed using ordinary one-way ANOVA with Tukey's multiple comparisons tests. P-values < 0.05 are shown.

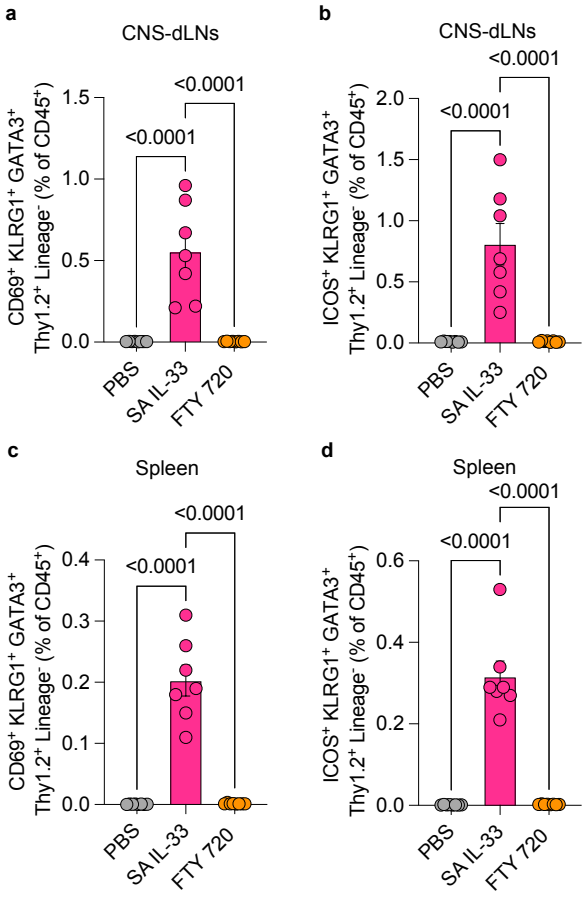

Figure 3.21: **Impact of prophylactic SA IL-33 therapy on ILC2 phenotype in the CNS-dLNs and spleen of EAE-bearing mice.** MOG_{35-55} EAE was induced as described in Figure 3.8e (n = 8 mice/group). EAE-bearing mice were prophylactically administered PBS, SA IL-33, or FTY 720 as described in Figure 3.8e. On day 21, the CNS-dLNs and spleen were excised and cells were processed for flow cytometric analysis. (a-d) Percentage of a) $CD69^+KLRG1^+GATA3^+Thy1.2^+Lin^-$ and b) $ICOS^+KLRG1^+GATA3^+Thy1.2^+Lin^-$ of $CD45^+$ cells in the CNS-dLNs. Percentage of c) $CD69^+KLRG1^+GATA3^+Thy1.2^+Lin^-$ and d) $ICOS^+KLRG1^+GATA3^+Thy1.2^+Lin^-$ of $CD45^+$ cells in the spleen. Data represent means ± s.e.m. Statistical analysis was performed using ordinary one-way ANOVA with Tukey's multiple comparisons tests. P-values < 0.05 are shown.

To characterize the impact of SA IL-33 on cytokine production in an antigen-specific manner, we restimulated CNS-dLN and spleen-derived cells, harvested from SA IL-33-treated EAE-bearing mice, with MOG protein for 72 hr *ex vivo* (Figure 3.16m-t, Figure 3.20h-o). Restimulated cells derived from the CNS-dLNs and spleen of SA IL-33-treated mice secreted significantly lower levels of the Th1 and Th17 cytokines IFN-γ (Figure 3.16m, Figure 3.20h), TNF-α (Figure 3.16n, Figure 3.20i), IL-17A (Figure 3.16o, Figure 3.20j), IL-17F (Figure 3.16p, Figure 3.20k), and IL-22 (Figure 3.16q, Figure 3.20l), as well as elevated levels of the Th2 cytokine IL-5 (Figure 3.16r, Figure 3.20m) compared to PBS. These results align with a previous study that noted a reduction in IL-17A and IFN-γ production by LN and spleen cells from EAE mice following WT IL-33 administration [281]. CNS-dLN but not spleen-derived cells from FTY 720-treated mice also secreted lower levels of Th1 and Th17 cytokines. Overall, the flow cytometric and *ex vivo* restimulation data indicate that prophylactic SA IL-33 therapy promotes immunoregulation in the SLOs of EAE-bearing mice.

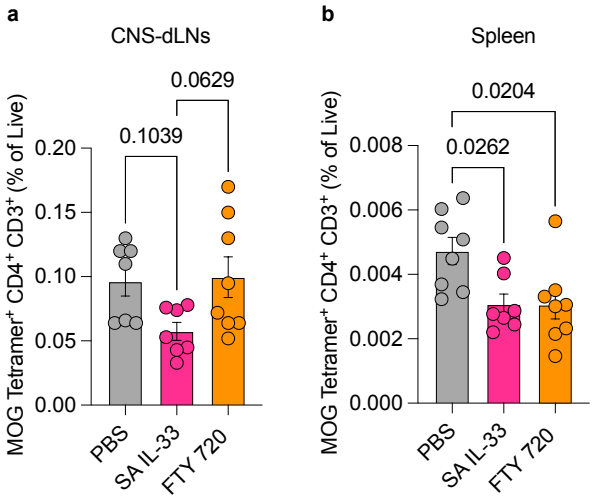

Figure 3.22: **Impact of prophylactic SA IL-33 therapy on MOG Tetramer$^+$ CD4$^+$ T cells in the CNS-dLNs and spleen of EAE-bearing mice.** MOG_{35-55} EAE was induced as described in Figure 3.8e (n = 8 mice/group). EAE-bearing mice were prophylactically administered PBS, SA IL-33, or FTY 720 as in Figure 3.8e. Continued on next page.

Figure 3.22: Continued: On day 21, the CNS-dLNs and spleen were excised and cells were processed for flow cytometric analysis.(a-b) Percentage of MOG Tetramer$^+$CD4$^+$CD3$^+$ of live cells in the a) CNS-dLNs and b) spleen. Data represent means ± s.e.m. Statistical analysis was performed using ordinary one-way ANOVA with Tukey's multiple comparisons tests. P-values < 0.05 are shown.

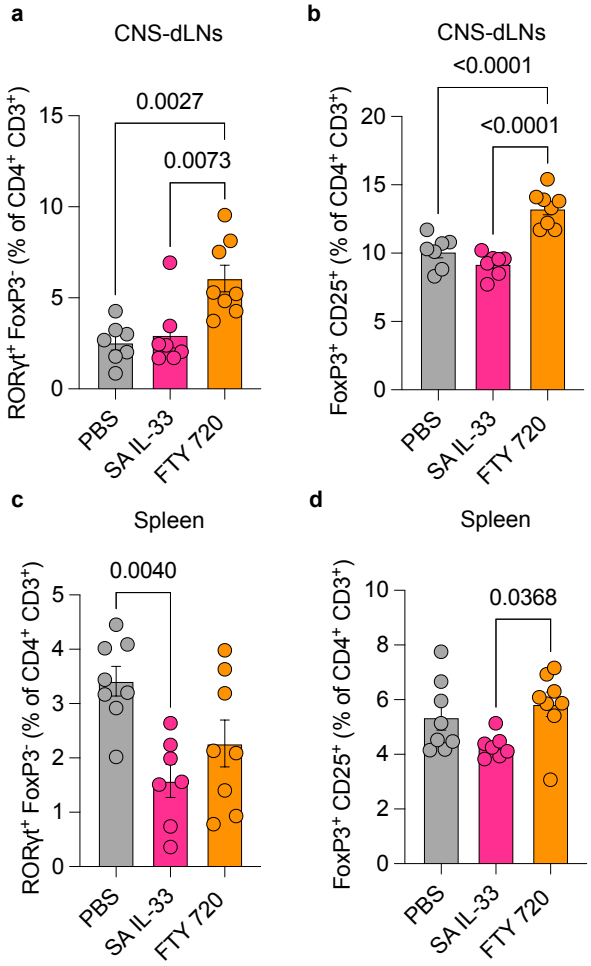

Figure 3.23: **Impact of prophylactic SA IL-33 therapy on RORγt$^+$FoxP3$^-$CD4$^+$ T cells and FoxP3$^+$CD25$^+$CD4$^+$ T cells in the CNS-dLNs and spleen of EAE-bearing mice.** MOG_{35-55} EAE was induced as described in Figure 3.8e (n = 8 mice/group). EAE-bearing mice were prophylactically administered PBS, SA IL-33, or FTY 720 as in in Figure 3.8e. On day 21, the CNS-dLNs and spleen were excised and cells were processed for flow cytometric analysis. (a-d) Percentage of a) RORγt$^+$FoxP3$^-$ and b) FoxP3$^+$CD25$^+$ of CD4$^+$CD3$^+$ cells in the CNS-dLNs. Percentage of c) RORγt$^+$FoxP3$^-$ and d) FoxP3$^+$CD25$^+$ of CD4$^+$CD3$^+$ cells in the spleen. Data represent means ± s.e.m. Statistical analysis was performed using ordinary one-way ANOVA with Tukey's multiple comparisons tests. P-values < 0.05 are shown.

3.4.6 Therapeutic SA IL-33 Reduces the Severity of MOG_{35-55}-Induced EAE and Modulates Immune Cells in the Spinal Cord and SLOs.

We next sought to determine whether SA IL-33 therapy, if initiated after MOG_{35-55}-EAE disease onset, could reverse the progression of already-established, severe disease. For this purpose, we s.c. administered PBS or SA IL-33 every-other day or orally gavaged FTY 720 daily, from day 20 post-EAE induction (Figure 3.24a). PBS-treated mice maintained chronic, severe hindlimb paralysis until endpoint (Figure 3.24b,c; Figure 3.25a), whereas therapeutic SA IL-33 (Figure 3.24b,c; Figure 3.25b) and FTY 720 (Figure 3.24b,c; Figure 3.25c) treatment reduced the severity of already-established disease, partially reversing paralysis.

In the spinal cord, therapeutic SA IL-33 and FTY 720 treatment significantly decreased the percentage of $CD45^+$ leukocytes (Figure 3.24d), $CD4^+$ T cells (Figure 3.24e), and disease-causing $ROR\gamma t^+$ Th17 T cells (Figure 3.24f), as well as trended towards reducing the percentage of MOG $Tetramer^+$ $CD4^+$ T cells (Figure 3.26). Furthermore, SA IL-33-treated mice also displayed elevated amphiregulin in the spinal cord homogenate (Figure 3.24g).

As in the prophylactic setting, therapeutic SA IL-33 also increased the percentage of ILC2s (Figure 3.24h) and their expression of activation markers CD25 (Figure 3.24i) and ICOS (Figure 3.27) in the spleen. In both the CNS-dLNs and spleen, therapeutic SA IL-33 elevated the percentage of $GATA3^+$ Th2 T cells (Figure 3.24j, Figure 3.28a) as well as the expression of ST2 (Figure 3.24k, Figure 3.28b) and CTLA-4 (Figure 3.24l, Figure 3.28c) on $FoxP3^+CD25^+$ Tregs without altering the level of $FoxP3^+CD25^+$ Tregs (Figure 3.29a,c). Although therapeutic SA IL-33 did not impact $ROR\gamma t^+$ Th17 cell levels in the CNS-dLNs (Figure 3.29b) or spleen (Figure 3.29d), SA IL-33-treated mice displayed significantly higher CTLA-4 expression on $ROR\gamma t^+$ Th17 cells in the CNS-dLNs (Figure 3.24m) compared to PBS and FTY 720.

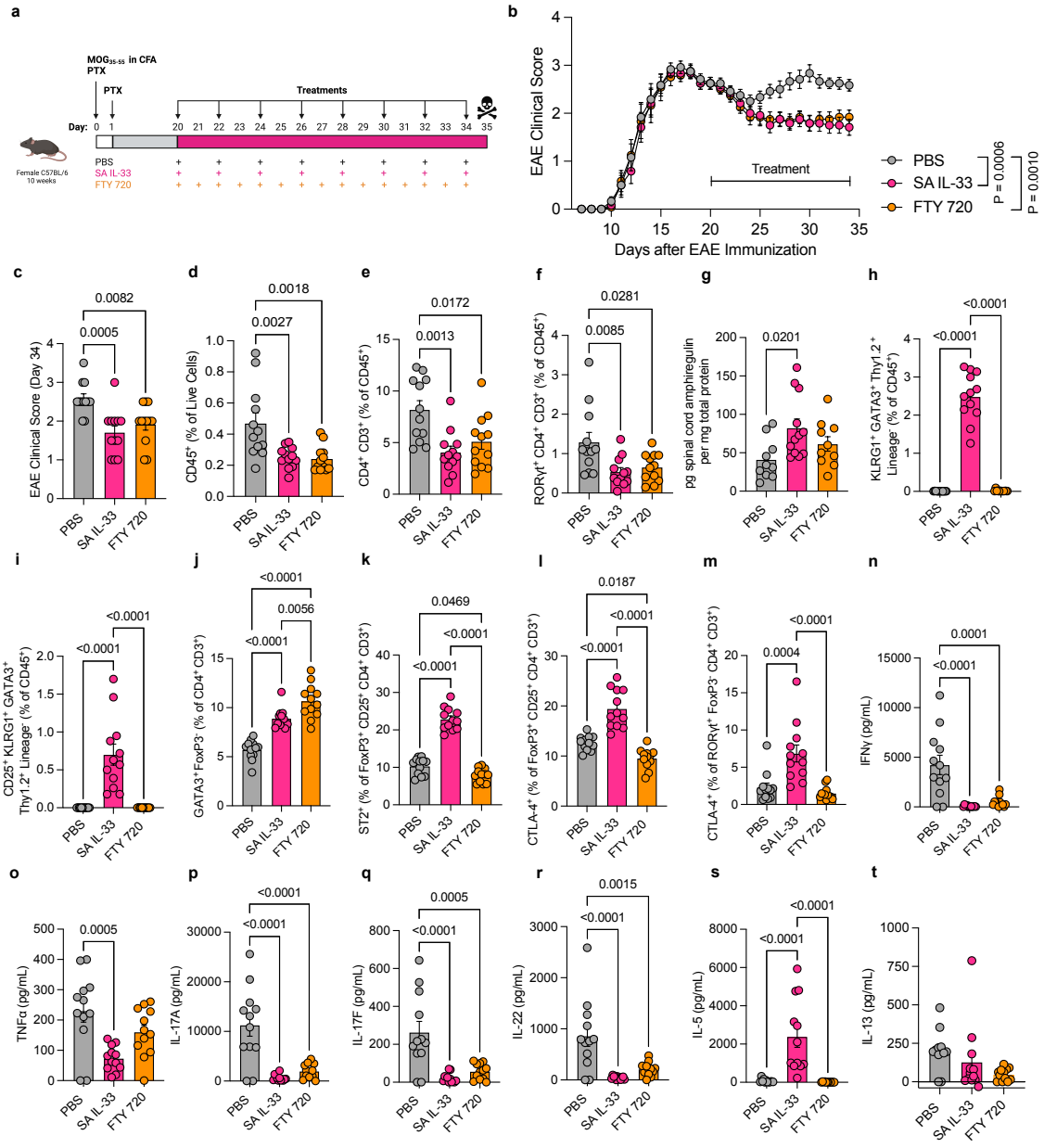

Figure 3.24: **Therapeutic SA IL-33 therapy reduces the severity of already-established MOG_{35-55}-induced EAE and modulates immune cells in the spinal cord, CNS-dLNs, and spleen.** (a) Overview of experimental design. EAE was induced in C56BL/6 mice by s.c. immunization with MOG_{35-55}/CFA followed by i.p. injections of PTX on days 0 and 1. On day 20 post MOG_{35-55} immunization, prior to the start of treatment, mice with established disease were assigned into groups of equal average clinical score. Each group was therapeutically administered s.c. PBS or s.c. 26 µg SA IL-33 (molar e.q. to WT IL-33) every other day, or oral gavage of FTY 720 (1 mg/kg body weight) daily from day 20 (n = 12 mice/group). (b) Disease progression. Clinical score of paralysis severity was assessed daily by a blinded investigator. Continued on next page.

Figure 3.24: Continued: (c) Disease score at final measurement. On day 35, spinal cords, CNS-dLNs, and spleen were excised, and cells were processed for flow cytometric and cytokine analysis. (d-f) Percentage of d) $CD45^+$ of live cells, e) $CD4^+CD3^+$ of $CD45^+$ cells, and f) $ROR\gamma t^+CD4^+$ of CD45+ cells in the spinal cord. (g) The concentration of amphiregulin in the spinal cord homogenate was measured using ELISA and normalized by total protein. Any values below the limit of detect were considered as the limit of detection. (h,i) Percentage of h) $KLRG1^+GATA3^+Thy1.2^+Lin^-$ and i) $CD25^+KLRG1^+GATA3^+Thy1.2^+Lin^-$ of $CD45^+$ cells in the spleen. (j-m) Percentage of j) $GATA3^+FoxP3^-$ of $CD4^+$ cells; k) $ST2^+$ and l) CTLA-4^+ of $FoxP3^+CD25^+CD4^+$ cells; and m) CTLA-4^+ of $ROR\gamma t^+FoxP3^-CD4^+$ cells in the CNS-dLNs. (n-t) The production of n) IFN-γ, o) TNF-α, p) IL-17A, q) IL-17F, r) IL-22, s) IL-5, and t) IL-13 was measured in the supernatant of spleen-derived cells from EAE-bearing mice following *ex vivo* restimulation with MOG protein for 72 hr. Values represent the difference between cytokine production of MOG-restimulated and unstimulated cells. Data represent means ± s.e.m. Statistical analysis on disease score AUC (from d20 to 35 in (b)), disease score at endpoint (c), flow cytometric analysis (d-f, h-m), and cytokine measurements (g, n-t) was performed using ordinary one-way ANOVA with Tukey's multiple comparisons tests. Diagram in (a) was created in BioRender.com. P-values < 0.05 are shown.

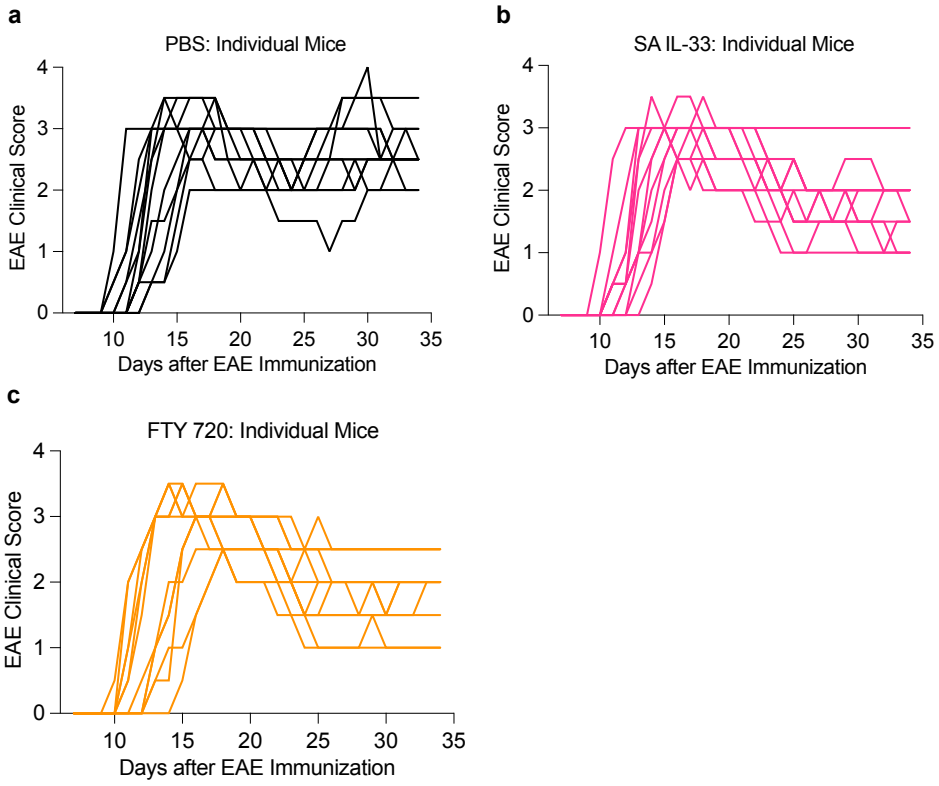

Figure 3.25: **Clinical scores of individual EAE-bearing mice in therapeutic SA IL-33 study.** (a-c) Mice were treated with a) PBS, b) SA IL-33, or c) FTY 720, as described in Figure 3.24a.

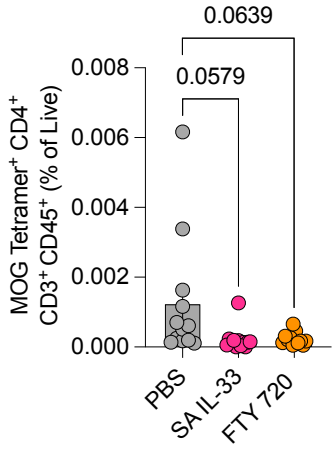

Figure 3.26: **Impact of therapeutic SA IL-33 on MOG-Tetramer CD4$^+$ T cells in the spinal cord of EAE-bearing mice.** MOG$_{35-55}$ EAE was induced as described in Figure 3.24a. EAE-bearing mice were therapeutically administered PBS, SA IL-33, or FTY 720 beginning on day 20 as in Figure 3.24a (n = 12 mice/group). On day 35, the spinal cord was excised and cells were processed for flow cytometric analysis. Graph displays percentage of MOG Tetramer$^+$CD4$^+$CD3$^+$CD45$^+$ of live cells in the spinal cord. Data represent means ± s.e.m. Statistical analysis was performed using ordinary one-way ANOVA with Tukey's multiple comparisons tests.

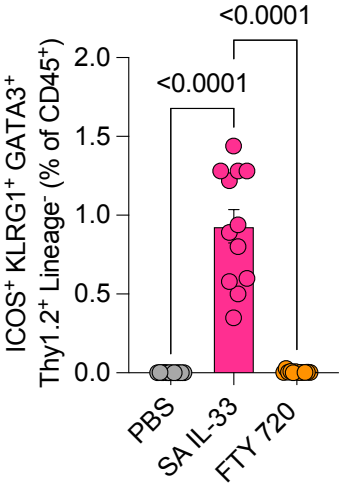

Figure 3.27: **Impact of therapeutic SA IL-33 therapy on ILC2 phenotype in the spleen of EAE-bearing mice.** MOG$_{35-55}$ EAE was induced as described in Figure 3.24a. EAE-bearing mice were therapeutically administered PBS, SA IL-33, or FTY 720 beginning on day 20 as in Figure 3.24a (n = 12 mice/group). On day 35, the spleen was excised and cells were processed for flow cytometric analysis. Continued on next page.

Figure 3.27: Continued: Graph displays percentage of ICOS$^+$ KLRG1$^+$ GATA3$^+$ Thy1.2$^+$ Lin$^-$ of CD45$^+$ cells in the spleen. Data represent means ± s.e.m. Statistical analysis was performed using ordinary one-way ANOVA with Tukey's multiple comparisons tests. P-values < 0.05 are shown.

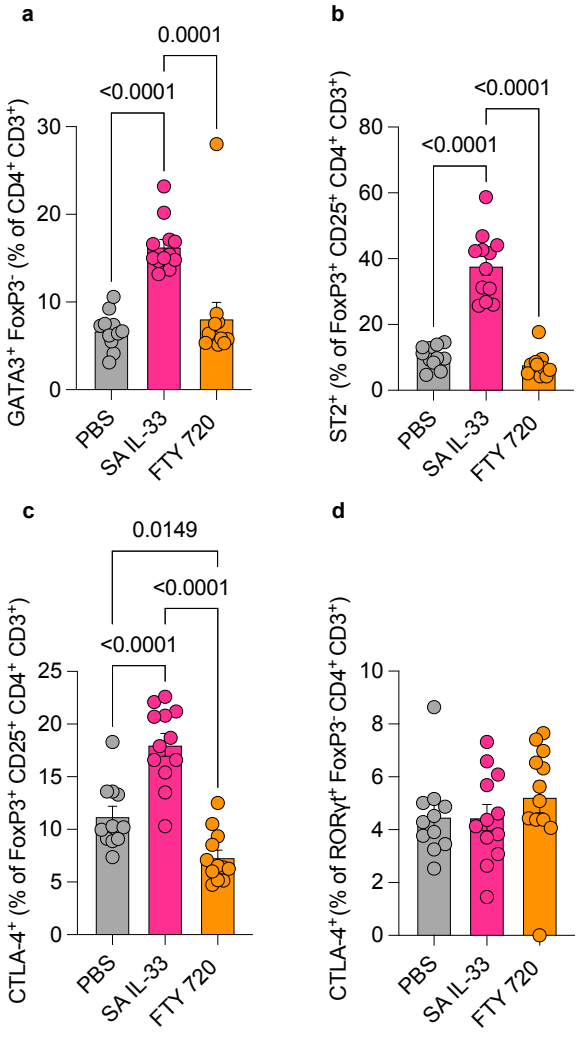

Figure 3.28: **Impact of therapeutic SA IL-33 therapy on CD4$^+$ T cell phenotype in the spleen of EAE-bearing mice.** MOG$_{35-55}$ EAE was induced as described in Fig. 6a. EAE-bearing mice were therapeutically administered PBS, SA IL-33, or FTY 720 beginning on day 20 as described in Figure 3.24a (n = 12 mice/group). On day 35, the spleens were excised and cells were processed for flow cytometric analysis. (a-d) Percentage of a) GATA3$^+$FoxP3$^-$ of CD4$^+$CD3$^+$ cells; b) ST2$^+$ and c) CTLA-4$^+$ of FoxP3$^+$CD25$^+$CD4$^+$ cells; and d) CTLA-4$^+$ of RORγt$^+$FoxP3$^-$CD4$^+$ cells in the spleen. Data represent means ± s.e.m. Statistical analysis was performed using ordinary one-way ANOVA with Tukey's multiple comparisons tests. P-values < 0.05 are shown.

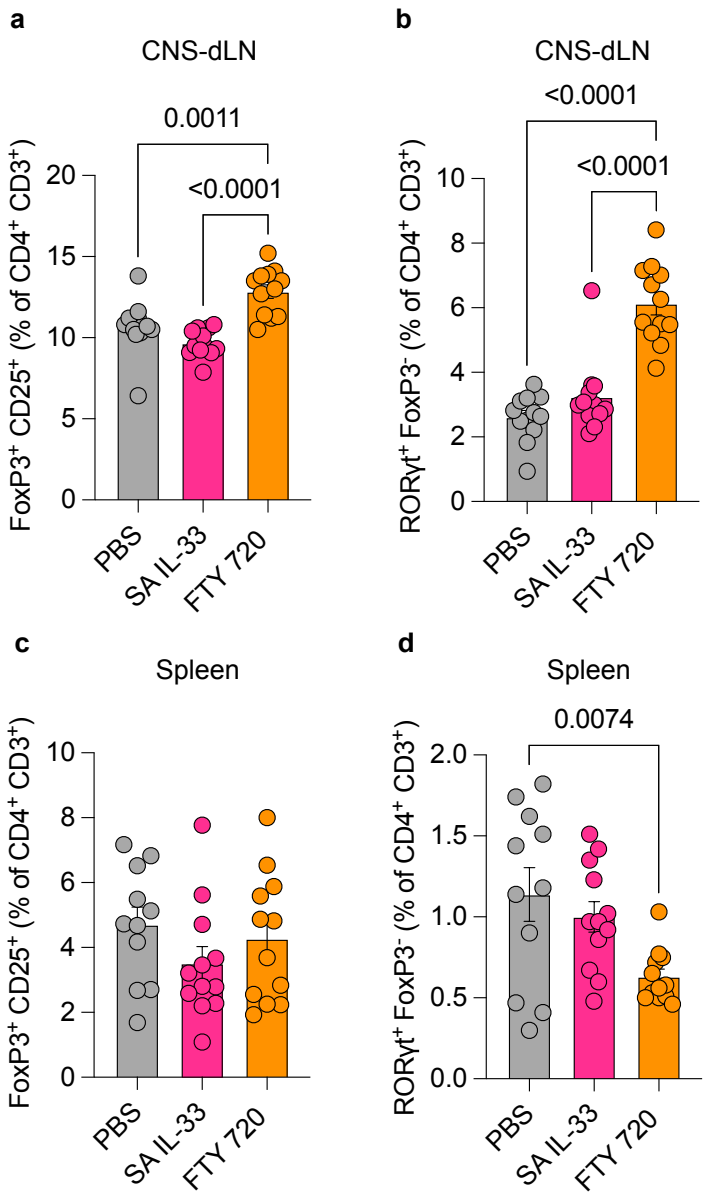

Figure 3.29: **Impact of therapeutic SA IL-33 therapy on FoxP3$^+$CD25$^+$CD4$^+$ T cells and RORγt$^+$FoxP3$^-$CD4$^+$ T cells in the CNS-dLNs and spleen of EAE-bearing mice.** MOG$_{35-55}$ EAE was induced as described in 3.24a (n = 12 mice/group). EAE-bearing mice were therapeutically administered PBS, SA IL-33, or FTY 720 beginning on day 20 as in Figure 3.24a. On day 35, the CNS-dLNs and spleen were excised and cells were processed for flow cytometric analysis. (a-d) Percentage of a) FoxP3$^+$CD25$^+$ and b) RORγt$^+$FoxP3$^-$ of CD4$^+$CD3$^+$ cells in the CNS-dLNs. Percentage of c) FoxP3$^+$CD25$^+$ and d) RORγt$^+$FoxP3$^-$ of CD4$^+$CD3$^+$ cells in the spleen. Data represent means ± s.e.m. Statistical analysis was performed using ordinary one-way ANOVA with Tukey's multiple comparisons tests. P-values < 0.05 are shown.

As in the prophylactic setting, spleen-derived cells from therapeutic SA IL-33-treated mice restimulated with MOG protein also secreted significantly lower levels of the Th1 and Th17 cytokines IFN-γ (Figure 3.24n), TNF-α (Figure 3.24o), IL-17A (Figure 3.24p), IL-17F (Figure 3.24q), and IL-22 (Figure 3.24r), as well as elevated levels of the Th2 cytokine IL-5 (Figure 3.24s) compared to PBS. Overall, these results suggest that SA IL-33 treatment reduces MOG_{35-55}-EAE severity and promotes immunomodulation in the chronic phase of disease.

3.4.7 Therapeutic SA IL-33 Reduces the Severity of Relapsing-Remitting $PLP_{139-151}$-EAE and Modulates Immune Cells in the SLOs

Lastly, we investigated the effectiveness of therapeutically administered SA IL-33 in a second disease model, relapsing-remitting (RR) EAE. RR-EAE was induced in SJL/J mice via immunization with native $PLP_{139-151}$ antigen emulsified in Complete Freud's Adjuvant followed by pertussis toxin [153][155]. During RR-EAE, mice initially develop acute disease, followed by period of partial or complete recovery called remission, and then a second wave of returning disease called relapse [309]. From day 18, after all mice entered remission, we s.c. administered PBS or SA IL-33 every other day until day 36, for a total of 10 doses (Figure 3.30a). Between the start of treatment and the study endpoint, SA IL-33 treatment significantly reduced disease score compared to PBS (Figure 3.30b, Figure 3.31a-b). Only 6 out of 11 SA IL-33-treated mice relapsed, while 9 out of 11 PBS-treated mice relapsed by the study endpoint (Figure 3.30c). Although SA IL-33 treatment did not significantly increase the probability of remaining relapse-free (Figure 3.31c), during remission, SA IL-33-treated mice displayed a significantly lower minimum EAE score compared to PBS mice (Figure 3.31e) and spent a greater number of remission days with minimal disease symptoms (EAE score ≤ 0.5) (Figure 3.31f).

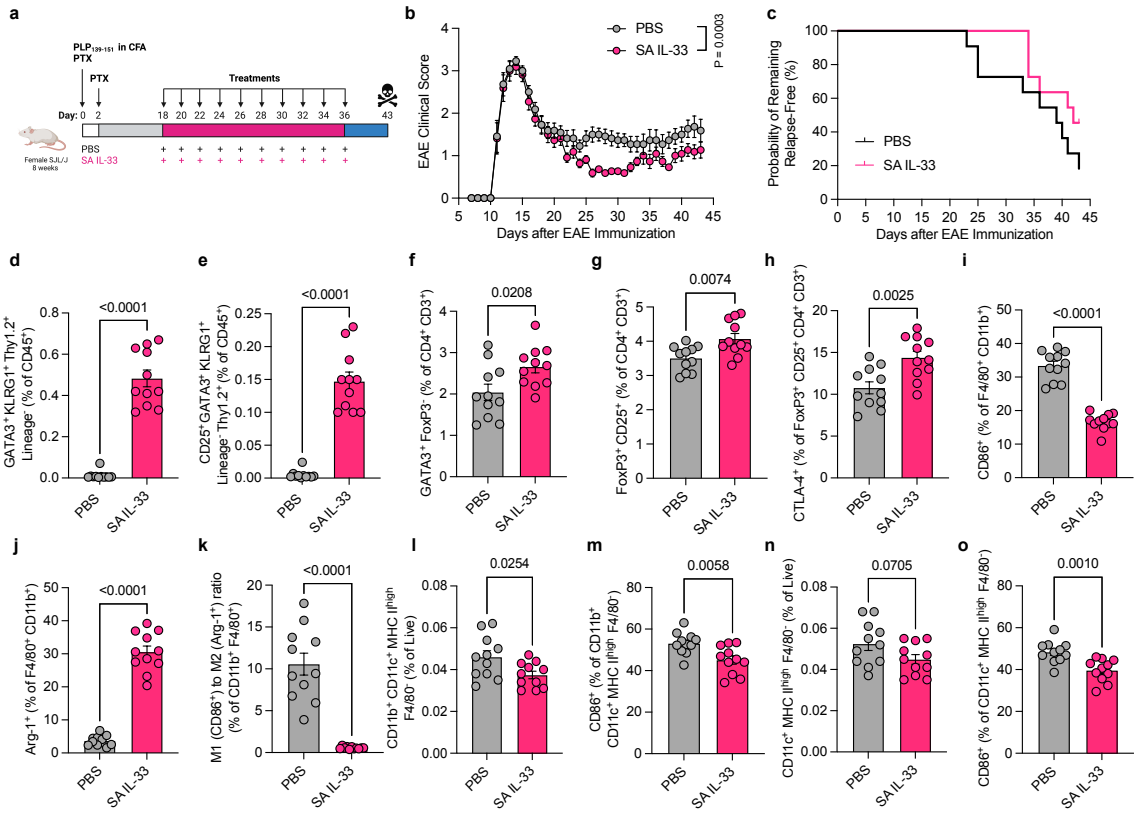

Figure 3.30: **SA IL-33 therapy reduces the severity of relapsing-remitting PLP-EAE and expands protective type 2 immune cells in the CNS-dLNs.** (a) Overview of experimental design. EAE was induced in SJL/J mice by s.c. immunization with $PLP_{139-151}$/CFA followed by i.p. injections of PTX on days 0 and 2. On day 18 post $PLP_{139-151}$ immunization, prior to the start of treatment, mice were assigned into groups of equal average clinical score. Each group was therapeutically administered s.c. PBS or s.c. 26 µg SA IL-33 (molar e.q. to WT IL-33) every other day from days 18 to 36 (n = 11 mice/group). (b) Disease progression. Clinical score of paralysis severity was assessed daily by a blinded investigator. (c) Probability of EAE mice remaining relapse-free. Acute phase, the first episode of disease, was defined as an increase in disease score by $\geq$ 1 grade for $\geq$ 2 consecutive days. Remission phase, a period of clinical improvement, was defined as the reduction of disease score for $\geq$ 2 consecutive days after peak disease score was attained. Relapse phase, a period of disease reoccurrence, was defined as the increase in disease score by $\geq$ 1 grade following remission. (d-o) On day 43, CNS-dLNs were excised and cells were processed for flow cytometric analysis. Percentage of d) $KLRG1^+GATA3^+Thy1.2^+Lin^-$ and e) $CD25^+KLRG1^+GATA3^+Thy1.2^+Lin^-$ of $CD45^+$ cells; f) $GATA3^+FoxP3^-$ and g) $FoxP3^+CD25^+$ of $CD4^+$ cells; h) CTLA-4^+ of $FoxP3^+$ $CD25^+$ cells; and i) $CD86^+$ and j) Arg-1^+ of $CD11b^+F4/80^+$ cells in the CNS-dLNs. k) M1 to M2 macrophage ratio in the CNS-dLNs. Percentage of l) $CD11b^+$ $CD11c^+MHCII^{high}F4/80^-$ of live cells; m) $CD86^+$ of $CD11b^+CD11c^+$ $MHCII^{high}F4/80^-$ cells; n) $CD11c^+MHCII^{high}F4/80^-$ of live cells; and o) $CD86^+$ of $CD11c^+MHCII^{high}F4/80^-$ cells in the CNS-dLNs. Continued on next page.

Figure 3.30: Continued: Data represent means ± s.e.m. Statistical analysis on disease score AUC (from d18 to 43 in (b)) and flow cytometric analysis (d-o) was performed using ordinary one-way ANOVA with Tukey's multiple comparisons tests, and on probability of relapsing (c) using Log-rank (Mantel-Cox) test comparing every two groups. P-values < 0.05 are shown. Diagram in (a) was created in BioRender.com. P-values < 0.05 are shown.

On day 43, the study endpoint, we performed immunophenotyping on the CNS-dLNs. We observed, as in the MOG-EAE model, that SA IL-33 treatment significantly increased the percentage of ILC2s (Figure 3.30d) and their expression of CD25 (Figure 3.30e) compared to PBS. In the T cell compartment, SA IL-33 also increased the percentage of GATA3$^+$ Th2 T cells (Figure 3.30f), as well as the percentage of FoxP3$^+$CD25$^+$ Tregs (Figure 3.30g) and the expression of CTLA-4 on these cells (Figure 3.30h). In the myeloid compartment, SA IL-33 treatment significantly reduced the percentage of CD86$^+$ M1-polarized macrophages (Figure 3.30i), while increasing the percentage of Arg-1$^+$ M2-macrophages (Figure 3.30j), overall reducing the M1 to M2 macrophage ratio (Figure 3.30k). Additionally, SA IL-33 significantly reduced the percentage of CD11b$^+$CD11c$^+$MHCII^{high}F4/80$^-$ DCs (Figure 3.30l), as well as their expression of CD86 (Figure 3.30m). SA IL-33 also trended towards reducing the percentage of CD11c$^+$MHCII^{high}F4/80$^-$ DCs (Figure 3.30n) and significantly reduced their expression of CD86 (Figure 3.30o). Overall, these results suggest that SA IL-33 treatment reduces PLP$_{139-151}$-EAE severity and promotes immunomodulation during later stages of disease.

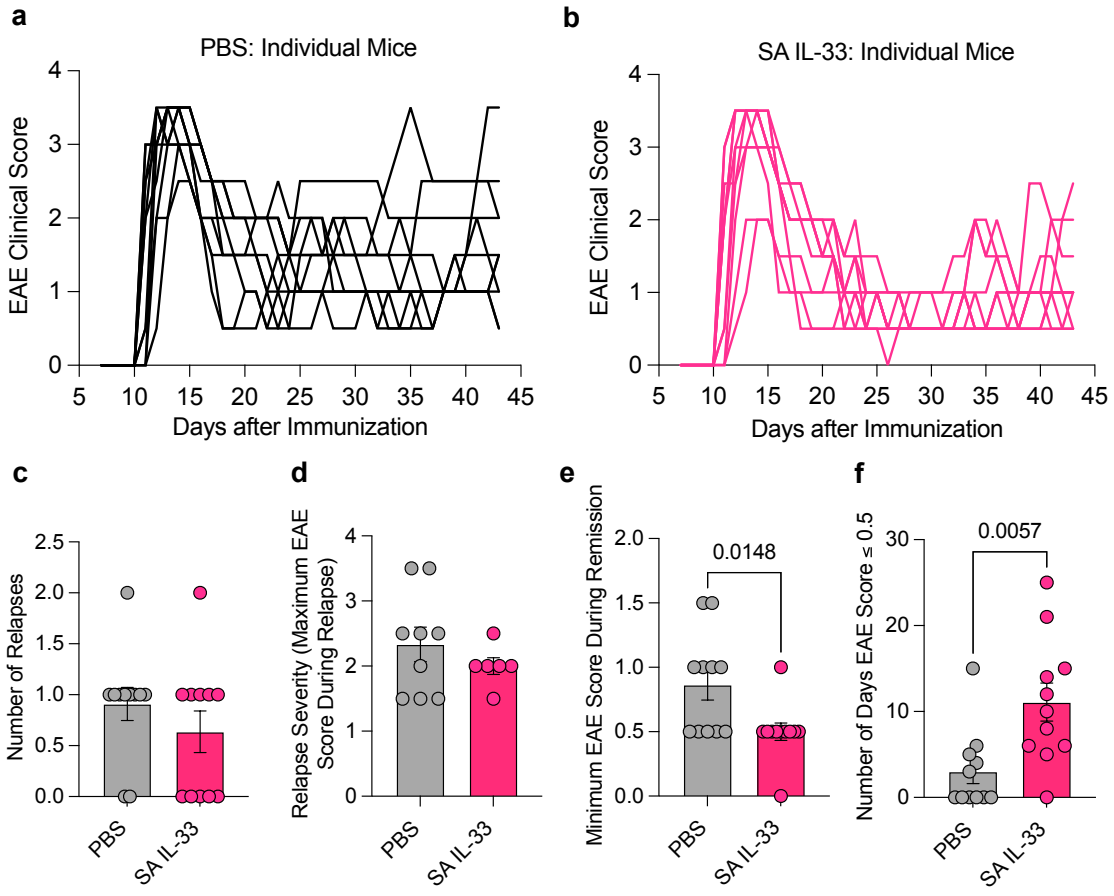

Figure 3.31: **Impact of SA IL-33 treatment on clinical scores of individual $PLP_{139-151}$-EAE mice and relapse parameters.** $PLP_{139-151}$ EAE was induced as described in Figure 3.30a. EAE-bearing mice were therapeutically administered PBS or SA IL-33 from day 18 to 36 as in Figure 3.30 a (n = 11 mice/group). (a-b) Clinical scores of individual mice treated with a) PBS or b) SA IL-33. Remission phase, a period of clinical improvement, was defined as the reduction of disease score for ≥ 2 consecutive days after peak disease score was attained. Relapse phase, a period of disease reoccurrence, was defined as the increase in disease score by ≥ 1 grade following remission. (c-f) Impact of SA IL-33 treatment on c) number of relapses, d) relapse severity, defined as the maximum disease score attained during a relapse, as well as e) minimum EAE score during remission and f) number of days EAE score ≤ 0.5. Data represent means $\pm$ s.e.m. Statistical analysis was performed using unpaired, two-tailed Student's T-test. P-values < 0.05 are shown.

3.5 Discussion

In this study, we engineered SA IL-33, a long-circulating, activity-attenuated fusion of the immunoregulatory cytokine, IL-33, and blood protein, SA. Following rigorous characterization of its pharmacokinetics, bioactivity, and immunotoxicity, we investigated the impact of subcutaneously administered SA IL-33 therapy on the prevention and treatment of EAE, a murine model of neuroinflammation. Through flow cytometric immunophenotyping and cytokine assays, we then explored several pathways by which SA IL-33 may promote immunomodulation in both the SLOs and CNS. Systemically administered, unmodified cytokines exhibit short *in vivo* plasma half-life and insufficient tissue residence [310][311] due to rapid degradation by proteolytic enzymes, receptor-mediated endocytosis, and renal clearance [279], necessitating high dosing frequency [312]. By recombinantly fusing IL-33 to SA, we generated an activity-attenuated protein with several advantages for clinical translation over WT IL-33, including prolonged plasma half-life, increased persistence in the SLOs and CNS, and greatly reduced immunotoxicity. Our results demonstrate that prophylactic SA IL-33 was significantly more effective than WT IL-33 in preventing the onset of EAE, and therapeutic treatment reduced the severity of already-established, chronic and relapsing-remitting EAE. In both treatment regimens, SA IL-33 suppressed pathogenic leukocyte infiltration and cytokine production in the CNS, while expanding protective type 2 immune cells and Treg subsets in the SLOs, compared to PBS-treated mice.

Genetic fusion of IL-33 to the non-immunogenic, water soluble, blood transport protein SA [284][313], prolonged the plasma half-life of IL-33 by approximately 27-fold and significantly increased its persistence in the SLOs both 6 hr and 48 hr post subcutaneous administration compared to WT IL-33. We also detected elevated levels of SA IL-33 in the spinal cord after 48 hr. These results align with previous studies that have demonstrated half-life extension of the cytokines IL-2 [314][315], IL-4 [219], IL-10 [218], IFN-α [316], IFN-β [317], and G-CSF [318] upon fusion to SA. SA likely prolongs cytokine half-life due to its

interaction with cellular receptors including neonatal Fc receptor (FcRn), megalin/cubulin complex, gp18, gp30, and gp60 [282][283][284][312][319][320][321][322]. Upon binding to intracellular FcRn in acidic endosomes, SA is translocated back to the cell surface, where at physiological pH, it dissociates from FcRn and returns to circulation[312][319][321]. In the clinical setting, cytokines with extended half-life require less frequent dosing, which may improve patient compliance [282][312].

Notably, we observed that fusion to SA attenuated the bioactivity of IL-33. Following stimulation with SA IL-33, murine ILC2s exhibited approximately 148-fold reduction in CD25 upregulation compared to WT IL-33-treated cells. Similar differences were noted in IL-33-induced ILC2 cytokine production. SA IL-33 also displayed approximately 233-fold lower bioactivity than WT IL-33 in human IL-33R-expressing HEK cells. It is possible that SA, a bulky 66.5 kD protein [284], may dampen IL-33 bioactivity due to steric hinderance. Evaluation of WT IL-33 and SA IL-33 binding to murine IL-33R, ST2, revealed only an approximately 3.2-fold difference in K_d, which suggests that SA fusion likely impacted IL-33 bioactivity downstream of receptor binding. SA-mediated activity-attenuation is not unprecidented, as we have previously observed that SA fused to the cytokine IL-4 displayed approximately 27-fold reduced bioactivity compared to WT IL-4 [219]. However, the magnitude of activity-attenuation was greater with IL-33 fusion.

Although IL-33-mediated Th2 skewing regulates hyperactive Th17 and Th1 responses [323], playing a protective role in neuroinflammatory diseases [263], overabundant IL-33 signaling contributes to excess type 2 cytokine production by ILC2s and Th2 T cells [280], which has been linked to conditions such as airway inflammation and anaphylactic shock [280]. Notably, SA IL-33 induced lower levels of IL-5 and IL-13, cytokines that promote eosinophil and basophil differentiation, activation, and survival [256][324][325][326][327], in the serum of naive mice than equimolar WT IL-33. These data parallel the elevated EC_{50} of SA IL-33-induced IL-5 and IL-13 production *in vitro*. In disease-bearing, MOG_{35-55}-

EAE mice administered WT IL-33, we observed 50% mortality, while all mice treated with equimolar SA IL-33 remained alive for the duration of the study. Although it remains to be determined whether mortality was caused by WT IL-33 alone or in synergy with the EAE induction components – CFA, an adjuvant derived from inactivated mycobacteria [328], and pertussis toxin, a virulence factor from *Bordetella pertussis* [328] – our results suggest that activity-attenuated SA IL-33 was less toxic than WT IL-33 in the context of this disease model. Future studies will endeavor to characterize the cellular mechanisms of IL-33-mediated immunotoxicity.

We next investigated subcutaneous SA IL-33 as a prophylactic treatment for MOG_{35-55}-induced EAE, a murine model of neuroinflammation triggered by MOG-specific $CD4^+$ T cells [156]. SA IL-33, when administered at an activity-equivalent dose to WT IL-33 on alternate days beginning on day 8, was significantly more effective at preventing EAE disease development, likely due to its prolonged retention, noted in the organ biodistribution study, in the SLOs and spinal cord, key sites of pathogenic T cell priming and inflammation-mediated tissue damage, respectively. WT IL-33 also delayed the onset of severe EAE, but to a lesser extent than SA IL-33. These results align with a previous study by Jiang et al. demonstrating that daily administration of WT IL-33 moderately suppressed EAE development [281] as well as prior work from our laboratory showing that SA-fused to another cytokine, IL-4, was superior to WT IL-4 in preventing EAE [219]. Notably, prophylactic SA IL-33 also displayed similar efficacy to FTY 720, an FDA-approved MS drug that systemically suppresses immunity [302]. Pathogenic leukocyte infiltration in the CNS is a key feature of MS and EAE [156]. Immunophenotyping of the spinal cord revealed that SA IL-33 treatment reduced the percentage of disease-causing MOG Tetramer$^+$RORγt$^+$ Th17 T cells, $CD86^+$ M1-polarized macrophages, and $CD11c^+MHCII^{high}$ dendritic cells in EAE-bearing mice. SA IL-33 treatment also suppressed pro-inflammatory cytokine IFN-γ and TNF-α levels in the spinal cord homogenate. Reduced migration of T cells and myeloid cells into the spinal cord

may prevent CNS damage and its clinical manifestations including loss of mobility [156].

Due to its ability to expand both type 2 immune cell and Treg subsets, IL-33 plays an important role in dampening overactive Th17 and Th1 responses [263]. In this study, we demonstrated that SA IL-33 treatment expanded type 2 immune cells ILC2s, GATA3$^+$ Th2 T cells, and M2-polarized macrophages in the CNS-dLNs and spleen of EAE-bearing mice, while suppressing pathogenic RORγt$^+$ Th17 cells in the spleen and M1-polarized macrophages in both the CNS-dLNs and spleen. These cellular changes were accompanied by a reduction in Th17/Th1 and an increase in Th2 cytokine production in *ex vivo*, restimulated CNS-dLN and spleen-derived cells from SA IL-33-treated, EAE-bearing mice. Our results align with previous reports demonstrating that ILC2s highly express IL-33R and expand upon WT IL-33 stimulation [266][299][298]. Although originally studied in the context of airway inflammation [280], ILC2s may play a protective role in neuroinflammation [329][330]. Studies from Russi et al. reveal that testosterone induces *il33* gene expression [329] and that IL-33-mediated expansion of ILC2s in the dLNs and CNS protects male SJL mice from developing $PLP_{139-151}$-EAE [330]. IL-33R is also highly expressed on Th2 T cells and contributes to their effector function [265]. Immunization of EAE-resistant, male SJL mice with the CNS antigen, MBP, has also been shown to preferentially expand Th2 T cells [331], and adoptive transfer of male-derived Th2 T cells protected female SJL recipients from developing passive EAE [331]. Additionally, IL-33 promotes M2-macrophage polarization [267][281][332][333]. Our results also align with a previous study showing that adoptively-transferred *ex vivo* IL-33 stimulated macrophages reduced EAE severity [281].

In addition to its role in Th2 skewing, SA IL-33 also modulated the Treg compartment in EAE-bearing mice. Tregs play a critical role in suppressing overactive immune responses, in part, by expressing the immune checkpoint markers CTLA-4 and PD-1 [334][335][336]. As CTLA-4 binds to the antigen-presenting cell (APC) costimulatory molecules CD80 and CD86 with greater avidity than CD28, CTLA-4$^+$ Tregs prevent conventional T cells from

receiving APC co-stimulation [335]. PD-1$^+$ Tregs bind to PD-L1-expressing T cells, B cells, and myeloid cells, and suppress their activation, proliferation, cytokine, and antibody production, resulting in apoptosis [336]. SA IL-33-treated mice displayed elevated CTLA-4 and PD-1 expression on FoxP3$^+$CD25$^+$ Tregs in both the CNS-dLNs and spleen of EAE-bearing mice, suggesting that SA IL-33 may augment the immunosuppressive capacity of Tregs. Notably, SA IL-33 treatment also expanded a subset of FoxP3$^+$ Tregs that express IL-33R (ST2$^+$ Tregs) in both the CNS-dLNs and spleen. This finding aligns with previous studies demonstrating that WT IL-33 promotes the expansion of ST2$^+$ Tregs [260][268][337], a heterogenous Treg population that co-express GATA3 [258][338]. IL-33 regulates FoxP3 expression on Tregs by causing the activation and recruitment of GATA3 onto the FoxP3 promoter via the MAP kinase pathway [258][339][340]. ST2$^+$FoxP3$^+$ Tregs contribute to the protective effects of IL-33 in allogenic cardiac [307] and skin [337] transplantation, graft-versus-host-disease [261], and colitis [258][308]. Future studies will seek to further characterize the phenotype and functions of ST2$^+$ Tregs. It is currently unknown whether FoxP3$^+$ Treg expression of ST2 and GATA3 is transient state on the path to becoming an "ex-Treg" or a long-term phenotype [13]. Whether ST2$^+$ Tregs act to broadly suppress the immune system or expand to solely prevent excessive type 2 immunity has also not been elucidated. However, a study by Siede et al. showed that ST2$^+$ Tregs are more effective than ST2$^-$ Tregs in suppressing naive CD4$^+$ T cell proliferation *in vitro* [260], suggesting broad suppression. Additionally, in a murine model of colitis, adoptively transferred ST2$^-$ cells displayed reduced FoxP3 levels, suggesting that IL-33 signaling may contribute to the maintenance of FoxP3 expression in inflammatory contexts [258].

As most MS patients are prescribed medication after onset of symptoms, we also studied the impact of therapeutic SA IL-33 treatment on EAE disease course. For this purpose, we administered SA IL-33 in the chronic phase of MOG_{35-55}-EAE and in the first remission phase of $PLP_{131-151}$-EAE. These murine models display some features of progressive

and relapsing-remitting MS, respectively [156]. Notably, therapeutic SA IL-33 significantly reduced disease score in both the chronic and relapsing-remitting EAE models. In chronic EAE, SA IL-33 also suppressed RORγt$^+$ Th17 cell infiltration in the spinal cord and expanded type 2 immune cells in the CNS-dLNs. Future studies could endeavor to improve the therapeutic efficacy of SA IL-33 in these models by altering the dose regimen or administering SA IL-33 in combination with additional therapies.

SA IL-33 displayed similar therapeutic efficacy to FTY 720, a clinically used MS drug that acts by broadly dampening the immune system [124]. Although effective in managing acute attacks, the majority of available MS therapies are unable to repair or regenerate damaged CNS components such as neurons, oligodendrocytes, or glia, rendering them less effective in reversing progressive forms of the disease, which are characterized by neurodegeneration and axon dysfunction [125]. Furthermore, by broadly suppressing the immune system, these therapies may also inhibit protective repair mechanisms. In healthy mice, IL-33 is highly expressed by mature oligodendrocytes and gray matter astrocytes [341][342] and modulates both CNS-resident immune and neuronal cell phenotype [263]. IL-33R is expressed by microglia [343], astrocytes [342][344], and neurons [281][344]. IL-33 stimulation polarizes microglia towards the M2 phenotype, which contributes to immunoregulation and tissue repair [263]. We observed elevated levels of amphiregulin, a tissue repair-associated growth factor, in the spinal cord homogenate of both prophylactically and therapeutically SA IL-33-treated EAE mice. Based on the tissue biodistribution study, we detected elevated IL-33 in the spinal cord and a trend towards increase in the brain 48 hr after SA IL-33 administration. Although we have yet to determine the cellular source of amphiregulin, it is possible that SA IL-33 may also be acting on CNS-resident cells to promote immunoregulation. In future studies, we intend to characterize the impact of SA IL-33 on these cellular populations via a combination of flow cytometric and immunofluorescence techniques.

In conclusion, we have demonstrated that SA IL-33, a long-circulating, activity-attenuated

fusion of IL-33 and SA, is a promising therapeutic for the treatment of EAE. Given its reduced immunotoxicity, prolonged half-life, and Th2/Treg-skewing mechanism of action, SA IL-33 therapy could be applied to the treatment of a broad array of autoimmune and inflammatory disorders.

3.6 Author Contributions

This chapter and the accompanying figures are adapted from the manuscript "Activity-attenuated albumin interleukin-33 fusion protein suppresses experimental autoimmune encephalomyelitis" by Erica Budina, Shijie Cao, Elyse A. Watkins, Joseph W. Reda, Ani Solanki, Mindy Nguyen, Phillip Ang, J. Emiliano Gomez Medellin, Hye-Rin Chun, Ha-Na Shim, Kevin Hultgren, Zahra Khosravi, Arjun Dhar, Suzana Gomes, Andrew C. Tremain, Ako Ishihara, Jun Ishihara, and Jeffrey A. Hubbell in preparation for publication. J.A.H. oversaw all research. E.B. and J.A.H. designed most of the experiments. E.B. prepared the materials. E.B., S.C., E.A.W., J.W.R., A.S., M.N., P.A., J.E.G.M., H.R.C., H.N.S., K.H., Z.K., A.D., S.G., A.C.T., A.I., and J.I. performed experiments. E.B. analyzed the data. E.B. and J.A.H. wrote the manuscript. All authors contributed to the article and approved the manuscript.

3.7 Acknowledgements

This work was supported by the Chicago Immunoengineering Innovation Center of the University of Chicago and the Alper Family Fund. We thank Dr. Anthony T. Reder and Dr. Aaron Esser-Kahn for helpful discussions. We also thank the Cytometry and Antibody Technology Core Facility (Cancer Center Support Grant P30CA014599) at the University of Chicago.

3.8 Competing Interests

E.B., E.A.W., A.I., J.I., and J.A.H. are inventors on a patent filed by the University of Chicago on uses of SA IL-33.

CHAPTER 4

CONCLUSIONS AND FUTURE DIRECTIONS

The objective of thesis was to develop engineering approaches for the treatment of multiple sclerosis (MS). For this purpose, we employed two different strategies, chemical conjugation and protein engineering, to prolong the bioavailability and *in vivo* half-life of the immunoregulatory molecules, butyrate and interleukin-33. We subsequently evaluated the efficacy of these engineered molecules in the treatment of EAE, a murine model of neuroinflammation that mimics several features of MS, and characterized their respective impact on pathogenic and immunoregulatory cell populations in disease-bearing mice.

In Chapter 2, we engineered the prodrug serine butyrate (SerBut) by esterifying the short chain fatty acid, butyrate, to the amino acid, L-serine. Taking advantage of the gut transport mechanism of amino acids, we hypothesized that serine conjugation would enable butyrate to bypass metabolism in the gut, enter the bloodstream, and exert its immunoregulatory effects systemically. We characterized the biodistribution of SerBut, and demonstrated that conjugation of L-serine to butyrate not only enhanced systemic bioavailability of butyrate but elevated butryate levels in the CNS. We then evaluated the efficacy of SerBut in preventing the onset of EAE, demonstrating that SerBut ameliorated EAE development more effectively than free sodium butyrate or free L-serine. We subsequently performed flow cytometric analysis to characterize the immunological changes induced by SerBut in the draining lymph nodes, spleen, and spinal cord. We observed a reduction in the infiltration of disease-causing RORγt$^+$CD4$^+$ Th17 T cells in the spinal cord. We also noted an expansion of Tregs and a downregulation of activation markers on myeloid cells in the secondary lymphoid organs. Additionally, we evaluated the impact of SerBut administration on global immune responses to vaccination and observed no changes in T cell frequency, B cell frequency, or antibody titers in SerBut-treated mice compared to PBS-treated mice following vaccination. These findings indicate that SerBut modulated immune responses in both the lymphoid and myeloid

compartments without blunting protective immune responses. One limitation of this work is that we administered SerBut therapy in the prophylactic context, prior to EAE disease onset. In future studies, we will evaluate the impact of therapeutic SerBut treatment in EAE-bearing mice with already-established, clinical symptoms of disease.

In Chapter 3, we engineered serum albumin interleukin-33 (SA IL-33), a recombinant fusion of the half-life prolonging blood protein, serum albumin, and the immunoregulatory cytokine, interleukin-33. We then characterized SA IL-33 bioactivity, biodistribution, and toxicity. We demonstrated that SA fusion not only extended the plasma half-life of IL-33 and increased its persistence in the SLOs, but also attenuated the cytokine's bioactivity, reducing drug-related adverse events in both healthy and disease-bearing mice at immunity-modulating doses. We subsequently evaluated the efficacy of prophylactic and therapeutic SA IL-33 administration in both chronic and relapsing-remitting EAE models. We observed that prophylactic SA IL-33 treatment prevented EAE development more effectively than WT IL-33, at biological-activity equivalent doses. Additionally, we showed that therapeutic SA IL-33 treatment reduced the severity of both chronic and relapsing-remitting EAE, in mice with already-established disease. We then performed flow cytometric analysis to characterize the immunological changes mediated by SA IL-33 in the spinal cord and SLOs. In the spinal cord, we observed that SA IL-33 suppressed the infiltration of $CD45^+$ cells, including disease-causing MOG $Tetramer^+$ Th17 T cells and M1-polarized macrophages. In the SLOs, SA IL-33 treatment expanded protective type 2 immune cells including ILC2s, M2-polarized macrophages, $ST2^+$ Tregs, and Th2 T cells. Together these findings suggest that SA IL-33 ameliorated neuroinflammation by promoting immunoregulation with minimal immunotoxicity. Future studies will endeavor to characterize the impact of SA IL-33 treatment on CNS-resident immune cells and neural cells in these various disease contexts.

In conclusion, this thesis seeks to contribute to the emerging field of neuro-immune engineering. We have developed two different approaches for the treatment of neuroinflam-

mation. Our findings provide evidence that these engineered molecules have the potential to serve as next-generation therapeutic agents for multiple sclerosis patients. Further studies, including preclinical and clinical studies, are needed to better understand their long-term safety and efficacy. Given the extensive immunomodulatory effects of SerBut and SA IL-33, it would also be valuable to explore their potential in the treatment of a broader range of immune-related conditions.

REFERENCES

[1] Lifeng Wang, Fu-Sheng Wang, and M. Eric Gershwin. Human autoimmune diseases: a comprehensive update. *Journal of Internal Medicine*, 278(4):369–395, October 2015.

[2] Michael D. Rosenblum, Iris K. Gratz, Jonathan S. Paw, and Abul K. Abbas. Treating Human Autoimmunity: Current Practice and Future Prospects. *Science Translational Medicine*, 4(125), March 2012.

[3] Maunil K. Desai and Roberta Diaz Brinton. Autoimmune Disease in Women: Endocrine Transition and Risk Across the Lifespan. *Frontiers in Endocrinology*, 10:265, April 2019.

[4] S. J. Walsh and L. M. Rau. Autoimmune diseases: a leading cause of death among young and middle-aged women in the United States. *American Journal of Public Health*, 90(9):1463–1466, September 2000.

[5] David S. Pisetsky. Pathogenesis of autoimmune disease. *Nature Reviews Nephrology*, 19(8):509–524, August 2023.

[6] Kenneth Murphy and Casey Weaver. *Janeway's immunobiology*. Garland Science/Taylor & Francis Group, LLC, New York, NY, 9th edition edition, 2016.

[7] Calliope A. Dendrou, Lars Fugger, and Manuel A. Friese. Immunopathology of multiple sclerosis. *Nature Reviews Immunology*, 15(9):545–558, September 2015.

[8] William L. Redmond and Linda A. Sherman. Peripheral Tolerance of CD8 T Lymphocytes. *Immunity*, 22(3):275–284, March 2005.

[9] Mark S. Anderson, Emily S. Venanzi, Ludger Klein, Zhibin Chen, Stuart P. Berzins, Shannon J. Turley, Harald Von Boehmer, Roderick Bronson, Andrée Dierich, Christophe Benoist, and Diane Mathis. Projection of an Immunological Self Shadow Within the Thymus by the Aire Protein. *Science*, 298(5597):1395–1401, November 2002.

[10] Y. Xing and K. A. Hogquist. T-Cell Tolerance: Central and Peripheral. *Cold Spring Harbor Perspectives in Biology*, 4(6):a006957–a006957, June 2012.

[11] Steven Z. Josefowicz, Li-Fan Lu, and Alexander Y. Rudensky. Regulatory T Cells: Mechanisms of Differentiation and Function. *Annual Review of Immunology*, 30(1):531–564, April 2012.

[12] Ludger Klein, Ellen A. Robey, and Chyi-Song Hsieh. Central CD4+ T cell tolerance: deletion versus regulatory T cell differentiation. *Nature Reviews Immunology*, 19(1):7–18, January 2019.

[13] Margarita Dominguez-Villar and David A. Hafler. Regulatory T cells in autoimmune disease. *Nature Immunology*, 19(7):665–673, July 2018.

[14] Eleonora Gambineri, Troy R. Torgerson, and Hans D. Ochs. Immune dysregulation, polyendocrinopathy, enteropathy, and X-linked inheritance (IPEX), a syndrome of systemic autoimmunity caused by mutations of FOXP3, a critical regulator of T-cell homeostasis:. *Current Opinion in Rheumatology*, 15(4):430–435, July 2003.

[15] A. Corthay. How do Regulatory T Cells Work? *Scandinavian Journal of Immunology*, 70(4):326–336, October 2009.

[16] Masaki Hara, Cherry I. Kingsley, Masanori Niimi, Simon Read, Stuart E. Turvey, Andrew R. Bushell, Peter J. Morris, Fiona Powrie, and Kathryn J. Wood. IL-10 Is Required for Regulatory T Cells to Mediate Tolerance to Alloantigens In Vivo. *The Journal of Immunology*, 166(6):3789–3796, March 2001.

[17] Kazuhiko Nakamura, Atsushi Kitani, and Warren Strober. Cell Contact–Dependent Immunosuppression by Cd4+Cd25+Regulatory T Cells Is Mediated by Cell Surface–Bound Transforming Growth Factor β. *The Journal of Experimental Medicine*, 194(5):629–644, September 2001.

[18] Lauren W. Collison, Creg J. Workman, Timothy T. Kuo, Kelli Boyd, Yao Wang, Kate M. Vignali, Richard Cross, David Sehy, Richard S. Blumberg, and Dario A. A. Vignali. The inhibitory cytokine IL-35 contributes to regulatory T-cell function. *Nature*, 450(7169):566–569, November 2007.

[19] Dario A. A. Vignali, Lauren W. Collison, and Creg J. Workman. How regulatory T cells work. *Nature Reviews Immunology*, 8(7):523–532, July 2008.

[20] Pushpa Pandiyan, Lixin Zheng, Satoru Ishihara, Jennifer Reed, and Michael J Lenardo. CD4+CD25+Foxp3+ regulatory T cells induce cytokine deprivation–mediated apoptosis of effector CD4+ T cells. *Nature Immunology*, 8(12):1353–1362, December 2007.

[21] Giovanna Borsellino, Markus Kleinewietfeld, Diletta Di Mitri, Alexander Sternjak, Adamo Diamantini, Raffaella Giometto, Sabine Höpner, Diego Centonze, Giorgio Bernardi, Maria Luisa Dell'Acqua, Paolo Maria Rossini, Luca Battistini, Olaf Rötzschke, and Kirsten Falk. Expression of ectonucleotidase CD39 by Foxp3+ Treg cells: hydrolysis of extracellular ATP and immune suppression. *Blood*, 110(4):1225–1232, August 2007.

[22] James J. Kobie, Pranav R. Shah, Li Yang, Jonathan A. Rebhahn, Deborah J. Fowell, and Tim R. Mosmann. T Regulatory and Primed Uncommitted CD4 T Cells Express CD73, Which Suppresses Effector CD4 T Cells by Converting 5-Adenosine Monophosphate to Adenosine. *The Journal of Immunology*, 177(10):6780–6786, November 2006.

[23] Silvia Deaglio, Karen M. Dwyer, Wenda Gao, David Friedman, Anny Usheva, Anna Erat, Jiang-Fan Chen, Keiichii Enjyoji, Joel Linden, Mohamed Oukka, Vijay K. Kuchroo, Terry B. Strom, and Simon C. Robson. Adenosine generation catalyzed by CD39 and CD73 expressed on regulatory T cells mediates immune suppression. *The Journal of Experimental Medicine*, 204(6):1257–1265, June 2007.

[24] Luca Antonioli, Pál Pacher, E. Sylvester Vizi, and György Haskó. CD39 and CD73 in immunity and inflammation. *Trends in Molecular Medicine*, 19(6):355–367, June 2013.

[25] György Haskó, Joel Linden, Bruce Cronstein, and Pál Pacher. Adenosine receptors: therapeutic aspects for inflammatory and immune diseases. *Nature Reviews Drug Discovery*, 7(9):759–770, September 2008.

[26] Behzad Rowshanravan, Neil Halliday, and David M. Sansom. CTLA-4: a moving target in immunotherapy. *Blood*, 131(1):58–67, January 2018.

[27] Francesca Fallarino, Ursula Grohmann, Kwang Woo Hwang, Ciriana Orabona, Carmine Vacca, Roberta Bianchi, Maria Laura Belladonna, Maria Cristina Fioretti, Maria-Luisa Alegre, and Paolo Puccetti. Modulation of tryptophan catabolism by regulatory T cells. *Nature Immunology*, 4(12):1206–1212, December 2003.

[28] Ching-Tai Huang, Creg J. Workman, Dallas Flies, Xiaoyu Pan, Aimee L. Marson, Gang Zhou, Edward L. Hipkiss, Sowmya Ravi, Jeanne Kowalski, Hyam I. Levitsky, Jonathan D. Powell, Drew M. Pardoll, Charles G. Drake, and Dario A.A. Vignali. Role of LAG-3 in Regulatory T Cells. *Immunity*, 21(4):503–513, October 2004.

[29] Bitao Liang, Craig Workman, Janine Lee, Claude Chew, Benjamin M. Dale, Lucrezia Colonna, Marcella Flores, Nianyu Li, Edina Schweighoffer, Steven Greenberg, Victor Tybulewicz, Dario Vignali, and Raphael Clynes. Regulatory T Cells Inhibit Dendritic Cells by Lymphocyte Activation Gene-3 Engagement of MHC Class II. *The Journal of Immunology*, 180(9):5916–5926, May 2008.

[30] Xin Yu, Kristin Harden, Lino C Gonzalez, Michelle Francesco, Eugene Chiang, Bryan Irving, Irene Tom, Sinisa Ivelja, Canio J Refino, Hilary Clark, Dan Eaton, and Jane L Grogan. The surface protein TIGIT suppresses T cell activation by promoting the generation of mature immunoregulatory dendritic cells. *Nature Immunology*, 10(1):48–57, January 2009.

[31] William J. Grossman, James W. Verbsky, Benjamin L. Tollefsen, Claudia Kemper, John P. Atkinson, and Timothy J. Ley. Differential expression of granzymes A and B in human cytotoxic lymphocyte subsets and T regulatory cells. *Blood*, 104(9):2840–2848, November 2004.

[32] Onder Alpdogan and Marcel R.M. Van Den Brink. Immune Tolerance and Transplantation. *Seminars in Oncology*, 39(6):629–642, December 2012.

[33] Daniel L Mueller. Mechanisms maintaining peripheral tolerance. *Nature Immunology*, 11(1):21–27, January 2010.

[34] Charles Janeway, editor. *Immunobiology: the immune system in health and disease ; [animated CD-ROM inside]*. Garland Publ. [u.a.], New York, NY, 5. ed edition, 2001.

[35] M. K. Jenkins, P. S. Taylor, S. D. Norton, and K. B. Urdahl. CD28 delivers a costimulatory signal involved in antigen-specific IL-2 production by human T cells. *Journal of Immunology (Baltimore, Md.: 1950)*, 147(8):2461–2466, October 1991.

[36] Leonard J. Appleman, Alla Berezovskaya, Isabelle Grass, and Vassiliki A. Boussiotis. CD28 Costimulation Mediates T Cell Expansion Via IL-2-Independent and IL-2-Dependent Regulation of Cell Cycle Progression. *The Journal of Immunology*, 164(1):144–151, January 2000.

[37] Ger J. J. C. Boonen, Astrid M. C. Van Dijk, Leo F. Verdonck, René A. W. Van Lier, Gert Rijksen, and René H. Medema. CD28 induces cell cycle progression by IL-2-independent down-regulation of p27kip1 expression in human peripheral T lymphocytes. *European Journal of Immunology*, 29(3):789–798, March 1999.

[38] Lawrence H. Boise, Andy J. Minn, Patricia J. Noel, Carl H. June, Mary Ann Accavitti, Tullia Lindsten, and Craig B. Thompson. CD28 costimulation can promote T cell survival by enhancing the expression of Bcl-xL. *Immunity*, 3(1):87–98, July 1995.

[39] William L. Redmond, Boris C. Marincek, and Linda A. Sherman. Distinct Requirements for Deletion versus Anergy during CD8 T Cell Peripheral Tolerance In Vivo. *The Journal of Immunology*, 174(4):2046–2053, February 2005.

[40] Pascal Chappert and Ronald H Schwartz. Induction of T cell anergy: integration of environmental cues and infectious tolerance. *Current Opinion in Immunology*, 22(5):552–559, October 2010.

[41] Laura Lossi. The concept of intrinsic versus extrinsic apoptosis. *Biochemical Journal*, 479(3):357–384, February 2022.

[42] Avi Ashkenazi and Vishva M. Dixit. Death Receptors: Signaling and Modulation. *Science*, 281(5381):1305–1308, August 1998.

[43] Peter D. Hughes, Gabrielle T. Belz, Karen A. Fortner, Ralph C. Budd, Andreas Strasser, and Philippe Bouillet. Apoptosis Regulators Fas and Bim Cooperate in Shutdown of Chronic Immune Responses and Prevention of Autoimmunity. *Immunity*, 28(2):197–205, February 2008.

[44] Douglas R. Green and Guido Kroemer. The Pathophysiology of Mitochondrial Cell Death. *Science*, 305(5684):626–629, July 2004.

[45] Victor L Perez, Luk Van Parijs, Andre Biuckians, Xin Xiao Zheng, Terry B Strom, and Abul K Abbas. Induction of Peripheral T Cell Tolerance In Vivo Requires CTLA-4 Engagement. *Immunity*, 6(4):411–417, April 1997.

[46] Andrew D. Wells. New Insights into the Molecular Basis of T Cell Anergy: Anergy Factors, Avoidance Sensors, and Epigenetic Imprinting. *The Journal of Immunology*, 182(12):7331–7341, June 2009.

[47] Richard V. Parry, Jens M. Chemnitz, Kenneth A. Frauwirth, Anthony R. Lanfranco, Inbal Braunstein, Sumire V. Kobayashi, Peter S. Linsley, Craig B. Thompson, and James L. Riley. CTLA-4 and PD-1 Receptors Inhibit T-Cell Activation by Distinct Mechanisms. *Molecular and Cellular Biology*, 25(21):9543–9553, November 2005.

[48] Honorio Torres-Aguilar, Sergio R. Aguilar-Ruiz, Gabriela González-Pérez, Rosario Munguía, Sandra Bajaña, Marco A. Meraz-Ríos, and Carmen Sánchez-Torres. Tolerogenic Dendritic Cells Generated with Different Immunosuppressive Cytokines Induce Antigen-Specific Anergy and Regulatory Properties in Memory CD4+ T Cells. *The Journal of Immunology*, 184(4):1765–1775, February 2010.

[49] Matthias P. Domogalla, Patricia V. Rostan, Verena K. Raker, and Kerstin Steinbrink. Tolerance through Education: How Tolerogenic Dendritic Cells Shape Immunity. *Frontiers in Immunology*, 8:1764, December 2017.

[50] B Rocha, A Grandien, and A A Freitas. Anergy and exhaustion are independent mechanisms of peripheral T cell tolerance. *The Journal of Experimental Medicine*, 181(3):993–1003, March 1995.

[51] Ethan M. Shevach and Angela M. Thornton. tTregs, pTregs, and iTregs: similarities and differences. *Immunological Reviews*, 259(1):88–102, May 2014.

[52] C. Garrison Fathman and Neil B. Lineberry. Molecular mechanisms of CD4+ T-cell anergy. *Nature Reviews Immunology*, 7(8):599–609, August 2007.

[53] Mahesh Yadav, Stephen Stephan, and Jeffrey A. Bluestone. Peripherally Induced Tregs – Role in Immune Homeostasis and Autoimmunity. *Frontiers in Immunology*, 4, 2013.

[54] Jeffrey A. Bluestone and Abul K. Abbas. Natural versus adaptive regulatory T cells. *Nature Reviews Immunology*, 3(3):253–257, March 2003.

[55] Karsten Kretschmer, Irina Apostolou, Daniel Hawiger, Khashayarsha Khazaie, Michel C Nussenzweig, and Harald Von Boehmer. Inducing and expanding regulatory T cell populations by foreign antigen. *Nature Immunology*, 6(12):1219–1227, December 2005.

[56] Maria A. Curotto De Lafaille and Juan J. Lafaille. Natural and Adaptive Foxp3+ Regulatory T Cells: More of the Same or a Division of Labor? *Immunity*, 30(5):626–635, May 2009.

[57] WanJun Chen, Wenwen Jin, Neil Hardegen, Ke-jian Lei, Li Li, Nancy Marinos, George McGrady, and Sharon M. Wahl. Conversion of Peripheral CD4+CD25- Naive T Cells to CD4+CD25+ Regulatory T Cells by TGF-β Induction of Transcription Factor *Foxp3*. *The Journal of Experimental Medicine*, 198(12):1875–1886, December 2003.

[58] E John Wherry. T cell exhaustion. *Nature Immunology*, 12(6):492–499, June 2011.

[59] E. John Wherry and Makoto Kurachi. Molecular and cellular insights into T cell exhaustion. *Nature Reviews Immunology*, 15(8):486–499, August 2015.

[60] Kemal Catakovic, Eckhard Klieser, Daniel Neureiter, and Roland Geisberger. T cell exhaustion: from pathophysiological basics to tumor immunotherapy. *Cell Communication and Signaling*, 15(1):1, December 2017.

[61] Zhanyan Gao, Yang Feng, Jinhua Xu, and Jun Liang. T-cell exhaustion in immune-mediated inflammatory diseases: New implications for immunotherapy. *Frontiers in Immunology*, 13:977394, September 2022.

[62] Ismo Ulmanen, Maria Halonen, Tanja Ilmarinen, and Leena Peltonen. Monogenic autoimmune diseases — lessons of self-tolerance. *Current Opinion in Immunology*, 17(6):609–615, December 2005.

[63] Kentaro Nagamine, Pärt Peterson, Hamish S. Scott, Jun Kudoh, Shinsei Minoshima, Maarit Heino, Kai J. E. Krohn, Maria D. Lalioti, Primus E. Mullis, Stylianos E. Antonarakis, Kazuhiko Kawasaki, Shuichi Asakawa, Fumiaki Ito, and Nobuyoshi Shimizu. Positional cloning of the APECED gene. *Nature Genetics*, 17(4):393–398, December 1997.

[64] Mark S. Anderson, Emily S. Venanzi, Ludger Klein, Zhibin Chen, Stuart P. Berzins, Shannon J. Turley, Harald Von Boehmer, Roderick Bronson, Andrée Dierich, Christophe Benoist, and Diane Mathis. Projection of an Immunological Self Shadow Within the Thymus by the Aire Protein. *Science*, 298(5597):1395–1401, November 2002.

[65] Department of Neurology, University of California at San Francisco, San Francisco, CA, USA, Alessandro Didonna, Jorge R. Oksenberg, and Department of Neurology, University of California at San Francisco, San Francisco, CA, USA. The Genetics of Multiple Sclerosis. In Department of Neural & Behavioral Sciences, Pennsylvania State University College of Medicine Hershey, Pennsylvania, USA, Ian S. Zagon, Patricia J. McLaughlin, and Department of Neural & Behavioral Sciences, Pennsylvania State University College of Medicine Hershey, Pennsylvania, USA, editors, *Multiple Sclerosis: Perspectives in Treatment and Pathogenesis*, pages 3–16. Codon Publications, November 2017.

[66] Roger Horton, Laurens Wilming, Vikki Rand, Ruth C. Lovering, Elspeth A. Bruford, Varsha K. Khodiyar, Michael J. Lush, Sue Povey, C. Conover Talbot, Mathew W. Wright, Hester M. Wain, John Trowsdale, Andreas Ziegler, and Stephan Beck. Gene map of the extended human MHC. *Nature Reviews Genetics*, 5(12):889–899, December 2004.

[67] Ludvig M Sollid, Wouter Pos, and Kai W Wucherpfennig. Molecular mechanisms for contribution of MHC molecules to autoimmune diseases. *Current Opinion in Immunology*, 31:24–30, December 2014.

[68] J A Hollenbach, M J Pando, S J Caillier, P-A Gourraud, and J R Oksenberg. The killer immunoglobulin-like receptor KIR3DL1 in combination with HLA-Bw4 is protective against multiple sclerosis in African Americans. *Genes & Immunity*, 17(3):199–202, April 2016.

[69] Samantha S. Soldan and Paul M. Lieberman. Epstein–Barr virus and multiple sclerosis. *Nature Reviews Microbiology*, 21(1):51–64, January 2023.

[70] Kathrine E. Attfield, Lise Torp Jensen, Max Kaufmann, Manuel A. Friese, and Lars Fugger. The immunology of multiple sclerosis. *Nature Reviews Immunology*, 22(12):734–750, December 2022.

[71] D. T. Okuda, R. Srinivasan, J. R. Oksenberg, D. S. Goodin, S. E. Baranzini, A. Beheshtian, E. Waubant, S. S. Zamvil, D. Leppert, P. Qualley, R. Lincoln, R. Gomez, S. Caillier, M. George, J. Wang, S. J. Nelson, B. A. C. Cree, S. L. Hauser, and D. Pelletier. Genotype–Phenotype correlations in multiple sclerosis: HLA genes influence disease severity inferred by 1HMR spectroscopy and MRI measures. *Brain*, 132(1):250–259, January 2009.

[72] B. C. Healy, M. Liguori, D. Tran, T. Chitnis, B. Glanz, C. Wolfish, S. Gauthier, G. Buckle, M. Houtchens, L. Stazzone, S. Khoury, R. Hartzmann, M. Fernandez-Vina, D. A. Hafler, H. L. Weiner, C. R. G. Guttmann, and P. L. De Jager. HLA B*44: Protective effects in MS susceptibility and MRI outcome measures. *Neurology*, 75(7):634–640, August 2010.

[73] Risk Alleles for Multiple Sclerosis Identified by a Genomewide Study. *New England Journal of Medicine*, 357(9):851–862, August 2007.

[74] Roberta Calabrese, Michele Zampieri, Rosella Mechelli, Viviana Annibali, Tiziana Guastafierro, Fabio Ciccarone, Giulia Coarelli, Renato Umeton, Marco Salvetti, and Paola Caiafa. Methylation-dependent *PAD2* upregulation in multiple sclerosis peripheral blood. *Multiple Sclerosis Journal*, 18(3):299–304, March 2012.

[75] Fabrizio G. Mastronardi, Abdul Noor, D. Denise Wood, Tara Paton, and Mario A. Moscarello. Peptidyl argininedeiminase 2 CpG island in multiple sclerosis white matter is hypomethylated. *Journal of Neuroscience Research*, 85(9):2006–2016, July 2007.

[76] Zhenyu Wu, Patrick Li, Yuzi Tian, Wenlu Ouyang, Jessie Wai-Yan Ho, Hasan B. Alam, and Yongqing Li. Peptidylarginine Deiminase 2 in Host Immunity: Current Insights and Perspectives. *Frontiers in Immunology*, 12:761946, November 2021.

[77] Chiharu Kumagai, Bernadette Kalman, Frank A. Middleton, Tamara Vyshkina, and Paul T. Massa. Increased promoter methylation of the immune regulatory gene SHP-1 in leukocytes of multiple sclerosis subjects. *Journal of Neuroimmunology*, 246(1-2):51–57, May 2012.

[78] George P Christophi, Chad A Hudson, Ross C Gruber, Christoforos P Christophi, Cornelia Mihai, Luis J Mejico, Burk Jubelt, and Paul T Massa. SHP-1 deficiency and increased inflammatory gene expression in PBMCs of multiple sclerosis patients. *Laboratory Investigation*, 88(3):243–255, March 2008.

[79] Manuel Rojas, Paula Restrepo-Jiménez, Diana M. Monsalve, Yovana Pacheco, Yeny Acosta-Ampudia, Carolina Ramírez-Santana, Patrick S.C. Leung, Aftab A. Ansari, M. Eric Gershwin, and Juan-Manuel Anaya. Molecular mimicry and autoimmunity. *Journal of Autoimmunity*, 95:100–123, December 2018.

[80] A. M. Powell and M. M. Black. Epitope spreading: protection from pathogens, but propagation of autoimmunity?: Epitope spreading. *Clinical and Experimental Dermatology*, 26(5):427–433, July 2001.

[81] Carol L. Vanderlugt and Stephen D. Miller. Epitope spreading in immune-mediated diseases: implications for immunotherapy. *Nature Reviews Immunology*, 2(2):85–95, February 2002.

[82] Kjetil Bjornevik, Marianna Cortese, Brian C. Healy, Jens Kuhle, Michael J. Mina, Yumei Leng, Stephen J. Elledge, David W. Niebuhr, Ann I. Scher, Kassandra L. Munger, and Alberto Ascherio. Longitudinal analysis reveals high prevalence of Epstein-Barr virus associated with multiple sclerosis. *Science*, 375(6578):296–301, January 2022.

[83] Samantha K. Dunmire, Priya S. Verghese, and Henry H. Balfour. Primary Epstein-Barr virus infection. *Journal of Clinical Virology*, 102:84–92, May 2018.

[84] Takayuki Murata, Atsuko Sugimoto, Tomoki Inagaki, Yusuke Yanagi, Takahiro Watanabe, Yoshitaka Sato, and Hiroshi Kimura. Molecular Basis of Epstein–Barr Virus Latency Establishment and Lytic Reactivation. *Viruses*, 13(12):2344, November 2021.

[85] Barbara Serafini, Barbara Rosicarelli, Diego Franciotta, Roberta Magliozzi, Richard Reynolds, Paola Cinque, Laura Andreoni, Pankaj Trivedi, Marco Salvetti, Alberto Faggioni, and Francesca Aloisi. Dysregulated Epstein-Barr virus infection in the multiple sclerosis brain. *The Journal of Experimental Medicine*, 204(12):2899–2912, November 2007.

[86] Monica A. Moreno, Noga Or-Geva, Blake T. Aftab, Rajiv Khanna, Ed Croze, Lawrence Steinman, and May H. Han. Molecular signature of Epstein-Barr virus infection in MS brain lesions. *Neurology - Neuroimmunology Neuroinflammation*, 5(4):e466, July 2018.

[87] Jan D. Lünemann, Ilijas Jelčić, Susanne Roberts, Andreas Lutterotti, Björn Tackenberg, Roland Martin, and Christian Münz. EBNA1-specific T cells from patients with multiple sclerosis cross react with myelin antigens and co-produce IFN-γ and IL-2. *The Journal of Experimental Medicine*, 205(8):1763–1773, August 2008.

[88] Trygve Holmøy, Espen Østhagen Kvale, and Frode Vartdal. Cerebrospinal fluid CD4 $^{+}$ T cells from a multiple sclerosis patient cross-recognize Epstein-Barr virus and myelin basic protein. *Journal of Neurovirology*, 10(5):278–283, January 2004.

[89] Tobias V. Lanz, R. Camille Brewer, Peggy P. Ho, Jae-Seung Moon, Kevin M. Jude, Daniel Fernandez, Ricardo A. Fernandes, Alejandro M. Gomez, Gabriel-Stefan Nadj, Christopher M. Bartley, Ryan D. Schubert, Isobel A. Hawes, Sara E. Vazquez, Manasi Iyer, J. Bradley Zuchero, Bianca Teegen, Jeffrey E. Dunn, Christopher B. Lock, Lucas B. Kipp, Victoria C. Cotham, Beatrix M. Ueberheide, Blake T. Aftab, Mark S. Anderson, Joseph L. DeRisi, Michael R. Wilson, Rachael J. M. Bashford-Rogers, Michael Platten, K. Christopher Garcia, Lawrence Steinman, and William H. Robinson. Clonally expanded B cells in multiple sclerosis bind EBV EBNA1 and GlialCAM. *Nature*, 603(7900):321–327, March 2022.

[90] Kai W Wucherpfennig and Jack L Strominger. Molecular mimicry in T cell-mediated autoimmunity: Viral peptides activate human T cell clones specific for myelin basic protein. *Cell*, 80(5):695–705, March 1995.

[91] Kaijian Hou, Zhuo-Xun Wu, Xuan-Yu Chen, Jing-Quan Wang, Dongya Zhang, Chuanxing Xiao, Dan Zhu, Jagadish B. Koya, Liuya Wei, Jilin Li, and Zhe-Sheng Chen. Microbiota in health and diseases. *Signal Transduction and Targeted Therapy*, 7(1):135, April 2022.

[92] Javier Ochoa-Repáraz and Lloyd H. Kasper. Gut microbiome and the risk factors in central nervous system autoimmunity. *FEBS Letters*, 588(22):4214–4222, November 2014.

[93] Gabriele Berg, Daria Rybakova, Doreen Fischer, Tomislav Cernava, Marie-Christine Champomier Vergès, Trevor Charles, Xiaoyulong Chen, Luca Cocolin, Kellye Eversole, Gema Herrero Corral, Maria Kazou, Linda Kinkel, Lene Lange, Nelson Lima, Alexander Loy, James A. Macklin, Emmanuelle Maguin, Tim Mauchline, Ryan McClure, Birgit Mitter, Matthew Ryan, Inga Sarand, Hauke Smidt, Bettina Schelkle, Hugo Roume, G. Seghal Kiran, Joseph Selvin, Rafael Soares Correa De Souza, Leo Van Overbeek, Brajesh K. Singh, Michael Wagner, Aaron Walsh, Angela Sessitsch, and Michael Schloter. Microbiome definition re-visited: old concepts and new challenges. *Microbiome*, 8(1):103, December 2020.

[94] Catherine A. Lozupone, Jesse I. Stombaugh, Jeffrey I. Gordon, Janet K. Jansson, and Rob Knight. Diversity, stability and resilience of the human gut microbiota. *Nature*, 489(7415):220–230, September 2012.

[95] Anastasia Revel-Muroz, Mikhail Akulinin, Polina Shilova, Alexander Tyakht, and Natalia Klimenko. Stability of human gut microbiome: Comparison of ecological modelling and observational approaches. *Computational and Structural Biotechnology Journal*, 21:4456–4468, 2023.

[96] Maayan Levy, Aleksandra A. Kolodziejczyk, Christoph A. Thaiss, and Eran Elinav. Dysbiosis and the immune system. *Nature Reviews Immunology*, 17(4):219–232, April 2017.

[97] Ruth E. Ley, Peter J. Turnbaugh, Samuel Klein, and Jeffrey I. Gordon. Human gut microbes associated with obesity. *Nature*, 444(7122):1022–1023, December 2006.

[98] Daniel W. Mielcarz and Lloyd H. Kasper. The Gut Microbiome in Multiple Sclerosis. *Current Treatment Options in Neurology*, 17(4):18, April 2015.

[99] Ivaylo I. Ivanov, Koji Atarashi, Nicolas Manel, Eoin L. Brodie, Tatsuichiro Shima, Ulas Karaoz, Dongguang Wei, Katherine C. Goldfarb, Clark A. Santee, Susan V. Lynch, Takeshi Tanoue, Akemi Imaoka, Kikuji Itoh, Kiyoshi Takeda, Yoshinori Umesaki, Kenya Honda, and Dan R. Littman. Induction of Intestinal Th17 Cells by Segmented Filamentous Bacteria. *Cell*, 139(3):485–498, October 2009.

[100] Pamela V. Chang, Liming Hao, Stefan Offermanns, and Ruslan Medzhitov. The microbial metabolite butyrate regulates intestinal macrophage function via histone deacetylase inhibition. *Proceedings of the National Academy of Sciences*, 111(6):2247–2252, February 2014.

[101] E Candido. Sodium butyrate inhibits histone deacetylation in cultured cells. *Cell*, 14(1):105–113, May 1978.

[102] Yukihiro Furusawa, Yuuki Obata, Shinji Fukuda, Takaho A. Endo, Gaku Nakato, Daisuke Takahashi, Yumiko Nakanishi, Chikako Uetake, Keiko Kato, Tamotsu Kato, Masumi Takahashi, Noriko N. Fukuda, Shinnosuke Murakami, Eiji Miyauchi, Shingo Hino, Koji Atarashi, Satoshi Onawa, Yumiko Fujimura, Trevor Lockett, Julie M. Clarke, David L. Topping, Masaru Tomita, Shohei Hori, Osamu Ohara, Tatsuya Morita, Haruhiko Koseki, Jun Kikuchi, Kenya Honda, Koji Hase, and Hiroshi Ohno. Commensal microbe-derived butyrate induces the differentiation of colonic regulatory T cells. *Nature*, 504(7480):446–450, December 2013.

[103] Patrick M. Smith, Michael R. Howitt, Nicolai Panikov, Monia Michaud, Carey Ann Gallini, Mohammad Bohlooly-Y, Jonathan N. Glickman, and Wendy S. Garrett. The Microbial Metabolites, Short-Chain Fatty Acids, Regulate Colonic T $_{\text{reg}}$ Cell Homeostasis. *Science*, 341(6145):569–573, August 2013.

[104] Koji Atarashi, Takeshi Tanoue, Minoru Ando, Nobuhiko Kamada, Yuji Nagano, Seiko Narushima, Wataru Suda, Akemi Imaoka, Hiromi Setoyama, Takashi Nagamori, Eiji Ishikawa, Tatsuichiro Shima, Taeko Hara, Shoichi Kado, Toshi Jinnohara, Hiroshi Ohno, Takashi Kondo, Kiminori Toyooka, Eiichiro Watanabe, Shin-ichiro Yokoyama, Shunji Tokoro, Hiroshi Mori, Yurika Noguchi, Hidetoshi Morita, Ivaylo I. Ivanov, Tsuyoshi Sugiyama, Gabriel Nuñez, J. Gray Camp, Masahira Hattori, Yoshinori Umesaki, and Kenya Honda. Th17 Cell Induction by Adhesion of Microbes to Intestinal Epithelial Cells. *Cell*, 163(2):367–380, October 2015.

[105] Teruyuki Sano, Wendy Huang, Jason A. Hall, Yi Yang, Alessandra Chen, Samuel J. Gavzy, June-Yong Lee, Joshua W. Ziel, Emily R. Miraldi, Ana I. Domingos, Richard Bonneau, and Dan R. Littman. An IL-23R/IL-22 Circuit Regulates Epithelial Serum Amyloid A to Promote Local Effector Th17 Responses. *Cell*, 163(2):381–393, October 2015.

[106] Emelyne Lécuyer, Sabine Rakotobe, Hélène Lengliné-Garnier, Corinne Lebreton, Marion Picard, Catherine Juste, Rémi Fritzen, Gérard Eberl, Kathy D. McCoy, Andrew J. Macpherson, Claude-Agnès Reynaud, Nadine Cerf-Bensussan, and Valérie Gaboriau-Routhiau. Segmented Filamentous Bacterium Uses Secondary and Tertiary Lymphoid Tissues to Induce Gut IgA and Specific T Helper 17 Cell Responses. *Immunity*, 40(4):608–620, April 2014.

[107] Tomas Hrncir. Gut Microbiota Dysbiosis: Triggers, Consequences, Diagnostic and Therapeutic Options. *Microorganisms*, 10(3):578, March 2022.

[108] Arianna K. DeGruttola, Daren Low, Atsushi Mizoguchi, and Emiko Mizoguchi. Current Understanding of Dysbiosis in Disease in Human and Animal Models:. *Inflammatory Bowel Diseases*, 22(5):1137–1150, May 2016.

[109] Jorge Correale, Reinhard Hohlfeld, and Sergio E. Baranzini. The role of the gut microbiota in multiple sclerosis. *Nature Reviews Neurology*, 18(9):544–558, September 2022.

[110] Jun Chen, Nicholas Chia, Krishna R. Kalari, Janet Z. Yao, Martina Novotna, M. Mateo Paz Soldan, David H. Luckey, Eric V. Marietta, Patricio R. Jeraldo, Xianfeng Chen, Brian G. Weinshenker, Moses Rodriguez, Orhun H. Kantarci, Heidi Nelson, Joseph A. Murray, and Ashutosh K. Mangalam. Multiple sclerosis patients have a distinct gut microbiota compared to healthy controls. *Scientific Reports*, 6(1):28484, June 2016.

[111] Sachiko Miyake, Sangwan Kim, Wataru Suda, Kenshiro Oshima, Masakazu Nakamura, Takako Matsuoka, Norio Chihara, Atsuko Tomita, Wakiro Sato, Seok-Won Kim, Hidetoshi Morita, Masahira Hattori, and Takashi Yamamura. Dysbiosis in the Gut Microbiota of Patients with Multiple Sclerosis, with a Striking Depletion of Species Belonging to Clostridia XIVa and IV Clusters. *PLOS ONE*, 10(9):e0137429, September 2015.

[112] Kerstin Berer, Marsilius Mues, Michail Koutrolos, Zakeya Al Rasbi, Marina Boziki, Caroline Johner, Hartmut Wekerle, and Gurumoorthy Krishnamoorthy. Commensal microbiota and myelin autoantigen cooperate to trigger autoimmune demyelination. *Nature*, 479(7374):538–541, November 2011.

[113] Egle Cekanaviciute, Bryan B. Yoo, Tessel F. Runia, Justine W. Debelius, Sneha Singh, Charlotte A. Nelson, Rachel Kanner, Yadira Bencosme, Yun Kyung Lee, Stephen L. Hauser, Elizabeth Crabtree-Hartman, Ilana Katz Sand, Mar Gacias, Yunjiao Zhu, Patrizia Casaccia, Bruce A. C. Cree, Rob Knight, Sarkis K. Mazmanian, and Sergio E.

Baranzini. Gut bacteria from multiple sclerosis patients modulate human T cells and exacerbate symptoms in mouse models. *Proceedings of the National Academy of Sciences*, 114(40):10713–10718, October 2017.

[114] Caroline C. Whitacre. Sex differences in autoimmune disease. *Nature Immunology*, 2(9):777–780, September 2001.

[115] María C. Ysrraelit and Jorge Correale. Impact of sex hormones on immune function and multiple sclerosis development. *Immunology*, 156(1):9–22, January 2019.

[116] Lucy Ryan and Kingston H. G. Mills. Sex differences regulate immune responses in experimental autoimmune encephalomyelitis and multiple sclerosis. *European Journal of Immunology*, 52(1):24–33, January 2022.

[117] Rhonda R Voskuhl. The effect of sex on multiple sclerosis risk and disease progression. *Multiple Sclerosis Journal*, 26(5):554–560, April 2020.

[118] Christian Confavreux, Michael Hutchinson, Martine Marie Hours, Patricia Cortinovis-Tourniaire, and Thibault Moreau. Rate of Pregnancy-Related Relapse in Multiple Sclerosis. *New England Journal of Medicine*, 339(5):285–291, July 1998.

[119] Charles Pierrot-Deseilligny and Jean-Claude Souberbielle. Vitamin D and multiple sclerosis: An update. *Multiple Sclerosis and Related Disorders*, 14:35–45, May 2017.

[120] Alberto Ascherio, Kassandra L Munger, and K Claire Simon. Vitamin D and multiple sclerosis. *The Lancet Neurology*, 9(6):599–612, June 2010.

[121] Cynthia Aranow. Vitamin D and the immune system. *Journal of Investigative Medicine: The Official Publication of the American Federation for Clinical Research*, 59(6):881–886, August 2011.

[122] K. L. Munger, S. M. Zhang, E. O'Reilly, M. A. Hernan, M. J. Olek, W. C. Willett, and A. Ascherio. Vitamin D intake and incidence of multiple sclerosis. *Neurology*, 62(1):60–65, January 2004.

[123] Clare Baecher-Allan, Belinda J. Kaskow, and Howard L. Weiner. Multiple Sclerosis: Mechanisms and Immunotherapy. *Neuron*, 97(4):742–768, February 2018.

[124] Dean M. Wingerchuk and Jonathan L. Carter. Multiple Sclerosis: Current and Emerging Disease-Modifying Therapies and Treatment Strategies. *Mayo Clinic Proceedings*, 89(2):225–240, February 2014.

[125] Stephen L. Hauser and Bruce A.C. Cree. Treatment of Multiple Sclerosis: A Review. *The American Journal of Medicine*, 133(12):1380–1390.e2, December 2020.

[126] F. D. Lublin, S. C. Reingold, J. A. Cohen, G. R. Cutter, P. S. Sorensen, A. J. Thompson, J. S. Wolinsky, L. J. Balcer, B. Banwell, F. Barkhof, B. Bebo, P. A. Calabresi,

M. Clanet, G. Comi, R. J. Fox, M. S. Freedman, A. D. Goodman, M. Inglese, L. Kappos, B. C. Kieseier, J. A. Lincoln, C. Lubetzki, A. E. Miller, X. Montalban, P. W. O'Connor, J. Petkau, C. Pozzilli, R. A. Rudick, M. P. Sormani, O. Stuve, E. Waubant, and C. H. Polman. Defining the clinical course of multiple sclerosis: The 2013 revisions. *Neurology*, 83(3):278–286, July 2014.

[127] M Pette, K Fujita, D Wilkinson, D M Altmann, J Trowsdale, G Giegerich, A Hinkkanen, J T Epplen, L Kappos, and H Wekerle. Myelin autoreactivity in multiple sclerosis: recognition of myelin basic protein in the context of HLA-DR2 products by T lymphocytes of multiple-sclerosis patients and healthy donors. *Proceedings of the National Academy of Sciences*, 87(20):7968–7972, October 1990.

[128] Bibiana Bielekova, Myong-Hee Sung, Nadja Kadom, Richard Simon, Henry McFarland, and Roland Martin. Expansion and Functional Relevance of High-Avidity Myelin-Specific CD4+ T Cells in Multiple Sclerosis. *The Journal of Immunology*, 172(6):3893–3904, March 2004.

[129] Niels Hellings, Mark Bare, Christof Verhoeven, Marie Beatrijs D'hooghe, Robert Medaer, Claude C.A. Bernard, Jef Raus, and Piet Stinissen. T-cell reactivity to multiple myelin antigens in multiple sclerosis patients and healthy controls. *Journal of Neuroscience Research*, 63(3):290–302, February 2001.

[130] Cm Pelfrey, Lr Tranquill, Ab Vogt, and Hf McFarland. T cell response to two immunodominant proteolipid protein (PLP) peptides in multiple sclerosis patients and healthy controls. *Multiple Sclerosis Journal*, 1(5):270–278, April 1996.

[131] P. Keskinen, T. Ronni, S. Matikainen, A. Lehtonen, and I. Julkunen. Regulation of HLA class I and II expression by interferons and influenza A virus in human peripheral blood mononuclear cells. *Immunology*, 91(3):421–429, July 1997.

[132] Jula Huppert, Dorothea Closhen, Andrew Croxford, Robin White, Paulina Kulig, Eweline Pietrowski, Ingo Bechmann, Burkhard Becher, Heiko J. Luhmann, Ari Waisman, and Christoph R. W. Kuhlmann. Cellular mechanisms of IL-17-induced blood-brain barrier disruption. *The FASEB Journal*, 24(4):1023–1034, April 2010.

[133] Bruce D. Trapp and Klaus-Armin Nave. Multiple Sclerosis: An Immune or Neurodegenerative Disorder? *Annual Review of Neuroscience*, 31(1):247–269, July 2008.

[134] Haley E. Titus, Yanan Chen, Joseph R. Podojil, Andrew P. Robinson, Roumen Balabanov, Brian Popko, and Stephen D. Miller. Pre-clinical and Clinical Implications of "Inside-Out" vs. "Outside-In" Paradigms in Multiple Sclerosis Etiopathogenesis. *Frontiers in Cellular Neuroscience*, 14:599717, October 2020.

[135] Josa M. Frischer, Stephan Bramow, Assunta Dal-Bianco, Claudia F. Lucchinetti, Helmut Rauschka, Manfred Schmidbauer, Henning Laursen, Per Soelberg Sorensen, and Hans Lassmann. The relation between inflammation and neurodegeneration in multiple sclerosis brains. *Brain*, 132(5):1175–1189, May 2009.

[136] Manuel A. Friese and Lars Fugger. Pathogenic CD8(+) T cells in multiple sclerosis. *Annals of Neurology*, 66(2):132–141, August 2009.

[137] Ying C. Q. Zang, Sufang Li, Victor M. Rivera, Jian Hong, Rachel R. Robinson, Wini T. Breitbach, James Killian, and Jingwu Z. Zhang. Increased CD8+ Cytotoxic T Cell Responses to Myelin Basic Protein in Multiple Sclerosis. *The Journal of Immunology*, 172(8):5120–5127, April 2004.

[138] C Malmestrom, J Lycke, S Haghighi, O Andersen, L Carlsson, H Wadenvik, and B Olsson. Relapses in multiple sclerosis are associated with increased CD8+ T-cell mediated cytotoxicity in CSF. *Journal of Neuroimmunology*, 196(1-2):159–165, May 2008.

[139] Nico Melzer, Sven G. Meuth, and Heinz Wiendl. CD8 $^{+}$ T cells and neuronal damage: direct and collateral mechanisms of cytotoxicity and impaired electrical excitability. *The FASEB Journal*, 23(11):3659–3673, November 2009.

[140] Jagannadha R. Avasarala, Anne H. Cross, and John L. Trotter. Oligoclonal Band Number as a Marker for Prognosis in Multiple Sclerosis. *Archives of Neurology*, 58(12):2044, December 2001.

[141] Rui Li, Ayman Rezk, Yusei Miyazaki, Ellen Hilgenberg, Hanane Touil, Ping Shen, Craig S. Moore, Laure Michel, Faisal Althekair, Sathy Rajasekharan, Jennifer L. Gommerman, Alexandre Prat, Simon Fillatreau, Amit Bar-Or, and on behalf of the Canadian B cells in MS Team. Proinflammatory GM-CSF–producing B cells in multiple sclerosis and B cell depletion therapy. *Science Translational Medicine*, 7(310), October 2015.

[142] Amit Bar-Or, Enedina M. L Oliveira, David E. Anderson, Jeff I. Krieger, Martin Duddy, Kevin C. O'Connor, and David A. Hafler. Immunological Memory: Contribution of Memory B Cells Expressing Costimulatory Molecules in the Resting State. *The Journal of Immunology*, 167(10):5669–5677, November 2001.

[143] Nicolas Molnarfi, Ulf Schulze-Topphoff, Martin S. Weber, Juan C. Patarroyo, Thomas Prod'homme, Michel Varrin-Doyer, Aparna Shetty, Christopher Linington, Anthony J. Slavin, Juan Hidalgo, Dieter E. Jenne, Hartmut Wekerle, Raymond A. Sobel, Claude C.A. Bernard, Mark J. Shlomchik, and Scott S. Zamvil. MHC class II–dependent B cell APC function is required for induction of CNS autoimmunity independent of myelin-specific antibodies. *Journal of Experimental Medicine*, 210(13):2921–2937, December 2013.

[144] Meike Mitsdoerffer and Anneli Peters. Tertiary Lymphoid Organs in Central Nervous System Autoimmunity. *Frontiers in Immunology*, 7, October 2016.

[145] Owain W. Howell, Cheryl A. Reeves, Richard Nicholas, Daniele Carassiti, Bishan Radotra, Steve M. Gentleman, Barbara Serafini, Francesca Aloisi, Federico Roncaroli,

Roberta Magliozzi, and Richard Reynolds. Meningeal inflammation is widespread and linked to cortical pathology in multiple sclerosis. *Brain*, 134(9):2755–2771, September 2011.

[146] Dmitri Lodygin, Moritz Hermann, Nils Schweingruber, Cassandra Flügel-Koch, Takashi Watanabe, Corinna Schlosser, Arianna Merlini, Henrike Körner, Hsin-Fang Chang, Henrike J. Fischer, Holger M. Reichardt, Marta Zagrebelsky, Brit Mollenhauer, Sebastian Kügler, Dirk Fitzner, Jens Frahm, Christine Stadelmann, Michael Haberl, Francesca Odoardi, and Alexander Flügel. β-Synuclein-reactive T cells induce autoimmune CNS grey matter degeneration. *Nature*, 566(7745):503–508, February 2019.

[147] Richard Macrez, Peter K Stys, Denis Vivien, Stuart A Lipton, and Fabian Docagne. Mechanisms of glutamate toxicity in multiple sclerosis: biomarker and therapeutic opportunities. *The Lancet Neurology*, 15(10):1089–1102, September 2016.

[148] R. Gold. Understanding pathogenesis and therapy of multiple sclerosis via animal models: 70 years of merits and culprits in experimental autoimmune encephalomyelitis research. *Brain*, 129(8):1953–1971, July 2006.

[149] Hans Lassmann and Monika Bradl. Multiple sclerosis: experimental models and reality. *Acta Neuropathologica*, 133(2):223–244, February 2017.

[150] Derrick P. McCarthy, Maureen H. Richards, and Stephen D. Miller. Mouse Models of Multiple Sclerosis: Experimental Autoimmune Encephalomyelitis and Theiler's Virus-Induced Demyelinating Disease. *Methods in Molecular Biology*, 900:381–401, 2012.

[151] Manu Rangachari and Vijay K. Kuchroo. Using EAE to better understand principles of immune function and autoimmune pathology. *Journal of Autoimmunity*, 45:31–39, September 2013.

[152] Lars Svensson, Khairul-Bariah Abdul-Majid, Jan Bauer, Hans Lassmann, RobertA. Harris, and Rikard Holmdahl. A comparative analysis of B cell-mediated myelin oligodendrocyte glycoprotein-experimental autoimmune encephalomyelitis pathogenesis in B cell-deficient mice reveals an effect on demyelination. *European Journal of Immunology*, 32(7):1939, July 2002.

[153] Bradford L. McRae, Mary K. Kennedy, Lit-Jen Tan, Mauro C. Dal Canto, Kathleen S. Picha, and Stephen D. Miller. Induction of active and adoptive relapsing experimental autoimmune encephalomyelitis (EAE) using an encephalitogenic epitope of proteolipid protein. *Journal of Neuroimmunology*, 38(3):229–240, June 1992.

[154] Eileen J McMahon, Samantha L Bailey, Carol Vanderlugt Castenada, Hanspeter Waldner, and Stephen D Miller. Epitope spreading initiates in the CNS in two mouse models of multiple sclerosis. *Nature Medicine*, 11(3):335–339, March 2005.

[155] B L McRae, C L Vanderlugt, M C Dal Canto, and S D Miller. Functional evidence for epitope spreading in the relapsing pathology of experimental autoimmune encephalomyelitis. *The Journal of experimental medicine*, 182(1):75–85, July 1995.

[156] Cris S Constantinescu, Nasr Farooqi, Kate O'Brien, and Bruno Gran. Experimental autoimmune encephalomyelitis (EAE) as a model for multiple sclerosis (MS): EAE as model for MS. *British Journal of Pharmacology*, 164(4):1079–1106, October 2011.

[157] Avraham Ben-Nun, Nathali Kaushansky, Naoto Kawakami, Gurumoorthy Krishnamoorthy, Kerstin Berer, Roland Liblau, Reinhard Hohlfeld, and Hartmut Wekerle. From classic to spontaneous and humanized models of multiple sclerosis: Impact on understanding pathogenesis and drug development. *Journal of Autoimmunity*, 54:33–50, November 2014.

[158] Narges Dargahi, Maria Katsara, Theodore Tselios, Maria-Eleni Androutsou, Maximilian De Courten, John Matsoukas, and Vasso Apostolopoulos. Multiple Sclerosis: Immunopathology and Treatment Update. *Brain Sciences*, 7(12):78, July 2017.

[159] Sivapriya Ramamoorthy and John A. Cidlowski. Corticosteroids: Mechanisms of Action in Health and Disease. *Rheumatic Diseases Clinics of North America*, 42(1):15–31, vii, February 2016.

[160] K. M. Myhr and S. I. Mellgren. Corticosteroids in the treatment of multiple sclerosis. *Acta Neurologica Scandinavica*, 120:73–80, August 2009.

[161] Giancarlo Comi and Marta Radaelli. Oral corticosteroids for multiple sclerosis relapse. *The Lancet*, 386(9997):937–939, September 2015.

[162] Carlo Pozzilli, Fabiana Marinelli, Silvia Romano, and Francesca Bagnato. Corticosteroids treatment. *Journal of the Neurological Sciences*, 223(1):47–51, August 2004.

[163] Mary Filipi and Samantha Jack. Interferons in the Treatment of Multiple Sclerosis. *International Journal of MS Care*, 22(4):165–172, July 2020.

[164] Xuan Feng, Riyue Bao, Lei Li, Florian Deisenhammer, Barry G.W. Arnason, and Anthony T. Reder. Interferon-β corrects massive gene dysregulation in multiple sclerosis: Short-term and long-term effects on immune regulation and neuroprotection. *eBioMedicine*, 49:269–283, November 2019.

[165] R. A. Rudick, D. E. Goodkin, L. D. Jacobs, D. L. Cookfair, R. M. Herndon, J. R. Richert, A. M. Salazar, J. S. Fischer, C. V. Granger, J. H. Simon, J. J. Alam, N. A. Simonian, M. K. Campion, D. M. Bartoszak, D. N. Bourdette, J. Braiman, C. M. Brownscheidle, M. E. Coats, S. L. Cohan, D. S. Dougherty, R. P. Kinkel, M. K. Mass, F. E. Munschauer, R. L. Priore, P. M. Pullicino, B. J. Scherokman, B. Weistock-Guttman, R. H. Whitham, and The Multiple Sclerosis Collaborative Research Group (MSCRG). Impact of interferon beta-1a on neurologic disability in relapsing multiple sclerosis. *Neurology*, 49(2):358–363, August 1997.

[166] PRISMS-4: Long-term efficacy of interferon- -1a in relapsing MS. *Neurology*, 56(12):1628–1636, June 2001.

[167] The IFNB Multiple Sclerosis Study Group. Interferon beta-1b is effective in relapsing-remitting multiple sclerosis: I. Clinical results of a multicenter, randomized, double-blind, placebo-controlled trial. *Neurology*, 43(4):655–655, April 1993.

[168] E. U. Walther and R. Hohlfeld. Multiple sclerosis: Side effects of interferon beta therapy and their management. *Neurology*, 53(8):1622–1622, November 1999.

[169] Niklas Bergvall, Charles Makin, Raquel Lahoz, Neetu Agashivala, Ashish Pradhan, Gorana Capkun, Allison A. Petrilla, Swapna U. Karkare, Catherine Balderston McGuiness, and Jonathan R. Korn. Relapse Rates in Patients with Multiple Sclerosis Switching from Interferon to Fingolimod or Glatiramer Acetate: A US Claims Database Study. *PLoS ONE*, 9(2):e88472, February 2014.

[170] Ludwig Kappos, Jeffrey Cohen, William Collins, Ana De Vera, Lixin Zhang-Auberson, Shannon Ritter, Philipp Von Rosenstiel, and Gordon Francis. Fingolimod in relapsing multiple sclerosis: An integrated analysis of safety findings. *Multiple Sclerosis and Related Disorders*, 3(4):494–504, July 2014.

[171] Jeffrey A. Cohen, Frederik Barkhof, Giancarlo Comi, Hans-Peter Hartung, Bhupendra O. Khatri, Xavier Montalban, Jean Pelletier, Ruggero Capra, Paolo Gallo, Guillermo Izquierdo, Klaus Tiel-Wilck, Ana De Vera, James Jin, Tracy Stites, Stacy Wu, Shreeram Aradhye, and Ludwig Kappos. Oral Fingolimod or Intramuscular Interferon for Relapsing Multiple Sclerosis. *New England Journal of Medicine*, 362(5):402–415, February 2010.

[172] Peter A Calabresi, Ernst-Wilhelm Radue, Douglas Goodin, Douglas Jeffery, Kottil W Rammohan, Anthony T Reder, Timothy Vollmer, Mark A Agius, Ludwig Kappos, Tracy Stites, Bingbing Li, Linda Cappiello, Philipp Von Rosenstiel, and Fred D Lublin. Safety and efficacy of fingolimod in patients with relapsing-remitting multiple sclerosis (FREEDOMS II): a double-blind, randomised, placebo-controlled, phase 3 trial. *The Lancet Neurology*, 13(6):545–556, June 2014.

[173] Stephen L. Hauser, Ludwig Kappos, Xavier Montalban, Licinio Craveiro, Cathy Chognot, Richard Hughes, Harold Koendgen, Noemi Pasquarelli, Ashish Pradhan, Kalpesh Prajapati, and Jerry S. Wolinsky. Safety of Ocrelizumab in Patients With Relapsing and Primary Progressive Multiple Sclerosis. *Neurology*, 97(16):e1546–e1559, October 2021.

[174] Timothy W. Houston, Quentin Howlett-Prieto, Colin Regenauer, Fernando D. Testai, Faith Yao, Xuan Feng, and Anthony T. Reder. Increased Percentage of CD8 $^{+}$ CD28 $^{-}$ Regulatory T Cells With Fingolimod Therapy in Multiple Sclerosis. *Neurology - Neuroimmunology Neuroinflammation*, 10(2):e200075, March 2023.

[175] Ralf A. Linker, De-Hyung Lee, Sarah Ryan, Anne M. Van Dam, Rebecca Conrad, Pradeep Bista, Weike Zeng, Xiaoping Hronowsky, Alex Buko, Sowmya Chollate, Gisa Ellrichmann, Wolfgang Brück, Kate Dawson, Susan Goelz, Stefan Wiese, Robert H. Scannevin, Matvey Lukashev, and Ralf Gold. Fumaric acid esters exert neuroprotective effects in neuroinflammation via activation of the Nrf2 antioxidant pathway. *Brain*, 134(3):678–692, March 2011.

[176] Robert H. Scannevin, Sowmya Chollate, Mi-young Jung, Melanie Shackett, Hiral Patel, Pradeep Bista, Weike Zeng, Sarah Ryan, Masayuki Yamamoto, Matvey Lukashev, and Kenneth J. Rhodes. Fumarates Promote Cytoprotection of Central Nervous System Cells against Oxidative Stress via the Nuclear Factor (Erythroid-Derived 2)-Like 2 Pathway. *Journal of Pharmacology and Experimental Therapeutics*, 341(1):274–284, April 2012.

[177] J. Oh and P. W. O'Connor. Teriflunomide. *Neurology: Clinical Practice*, 3(3):254–260, June 2013.

[178] Wiebke Schrempf and Tjalf Ziemssen. Glatiramer acetate: Mechanisms of action in multiple sclerosis. *Autoimmunity Reviews*, 6(7):469–475, August 2007.

[179] Foziah Alshamrani, Hind Alnajashi, and Mohammed F Almuaigel. Efficacy and Safety of Intravenous Cladribine in Patients with Rapidly Evolving or Early Secondary Progressive Multiple Sclerosis. *Cureus*, February 2020.

[180] Gavin Giovannoni. Cladribine to Treat Relapsing Forms of Multiple Sclerosis. *Neurotherapeutics*, 14(4):874–887, October 2017.

[181] Ted A. Yednock, Catherine Cannon, Lawrence C. Fritz, Francisco Sanchez-Madrid, Lawrence Steinman, and Nathan Karin. Prevention of experimental autoimmune encephalomyelitis by antibodies against $\alpha 4 \beta$l integrin. *Nature*, 356(6364):63–66, March 1992.

[182] Chris H. Polman, Paul W. O'Connor, Eva Havrdova, Michael Hutchinson, Ludwig Kappos, David H. Miller, J. Theodore Phillips, Fred D. Lublin, Gavin Giovannoni, Andrzej Wajgt, Martin Toal, Frances Lynn, Michael A. Panzara, and Alfred W. Sandrock. A Randomized, Placebo-Controlled Trial of Natalizumab for Relapsing Multiple Sclerosis. *New England Journal of Medicine*, 354(9):899–910, March 2006.

[183] Richard A. Rudick, William H. Stuart, Peter A. Calabresi, Christian Confavreux, Steven L. Galetta, Ernst-Wilhelm Radue, Fred D. Lublin, Bianca Weinstock-Guttman, Daniel R. Wynn, Frances Lynn, Michael A. Panzara, and Alfred W. Sandrock. Natalizumab plus Interferon Beta-1a for Relapsing Multiple Sclerosis. *New England Journal of Medicine*, 354(9):911–923, March 2006.

[184] Per Soelberg Sorensen and Morten Blinkenberg. The potential role for ocrelizumab in the treatment of multiple sclerosis: current evidence and future prospects. *Therapeutic Advances in Neurological Disorders*, 9(1):44–52, January 2016.

[185] Rui Li, Kristina R. Patterson, and Amit Bar-Or. Reassessing B cell contributions in multiple sclerosis. *Nature Immunology*, 19(7):696–707, July 2018.

[186] Xavier Montalban, Stephen L. Hauser, Ludwig Kappos, Douglas L. Arnold, Amit Bar-Or, Giancarlo Comi, Jérôme De Seze, Gavin Giovannoni, Hans-Peter Hartung, Bernhard Hemmer, Fred Lublin, Kottil W. Rammohan, Krzysztof Selmaj, Anthony Traboulsee, Annette Sauter, Donna Masterman, Paulo Fontoura, Shibeshih Belachew, Hideki Garren, Nicole Mairon, Peter Chin, and Jerry S. Wolinsky. Ocrelizumab versus Placebo in Primary Progressive Multiple Sclerosis. *New England Journal of Medicine*, 376(3):209–220, January 2017.

[187] Ashwin N. Skelly, Yuko Sato, Sean Kearney, and Kenya Honda. Mining the microbiota for microbial and metabolite-based immunotherapies. *Nature Reviews Immunology*, 19(5):305–323, May 2019.

[188] Allison Agus, Karine Clément, and Harry Sokol. Gut microbiota-derived metabolites as central regulators in metabolic disorders. *Gut*, 70(6):1174–1182, June 2021.

[189] Eiji Miyauchi, Chikako Shimokawa, Alex Steimle, Mahesh S. Desai, and Hiroshi Ohno. The impact of the gut microbiome on extra-intestinal autoimmune diseases. *Nature Reviews Immunology*, 23(1):9–23, January 2023.

[190] Kenya Honda and Dan R. Littman. The microbiota in adaptive immune homeostasis and disease. *Nature*, 535(7610):75–84, July 2016.

[191] Dallas R. Donohoe, Nikhil Garge, Xinxin Zhang, Wei Sun, Thomas M. O'Connell, Maureen K. Bunger, and Scott J. Bultman. The Microbiome and Butyrate Regulate Energy Metabolism and Autophagy in the Mammalian Colon. *Cell Metabolism*, 13(5):517–526, May 2011.

[192] Jerry M. Wells, Robert J. Brummer, Muriel Derrien, Thomas T. MacDonald, Freddy Troost, Patrice D. Cani, Vassilia Theodorou, Jan Dekker, Agnes Méheust, Willem M. De Vos, Annick Mercenier, Arjen Nauta, and Clara L. Garcia-Rodenas. Homeostasis of the gut barrier and potential biomarkers. *American Journal of Physiology-Gastrointestinal and Liver Physiology*, 312(3):G171–G193, March 2017.

[193] Ruyi Wang, Shijie Cao, Mohamed Elfatih H. Bashir, Lauren A. Hesser, Yanlin Su, Sung Min Choi Hong, Andrew Thompson, Elliot Culleen, Matthew Sabados, Nicholas P. Dylla, Evelyn Campbell, Riyue Bao, Eric B. Nonnecke, Charles L. Bevins, D. Scott Wilson, Jeffrey A. Hubbell, and Cathryn R. Nagler. Treatment of peanut allergy and colitis in mice via the intestinal release of butyrate from polymeric micelles. *Nature Biomedical Engineering*, 7(1):38–55, December 2022.

[194] Ara Koh, Filipe De Vadder, Petia Kovatcheva-Datchary, and Fredrik Bäckhed. From Dietary Fiber to Host Physiology: Short-Chain Fatty Acids as Key Bacterial Metabolites. *Cell*, 165(6):1332–1345, June 2016.

[195] Luying Peng, Zhong-Rong Li, Robert S. Green, Ian R. Holzmanr, and Jing Lin. Butyrate Enhances the Intestinal Barrier by Facilitating Tight Junction Assembly via Activation of AMP-Activated Protein Kinase in Caco-2 Cell Monolayers. *The Journal of Nutrition*, 139(9):1619–1625, September 2009.

[196] Luying Peng, Zhenjuan He, Wei Chen, Ian R Holzman, and Jing Lin. Effects of Butyrate on Intestinal Barrier Function in a Caco-2 Cell Monolayer Model of Intestinal Barrier. *Pediatric Research*, 61(1):37–41, January 2007.

[197] J. A. McKay and J. C. Mathers. Diet induced epigenetic changes and their implications for health: Nutrition, epigenetics and health. *Acta Physiologica*, 202(2):103–118, June 2011.

[198] Roberto Berni Canani, Margherita Di Costanzo, and Ludovica Leone. The epigenetic effects of butyrate: potential therapeutic implications for clinical practice. *Clinical Epigenetics*, 4(1):4, December 2012.

[199] Jian Tan, Craig McKenzie, Maria Potamitis, Alison N. Thorburn, Charles R. Mackay, and Laurence Macia. The Role of Short-Chain Fatty Acids in Health and Disease. In *Advances in Immunology*, volume 121, pages 91–119. Elsevier, 2014.

[200] H. M. Hamer, D. Jonkers, K. Venema, S. Vanhoutvin, F. J. Troost, and R.-J. Brummer. Review article: the role of butyrate on colonic function. *Alimentary Pharmacology & Therapeutics*, 27(2):104–119, January 2008.

[201] Nicholas Arpaia, Clarissa Campbell, Xiying Fan, Stanislav Dikiy, Joris Van Der Veeken, Paul deRoos, Hui Liu, Justin R. Cross, Klaus Pfeffer, Paul J. Coffer, and Alexander Y. Rudensky. Metabolites produced by commensal bacteria promote peripheral regulatory T-cell generation. *Nature*, 504(7480):451–455, December 2013.

[202] Kees Meijer, Paul De Vos, and Marion G Priebe. Butyrate and other short-chain fatty acids as modulators of immunity: what relevance for health?:. *Current Opinion in Clinical Nutrition and Metabolic Care*, 13(6):715–721, November 2010.

[203] Maria M. M. Kaisar, Leonard R. Pelgrom, Alwin J. Van Der Ham, Maria Yazdanbakhsh, and Bart Everts. Butyrate Conditions Human Dendritic Cells to Prime Type 1 Regulatory T Cells via both Histone Deacetylase Inhibition and G Protein-Coupled Receptor 109A Signaling. *Frontiers in Immunology*, 8:1429, October 2017.

[204] Claudia Nastasi, Marco Candela, Charlotte Menné Bonefeld, Carsten Geisler, Morten Hansen, Thorbjørn Krejsgaard, Elena Biagi, Mads Hald Andersen, Patrizia Brigidi, Niels Ødum, Thomas Litman, and Anders Woetmann. The effect of short-chain fatty acids on human monocyte-derived dendritic cells. *Scientific Reports*, 5(1):16148, November 2015.

[205] Zhiwei Ang and Jeak Ling Ding. GPR41 and GPR43 in Obesity and Inflammation – Protective or Causative? *Frontiers in Immunology*, 7, February 2016.

[206] Andrew J. Brown, Susan M. Goldsworthy, Ashley A. Barnes, Michelle M. Eilert, Lili Tcheang, Dion Daniels, Alison I. Muir, Mark J. Wigglesworth, Ian Kinghorn, Neil J. Fraser, Nicholas B. Pike, Jay C. Strum, Klaudia M. Steplewski, Paul R. Murdock, Julie C. Holder, Fiona H. Marshall, Philip G. Szekeres, Shelagh Wilson, Diane M. Ignar, Steve M. Foord, Alan Wise, and Simon J. Dowell. The Orphan G Protein-coupled Receptors GPR41 and GPR43 Are Activated by Propionate and Other Short Chain Carboxylic Acids. *Journal of Biological Chemistry*, 278(13):11312–11319, March 2003.

[207] Lars Fugger, Lise Torp Jensen, and Jamie Rossjohn. Challenges, Progress, and Prospects of Developing Therapies to Treat Autoimmune Diseases. *Cell*, 181(1):63–80, April 2020.

[208] Gabriel Horta-Baas, María Del Socorro Romero-Figueroa, Alvaro José Montiel-Jarquín, María Luisa Pizano-Zárate, Jaime García-Mena, and Ninfa Ramírez-Durán. Intestinal Dysbiosis and Rheumatoid Arthritis: A Link between Gut Microbiota and the Pathogenesis of Rheumatoid Arthritis. *Journal of Immunology Research*, 2017:1–13, 2017.

[209] Matthew L Stoll, Ranjit Kumar, Casey D Morrow, Elliot J Lefkowitz, Xiangqin Cui, Anna Genin, Randy Q Cron, and Charles O Elson. Altered microbiota associated with abnormal humoral immune responses to commensal organisms in enthesitis-related arthritis. *Arthritis Research & Therapy*, 16(6):486, December 2014.

[210] Sushrut Jangi, Roopali Gandhi, Laura M. Cox, Ning Li, Felipe Von Glehn, Raymond Yan, Bonny Patel, Maria Antonietta Mazzola, Shirong Liu, Bonnie L. Glanz, Sandra Cook, Stephanie Tankou, Fiona Stuart, Kirsy Melo, Parham Nejad, Kathleen Smith, Begüm D. Topçuolu, James Holden, Pia Kivisäkk, Tanuja Chitnis, Philip L. De Jager, Francisco J. Quintana, Georg K. Gerber, Lynn Bry, and Howard L. Weiner. Alterations of the human gut microbiome in multiple sclerosis. *Nature Communications*, 7(1):12015, June 2016.

[211] Brandi L. Cantarel, Emmanuelle Waubant, Christel Chehoud, Justin Kuczynski, Todd Z. DeSantis, Janet Warrington, Arun Venkatesan, Claire M. Fraser, and Ellen M. Mowry. Gut Microbiota in Multiple Sclerosis: Possible Influence of Immunomodulators. *Journal of Investigative Medicine*, 63(5):729–734, June 2015.

[212] Miho Mizuno, Daisuke Noto, Naoko Kaga, Asako Chiba, and Sachiko Miyake. The dual role of short fatty acid chains in the pathogenesis of autoimmune disease models. *PLOS ONE*, 12(2):e0173032, February 2017.

[213] Hu Liu, Ji Wang, Ting He, Sage Becker, Guolong Zhang, Defa Li, and Xi Ma. Butyrate: A Double-Edged Sword for Health? *Advances in Nutrition*, 9(1):21–29, January 2018.

[214] Richard I. Breuer, Stephen K. Buto, Miriam L. Christ, Judy Bean, Piero Vernia, P. Paoluzi, M. C. Di Paolo, and Renzo Caprilli. Rectal irrigation with short-chain

fatty acids for distal ulcerative colitis: Preliminary report. *Digestive Diseases and Sciences*, 36(2):185–187, February 1991.

[215] R I Breuer, K H Soergel, B A Lashner, M L Christ, S B Hanauer, A Vanagunas, J M Harig, A Keshavarzian, M Robinson, J H Sellin, D Weinberg, D E Vidican, K L Flemal, and A W Rademaker. Short chain fatty acid rectal irrigation for left-sided ulcerative colitis: a randomised, placebo controlled trial. *Gut*, 40(4):485–491, April 1997.

[216] Graham D. Sher, Gordon D. Ginder, Jane Little, Suya Yang, George J. Dover, and Nancy F. Olivieri. Extended Therapy with Intravenous Arginine Butyrate in Patients with β-Hemoglobinopathies. *New England Journal of Medicine*, 332(24):1606–1610, June 1995.

[217] P. Vernia, M. Cittadini, R. Caprilli, and A. Torsoli. Topical treatment of refractory distal ulcerative colitis with 5-ASA and sodium butyrate. *Digestive Diseases and Sciences*, 40(2):305–307, February 1995.

[218] Eiji Yuba, Erica Budina, Kiyomitsu Katsumata, Ako Ishihara, Aslan Mansurov, Aaron T. Alpar, Elyse A. Watkins, Peyman Hosseinchi, Joseph W. Reda, Abigail L. Lauterbach, Mindy Nguyen, Ani Solanki, Takahiro Kageyama, Melody A. Swartz, Jun Ishihara, and Jeffrey A. Hubbell. Suppression of Rheumatoid Arthritis by Enhanced Lymph Node Trafficking of Engineered Interleukin-10 in Murine Models. *Arthritis & Rheumatology*, 73(5):769–778, May 2021.

[219] Ako Ishihara, Jun Ishihara, Elyse A. Watkins, Andrew C. Tremain, Mindy Nguyen, Ani Solanki, Kiyomitsu Katsumata, Aslan Mansurov, Erica Budina, Aaron T. Alpar, Peyman Hosseinchi, Lea Maillat, Joseph W. Reda, Takahiro Kageyama, Melody A. Swartz, Eiji Yuba, and Jeffrey A. Hubbell. Prolonged residence of an albumin–IL-4 fusion protein in secondary lymphoid organs ameliorates experimental autoimmune encephalomyelitis. *Nature Biomedical Engineering*, 5(5):387–398, October 2020.

[220] Manfred B Lutz, Nicole Kukutsch, Alexandra L.J Ogilvie, Susanne Rößner, Franz Koch, Nikolaus Romani, and Gerold Schuler. An advanced culture method for generating large quantities of highly pure dendritic cells from mouse bone marrow. *Journal of Immunological Methods*, 223(1):77–92, February 1999.

[221] T Torii, K Kanemitsu, T Wada, S Itoh, K Kinugawa, and A Hagiwara. Measurement of short-chain fatty acids in human faeces using high-performance liquid chromatography: specimen stability. *Annals of Clinical Biochemistry: International Journal of Laboratory Medicine*, 47(5):447–452, September 2010.

[222] A L Millard, P M Mertes, D Ittelet, F Villard, P Jeannesson, and J Bernard. Butyrate affects differentiation, maturation and function of human monocyte-derived dendritic cells and macrophages. *Clinical and Experimental Immunology*, 130(2):245–255, October 2002.

[223] Stefan Bröer. Amino acid transport across mammalian intestinal and renal epithelia. *Physiological Reviews*, 88(1):249–286, January 2008.

[224] Ivan Tayarani, Jeanne-Marie Lefauconnier, Françoise Roux, and Jean-Marie Bourre. Evidence for an Alanine, Serine, and Cysteine System of Transport in Isolated Brain Capillaries. *Journal of Cerebral Blood Flow & Metabolism*, 7(5):585–591, October 1987.

[225] Richard A Hawkins, Robyn L O'Kane, Ian A Simpson, and Juan R Viña. Structure of the Blood–Brain Barrier and Its Role in the Transport of Amino Acids. *The Journal of Nutrition*, 136(1):218S–226S, January 2006.

[226] Ahmed B. Montaser, Juulia Järvinen, Susanne Löffler, Johanna Huttunen, Seppo Auriola, Marko Lehtonen, Aaro Jalkanen, and Kristiina M. Huttunen. L-Type Amino Acid Transporter 1 Enables the Efficient Brain Delivery of Small-Sized Prodrug across the Blood–Brain Barrier and into Human and Mouse Brain Parenchymal Cells. *ACS Chemical Neuroscience*, 11(24):4301–4315, December 2020.

[227] Yuichi Maeda and Kiyoshi Takeda. Role of Gut Microbiota in Rheumatoid Arthritis. *Journal of Clinical Medicine*, 6(6):60, June 2017.

[228] Da Som Kim, Jeong-Eun Kwon, Seung Hoon Lee, Eun Kyung Kim, Jun-Geol Ryu, Kyung-Ah Jung, Jeong-Won Choi, Min-Jung Park, Young-Mee Moon, Sung-Hwan Park, Mi-La Cho, and Seung-Ki Kwok. Attenuation of Rheumatoid Inflammation by Sodium Butyrate Through Reciprocal Targeting of HDAC2 in Osteoclasts and HDAC8 in T Cells. *Frontiers in Immunology*, 9:1525, July 2018.

[229] Elizabeth C. Rosser, Christopher J.M. Piper, Diana E. Matei, Paul A. Blair, André F. Rendeiro, Michael Orford, Dagmar G. Alber, Thomas Krausgruber, Diego Catalan, Nigel Klein, Jessica J. Manson, Ignat Drozdov, Christoph Bock, Lucy R. Wedderburn, Simon Eaton, and Claudia Mauri. Microbiota-Derived Metabolites Suppress Arthritis by Amplifying Aryl-Hydrocarbon Receptor Activation in Regulatory B Cells. *Cell Metabolism*, 31(4):837–851.e10, April 2020.

[230] K. Terato, K. A. Hasty, R. A. Reife, M. A. Cremer, A. H. Kang, and J. M. Stuart. Induction of arthritis with monoclonal antibodies to collagen. *Journal of Immunology (Baltimore, Md.: 1950)*, 148(7):2103–2108, April 1992.

[231] Pilaiwanwadee Hutamekalin, Takayuki Saito, Kouya Yamaki, Nobuaki Mizutani, David D. Brand, Takaki Waritani, Kuniaki Terato, and Shin Yoshino. Collagen antibody-induced arthritis in mice: Development of a new arthritogenic 5-clone cocktail of monoclonal anti-type II collagen antibodies. *Journal of Immunological Methods*, 343(1):49–55, March 2009.

[232] Merrill J. Rowley, Kutty Selva Nandakumar, and Rikard Holmdahl. The role of collagen antibodies in mediating arthritis. *Modern Rheumatology*, 18(5):429–441, October 2008.

[233] Ioannis Kalampokis, Ayumi Yoshizaki, and Thomas F Tedder. IL-10-producing regulatory B cells (B10 cells) in autoimmune disease. *Arthritis Research & Therapy*, 15(Suppl 1):S1, 2013.

[234] Alexander Swidsinski, Yvonne Dörffel, Vera Loening-Baucke, Christoph Gille, Önder Göktas, Anne Reißhauer, Jürgen Neuhaus, Karsten-Henrich Weylandt, Alexander Guschin, and Markus Bock. Reduced Mass and Diversity of the Colonic Microbiome in Patients with Multiple Sclerosis and Their Improvement with Ketogenic Diet. *Frontiers in Microbiology*, 8:1141, June 2017.

[235] Kerstin Berer, Lisa Ann Gerdes, Egle Cekanaviciute, Xiaoming Jia, Liang Xiao, Zhongkui Xia, Chuan Liu, Luisa Klotz, Uta Stauffer, Sergio E. Baranzini, Tania Kümpfel, Reinhard Hohlfeld, Gurumoorthy Krishnamoorthy, and Hartmut Wekerle. Gut microbiota from multiple sclerosis patients enables spontaneous autoimmune encephalomyelitis in mice. *Proceedings of the National Academy of Sciences*, 114(40):10719–10724, October 2017.

[236] Suzana Stanisavljević, Miroslav Dinić, Bojan Jevtić, Neda Đedović, Miljana Momčilović, Jelena Đokić, Nataša Golić, Marija Mostarica Stojković, and Đorđe Miljković. Gut Microbiota Confers Resistance of Albino Oxford Rats to the Induction of Experimental Autoimmune Encephalomyelitis. *Frontiers in Immunology*, 9:942, May 2018.

[237] Ilaria Cosorich, Gloria Dalla-Costa, Chiara Sorini, Roberto Ferrarese, Maria Josè Messina, Jayashree Dolpady, Elisa Radice, Alberto Mariani, Pier Alberto Testoni, Filippo Canducci, Giancarlo Comi, Vittorio Martinelli, and Marika Falcone. High frequency of intestinal T $_{\mathrm{h}}$ 17 cells correlates with microbiota alterations and disease activity in multiple sclerosis. *Science Advances*, 3(7):e1700492, July 2017.

[238] Aiden Haghikia, Stefanie Jörg, Alexander Duscha, Johannes Berg, Arndt Manzel, Anne Waschbisch, Anna Hammer, De-Hyung Lee, Caroline May, Nicola Wilck, Andras Balogh, Annika I. Ostermann, Nils Helge Schebb, Denis A. Akkad, Diana A. Grohme, Markus Kleinewietfeld, Stefan Kempa, Jan Thöne, Seray Demir, Dominik N. Müller, Ralf Gold, and Ralf A. Linker. Dietary Fatty Acids Directly Impact Central Nervous System Autoimmunity via the Small Intestine. *Immunity*, 43(4):817–829, October 2015.

[239] Tong Chen, Daisuke Noto, Yasunobu Hoshino, Miho Mizuno, and Sachiko Miyake. Butyrate suppresses demyelination and enhances remyelination. *Journal of Neuroinflammation*, 16(1):165, December 2019.

[240] Bing Zhu, Yoshio Bando, Sheng Xiao, Kaiyong Yang, Ana C. Anderson, Vijay K. Kuchroo, and Samia J. Khoury. CD11b+Ly-6Chi Suppressive Monocytes in Experimental Autoimmune Encephalomyelitis. *The Journal of Immunology*, 179(8):5228–5237, October 2007.

[241] Ulf Schulze-Topphoff, Michel Varrin-Doyer, Kara Pekarek, Collin M. Spencer, Aparna Shetty, Sharon A. Sagan, Bruce A. C. Cree, Raymond A. Sobel, Brian T. Wipke, Lawrence Steinman, Robert H. Scannevin, and Scott S. Zamvil. Dimethyl fumarate treatment induces adaptive and innate immune modulation independent of Nrf2. *Proceedings of the National Academy of Sciences*, 113(17):4777–4782, April 2016.

[242] Ilya Ayzenberg, Robert Hoepner, and Ingo Kleiter. Fingolimod for multiple sclerosis and emerging indications: appropriate patient selection, safety precautions, and special considerations. *Therapeutics and Clinical Risk Management*, 12:261–272, 2016.

[243] Jerold Chun and Hans-Peter Hartung. Mechanism of Action of Oral Fingolimod (FTY720) in Multiple Sclerosis. *Clinical Neuropharmacology*, 33(2):91–101, March 2010.

[244] Lin Zhang, Chudan Liu, Qingyan Jiang, and Yulong Yin. Butyrate in Energy Metabolism: There Is Still More to Learn. *Trends in Endocrinology & Metabolism*, 32(3):159–169, March 2021.

[245] Nagendra Singh, Ashish Gurav, Sathish Sivaprakasam, Evan Brady, Ravi Padia, Huidong Shi, Muthusamy Thangaraju, Puttur D. Prasad, Santhakumar Manicassamy, David H. Munn, Jeffrey R. Lee, Stefan Offermanns, and Vadivel Ganapathy. Activation of Gpr109a, Receptor for Niacin and the Commensal Metabolite Butyrate, Suppresses Colonic Inflammation and Carcinogenesis. *Immunity*, 40(1):128–139, January 2014.

[246] Harold L. Newmark, Joanne R. Lupton, and Charles W. Young. Butyrate as a differentiating agent: pharmacokinetics, analogues and current status. *Cancer Letters*, 78(1-3):1–5, April 1994.

[247] J H Cummings, E W Pomare, W J Branch, C P Naylor, and G T Macfarlane. Short chain fatty acids in human large intestine, portal, hepatic and venous blood. *Gut*, 28(10):1221–1227, October 1987.

[248] Nicholas A. Scott, Anna Andrusaite, Peter Andersen, Melissa Lawson, Cristina Alcon-Giner, Charlotte Leclaire, Shabhonam Caim, Gwenaelle Le Gall, Tovah Shaw, James P. R. Connolly, Andrew J. Roe, Hannah Wessel, Alberto Bravo-Blas, Carolyn A. Thomson, Verena Kästele, Ping Wang, Daniel A. Peterson, Allison Bancroft, Xuhang Li, Richard Grencis, Allan McI Mowat, Lindsay J. Hall, Mark A. Travis, Simon W. F. Milling, and Elizabeth R. Mann. Antibiotics induce sustained dysregulation of intestinal T cell immunity by perturbing macrophage homeostasis. *Science Translational Medicine*, 10(464):eaao4755, October 2018.

[249] D. M. Sansom. CD28, CTLA-4 and their ligands: who does what and to whom? *Immunology*, 101(2):169–177, October 2000.

[250] P S Linsley and J A Ledbetter. The Role of the CD28 Receptor During T Cell Responses to Antigen. *Annual Review of Immunology*, 11(1):191–212, April 1993.

[251] Lucy S. K. Walker and David M. Sansom. The emerging role of CTLA4 as a cell-extrinsic regulator of T cell responses. *Nature Reviews Immunology*, 11(12):852–863, December 2011.

[252] Arnaud M. Didierlaurent, Sandra Morel, Laurence Lockman, Sandra L. Giannini, Michel Bisteau, Harald Carlsen, Anders Kielland, Olivier Vosters, Nathalie Vanderheyde, Francesca Schiavetti, Daniel Larocque, Marcelle Van Mechelen, and Nathalie Garçon. AS04, an Aluminum Salt- and TLR4 Agonist-Based Adjuvant System, Induces a Transient Localized Innate Immune Response Leading to Enhanced Adaptive Immunity. *The Journal of Immunology*, 183(10):6186–6197, November 2009.

[253] Ari B. Molofsky, Adam K. Savage, and Richard M. Locksley. Interleukin-33 in Tissue Homeostasis, Injury, and Inflammation. *Immunity*, 42(6):1005–1019, June 2015.

[254] Jochen Schmitz, Alexander Owyang, Elizabeth Oldham, Yaoli Song, Erin Murphy, Terril K. McClanahan, Gerard Zurawski, Mehrdad Moshrefi, Jinzhong Qin, Xiaoxia Li, Daniel M. Gorman, J. Fernando Bazan, and Robert A. Kastelein. IL-33, an Interleukin-1-like Cytokine that Signals via the IL-1 Receptor-Related Protein ST2 and Induces T Helper Type 2-Associated Cytokines. *Immunity*, 23(5):479–490, November 2005.

[255] Neil E. Humphreys, Damo Xu, Matthew R. Hepworth, Foo Y. Liew, and Richard K. Grencis. IL-33, a Potent Inducer of Adaptive Immunity to Intestinal Nematodes. *The Journal of Immunology*, 180(4):2443–2449, February 2008.

[256] Ben C. L. Chan, Christopher W. K. Lam, Lai-Shan Tam, and Chun K. Wong. IL33: Roles in Allergic Inflammation and Therapeutic Perspectives. *Frontiers in Immunology*, 10:364, March 2019.

[257] Nicholas Arpaia, Jesse A. Green, Bruno Moltedo, Aaron Arvey, Saskia Hemmers, Shaopeng Yuan, Piper M. Treuting, and Alexander Y. Rudensky. A Distinct Function of Regulatory T Cells in Tissue Protection. *Cell*, 162(5):1078–1089, August 2015.

[258] Chris Schiering, Thomas Krausgruber, Agnieszka Chomka, Anja Fröhlich, Krista Adelmann, Elizabeth A. Wohlfert, Johanna Pott, Thibault Griseri, Julia Bollrath, Ahmed N. Hegazy, Oliver J. Harrison, Benjamin M. J. Owens, Max Löhning, Yasmine Belkaid, Padraic G. Fallon, and Fiona Powrie. The alarmin IL-33 promotes regulatory T-cell function in the intestine. *Nature*, 513(7519):564–568, September 2014.

[259] Saskia Hemmers, Michail Schizas, and Alexander Y. Rudensky. T reg cell–intrinsic requirements for ST2 signaling in health and neuroinflammation. *Journal of Experimental Medicine*, 218(2):e20201234, February 2021.

[260] Julia Siede, Anja Fröhlich, Angeliki Datsi, Ahmed N. Hegazy, Domonkos V. Varga, Vivien Holecska, Hirohisa Saito, Susumu Nakae, and Max Löhning. IL-33 Receptor-Expressing Regulatory T Cells Are Highly Activated, Th2 Biased and Suppress CD4 T Cell Proliferation through IL-10 and TGFβ Release. *PLOS ONE*, 11(8):e0161507, August 2016.

[261] Benjamin M. Matta, Dawn K. Reichenbach, Xiaoli Zhang, Lisa Mathews, Brent H. Koehn, Gaelen K. Dwyer, Jeremy M. Lott, Franziska M. Uhl, Dietmar Pfeifer, Colby J. Feser, Michelle J. Smith, Quan Liu, Robert Zeiser, Bruce R. Blazar, and Hēth R. Turnquist. Peri-alloHCT IL-33 administration expands recipient T-regulatory cells that protect mice against acute GVHD. *Blood*, 128(3):427–439, July 2016.

[262] Lei Xu, Wei Li, Xiaofan Wang, Lina Zhang, Qianqian Qi, Liyang Dong, Chuan Wei, Yanan Pu, Yalin Li, Jifeng Zhu, Sha Zhou, Feng Liu, Xiaojun Chen, and Chuan Su. The IL-33-ST2-MyD88 axis promotes regulatory T cell proliferation in the murine liver. *European Journal of Immunology*, 48(8):1302–1307, August 2018.

[263] Foo Yew Liew, Jean-Philippe Girard, and Heth Roderick Turnquist. Interleukin-33 in health and disease. *Nature Reviews Immunology*, 16(11):676–689, November 2016.

[264] Dietmar M.W. Zaiss, William C. Gause, Lisa C. Osborne, and David Artis. Emerging Functions of Amphiregulin in Orchestrating Immunity, Inflammation, and Tissue Repair. *Immunity*, 42(2):216–226, February 2015.

[265] Max Löhning, Arne Stroehmann, Anthony J. Coyle, Jane L. Grogan, Steven Lin, Jose-Carlos Gutierrez-Ramos, Douglas Levinson, Andreas Radbruch, and Thomas Kamradt. T1/ST2 is preferentially expressed on murine Th2 cells, independent of interleukin 4, interleukin 5, and interleukin 10, and important for Th2 effector function. *Proceedings of the National Academy of Sciences*, 95(12):6930–6935, June 1998.

[266] Daniel R. Neill, See Heng Wong, Agustin Bellosi, Robin J. Flynn, Maria Daly, Theresa K. A. Langford, Christine Bucks, Colleen M. Kane, Padraic G. Fallon, Richard Pannell, Helen E. Jolin, and Andrew N. J. McKenzie. Nuocytes represent a new innate effector leukocyte that mediates type-2 immunity. *Nature*, 464(7293):1367–1370, April 2010.

[267] Mariola Kurowska-Stolarska, Bartosz Stolarski, Peter Kewin, Grace Murphy, Christopher J. Corrigan, Sun Ying, Nick Pitman, Ananda Mirchandani, Batika Rana, Nico Van Rooijen, Malcolm Shepherd, Charlie McSharry, Iain B. McInnes, Damo Xu, and Foo Y. Liew. IL-33 Amplifies the Polarization of Alternatively Activated Macrophages That Contribute to Airway Inflammation. *The Journal of Immunology*, 183(10):6469–6477, November 2009.

[268] Benjamin M. Matta, Jeremy M. Lott, Lisa R. Mathews, Quan Liu, Brian R. Rosborough, Bruce R. Blazar, and Hēth R. Turnquist. IL-33 Is an Unconventional Alarmin That Stimulates IL-2 Secretion by Dendritic Cells To Selectively Expand IL-33R/ST2+ Regulatory T Cells. *The Journal of Immunology*, 193(8):4010–4020, October 2014.

[269] Li-Yin Hung, Yukinori Tanaka, Karl Herbine, Christopher Pastore, Brenal Singh, Annabel Ferguson, Nisha Vora, Bonnie Douglas, Kelly Zullo, Edward M. Behrens, Tiffany Li Hui Tan, Michael A. Kohanski, Paul Bryce, Cailu Lin, Taku Kambayashi, Danielle R. Reed, Breann L. Brown, Noam A. Cohen, and De'Broski R. Herbert. Cellular context of IL-33 expression dictates impact on anti-helminth immunity. *Science Immunology*, 5(53):eabc6259, November 2020.

[270] A. Pascual-Reguant, J. Bayat Sarmadi, C. Baumann, R. Noster, D. Cirera-Salinas, C. Curato, P. Pelczar, S. Huber, C.E. Zielinski, M. Löhning, A.E. Hauser, and E. Esplugues. TH17 cells express ST2 and are controlled by the alarmin IL-33 in the small intestine. *Mucosal Immunology*, 10(6):1431–1442, November 2017.

[271] Zeyu Chen, Yifan Hu, Yu Gong, Xilin Zhang, Lian Cui, Rongfen Chen, Yingyuan Yu, Qian Yu, Youdong Chen, Hongyue Diao, Jia Chen, Yuanyuan Wang, and Yuling Shi. Interleukin-33 alleviates psoriatic inflammation by suppressing the T helper type 17 immune response. *Immunology*, 160(4):382–392, August 2020.

[272] Junfeng Zhu, Yuanyuan Wang, Fangli Yang, Lixuan Sang, Jingbo Zhai, Shengjun Li, Yan Li, Danan Wang, Changlong Lu, and Xun Sun. IL-33 alleviates DSS-induced chronic colitis in C57BL/6 mice colon lamina propria by suppressing Th17 cell response as well as Th1 cell response. *International Immunopharmacology*, 29(2):846–853, December 2015.

[273] Jun-feng Zhu, Ying Xu, Jian Zhao, Xue Li, Xinrui Meng, Tian-qi Wang, Ben-yao Zou, Peng-yan Zhao, Qi Liu, Chang-long Lu, Fang-liang Zheng, and Hong-sheng Liu. IL-33 Protects Mice against DSS-Induced Chronic Colitis by Increasing Both Regulatory B Cell and Regulatory T Cell Responses as Well as Decreasing Th17 Cell Response. *Journal of Immunology Research*, 2018:1–12, November 2018.

[274] Mark Barbour, Debbie Allan, Heping Xu, Cheng Pei, Mei Chen, Wanda Niedbala, Sandra Y. Fukada, Anne-Galle Besnard, Jose C. Alves-Filho, Xiaoguang Tong, John V. Forrester, Foo Yew Liew, and Hui-Rong Jiang. IL-33 attenuates the development of experimental autoimmune uveitis: Immunomodulation. *European Journal of Immunology*, 44(11):3320–3329, November 2014.

[275] Rodrigo Vazquez-Lombardi, Brendan Roome, and Daniel Christ. Molecular Engineering of Therapeutic Cytokines. *Antibodies*, 2(4):426–451, July 2013.

[276] Jon D. Laman and Roy O. Weller. Drainage of Cells and Soluble Antigen from the CNS to Regional Lymph Nodes. *Journal of Neuroimmune Pharmacology*, 8(4):840–856, September 2013.

[277] Marian J. Phillips, Michelle Needham, and Roy O. Weller. Role of cervical lymph nodes in autoimmune encephalomyelitis in the Lewis rat. *The Journal of Pathology*, 182(4):457–464, August 1997.

[278] Marloes Van Zwam, Ruth Huizinga, Nicole Heijmans, Marjan Van Meurs, Annet F Wierenga-Wolf, Marie-José Melief, Rogier Q Hintzen, Bert A 'T Hart, Sandra Amor, Leonie A Boven, and Jon D Laman. Surgical excision of CNS-draining lymph nodes reduces relapse severity in chronic-relapsing experimental autoimmune encephalomyelitis. *The Journal of Pathology*, 217(4):543–551, March 2009.

[279] Jalal A Jazayeri and Graeme J Carroll. Fc-Based Cytokines: Prospects for Engineering Superior Therapeutics. *BioDrugs*, 22(1):11–26, 2008.

[280] Foo Y. Liew, Nick I. Pitman, and Iain B. McInnes. Disease-associated functions of IL-33: the new kid in the IL-1 family. *Nature Reviews Immunology*, 10(2):103–110, February 2010.

[281] Hui-Rong Jiang, Marija Milovanović, Debbie Allan, Wanda Niedbala, Anne-Galle Besnard, Sandra Y. Fukada, Jose C. Alves-Filho, Dieudonnée Togbe, Carl S. Goodyear, Christopher Linington, Damo Xu, Miodrag L. Lukic, and Foo Y. Liew. IL-33 attenuates EAE by suppressing IL-17 and IFN-γ production and inducing alternatively activated macrophages: Immunomodulation. *European Journal of Immunology*, 42(7):1804–1814, July 2012.

[282] Roland E Kontermann. Strategies for extended serum half-life of protein therapeutics. *Current Opinion in Biotechnology*, 22(6):868–876, December 2011.

[283] Jürgen Scheller, Erika Engelowski, Jens M. Moll, and Doreen M. Floss. Immunoreceptor Engineering and Synthetic Cytokine Signaling for Therapeutics. *Trends in Immunology*, 40(3):258–272, March 2019.

[284] Maja Thim Larsen, Matthias Kuhlmann, Michael Lykke Hvam, and Kenneth A. Howard. Albumin-based drug delivery: harnessing nature to cure disease. *Molecular and Cellular Therapies*, 4(1):3, December 2016.

[285] Jun Ishihara, Ako Ishihara, Koichi Sasaki, Steve Seung-Young Lee, John-Michael Williford, Mariko Yasui, Hiroyuki Abe, Lambert Potin, Peyman Hosseinchi, Kazuto Fukunaga, Michal M. Raczy, Laura T. Gray, Aslan Mansurov, Kiyomitsu Katsumata, Masashi Fukayama, Stephen J. Kron, Melody A. Swartz, and Jeffrey A. Hubbell. Targeted antibody and cytokine cancer immunotherapies through collagen affinity. *Science Translational Medicine*, 11(487):eaau3259, April 2019.

[286] Aslan Mansurov, Jun Ishihara, Peyman Hosseinchi, Lambert Potin, Tiffany M. Marchell, Ako Ishihara, John-Michael Williford, Aaron T. Alpar, Michal M. Raczy, Laura T. Gray, Melody A. Swartz, and Jeffrey A. Hubbell. Collagen-binding IL-12 enhances tumour inflammation and drives the complete remission of established immunologically cold mouse tumours. *Nature Biomedical Engineering*, 4(5):531–543, April 2020.

[287] Aslan Mansurov, Peyman Hosseinchi, Kevin Chang, Abigail L. Lauterbach, Laura T. Gray, Aaron T. Alpar, Erica Budina, Anna J. Slezak, Seounghun Kang, Shijie Cao, Ani Solanki, Suzana Gomes, John-Michael Williford, Melody A. Swartz, Juan L. Mendoza, Jun Ishihara, and Jeffrey A. Hubbell. Masking the immunotoxicity of interleukin-12 by fusing it with a domain of its receptor via a tumour-protease-cleavable linker. *Nature Biomedical Engineering*, 6(7):819–829, May 2022.

[288] John-Michael Williford, Jun Ishihara, Ako Ishihara, Aslan Mansurov, Peyman Hosseinchi, Tiffany M. Marchell, Lambert Potin, Melody A. Swartz, and Jeffrey A.

Hubbell. Recruitment of CD103 $^{+}$ dendritic cells via tumor-targeted chemokine delivery enhances efficacy of checkpoint inhibitor immunotherapy. *Science Advances*, 5(12):eaay1357, December 2019.

[289] Jun Ishihara, Ako Ishihara, Kazuto Fukunaga, Koichi Sasaki, Michael J. V. White, Priscilla S. Briquez, and Jeffrey A. Hubbell. Laminin heparin-binding peptides bind to several growth factors and enhance diabetic wound healing. *Nature Communications*, 9(1):2163, June 2018.

[290] Andrew C. Tremain, Rachel P. Wallace, Kristen M. Lorentz, Thomas B. Thornley, Jennifer T. Antane, Michal R. Raczy, Joseph W. Reda, Aaron T. Alpar, Anna J. Slezak, Elyse A. Watkins, Chitavi D. Maulloo, Erica Budina, Ani Solanki, Mindy Nguyen, David J. Bischoff, Jamie L. Harrington, Rabinarayan Mishra, Gregory P. Conley, Romain Marlin, Nathalie Dereuddre-Bosquet, Anne-Sophie Gallouët, Roger LeGrand, D. Scott Wilson, Stephan Kontos, and Jeffrey A. Hubbell. Synthetically glycosylated antigens for the antigen-specific suppression of established immune responses. *Nature Biomedical Engineering*, 7(9):1142–1155, September 2023.

[291] Elyse A. Watkins, Jennifer T. Antane, Jaeda L. Roberts, Kristen M. Lorentz, Sarah Zuerndorfer, Anya C. Dunaif, Lucas J. Bailey, Andrew C. Tremain, Mindy Nguyen, Roberto C. De Loera, Rachel P. Wallace, Rachel K. Weathered, Stephan Kontos, and Jeffrey A. Hubbell. Persistent antigen exposure via the eryptotic pathway drives terminal T cell dysfunction. *Science Immunology*, 6(56):eabe1801, February 2021.

[292] Emma Lefrançais, Anais Duval, Emilie Mirey, Stéphane Roga, Eric Espinosa, Corinne Cayrol, and Jean-Philippe Girard. Central domain of IL-33 is cleaved by mast cell proteases for potent activation of group-2 innate lymphoid cells. *Proceedings of the National Academy of Sciences*, 111(43):15502–15507, October 2014.

[293] Natalie Fursov, Jin Lu, Catherine Healy, Sheng-Jiun Wu, Eilyn Lacy, Angela Filer, Yawei Li, Changbao Liu, Roberta Lamb, Brian Jones, Ramachandra Reddy, Ted Petley, and Karen Duffy. Monoclonal antibodies targeting ST2L Domain 1 or Domain 3 differentially modulate IL-33-induced cytokine release by human mast cell and basophilic cell lines. *Molecular Immunology*, 75:178–187, July 2016.

[294] Abdulraouf M. Ramadan, Etienne Daguindau, Jason C. Rech, Krishnapriya Chinnaswamy, Jilu Zhang, Greg L. Hura, Brad Griesenauer, Zachary Bolten, Aaron Robida, Martha Larsen, Jeanne A. Stuckey, Chao-Yie Yang, and Sophie Paczesny. From proteomics to discovery of first-in-class ST2 inhibitors active in vivo. *JCI Insight*, 3(14):e99208, July 2018.

[295] Marc Charabati, Camille Grasmuck, Soufiane Ghannam, Lyne Bourbonnière, Antoine P. Fournier, Marc-André Lécuyer, Olivier Tastet, Hania Kebir, Rose-Marie Rébillard, Chloé Hoornaert, Elizabeth Gowing, Sandra Larouche, Olivier Fortin, Camille Pittet, Ali Filali-Mouhim, Boaz Lahav, Robert Moumdjian, Alain Bouthillier, Marc Girard, Pierre Duquette, Romain Cayrol, Evelyn Peelen, Francisco J. Quintana, Jack P.

Antel, Alexander Flügel, Catherine Larochelle, Nathalie Arbour, Stephanie Zandee, and Alexandre Prat. DICAM promotes T $_{h}$ 17 lymphocyte trafficking across the blood-brain barrier during autoimmune neuroinflammation. *Science Translational Medicine*, 14(626):eabj0473, January 2022.

[296] Michael U. Martin. Special aspects of interleukin-33 and the IL-33 receptor complex. *Seminars in Immunology*, 25(6):449–457, December 2013.

[297] Mohammad Faruq Abd Rachman Isnadi, Voon Kin Chin, Roslaini Abd Majid, Tze Yan Lee, Maizaton Atmadini Abdullah, Ramatu Bello Omenesa, Zaid Osamah Ibraheem, and Rusliza Basir. Critical Roles of IL-33/ST2 Pathway in Neurological Disorders. *Mediators of Inflammation*, 2018:1–9, 2018.

[298] Thomas Hoyler, Christoph S.N. Klose, Abdallah Souabni, Adriana Turqueti-Neves, Dietmar Pfeifer, Emma L. Rawlins, David Voehringer, Meinrad Busslinger, and Andreas Diefenbach. The Transcription Factor GATA-3 Controls Cell Fate and Maintenance of Type 2 Innate Lymphoid Cells. *Immunity*, 37(4):634–648, October 2012.

[299] April E. Price, Hong-Erh Liang, Brandon M. Sullivan, R. Lee Reinhardt, Chris J. Eisley, David J. Erle, and Richard M. Locksley. Systemically dispersed innate IL-13–expressing cells in type 2 immunity. *Proceedings of the National Academy of Sciences*, 107(25):11489–11494, June 2010.

[300] Corinne Cayrol and Jean-Philippe Girard. Interleukin-33 (IL-33): A nuclear cytokine from the IL-1 family. *Immunological Reviews*, 281(1):154–168, January 2018.

[301] Samuel S. Dychter, David A. Gold, and Michael F. Haller. Subcutaneous Drug Delivery: A Route to Increased Safety, Patient Satisfaction, and Reduced Costs. *Journal of Infusion Nursing*, 35(3):154–160, May 2012.

[302] Ludwig Kappos, Ernst-Wilhelm Radue, Paul O'Connor, Chris Polman, Reinhard Hohlfeld, Peter Calabresi, Krzysztof Selmaj, Catherine Agoropoulou, Malgorzata Leyk, Lixin Zhang-Auberson, and Pascale Burtin. A Placebo-Controlled Trial of Oral Fingolimod in Relapsing Multiple Sclerosis. *New England Journal of Medicine*, 362(5):387–401, February 2010.

[303] Marc Veldhoen, Richard J. Hocking, Christopher J. Atkins, Richard M. Locksley, and Brigitta Stockinger. TGFβ in the Context of an Inflammatory Cytokine Milieu Supports De Novo Differentiation of IL-17-Producing T Cells. *Immunity*, 24(2):179–189, February 2006.

[304] Rama Krishna Gurram and Jinfang Zhu. Orchestration between ILC2s and Th2 cells in shaping type 2 immune responses. *Cellular & Molecular Immunology*, 16(3):225–235, March 2019.

[305] Mousa Komai-Koma, Damo Xu, Yubin Li, AndrewN.J. McKenzie, IainB. McInnes, and FooY. Liew. IL-33 is a chemoattractant for human Th2 cells. *European Journal of Immunology*, 37(10):2779–2786, October 2007.

[306] Liying Guo, Gang Wei, Jinfang Zhu, Wei Liao, Warren J. Leonard, Keji Zhao, and William Paul. IL-1 family members and STAT activators induce cytokine production by Th2, Th17, and Th1 cells. *Proceedings of the National Academy of Sciences*, 106(32):13463–13468, August 2009.

[307] Hēth R. Turnquist, Zhenlin Zhao, Brian R. Rosborough, Quan Liu, Antonino Castellaneta, Kumiko Isse, Zhiliang Wang, Megan Lang, Donna Beer Stolz, Xin Xiao Zheng, A. Jake Demetris, Foo Y. Liew, Kathryn J. Wood, and Angus W. Thomson. IL-33 Expands Suppressive CD11b+ Gr-1int and Regulatory T Cells, including ST2L+ Foxp3+ Cells, and Mediates Regulatory T Cell-Dependent Promotion of Cardiac Allograft Survival. *The Journal of Immunology*, 187(9):4598–4610, November 2011.

[308] Lihua Duan, Jie Chen, Hongwei Zhang, Heng Yang, Ping Zhu, Ali Xiong, Quansong Xia, Fang Zheng, Zheng Tan, Feili Gong, and Min Fang. Interleukin-33 Ameliorates Experimental Colitis through Promoting Th2/Foxp3+ Regulatory T-Cell Responses in Mice. *Molecular Medicine*, 18(5):753–761, May 2012.

[309] Stephen D. Miller and William J. Karpus. Experimental Autoimmune Encephalomyelitis in the Mouse. *Current Protocols in Immunology*, 77(1), May 2007.

[310] Jeroen Deckers, Tom Anbergen, Ayla M. Hokke, Anne De Dreu, David P. Schrijver, Koen De Bruin, Yohana C. Toner, Thijs J. Beldman, Jamie B. Spangler, Tom F. A. De Greef, Francesca Grisoni, Roy Van Der Meel, Leo A. B. Joosten, Maarten Merkx, Mihai G. Netea, and Willem J. M. Mulder. Engineering cytokine therapeutics. *Nature Reviews Bioengineering*, 1(4):286–303, February 2023.

[311] Aslan Mansurov, Abigail Lauterbach, Erica Budina, Aaron T. Alpar, Jeffrey A. Hubbell, and Jun Ishihara. Immunoengineering approaches for cytokine therapy. *American Journal of Physiology-Cell Physiology*, 321(2):C369–C383, August 2021.

[312] Darrell Sleep, Jason Cameron, and Leslie R. Evans. Albumin as a versatile platform for drug half-life extension. *Biochimica et Biophysica Acta (BBA) - General Subjects*, 1830(12):5526–5534, December 2013.

[313] Michal Pyzik, Timo Rath, Wayne I. Lencer, Kristi Baker, and Richard S. Blumberg. FcRn: The Architect Behind the Immune and Nonimmune Functions of IgG and Albumin. *Journal of Immunology (Baltimore, Md.: 1950)*, 194(10):4595–4603, May 2015.

[314] Robert J. Melder, Blaire L. Osborn, Todd Riccobene, Palanisamy Kanakaraj, Ping Wei, Guoxian Chen, David Stolow, Wendy Green Halpern, Thi-Sau Migone, Qi Wang, Krzysztof J. Grzegorzewski, and Gilles Gallant. Pharmacokinetics and in vitro and in vivo anti-tumor response of an interleukin-2-human serum albumin fusion protein in mice. *Cancer Immunology, Immunotherapy*, 54(6):535–547, June 2005.

[315] Zhengsheng Yao, Weili Dai, James Perry, Martin W. Brechbiel, and Cynthia Sung. Effect of albumin fusion on the biodistribution of interleukin-2. *Cancer Immunology, Immunotherapy*, 53(5):404–410, May 2004.

[316] Vinod K. Rustgi. Albinterferon alfa-2b, a novel fusion protein of human albumin and human interferon alfa-2b, for chronic hepatitis C. *Current Medical Research and Opinion*, 25(4):991–1002, April 2009.

[317] Cynthia Sung, Bernardetta Nardelli, David W. LaFleur, Erich Blatter, Marta Corcoran, Henrik S. Olsen, Charles E. Birse, Oxana K. Pickeral, Junli Zhang, Devanshi Shah, Gordon Moody, Solange Gentz, Lisa Beebe, and Paul A. Moore. An IFN- β -Albumin Fusion Protein That Displays Improved Pharmacokinetic and Pharmacodynamic Properties in Nonhuman Primates. *Journal of Interferon & Cytokine Research*, 23(1):25–36, January 2003.

[318] Wendy Halpern, Todd A. Riccobene, Heidi Agostini, Kevin Baker, David Stolow, Mi-Li Gu, Jonathan Hirsch, Angela Mahoney, Jeffrey Carrell, Ernest Boyd, and Krzysztof J. Grzegorzewski. Albugranin, a Recombinant Human Granulocyte Colony Stimulating Factor (G-CSF) Genetically Fused to Recombinant Human Albumin Induces Prolonged Myelopoietic Effects in Mice and Monkeys. *Pharmaceutical Research*, 19(11):1720–1729, 2002.

[319] Chaity Chaudhury, Samina Mehnaz, John M. Robinson, William L. Hayton, Dennis K. Pearl, Derry C. Roopenian, and Clark L. Anderson. The Major Histocompatibility Complex–related Fc Receptor for IgG (FcRn) Binds Albumin and Prolongs Its Lifespan. *The Journal of Experimental Medicine*, 197(3):315–322, February 2003.

[320] William R. Strohl. Fusion Proteins for Half-Life Extension of Biologics as a Strategy to Make Biobetters. *BioDrugs*, 29(4):215–239, August 2015.

[321] Derry C. Roopenian and Shreeram Akilesh. FcRn: the neonatal Fc receptor comes of age. *Nature Reviews Immunology*, 7(9):715–725, September 2007.

[322] Shreeram Akilesh, Gregory J. Christianson, Derry C. Roopenian, and Andrey S. Shaw. Neonatal FcR Expression in Bone Marrow-Derived Cells Functions to Protect Serum IgG from Catabolism. *The Journal of Immunology*, 179(7):4580–4588, October 2007.

[323] Taylor B. Smallwood, Paul R. Giacomin, Alex Loukas, Jason P. Mulvenna, Richard J. Clark, and John J. Miles. Helminth Immunomodulation in Autoimmune Disease. *Frontiers in Immunology*, 8:453, April 2017.

[324] S. Greenfeder, S. P. Umland, F. M. Cuss, R. W. Chapman, and R. W. Egan. Th2 cytokines and asthma. The role of interleukin-5 in allergic eosinophilic disease. *Respiratory Research*, 2(2):71–79, 2001.

[325] Corrado Pelaia, Giovanni Paoletti, Francesca Puggioni, Francesca Racca, Girolamo Pelaia, Giorgio Walter Canonica, and Enrico Heffler. Interleukin-5 in the Pathophysiology of Severe Asthma. *Frontiers in Physiology*, 10:1514, 2019.

[326] Jonathan Corren. Role of Interleukin-13 in Asthma. *Current Allergy and Asthma Reports*, 13(5):415–420, October 2013.

[327] Larry Borish and John W. Steinke. Interleukin-33 in Asthma: How Big of a Role Does It Play? *Current Allergy and Asthma Reports*, 11(1):7–11, February 2011.

[328] Cris S Constantinescu and Brendan A Hilliard. Adjuvants in EAE. In Ehud Lavi and Cris S. Constantinescu, editors, *Experimental Models of Multiple Sclerosis*, pages 73–84. Springer US, Boston, MA, 2005.

[329] Abigail E. Russi, Mark E. Ebel, Yuchen Yang, and Melissa A. Brown. Male-specific IL-33 expression regulates sex-dimorphic EAE susceptibility. *Proceedings of the National Academy of Sciences*, 115(7), February 2018.

[330] Abigail E. Russi, Margaret E. Walker-Caulfield, Mark E. Ebel, and Melissa A. Brown. Cutting Edge: c-Kit Signaling Differentially Regulates Type 2 Innate Lymphoid Cell Accumulation and Susceptibility to Central Nervous System Demyelination in Male and Female SJL Mice. *The Journal of Immunology*, 194(12):5609–5613, June 2015.

[331] D J Cua, D R Hinton, and S A Stohlman. Self-antigen-induced Th2 responses in experimental allergic encephalomyelitis (EAE)-resistant mice. Th2-mediated suppression of autoimmune disease. *The Journal of Immunology*, 155(8):4052–4059, October 1995.

[332] Rongguo He, Hui Yin, Baohong Yuan, Tao Liu, Li Luo, Ping Huang, Liangcheng Dai, and Kang Zeng. IL-33 improves wound healing through enhanced M2 macrophage polarization in diabetic mice. *Molecular Immunology*, 90:42–49, October 2017.

[333] Anne-Gaelle Besnard, Rodrigo Guabiraba, Wanda Niedbala, Jennifer Palomo, Flora Reverchon, Tovah N. Shaw, Kevin N. Couper, Bernhard Ryffel, and Foo Y. Liew. IL-33-Mediated Protection against Experimental Cerebral Malaria Is Linked to Induction of Type 2 Innate Lymphoid Cells, M2 Macrophages and Regulatory T Cells. *PLOS Pathogens*, 11(2):e1004607, February 2015.

[334] Jiajing Cai, Dongsheng Wang, Guoyuan Zhang, and Xiaolan Guo. The Role Of PD-1/PD-L1 Axis In Treg Development And Function: Implications For Cancer Immunotherapy. *OncoTargets and Therapy*, Volume 12:8437–8445, October 2019.

[335] Lucy S.K. Walker. Treg and CTLA-4: Two intertwining pathways to immune tolerance. *Journal of Autoimmunity*, 45:49–57, September 2013.

[336] Elena Gianchecchi and Alessandra Fierabracci. Inhibitory Receptors and Pathways of Lymphocytes: The Role of PD-1 in Treg Development and Their Involvement in Autoimmunity Onset and Cancer Progression. *Frontiers in Immunology*, 9:2374, October 2018.

[337] Kento Kawai, Masateru Uchiyama, Joanna Hester, and Fadi Issa. IL-33 drives the production of mouse regulatory T cells with enhanced in vivo suppressive activity in skin transplantation. *American Journal of Transplantation*, 21(3):978–992, March 2021.

[338] Michael Delacher, Charles D Imbusch, Dieter Weichenhan, Achim Breiling, Agnes Hotz-Wagenblatt, Ulrike Träger, Ann-Cathrin Hofer, Danny Kägebein, Qi Wang, Felix Frauhammer, Jan-Philipp Mallm, Katharina Bauer, Carl Herrmann, Philipp A Lang, Benedikt Brors, Christoph Plass, and Markus Feuerer. Genome-wide DNA-methylation landscape defines specialization of regulatory T cells in tissues. *Nature Immunology*, 18(10):1160–1172, October 2017.

[339] Yunqi Wang, Maureen A. Su, and Yisong Y. Wan. An Essential Role of the Transcription Factor GATA-3 for the Function of Regulatory T Cells. *Immunity*, 35(3):337–348, September 2011.

[340] Michael Peine, Roman M. Marek, and Max Löhning. IL-33 in T Cell Differentiation, Function, and Immune Homeostasis. *Trends in Immunology*, 37(5):321–333, May 2016.

[341] Sachin P. Gadani, James T. Walsh, Igor Smirnov, Jingjing Zheng, and Jonathan Kipnis. The Glia-Derived Alarmin IL-33 Orchestrates the Immune Response and Promotes Recovery following CNS Injury. *Neuron*, 85(4):703–709, February 2015.

[342] Chad A Hudson, George P Christophi, Ross C Gruber, Joel R Wilmore, David A Lawrence, and Paul T Massa. Induction of IL-33 expression and activity in central nervous system glia. *Journal of Leukocyte Biology*, 84(3):631–643, September 2008.

[343] Ilia D. Vainchtein, Gregory Chin, Frances S. Cho, Kevin W. Kelley, John G. Miller, Elliott C. Chien, Shane A. Liddelow, Phi T. Nguyen, Hiromi Nakao-Inoue, Leah C. Dorman, Omar Akil, Satoru Joshita, Ben A. Barres, Jeanne T. Paz, Ari B. Molofsky, and Anna V. Molofsky. Astrocyte-derived interleukin-33 promotes microglial synapse engulfment and neural circuit development. *Science*, 359(6381):1269–1273, March 2018.

[344] Satoko Yasuoka, Jun Kawanokuchi, Bijay Parajuli, Shijie Jin, Yukiko Doi, Mariko Noda, Yoshifumi Sonobe, Hideyuki Takeuchi, Tetsuya Mizuno, and Akio Suzumura. Production and functions of IL-33 in the central nervous system. *Brain Research*, 1385:8–17, April 2011.